

Aus dem Pathologischen Institut der Universität München
Institut der Universität München
Direktor: Prof. Dr. med. Frederick Klauschen

***Csf1r* mediates enhancement of intestinal
tumorigenesis caused by inactivation of *Mir34a***

Dissertation
zum Erwerb des Doktorgrades der Humanbiologie
an der Medizinischen Fakultät der
Ludwig-Maximilians-Universität zu München

vorgelegt von

Fangteng Liu

aus

Jiangxi, Volksrepublik China

2023

Mit Genehmigung der Medizinischen Fakultät
der Universität München

Berichterstatter: Prof. Dr. rer. nat. Heiko Hermeking

Mitberichterstatter: Prof. Dr. Peter Nelson
Prof. Dr. Enrico De Toni

Mitbetreuung durch den
promovierten Mitarbeiter:

Dekan: Prof. Dr. med. Thomas Gudermann

Tag der mündlichen Prüfung: 27.07.2023

Publications

The results of this thesis have been published in:

Original article:

Liu, F., Bouznad, N., Kaller, M., Shi, X., König, J., Jaeckel, S., & Hermeking, H. (2022). Csf1r mediates enhancement of intestinal tumorigenesis caused by inactivation of Mir34a. *International Journal of Biological Sciences*, 18(14), 5415-5437. doi:10.7150/ijbs.75503

(IF₂₀₂₂: 10.75)

Table of content

Table of content.....	4
Zusammenfassung (Deutsch):.....	6
Summary (English):	8
List of abbreviations	10
1. Introduction	12
1.1 Colorectal cancer incidence.....	12
1.2 Genetics of colorectal cancer	15
1.3 <i>Apc</i> ^{Min/+} mouse model.....	19
1.4 Role of miR-34a in cancer	20
1.5 CSF1R signaling	24
2. Aims of the thesis	30
3. Materials and Methods	31
3.1 Materials.....	31
3.1.1 Chemicals and reagents	31
3.1.2 Enzymes	33
3.1.3 Kits	33
3.1.4 Antibodies	34
3.1.5 Buffers and solutions	36
3.1.6 Oligonucleotides	40
3.1.7 miRNA mimics	44
3.1.8 Vectors	45
3.1.9 Mice.....	45
3.1.10 Cell lines.....	46
3.1.11 Software	46
3.1.12 Laboratory equipment	47
3.2 Methods	49
3.2.1 Generation and breeding of mice	49
3.2.2 Genotyping.....	49
3.2.3 Specimen preparation and adenoma counting	52
3.2.4 Histology and immunohistochemistry	53
3.2.5 <i>In situ</i> hybridization analysis	54
3.2.6 Assessment of immunodetections	55
3.2.7 Cell lines and tumoroid culture	56
3.2.8 Immunofluorescence (IF) staining of tumoroids.....	56
3.2.9 Cryopreservation of mammalian cells and tumoroids.....	57
3.2.10 Generation of cell pools stably expressing conditional alleles.....	58
3.2.11 Dual 3'-UTR luciferase reporter assays.....	58
3.2.12 Acquisition of plasmids	59
3.2.13 DNA sequencing	60
3.2.14 Quantitative real-time PCR (qPCR) analysis	61
3.2.15 Western blot analysis.....	62

3.2.16	Transcriptomic analysis	63
3.2.17	Analysis of expression and clinical data from public databases.....	64
3.3	Statistical analyses	65
4.	Results	67
4.1	Combined deletion of <i>Mir34a</i> and <i>Csf1r</i> in murine intestinal epithelium	67
4.2	<i>Csf1r</i> mediates effects of <i>Mir34a</i> loss on intestinal architecture and secretory cell homeostasis	68
4.3	<i>Mir34a</i> loss enhances intestinal tumorigenesis in a <i>Csf1r</i> -dependent manner	72
4.4	<i>Csf1r</i> loss largely reversed the effects of <i>Mir34a</i> deletion on tumor microenvironment	76
4.5	Role of <i>Csf1r</i> in <i>Mir34a</i> -loss induced stemness and Wnt signaling	78
4.6	Expression profiling of <i>Mir34a</i> - and/or <i>Csf1r</i> -deficient adenomas and tumoroids.....	81
4.7	Analysis of <i>Mir34a</i> target expression.....	87
4.8	Clinical associations of <i>Mir34a</i> -related expression signatures	94
4.9	<i>Mir34a</i> and <i>Csf1r</i> influence therapeutic responses in tumoroids.....	98
5.	Discussion	100
6.	References.....	110
7.	Supplements	135
7.1	Supplemental Data 1	135
7.2	Supplemental Data 2	136
7.3	Supplemental Data 3	138
7.4	Supplemental Data 4	139
7.5	Supplemental Data 5	140
7.6	Supplemental Data 6	146
7.7	Supplemental Data 7	147
7.8	Supplemental Data 8	148
7.9	Supplemental Data 9	153
7.10	Supplemental Data 10	156
	Acknowledgements	158
	Affidavit	159
	List of publications	160

Zusammenfassung (Deutsch):

Das p53-induzierbare *Mir34a*-Gen wird bei Darmkrebs (CRC) häufig epigenetisch stillgelegt. Kürzlich haben wir CSF1R als miR-34a-Ziel identifiziert und CSF1R als Effektor der miR-34a-vermittelten CRC-Unterdrückung in menschlichen Zellen charakterisiert. Die *in vivo* Rolle der CSF1R/miR-34a-Achse bei der intestinalen Tumorentstehung blieb jedoch unbekannt. In dieser Studie bestätigten wir, dass *Csf1r*-mRNA ein direktes, konserviertes *Mir34a*-Ziel in Mäusen ist. Um die *in vivo* Relevanz der *Csf1r*-Regulation durch *Mir34a* während der Bildung von Darmtumoren zu untersuchen, haben wir außerdem *Apc*^{Min/+}-Mäuse mit Intestinal-Epithelial Zell-spezifischen Deletionen der *Mir34a*- und/oder *Csf1r*-Gene generiert. Wir fanden heraus, dass *Mir34a*-defiziente *Apc*^{Min/+}-Mäuse eine erhöhte Anzahl und Größe von Darmadenomen und eine verkürzte Überlebenszeit aufwiesen, während *Csf1r*-defiziente *Apc*^{Min/+}-Mäuse eine verringerte Tumorlast und ein verlängertes Überleben aufwiesen. Adenome mit *Mir34a*-Defizienz zeigten eine erhöhte Proliferation und verringerte Apoptose, eine verstärkte STAT3-Signalübertragung, eine stärkere Infiltration von Fibroblasten, Immunzellen und Bakterien sowie eine erhöhte Häufigkeit von Krebsstammzellen. Die Deletion von *Csf1r* hatte die gegenteiligen Wirkungen, und die kombinierte Deletion von *Mir34a* und *Csf1r* kehrte die Wirkungen der *Mir34a*-Deletion weitgehend um. Darüber hinaus wurden die Homöostase von Stamm- und sekretorischen Zellen, die Darmarchitektur und die Bildung von Tumoroiden durch die Deletion von *Mir34a* und *Csf1r* in entgegengesetzter Richtung beeinflusst. Die gleichzeitige Deletion von *Csf1r* und *Mir34a* neutralisierte die Wirkungen der einzelnen Deletionen. Darüber hinaus zeigte eine umfassende Analyse von mRNA-Expressionsprofilen in Adenomen und Tumoroiden, dass mRNAs mit *Mir34a*-Seed-Matching-Sites, die für Proteine im

Zusammenhang mit EMT (Epithel-Mesenchymal-Übergang), Stemness und Wnt-Signalisierung kodieren, nach der *Mir34a*-Inaktivierung angereichert wurden. *Netrin-1/Ntn1* und *Transgelin/Tagln* wurden als direkte Ziele der *Mir34a*- und *Csf1r*-Signalgebung in menschlichen und murinen Zellen charakterisiert. Mit der *Mir34a*-Inaktivierung in Zusammenhang stehende Expressionssignaturen waren mit den molekularen CRC-Subtypen CMS4/CRISB+D, CRCs im Stadium 4 und einem schlechten Überleben der Patienten assoziiert. Darüber hinaus vermittelte *Csf1r* die Resistenz gegen 5-FU, die durch den Verlust von *Mir34a* in Tumoroiden verursacht wurde. Diese Studie liefert genetische Beweise dafür, dass die *Csf1r*-Hochregulierung eine durch *Mir34a*-Verlust induzierte verstärkte intestinale Tumorentstehung vermittelt und weist auf eine Notwendigkeit der *Mir34a*-vermittelten *Csf1r*-Unterdrückung für die Homöostase intestinaler Stammzellen/sekretorischer Zellen und die Tumorunterdrückung hin. Zudem legen die Ergebnisse nahe, dass CSF1R ein wirksames therapeutisches Ziel bei p53/miR-34a-Pathway-defiziente CRCs.

Summary (English):

The p53-inducible *Mir34a* gene is frequently epigenetically silenced in colorectal cancer (CRC). Recently, we identified *CSF1R* as a miR-34a target and characterized CSF1R as an effector of miR-34a-mediated CRC suppression in human cells. However, the *in vivo* role of the CSF1R/miR-34a axis in intestinal tumorigenesis remained unknown. In this study, we confirmed that *Csf1r* mRNA is a direct, conserved *Mir34a* target in mice. To address the *in vivo* relevance of *Csf1r* regulation by *Mir34a* during intestinal tumor formation we further generated *Apc*^{Min/+} mice with intestinal-epithelial cell (IEC)-specific deletions of the *Mir34a* and/or *Csf1r* genes. We found that *Mir34a*-deficient *Apc*^{Min/+} mice displayed an increased number and size of intestinal adenomas, and reduced survival time, whereas *Csf1r*-deficient *Apc*^{Min/+} mice exhibited decreased tumor burden, and prolonged survival. *Mir34a*-deficient adenomas showed elevated proliferation and decreased apoptosis, enhanced STAT3 signaling, greater infiltrations of fibroblasts, immune cells, and bacteria, as well as increased abundance of cancer stem cells. Deletion of *Csf1r* had the opposite effects, and combined deletion of *Mir34a* and *Csf1r* largely reversed the effects of *Mir34a* deletion. In addition, stem and secretory cell homeostasis, intestinal architecture and tumoroid formation were affected in opposite directions by deletion of *Mir34a* and *Csf1r*. Concomitant deletion of *Csf1r* and *Mir34a* neutralized the effects of the single deletions. Furthermore, comprehensive analysis of mRNA expression profiles within adenomas and tumoroids showed that mRNAs containing *Mir34a* seed-matching sites, which encode proteins related to EMT (epithelial-mesenchymal transition), stemness and Wnt signaling, were enriched after *Mir34a* inactivation. *Netrin-1/Ntn1* and *Transgelin/Tagln* were characterized as direct targets of *Mir34a* and *Csf1r* signaling in human and murine cells. *Mir34a*-inactivation related expression

signatures were associated with CRC molecular subtypes CMS4/CRISB+D, stage 4 CRCs and poor patient survival. In addition, *Csf1r* mediated the resistance to 5-FU induced caused by loss of *Mir34a* in tumoroids. This study provides genetic evidence that *Csf1r* upregulation mediates enhanced intestinal tumorigenesis induced by *Mir34a* loss, indicates a requirement of *Mir34a*-mediated *Csf1r* suppression for intestinal stem/secretory cell homeostasis and tumor suppression, and suggests that CSF1R may be an effective therapeutic target in p53/miR-34a pathway-deficient CRCs.

List of abbreviations

5-FU	5-Fluorouracil
ABPs	Actin-binding proteins
AEC	Aminoethyl carbazole
APC	Adenomatous polyposis coli
APS	Ammonium peroxodisulfate
CCLE	Cancer Cell Line Encyclopedia
CD115	Cluster of Differentiation 115
CD146	Cluster of Differentiation 146
CHAPS	3-[(3-cholamidopropyl)dimethyl-ammonio]-1- propane sulfonate
CRC	Colorectal cancer
CRCSC	Colorectal Cancer Subtyping Consortium
CRIS	CRC intrinsic subtypes
CSF1	Colony stimulating factor 1
CSF1R	Colony stimulating factor 1 receptor
DAB	3,3'-Diaminobenzidine
DAPI	4',6-diamidino-2-phenylindole
DCC	Deleted in colorectal cancer
DEPC	Diethyl pyrocarbonate
DIG	Digoxigenin
DSCAM	Down syndrome cell adhesion molecule
DMEM	Dulbecco's modified Eagle's medium
DMSO	Dimethyl Sulfoxide
dNTPs	Deoxynucleotides
DOX	Doxycycline
ECM	Extracellular matrix
EMT	Epithelial mesenchymal transition
FAP	Familial adenomatous polyposis
FBS	Fetal Bovine Serum
FISH	Fluorescence <i>in situ</i> hybridization
GEO	Gene Expression Omnibus
GSEA	Gene Set Enrichment Analysis
HBSS	Hank's Balanced Salt Solution
HDI	Human Development Index
H&E	Hematoxylin and eosin
IEC	Intestinal-epithelial cell
IF	Immunofluorescence
IHC	Immunohistochemistry
ISCs	Intestinal stem cells
ISH	<i>In situ</i> hybridization
IVC	Individually ventilated cages
KD	Knockdown
KO	Knockout
M-CSFR	Macrophage colony-stimulating factor receptor
NES	Normalized enrichment scores

ORF	Open reading frame
PAS	Periodic acid-Schiff
PCA	Principal component analysis
PFA	Paraformaldehyde
PKA	Protein kinase A
SDS	Sodium dodecyl sulfate
SMS	Seed-matching sequence
TEMED	Tetramethylethylenediamine
WB	Western blot

1. Introduction

1.1 Colorectal cancer incidence

Colorectal cancer (CRC) is a malignant disease originating in the large intestine or rectum, which represents a serious problem to the global public health security (Rabeneck, Chiu, & Senore, 2020) and causes a heavy financial burden (Azzani, Roslani, & Su, 2016; Henderson et al., 2021). According to the results from GLOBOCAN 2020 produced by the International Agency for Research on Cancer, an estimated 1,930,000 CRC cases were diagnosed worldwide in 2020, accounting for 10% of the new cancer cases, ranking the 3rd among malignancies (**Figure 1**) (H. Sung et al., 2021). In the same year, there were an estimated 930,000 CRC-caused deaths, representing 9.4% of the cancer deaths, and thereby the 2nd leading cause for tumor-related deaths globally (**Figure 1**) (H. Sung et al., 2021).

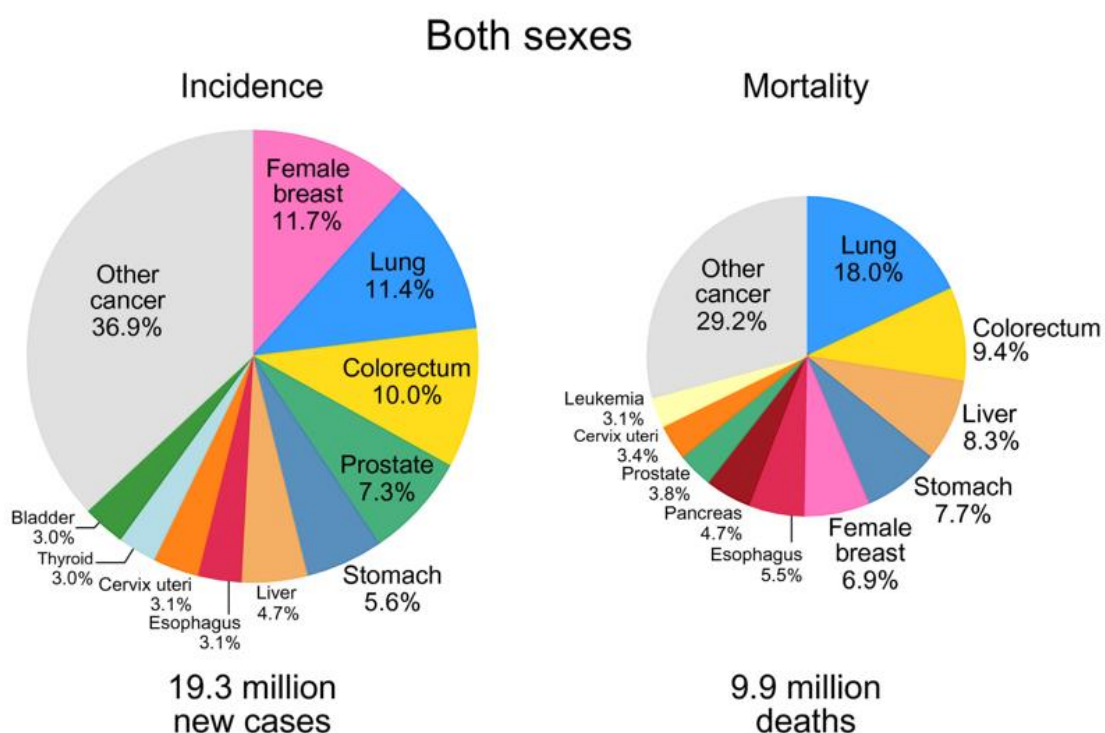


Figure 1. Ten top most common cancers for new cases and deaths for both sexes in 2020 worldwide. Figure is taken from (H. Sung et al., 2021).

China and the United States had the highest number of new CRC cases in 2020, with about 560,000 and 160,000 cases, respectively (**Figure 2**) (Xi & Xu, 2021). It is estimated that by 2040, the number of new CRC cases in China and the United States may presumably reach 910,000 and 210,000, respectively (**Figure 2**) (Xi & Xu, 2021). In 2020, the estimated number of CRC deaths in China, Japan, and the United States represented the highest three in the world, with 286,000, 60,000, and 54,000 deaths, respectively (**Figure 2**) (Xi & Xu, 2021). By 2040, the number of CRC deaths in China, Japan, and the United States is expected to reach 546,000, 73,000, and 80,000, respectively (**Figure 2**) (Xi & Xu, 2021). Additionally, Russia, India, and Germany were among the top 10 countries with the highest CRC incidence in 2020 (**Figure 2**) (Xi & Xu, 2021).

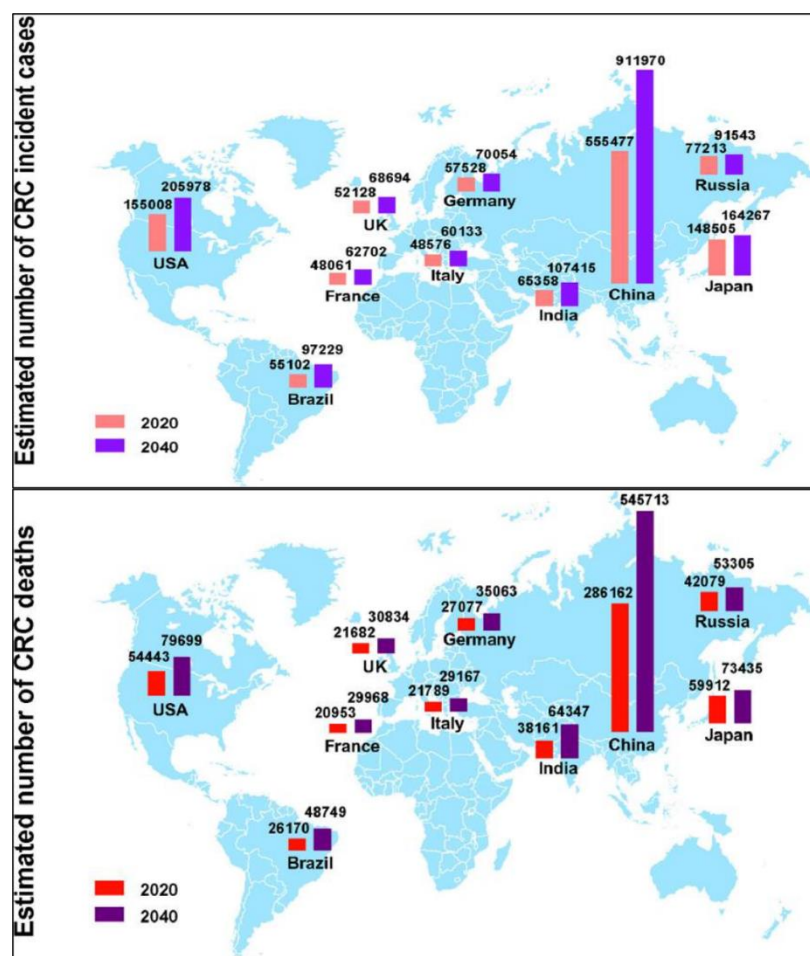


Figure 2. Estimated number of new cases and deaths of CRC in the top 10 countries with highest incident cases in 2020 and projections for 2040. Figures are taken from (Xi & Xu, 2021).

The frequency of CRC varies in different countries and regions (H. Sung et al., 2021; Xi & Xu, 2021). In 2020, the three countries with the top incidence of CRC in the world are all in Europe, among which Hungary had the highest incidence rate of CRC - 0.453%, followed by Slovakia and Norway, the incidence rate is 0.439% and 0.419%, respectively (Xi & Xu, 2021). Countries with the incidence of CRC at bottom in the world are mostly located in Africa and parts of Asia, among which Guinea in West Africa has the lowest incidence rate of CRC - 0.033%, which is only about one-thirteenth of that in Hungary (Xi & Xu, 2021). And at the level of Human Development Index (HDI), the incidence rates of CRC in very high, high, medium and low HDI countries are 29.4, 20.4, 6.1, and 7.40 cases per 100,000 persons, respectively (Xi & Xu, 2021). This seems to indicate a positive correlation between the incidence rate of CRC and HDI, which supports the conclusion that the incidence of CRC is higher in developed countries and relatively lower in less developed countries and regions. Although the incidence of CRC in highly developed countries is at a high basal level, the incidence of CRC has shown a stable or declining trend, while the incidence rate of CRC is increasing rapidly in lower-to-middle-income countries (M. Arnold et al., 2017; Xi & Xu, 2021). This distribution and trends correlate with more westernized lifestyles in transition countries, with greater exposure to risk factors, and in high-income countries with popularized CRC screening and early detection and removal of precancerous lesions and healthier lifestyles changes (M. Arnold et al., 2017; Bishehsari, Mahdavinia, Vacca, Malekzadeh, & Mariani-Costantini, 2014; Murphy et al., 2019; Xi & Xu, 2021).

In addition, the incidence of CRC also varies by age and sex. Studies found that the incidence of CRC increases with age (Amersi, Agustin, & Ko, 2005), especially when the age exceeds 50 years (Bibbins-Domingo et al., 2016). And

among people aged 50-64, the incidence of CRC increased by 1% per year (Siegel et al., 2020). Strikingly, mounting evidence recently attests that the incidence of CRC is increasing in younger populations (Saad El Din et al., 2020; J. J. Y. Sung et al., 2019; Vuik et al., 2019). And it is predicted that by 2030, the average incidence rate of CRC in the United States will increase by approximately 107% in patients aged 20 to 34, and by about 37% in patients aged 35 to 49 (Bailey et al., 2015). The observed rise in CRC incidence among young adults may be related to changes in early-life risk factor exposure (Gu et al., 2022; O'Sullivan et al., 2022; Young et al., 2015). Behavioral and lifestyle changes, like overweight or obese (Patel & De, 2016), physical inactivity (Nguyen et al., 2018), low-fiber and high-fat diets (Carroll, Frugé, Heslin, Lipke, & Greene, 2022), and tobacco use (Buc et al., 2006), all are risk factors that contribute to an increased likelihood of developing early-onset CRC. And the incidence rate of CRC in men is substantially higher than that in women, the age-standardized incidence rate for CRC in men is 45% higher than in women (Abancens, Bustos, Harvey, McBryan, & Harvey, 2020). The sexual dimorphism in CRC incidence may be due to the protective effect of the sex steroid hormone estrogen in the development of CRC in females (Abancens et al., 2020).

1.2 Genetics of colorectal cancer

The carcinogenesis and development of CRC is a multistep, multifactorial process. Hereditary, environmental and individual factors all influence the occurrence of CRC (Munteanu & Mastalier, 2014). Familial inherited conditions, e.g. Familial adenomatous polyposis (FAP), MUTYH-associated polyposis and Lynch syndrome, lead to significantly increased risk of CRC (R. M. Byrne & Tsikitis, 2018; Stoffel & Kastrinos, 2014). In addition, individuals with mentioned

above such as FAP family history have an increased risk of developing CRC (Aihara, Kumar, & Thompson, 2014; Jenkins et al., 2006; Smith-Ravin et al., 1994).

Genome stability is a fundamental biological trait that maintains the integrity of the genetic material transmitted across generations and in somatic cells (Kovalchuk, 2016). Loss of genome stability is closely implicated in cancer progression (Shen, 2011), and the acquisition of genomic instability is accepted as an important factor in the pathogenesis of CRC (Beckman & Loeb, 2005; H. Yamagishi, Kuroda, Imai, & Hiraishi, 2016). There are three levels of genomic instability, the most common of which is chromosomal instability, which causes changes in the chromosome number (so-called aneuploidy) and structure (Lengauer, Kinzler, & Vogelstein, 1998). Up to 65%–70% of sporadic CRCs display chromosomal instability (Pino & Chung, 2010). Microsatellite instability refers to mutations of repetitive sequences resulting from deletions or expansions within these which also affect coding sequences of oncogenes and tumor suppressor genes, such as *APC* and *β-catenin* (W. S. Chen et al., 1997; Pikor, Thu, Vucic, & Lam, 2013). It is caused by loss of the DNA mismatch repair and has been studied extensively in a number of cancers (Halling et al., 1999; W. S. Kim et al., 2000; Koopman et al., 2009; Risinger et al., 1993). Approximately 15% of CRCs exhibit microsatellite instability (Lothe et al., 1993; Pikor et al., 2013). Mutations of mismatch repair genes, including *MLH1*, *MSH2*, *MSH6*, *PMS1* and *PMS2*, have been shown to cause CRC, reviewed in (Wheeler, Bodmer, & Mortensen, 2000). Nucleotide instability, although less common than other forms of genomic instability, can also cause significant phenotypes when present, as monoallelic MYH somatic variants, G:C-->T:A, which leads to genomic instability

and accumulation of DNA mutations that predispose these individuals to colon cancer (Al-Tassan et al., 2002; Kambara et al., 2004). In addition, global hypomethylation and promoter-specific DNA methylation are regarded as the prominent characteristics of CRCs (Tse, Jenkins, Chionh, & Mariadason, 2017), and aberrant DNA CpG-methylation is found to be closely associated with CRC. For examples, genes of *ADAMTS16* (Kordowski et al., 2018) and *MLH1* (Wong, Hawkins, Ward, & Hitchins, 2011) showing altered DNA methylation are linked to CRC development.

Notably, dysregulation of tumor suppressor genes and oncogenes is frequently detected in CRC tissues, the activation of oncogenes and mutations of tumor suppressor genes are closely related to the occurrence and development of CRC. *KRAS* (Bos et al., 1987), *BRAF* (Caputo et al., 2019), *PIK3CA* (Cathomas, 2014), *CTNNB1* (A. Arnold et al., 2020) are proven to be oncogenes involved in CRC, while *APC* (Kinzler et al., 1991; Powell et al., 1992), *TP53* (Baker et al., 1989; Hollstein, Sidransky, Vogelstein, & Harris, 1991), *PTEN* (Salvatore et al., 2019) and *DCC* (Peltomäki et al., 1991) are suppressor genes associated with CRC.

In the “adenoma to carcinoma” process, each step is accompanied by distinct molecular changes (Fearon & Vogelstein, 1990; Menter et al., 2019). Generally accepted, the mutation in the adenomatous polyposis coli (*APC*) gene, which occurs in ca. 80% of CRCs, triggers the transformation from normal mucosa to benign adenoma, and is followed by alterations of *KRAS* and *p53* genes, which further promote tumorigenesis and progression. About 10% of CRCs cases lack alterations of *APC* and show activating mutations of β -catenin (Parker, Rudeen, & Neufeld, 2020). Mutations required for transformation from

adenoma to carcinoma result in promotion of malignant phenotype through selection of variants with optimal growth and invasion of tumor cell colonies (Vogelstein & Kinzler, 2002). With the development of sequencing technology and bioinformatics, further advances have been made in characterizing the molecular expression signatures of colorectal cancer (**Figure 3**) (Menter et al., 2019).

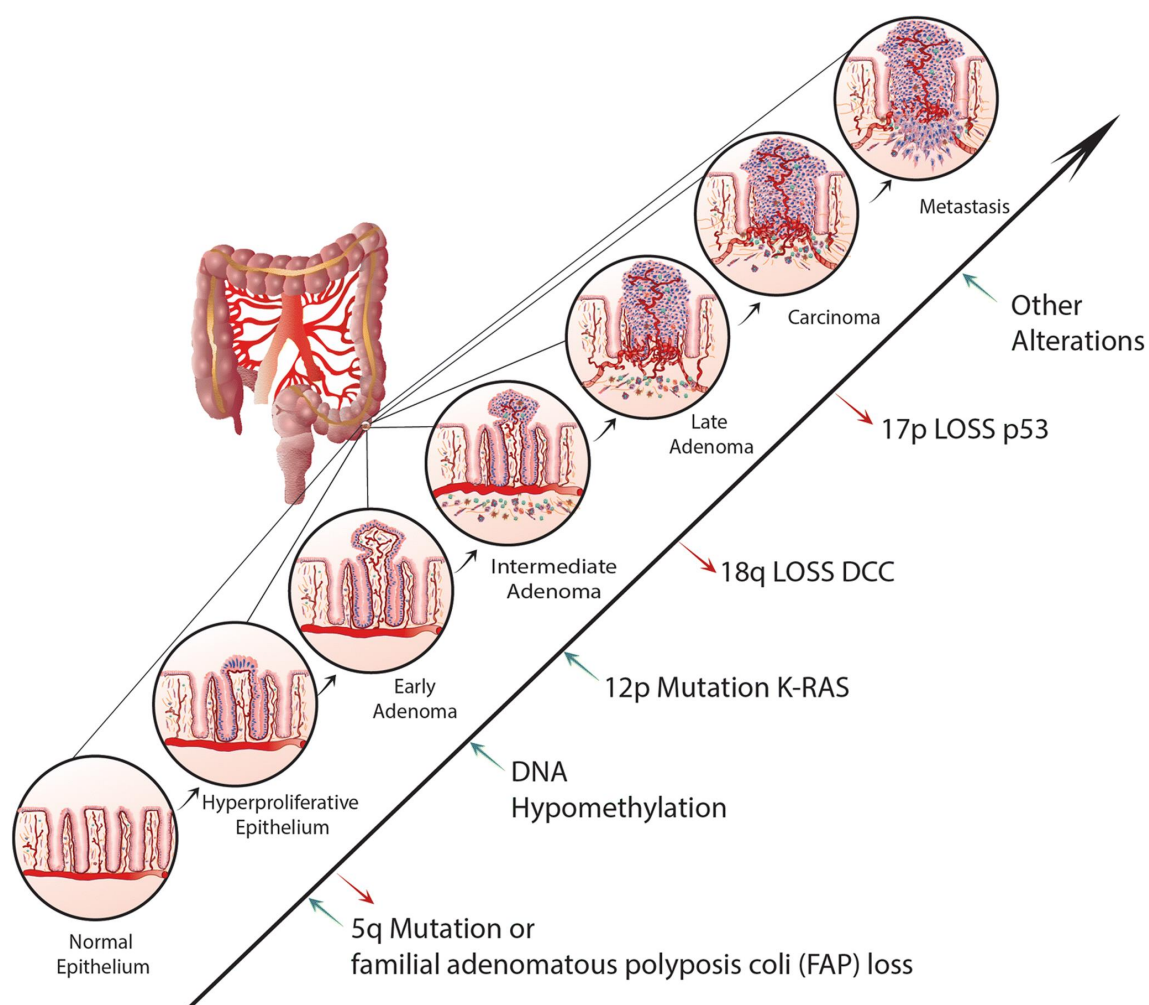


Figure 3. Genetic and epigenetic alterations in the tumorigenesis and progression of colorectal cancer. A spectrum of genetic changes drives the development of colorectal cancer, including the modifications of multiple oncogenes and tumor suppressor genes. During these processes 5q mutation or *FAP* loss is the early alterations involving hyperproliferation of epithelial cells and DNA hypomethylation. *K-ras* mutations may occur in adenomas at early and intermediate stages. Loss of 18q or deleted in colorectal cancer (*DCC*) contributes to late adenoma. 17p loss (*p53*) causes adenoma to eventually develop into carcinoma. Prior to tumor metastasis, there may be other alterations. Figure is taken from (Menter et al., 2019).

1.3 *Apc*^{Min/+} mouse model

The development of human CRC is a complex process involving multiple interactions of genes and environment (Ahmed, 2006). To assess the relevant biological features of CRC and further reveal the underlying mechanism of CRC progression, many useful mouse models for CRC have been established (Bürtin, Mullins, & Linnebacher, 2020; Jackstadt & Sansom, 2016). These can be broadly divided into three groups: genetically-engineered, chemically-induced, and inoculated models (Tong, Yang, & Koeffler, 2011). The chemical-induced mouse model is the oldest approach to induce CRC in animals, and the AOM/DSS model is a powerful and reproducible chemically induced mouse model for studying colon cancer carcinogenesis (De Robertis et al., 2011). Genetically engineered mouse models can well simulate the pathogenesis of CRC, contributing to study the role of specific molecular pathway in CRC (Bürtin et al., 2020).

The *Apc*^{Min} (Multiple intestinal neoplasia) mouse model represents the most widely used model for colorectal tumorigenesis (Moser et al., 1995; Ren, Sui, Fang, Li, & Li, 2019). Activation of the Wnt signaling pathway by genetic alterations of the *APC* or *CTNNB1* gene is a hallmark of CRC (Bienz & Clevers, 2000). In humans, the familial adenomatous polyposis (FAP) syndrome caused by the mutations of tumor-suppressor gene *Apc* leads to 100-1000 adenomatous polyps in the large intestine at early adolescence, and ultimately develop into malignant colorectal cancer in all cases (Galiatsatos & Foulkes, 2006; Half, Bercovich, & Rozen, 2009). The *Apc*^{Min/+} mouse harbors a point mutation within one *Apc* allele, resulting in an incomplete *Apc* protein - a truncated form of APC with 850 amino acids, and activation of Wnt signaling. Similar to patients with FAP, *Apc*^{Min} mice are predisposed to multiple intestinal neoplasms- roughly 100 small intestinal adenomas and few colon adenomas, which correspond to an early stage of

colorectal cancer. The adenomas in *Apc^{Min/+}* mice do not progress to invasive cancers and therefore do not form local or distant metastases (Halberg et al., 2009; Moser, Pitot, & Dove, 1990). The human and mouse *Apc* genes have about 90% sequence similarity (Su et al., 1992), and the *Apc^{Min}* mouse model and the human inherited FAP syndrome display high genetic and phenotypic similarities. The *Apc^{Min/+}* mouse model is therefore appropriate for simulating human familial adenomatous polyposis and colorectal tumors, and allow to explore the earliest mechanisms in the development of CRC. And *Apc^{Min/+}* mouse has become an excellent animal model for studying the genes involved in colorectal tumorigenesis (**Figure 4**) (Jackstadt & Sansom, 2016; Ren et al., 2019).

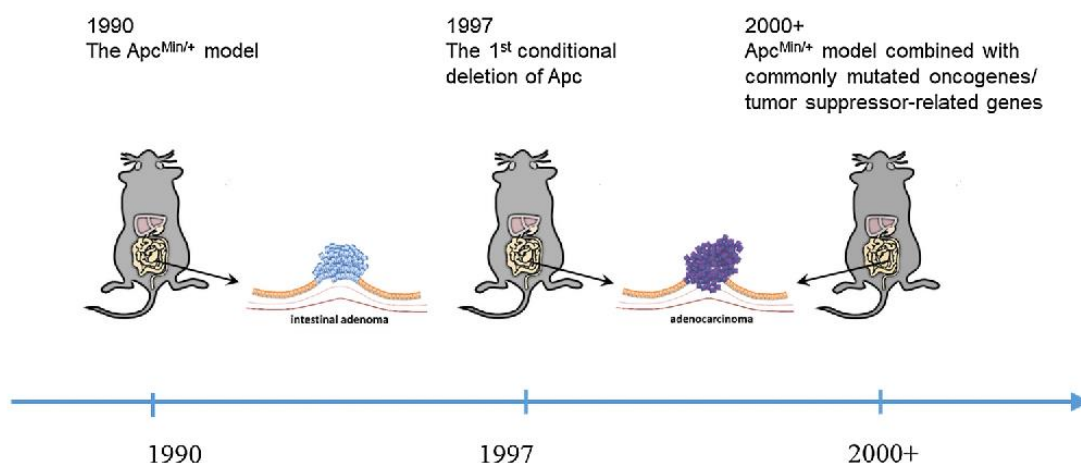


Figure 4. Overview of the historical evolution of the *Apc^{Min/+}* mice models. The *Apc^{Min/+}* mouse was developed in the year of 1990 and imitates the conditions that seen in FAP patients. Models for colonic adenomas were obtained later in 1997 when the first conditional deletion of *Apc* was accomplished in the colon. Since 2000, *Apc^{Min/+}* models combined with specific mutations of oncogenes or tumor suppressor genes have been established. Figure is taken from (Ren et al., 2019).

1.4 Role of miR-34a in cancer

miR-34a was one of the identified p53-regulated microRNAs, has attracted widespread interest (Hermeking, 2007, 2012). By binding to the promoter of *miR-34a*, activation of *p53* leads to the upregulation of miR-34a expression (**Figure 5**) (Misso et al., 2014; Tarasov et al., 2007). Decreased expression of miR-34a

widely exists in a wide range of human cancer tissues, and has been associated with tumor progression and clinical prognosis of cancer patients (Hermeking, 2012; Lodygin et al., 2008; Vogt et al., 2011). Through down-stream targets, miR-34a suppresses a variety of tumor-associated processes (**Figure 6**) (Hermeking, 2012; S. Li et al., 2021; Rokavec, Li, Jiang, & Hermeking, 2014), such as cell cycle (Singh, Sharma, & Singh, 2022), proliferation and apoptosis (Hermeking, 2010; B. Wang et al., 2018), invasion (Rui et al., 2018), stemness (C. Liu et al., 2011), and epithelial-mesenchymal transition (EMT) (Kaller & Hermeking, 2016). As a network hub miR-34a, participates in the regulation of numerous signal pathways including MAPK/ERK signaling (Y. Zhou, Ding, Lin, & Wang, 2018), the PI3K/AKT pathway (Ma, Qin, & Cui, 2013), STAT3 signaling (X. Lin et al., 2017) and the Wnt signaling pathway (N. H. Kim et al., 2011).

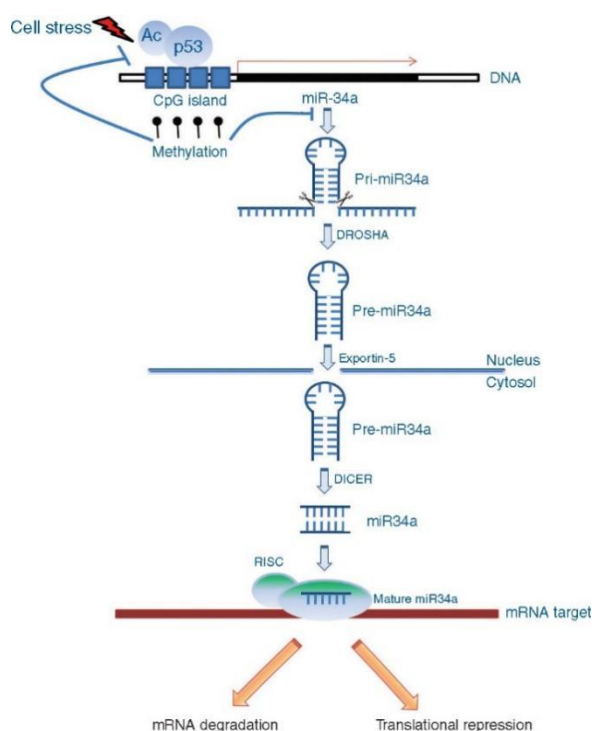


Figure 5. MiR-34a biogenesis displaying miR-34a upregulation after p53 activation. When DNA is damaged, the p53 gene is activated, and p53 binds to the miR-34a promoter to induce the expression of pri-miR-34a. The production of the associated miRNAs is decreased as a result of a mutation in p53's DNA-binding domain, which has an adverse effect on this processing. After DNA damage, p53 transactivates miR-34a, however CpG DNA-methylation of the miR-34a promoter results in dominant silencing of miR-34a. The human RNase III DROSHA converts miR-34a from its initial long hairpin molecule (pri-miRNA) transcript into a stem-loop precursor with a

length of around 70 nucleotides (pre-miRNAs). MiR-34a is transported from the nucleus to the cytoplasm via exportin-5. MiR-34a is fragmented into duplexes with ultimate lengths of 22-23 nt by another human RNase III, DICER, in a series of steps. The RNA-induced silencing complex (RISC) is the last stage, in which one strand of the miRNA duplex (the "mature strand") is integrated while the other is destroyed. Once it has been incorporated into the RISC, miR-34a directs this complex to partially or completely complementary binding sites found in the 3' untranslated region (UTR) of target mRNAs, where it then inhibits the translation of those mRNAs. The target mRNA is degraded when the alignment is perfect, whereas mRNA translation is hampered by imperfect alignment. Figure is taken from (Misso et al., 2014).

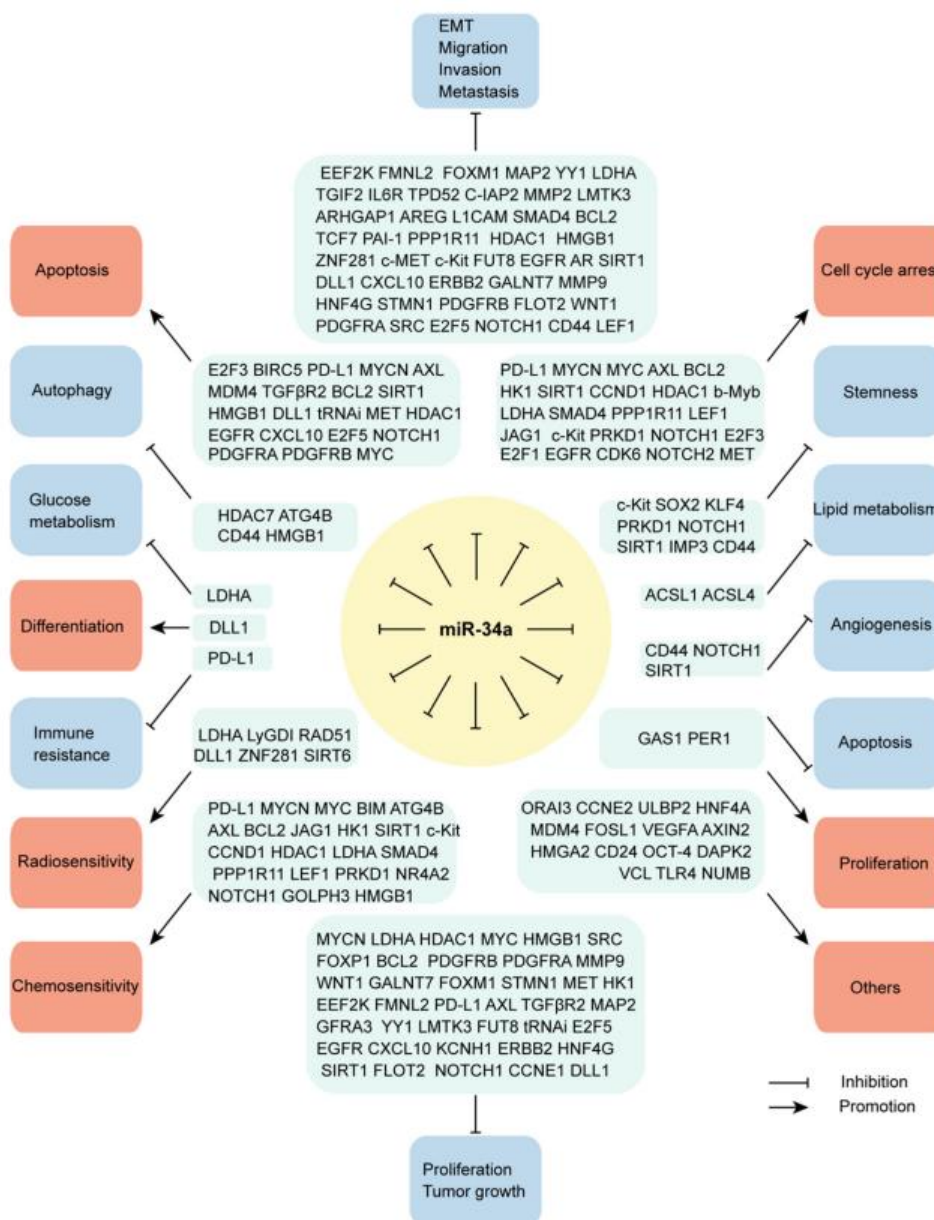


Figure 6. Multifaceted antitumor effects of miR-34a regulated by down-stream targets.

To prevent cancer progression, miR-34a mediates a variety of biological effects by targeting downstream genes and related signaling pathways. As a well-known and powerful tumor suppressor, various critical effects of miR-34a have been characterized, including the inhibitory roles on tumor migration, invasion, metastasis, stemness, angiogenesis, proliferation, tumor growth, immune resistance and autophagy. In addition, miR-34a mediates cell cycle arrest, chemo- and radio-sensitivity. In addition, miR-34a was reported to suppress the metabolism of lipid and glucose via modulating associated downstream targets. Figure is taken from (S. Li et al., 2021).

miR-34a was found to be frequently epigenetically inactivated by CpG methylation in solid tumors as well as hematological malignancies (Chim et al., 2010; Lodygin et al., 2008). For instances, in CRCs the rate of *miR-34a* silencing was at ca. 75% and for *miR-34b/c* at 100% (Lodygin et al., 2008; Vogt et al., 2011). Also in non-Hodgkin's lymphoma, the rate of *miR-34a* methylation was reported as high as 18.8% (Chim et al., 2010). In neuroblastoma, specific deletions of *miR-34a*, which resides on 1p36, have been detected (Hermeking, 2010; Welch, Chen, & Stallings, 2007). The restoration of *miR-34a* is therefore a potential therapeutic approach to treat human tumors, including CRCs (Abd-Aziz, Kamaruzman, & Poh, 2020; Bader, Brown, Stoudemire, & Lammers, 2011; W. J. Li et al., 2021). Whereas, in mice models, an increase in the rate of tumor formation could not be observed after inactivation of *Mir34a* or *Mir34b/c* genes alone, *Mir34* loss combined with mutation of other genes or carcinogenic treatments promoted tumor development. For example, no tumorigenic lesions were observed in mice with prostate epithelium-specific inactivation of the *miR-34* genes alone, but combined deficiency for *miR-34* and *p53* resulted in high-grade prostate intraepithelial neoplasia and invasive adenocarcinomas (C. Y. Cheng et al., 2014). In mouse model of pancreatic cancer, no obvious phenotypes are exhibited in *Mir34a*^{Δ/Δ} mice, while pancreatic pre-neoplastic lesions and adenocarcinomas rapidly developed in *Kras*^{G12D}; *Mir34a*^{Δ/Δ} mice (Hidalgo-Sastre et al., 2020). In a *Kras*-induced lung cancer mouse model, *miR-34a* inactivation alone does not display a strong oncogenic effect, while in combination with *p53* haplo-insufficiency it significantly accelerated the development of lung tumorigenesis (Okada et al., 2014). In a colitis-associated cancer mouse model, the deficiency of *Mir34a* enhanced the formation and invasion of colon tumors after AOM/DSS treatment (Rokavec, Li, et al., 2014).

Furthermore, combined deletion of *Mir34a* and *Tp53* in colonic epithelial cells promoted the progression and invasiveness of CRC after azoxymethane treatment (Öner et al., 2018). In the *Apc*^{Min/+} mouse model, combined deletion of the *miR-34a* and *miR-34b/c* genes significantly enhanced the intestinal tumorigenesis caused by inactivation of the *Apc* gene (Jiang & Hermeking, 2017).

In addition, miR-34a expression is related to clinical progression, and was identified as potential prognostic markers of CRC (Gao et al., 2015; Siemens et al., 2013). Moreover, deletion of miR-34a inhibits asymmetric division and exacerbates Lgr5⁺ intestinal stem cells proliferation (Bu et al., 2016). It has been shown that the IL-6R/STAT3/miR-34a feedback loop facilitates EMT-mediated CRC invasion and metastasis (Rokavec, Oner, et al., 2014). Furthermore, in human CRC cell lines, miR-34a-mediated regulation of CSF1R expression results from p53 activation, and a double-negative feedback loop formed by miR-34a, CSF1R, and STAT3 allow CRC cells to integrate antagonistic mitogenic and antiproliferative signals (Shi et al., 2020). miR-34a-mediated CSF1R/STAT3 signaling has been shown to be involved in multiple tumor-related processes and properties. miR-34a downregulation and resulting CSF1R upregulation mediates EMT, enhanced migration and invasion, and drug resistance in CRC cells. And epigenetic silencing of *miR-34a* that upregulates CSF1R promotes 5-FU resistance and development of CRC (Shi et al., 2020).

1.5 CSF1R signaling

As mentioned above CSF1R was identified as a target of miR-34a by the hosting lab of Prof. Hermeking before (Shi et al., 2020). Colony stimulating factor 1 receptor (CSF1R), also called macrophage colony-stimulating factor receptor

(M-CSFR) or cluster of differentiation 115 (CD115), is a cell-surface membrane protein encoded by the *c-FMS* proto-oncogene, and acts as the receptor for colony stimulating factor 1 (CSF1) and interleukin 34 (IL-34) (H. Lin et al., 2008). CSF1R belongs to the group of class III receptor tyrosine kinases, with characteristic extracellular IgG, a transmembrane and intracellular kinase domains (**Figure 7**) (Abu-Duhier et al., 2003; Mun, Park, & Park-Min, 2020).

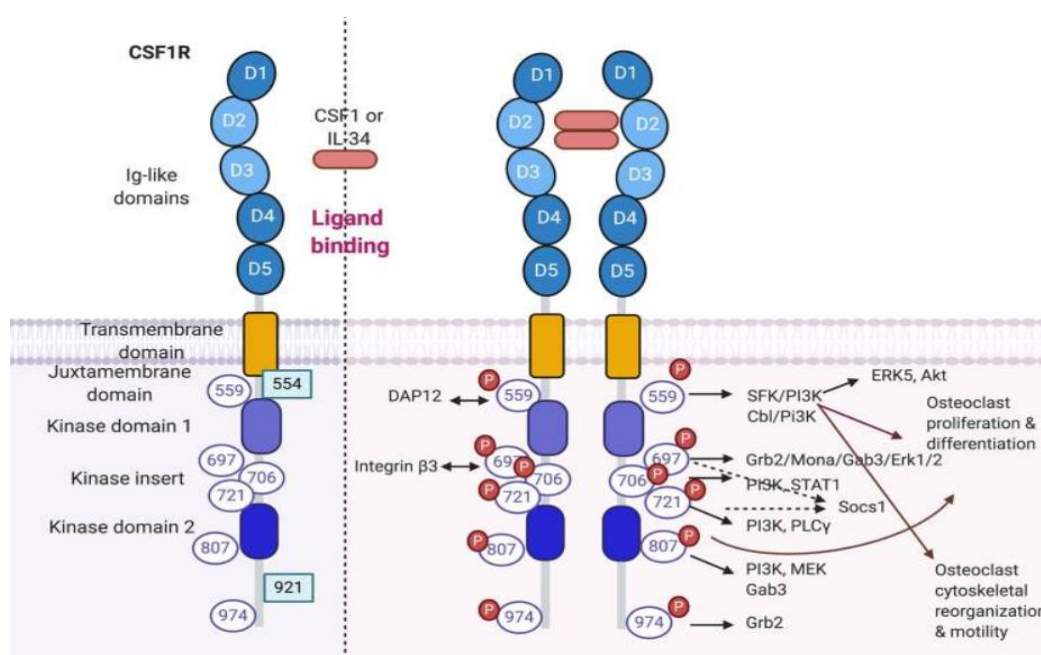


Figure 7. Structure of CSF1R protein showing the receptor binding sites and regulatory domains. The CSF1R protein is comprised of extracellular and intracellular regions. Five Ig-like domains (D1 to D5), including ligand-binding D2 and D3 domains, are present in the extracellular region. Kinase domain 1 and 2, a kinase insert, and transmembrane, juxtamembrane and cytoplasmic domains constitute the intracellular region. As a receptor tyrosine kinase, CSF1R contains six tyrosine residues that are phosphorylated upon ligand (CSF1 or IL34) binding (purple circles). Figure is taken from (Mun et al., 2020).

Ligand binding activates CSF1R through dimerization, followed by phosphorylation of at least six intracellular tyrosine residues in its intracellular domain and the binding of a number of effector proteins, these proteins subsequently activate multiple downstream signal transduction cascades to regulate cell proliferation, differentiation, migration and survival (**Figure 8**) (Mun et al., 2020; Pixley & Stanley, 2004).

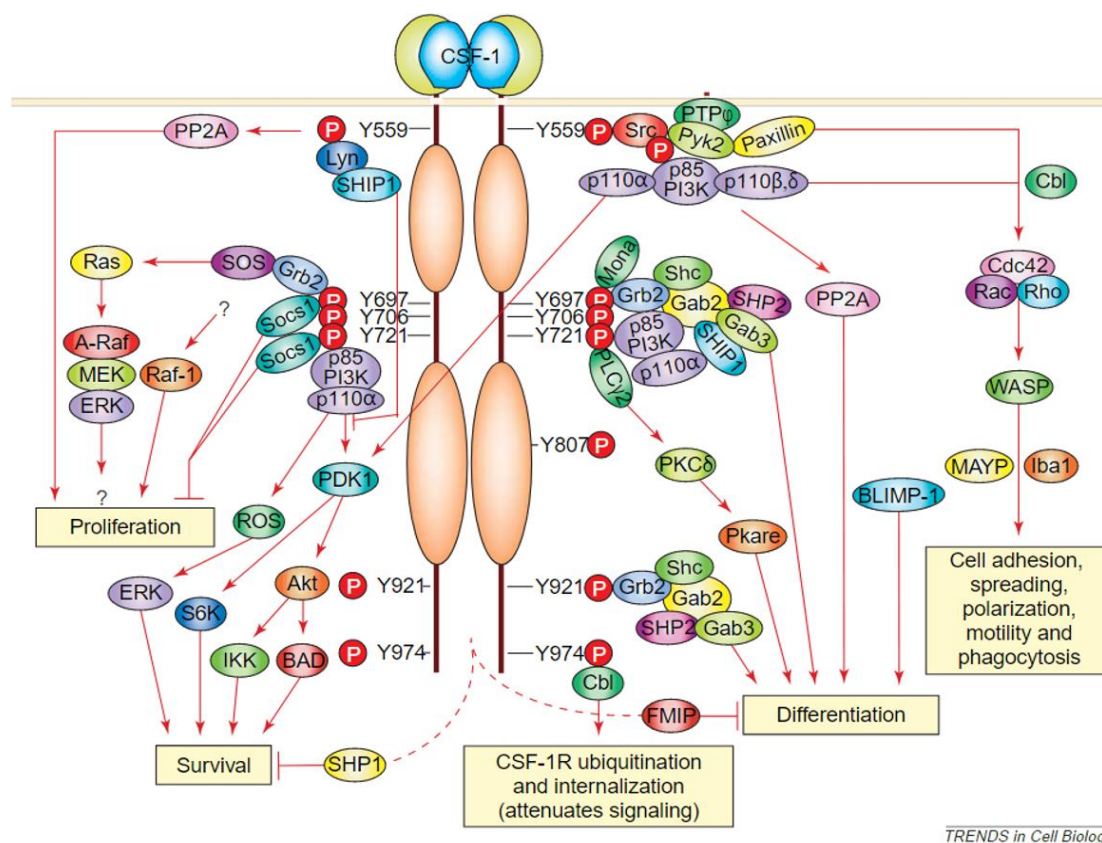


Figure 8. Downstream signaling pathways and biological functions regulated by CSF1R.

Ligand binding of CSF1R induces dimerization and phosphorylation of tyrosine residues, and phosphorylated tyrosine serves as a docking site for signaling molecules, thereby activating multiple signaling pathways, including Ras/Raf/MEK/ERK pathway, PI3K/AKT signaling, and Rac signaling, and promoting cell proliferation, adhesion, survival, differentiation, motility. Figure is taken from (Pixley & Stanley, 2004).

It has been reported that a number of signaling pathways can be activated upon CSF1R stimulation by its ligands (Shouqing & Dexian, 1998). The Ras/Raf/MEK/ERK pathway is evolutionarily conserved (Kolch, 2005) and represents a principal signaling cascade among MAPKs (L. Li et al., 2016). It participates in diverse cellular activities and plays a crucial role in carcinogenesis and drug resistance (Guo et al., 2020; McCubrey et al., 2007). Studies showed that CSF1R activates cell proliferation (Roussel, Cleveland, Shurtleff, & Sherr, 1991; Roussel, Davis, Cleveland, Ghysdael, & Hiebert, 1994) and survival (Lee, 1999; Lee & States, 2000) by inducing the Ras/Raf/MEK/ERK pathway. In

addition, CSF1R activates the MAPK pathway to promote the pro-tumorigenic phenotypes of M2 tumor-associated macrophages (TAMs) (Ramesh, Brouillard, Kumar, Nandi, & Kulkarni, 2020). CSF1R also promoted proliferation of breast cancer cells by ERK1/2 activation (Morandi, Barbetti, Rivero, Dello Sbarba, & Rovida, 2011). In line with these findings, the successful treatment of a patient with Erdheim-Chester disease (ECD), which is associated with activation of ERK/MAPK axis, was achieved by applying Pexidartinib, a specific CSF1R inhibitor (Abeykoon et al., 2022).

CSF1R activates STAT1 and STAT3 (Gérard, De Mot, Cordi, van Eyll, & Lemaigre, 2021; Novak et al., 1995), which are cytoplasmic transcription factors are involved in inflammatory responses, angiogenesis, proliferation and apoptosis (B. H. Kim, Yi, & Ye, 2016; Loh et al., 2019; Y. Zhang & Liu, 2017). CSF1R also activates the JAK/STAT pathway (Truong et al., 2018). IL-34 binding to CSF1R and the subsequent STAT3 activation results in proliferation and migration of hepatitis B virus-associated hepatocarcinoma cells (Kong et al., 2019). And in rheumatoid arthritis, p-STAT3/STAT3 protein levels were found to be decreased after CSF1R blockade (S. Yang et al., 2016).

Phosphorylation of CSF1R activates phosphoinositide 3-kinase (PI3K) (Reedijk et al., 1992; Shouqing & Dexian, 1998; Zwaenepoel et al., 2012). Activated PI3K enhances ERK and Rac signaling to promote tumorigenesis (Campa, Ciraolo, Ghigo, Germena, & Hirsch, 2015; Ebi et al., 2013; Parri & Chiarugi, 2010; Royal, Lamarche-Vane, Lamorte, Kaibuchi, & Park, 2000). CSF1R also stimulates macrophage motility and enhances invasion and metastasis of tumor cells via the PI3K pathway (Mouchemore et al., 2013; Sampaio et al., 2011). The proliferation of macrophages regulated through

CSF1R is mediated by the PI3K and ERK1/2 pathways (W. Yu et al., 2012). CSF1R also promotes macrophage migration, invasion and M2 polarization via activation of the PI3K/AKT/FOXO1 axis (Dwyer, Greenland, & Pixley, 2017; Y. Zhou et al., 2021). CSF1R promotes T-cell lymphoma growth through activation of PI3K/AKT/mTOR pathways (Murga-Zamalloa et al., 2020). PI3K blockade combined with CSF1R inhibition may provide a promising immunotherapeutic strategy for the treatment of pancreatic cancer (M. Li et al., 2020) and glioblastoma multiforme (Quail et al., 2016) by targeting macrophages and remodeling the tumor microenvironment. In addition, CSF1R also activates the phosphatidylcholine-specific phospholipase C pathway, which is involved in the modulation of cellular metabolism, growth and proliferation during tumor progression (M. Cheng, Bhujwalla, & Glunde, 2016; Mercurio et al., 2017; Podo et al., 2016).

CSF1R was initially found to be expressed mainly in macrophages and their progenitors (P. V. Byrne, Guilbert, & Stanley, 1981; Guilbert & Stanley, 1980), but was later found to be also expressed in other cell types, such as osteoclasts, myeloid dendritic cells (MacDonald et al., 2005), and microglia (Nandi et al., 2012). CSF1R signaling is critical for the differentiation, survival and polarization, and chemotaxis of macrophages (Stanley & Chitu, 2014). Macrophages promote tumorigenesis and progression by stimulating angiogenesis, facilitating tumor cell expansion, growth, invasion, and metastasis and suppressing anti-tumor immunity (Cassetta & Pollard, 2018; Noy & Pollard, 2014; Salmaninejad et al., 2019). CSF1R expression has also been detected in the murine intestinal epithelial cells (Akcora et al., 2013; Huynh et al., 2009). The CSF1R controls the development of Paneth cells, and is required for support of the intestinal stem cell niche. *Csf1r*-deficient mice displayed a reduced size of

intestinal crypts and villi, and a dramatic reduction of Paneth cell numbers (Huynh et al., 2009). In addition, *Csf1r* loss was associated with reduced crypt proliferation and lowered expression of stem cell genes (Akcora et al., 2013). CSF1R also plays an important role in murine colon development, homeostasis and inflammatory stress response, a study by (Huynh et al., 2013) found thinner colonic mucosa, fewer cells per crypt, more mucin staining, and less enteroendocrine cells in the large intestines of *Csf1r* mutant mice, and the mRNAs expression of cell cycle genes and stem cell marker gene were significantly reduced in *Csf1r*-loss colonic crypts. The inflammatory response examination showed that *Csf1r*^{+/-} male mice were protected from adverse effects associated with DSS-induced colitis compared with wild-type mice (Huynh et al., 2013). CSF1R expression was detected in tumor tissues and up-regulation of CSF1R is associated with an unfavourable prognosis for cancer patients, including breast, colorectal, renal and lung carcinoma (Baghdadi et al., 2018; Guan et al., 2021; Maher et al., 1998; L. Yang et al., 2016). Interestingly, treatment of osteosarcoma cell lines with the CSF1R inhibitor PLX3397 results in the inhibition of oncogenic ERK signaling and the repression of tumor growth and metastasis (Smeester et al., 2020). The hosting lab could show that CSF1R mediates EMT, migration, invasion and resistance to 5-fluorouracil (5-FU) in CRC cells (Shi et al., 2020). Taking together, these results indicate a significant role of CSF1R signaling in promoting tumorigenesis and the potential value of CSF1R as therapeutic target for cancer patients. Accordingly, there are currently a number of agents in clinical development that target CSF1R signaling (Cannarile et al., 2017; Peyraud, Cousin, & Italiano, 2017; Xiang, Li, & Tang, 2022).

2. Aims of the thesis

This thesis had the following aims:

- Characterization of the effects of intestinal epithelial cell (IEC)-specific deletion of *Mir34a* and/or its target *Csf1r* in intestinal tumorigenesis using *Apc*^{Min/+} mice.
- Comprehensive analysis of the *Mir34a/Csf1r* double-negative feedback loop in intestinal adenoma development at the organismal and molecular level.

3. Materials and Methods

3.1 Materials

3.1.1 Chemicals and reagents

Chemical compound	Supplier
2.5% Normal Horse Serum	Vector
3-[(3-cholamidopropyl)dimethyl-ammonio]-1-propane sulfonate (CHAPS)	Sigma-Aldrich
4',6-diamidino-2-phenylindole (DAPI)	Carl Roth
5-Flourouracil	Sigma-Aldrich
Advanced DMEM/F12	Thermo Fisher Scientific
Alcian blue	BioOptica
Ammonium peroxodisulfate (APS)	Carl Roth
Ampicillin	Sigma-Aldrich
Antibody diluent, background-reducing	Dako
Aqueous Mounting Media	Abcam
B-27™ Supplement (50X)	Thermo Fisher Scientific
BD Matrigel™ Basement Membrane Matrix	BD Bioscience
Blocking solution	Roche Diagnostics
Bovine Serum Albumin	Thermo Fisher Scientific
Cell Recovery Solution	Corning
Complete Mini Protease Inhibitor Cocktail	Roche
Deoxynucleotides (dNTPs)	Thermo Fisher Scientific
Diethyl pyrocarbonate (DEPC)	Sigma-Aldrich
Distilled Water	Thermo Fisher Scientific
Dulbecco's Modified Eagle medium (DMEM)	Thermo Fisher Scientific
Dimethyl Sulfoxide (DMSO)	Carl Roth
Doxycycline (DOX)	Sigma-Aldrich
Eosin	Sigma-Aldrich
Ethidium bromide	Carl Roth
Fast SYBR® green master mix	Applied Biosystems
Formamide	Sigma-Aldrich
Formalin, 4% neutral-buffered	CLN GmbH
FuGENE6	Roche
Gene ruler 100bp plus DNA ladder	Thermo Fisher Scientific
Gene ruler 1kb DNA ladder	Thermo Fisher Scientific
Gene ruler low range DNA ladder	Thermo Fisher Scientific
Gibco™ Fetal Bovine Serum (FBS)	Thermo Fisher Scientific
GlutaMAX™ Supplement	Thermo Fisher Scientific
Growth Factor Reduced Basement Membrane Matrix, Phenol Red-free Matrigel	Corning
Hank's Balanced Salt Solution (HBSS)	Thermo Fisher Scientific

Chemical compound	Supplier
Hematoxylin	Vector
Heparin sodium	Sigma-Aldrich
HEPES	Thermo Fisher Scientific
Hi-Di™ Formamide	Applied Biosystems
HiPerFect transfectin reagent	QIAGEN
Human EGF Receptor	Thermo Fisher Scientific
Hydrogen peroxide 30%	Carl Roth
Immobilon® Western Chemiluminescent HRP Substrate	Merck Millipore
Immobilon-P Transfer membrane	Merck Millipore
Kaiser glycerine gelatin	Merck Millipore
LB-Agar (Lennox)	Carl Roth
LB-Medium (Luria/Miller)	Carl Roth
Lipofectamin 2000	Invitrogen
McCoy's 5A (Modified) Medium	Thermo Fisher Scientific
Methanol	Carl Roth
N-2 Supplement (100X)	Thermo Fisher Scientific
NBT/BCIP solution, ready to use	Sigma-Aldrich
Normocin™ (50mg/ml)	InvivoGen
Opti-MEM® Reduced Serum Medium	Gibco/Life Technologies
PageRuler™ prestained protein ladder	Thermo Fisher Scientific
Paraformaldehyde solution 4% in PBS	Santa Cruz
Paraformaldehyd	Merck Millipore
Penicillin-streptomycin	Thermo Fisher Scientific
Periodic acid	Merck Millipore
PhosSTOP Phosphatase Inhibitor Cocktail	Roche
ProLong gold antifade reagent	Thermo Fisher Scientific
Puromycin dihydrochloride	Sigma-Aldrich
RNA from Yeast	Sigma-Aldrich
Roti®-Histokitt II	Carl Roth
Rotiphorese gel 30 (37,5:1)	Carl Roth
RPMI 1640 Medium with L-glutamine	Thermo Fisher Scientific
Schiff's reagent	Sigma-Aldrich
Skim milk powder	Sigma-Aldrich
Sodium dodecyl sulfate (SDS)	Carl Roth
Target retrieval solution, citrate pH 6	Dako
Tetramethylethylenediamine (TEMED)	Carl Roth
Triton X 100	Carl Roth
Trizol	Invitrogen
TWEEN® 20	Sigma-Aldrich
Universal agarose PeqGold	PeqLab
Water (molecular biological grade)	Life Technologies
Western lightning plus ECL	Perkin Elmer
Xylol	Carl Roth

Chemical compound	Supplier
Y-27632	MedBiochem Express
β -mercaptoethanol	Sigma-Aldrich

3.1.2 Enzymes

Application	Enzyme	Supplier
PCR	FIREPol® DNA Polymerase	Solis BioDyne
	Hot FIREPol® DNA Polymerase	Solis BioDyne
qPCR	DNase I, recombinant, RNase-free	Roche
ISH	Proteinase K	Sigma-Aldrich
Cell culture	Trypsin-EDTA (0.5%, 10x, phenol-red free)	Gibco/Life Technologies
	Accutase® solution	Sigma-Aldrich
	Trypsin-EDTA (0.05%, 1x)	Gibco/Life Technologies
Tumoroids	Collagenase Type IV	Merck Millipore
	Dispase Type II	Sigma-Aldrich
	TrypLE™ Select Enzyme (10X, no phenol red)	Thermo Fisher Scientific
Generation of vectors	Restriction endonucleases	New England Biolabs
	T4 DNA ligase	Thermo Fisher Scientific

3.1.3 Kits

Application	Kit	Supplier
IHC	Streptavidin/Biotin Blocking Kit	Vector
	DAB Peroxidase Substrate Kit	Vector
	VECTASTAIN Elite ABC-HRP Kit	Vector
	ImmPRESS™ HRP Anti-Rabbit IgG (Peroxidase) Polymer Detection Kit	Vector
	ImmPRESS™ HRP Anti-Rat IgG (Peroxidase) Polymer Detection Kit	Vector
	AEC Substrate Kit	Abcam
ISH	DIG Northern Starter Kit	Roche
	BCIP/NBT substrate system	Sigma-Aldrich
Cloning/ generation of vectors	QIAquick Gel Extraction Kit	QIAGEN
	QIAquick PCR Purification Kit	QIAGEN
	Monarch® DNA Gel Extraction Kit	New England Biolabs
	Monarch® PCR&DNA Cleanup Kit	New England Biolabs
	Pure Yield™ Plasmid Midiprep System	Promega
	QIAprep Spin Miniprep Kit	QIAGEN
	BigDye Terminator v1.1 cycle sequencing Kit	Applied Biosystems

Application	Kit	Supplier
	DyeEx 2.0 Spin Kit	QIAGEN
	QuikChange II XL Site-Directed Mutagenesis Kit	Stratagene
	Mut Express II Fast Mutagenesis Kit V2	Vazyme Biotech
WB	Micro BCA™ Protein Assay Kit	Thermo Fisher Scientific
IF	EdU Click 555 Kit	baseclick GmbH
Luciferase reporter assays	Dual-Luciferase® Reporter Assay System	Promega
qPCR	High Pure RNA Isolation Kit	Roche
	RNeasy Plus Mini Kit	QIAGEN
	Verso cDNA Synthesis Kit	Thermo Fisher Scientific

3.1.4 Antibodies

3.1.4.1 Primary antibodies

Name	Species	Catalog No.	Company	Use	Dilution	Source
CSF1R	Mouse	# SAB4500500	Sigma-Aldrich	IHC	1:100	Rabbit
MUC2	Mouse	E-AB-70212	Elabscience	IHC	1:2000	Rabbit
Lysozyme	Mouse	ab108508	Abcam	IHC	1:1000	Rabbit
Chromogranin A	Mouse	E-AB-40339	Elabscience	IHC	1:800	Rabbit
Ki-67	Mouse	#12202	Cell Signaling	IHC	1:400	Rabbit
Cleaved-Caspase-3	Mouse	#9664	CST	IHC, IF	1:500, 1:100	Rabbit
p-STAT3	Mouse	#9145	CST	IHC	1:200	Rabbit
Vimentin	Mouse	ab92547	Abcam	IHC	1:500	Rabbit
CD3	Mouse	A 0452	DAKO	IHC	1:100	Rabbit
CD45R	Mouse	550286	BD	IHC	1:100	Rat
CD68	Mouse	E-AB-70389	Elabscience	IHC	1:300	Rabbit

Name	Species	Catalog No.	Company	Use	Dilution	Source
Ly6G	Mouse	E-AB-70094	Elabscience	IHC	1:400	Rabbit
β -catenin	Mouse	ab32572	Abcam	IHC	1:500	Rabbit
NTN1	Human/ mouse	bs-1858R	Bioss Antibodies	WB	1:1000	Rabbit
TAGLN	Human/ mouse	PA5-29767	Invitrogen	WB	1:1000	Rabbit
β -actin	Human/ mouse	# A2066	Sigma- Aldrich	WB	1:1000	Rabbit

IHC: Immunohistochemistry, WB: Western blot, IF: Immunofluorescence

3.1.4.2 Secondary antibodies

Name	Species	Catalog No.	Company	Use	Dilution	Source
ImmPRESS REAGENT Anti-Rabbit IgG	Rabbit	MP-7401	Vector	IHC	Ready- to use	Horse
ImmPRESS REAGENT Anti-Rat IgG	Rat	MP-7444	Vector	IHC	Ready- to use	Goat
Anti-Rabbit HRP	Rabbit	# A0545	Sigma	WB	1:10000	Goat
Anti-Rabbit- Cy3	Rabbit	711-165-152	Jackson Immuno- Research	IF	1:100	donkey

IHC: Immunohistochemistry, WB: Western blot, IF: Immunofluorescence

3.1.5 Buffers and solutions

Genotyping of mice:

10x Gitschier`s Buffer (10x GB):

670 mM Tris (pH 8.8); 166 mM $(\text{NH}_4)_2\text{SO}_4$; 65 mM MgCl_2

Soriano Buffer:

10.08 ml ddH₂O; 1.2 ml 10x GB; 0.6 ml 10% Triton X-100; 0.12 ml β -mercaptoethanol

Proteinase K buffer:

0.1 M Tris (pH 8.5); 0.2 M NaCl; 5 mM EDTA (pH 8.0); 0.2% SDS

10x Vogelstein PCR buffer:

166 mM $(\text{NH}_4)_2\text{SO}_4$; 670 mM Tris/HCl (pH 8.8); 67 mM MgCl_2 ; 100 mM β -mercaptoethanol

Immunohistochemistry:

10x PBS:

80g NaCl; 2 g KCl; 17.8 g Na_2HPO_4 ; 2.4 g KH_2PO_4 ; add ddH₂O to 1 l

Tris-EDTA Buffer (pH 9.0):

1.21 g Tris Base; 0.37 g of EDTA in 1 l ddH₂O. Adjust the pH to 9.0 with 1N sodium hydroxide and then add 0.5 ml of Tween 20.

In situ Hybridization:

DEPC-H₂O:

1 ml Diethyl pyrocarbonate (DEPC) in 1 l H₂O (autoclave to inactivate DEPC)

20x SSC:

175.3g NaCl; 88.2g sodium citrate·2H₂O; add DEPC-H₂O to 1l (adjust pH to 4.5 or 7.5)

Heparin stock solution (50 mg/ml):

0.05 g Heparin in 1 ml DEPC-H₂O

Yeast RNA stock solution (10 mg/ml):

0.1 g Yeast RNA in 10 ml DEPC-H₂O (Heat to 65°C and vortex vigorously)

Hybridization solution:

15 ml DEPC-H₂O; 50 ml Formamide; 25 ml 20x SSC (pH 4.5); 2.5 ml 0.2M EDTA (pH 8.0); 2 g Blocking reagent powder; 0.05 g CHAPS powder; 100 ul Heparin stock solution (50 mg/ml); 10 ul yeast RNA stock solution (10mg/ml), add DEPC-H₂O to 100ml. Heat to 65°C to dissolve.

Acetic anhydride solution:

1 ml acetic anhydride in 400 ml 0.1M Triethanolamine (pH 8.0)

4% PFA:

8 g Paraformaldehyde (PFA) in 200 ml 1x PBS (heat to 65°C and add one NaOH pellet to dissolve)

Blocking Solution:

0.2 g blocking powder in 20 ml Tris/NaCl buffer (heat to 65°C to dissolve)

1x Tris/NaCl Buffer:

100 ml 10x Tris/NaCl; 900 ml DEPC-H₂O; 1 ml Tween20

NTM Buffer:

60 ml 1M Tris (pH9.5) + 12 ml 5M NaCl + 30 ml 1M MgCl₂ + 498 ml DEPC-H₂O

Tumoroid culture medium:

1% Glutamate; 1% HEPES; 1% Penicillin/Streptomycin; 1% N-2 Supplement; 2% B-27 Supplement; 50 ng/ml EGF; 0.1 mg/ml Normocin and 10 μM Y-27632 to advanced DMEM/F12. Y-27632 is only required for the first 2 days after isolation or passaging.

Western Blotting:

2x Laemmli buffer:

120 mM Tris/HCl (pH 6.8); 4% SDS; 20% glycerol; 0.02% bromophenol blue (in H₂O); 10% β-mercaptoethanol (added right before use)

RIPA lysis buffer:

50 mM Tris/HCl, pH 8.0; 250 mM NaCl; 1% NP40 (Nonidet P-40); 0.5% (w/v) sodium deoxycholate; 0.1% sodium dodecylsulfate. 1 tablet of protease inhibitor cocktail (Roche) and 1 tablet of phosphatase inhibitor cocktail (Roche) to 10 ml of RIPA buffer.

10x Tris-glycine-SDS running buffer:

192mM Glycine; 25mM Tris; 0.1% SDS, pH 8.3-8.7; add 1 l ddH₂O

Towbin buffer:

192 mM Glycine (pH 8.3); 20% Methanol; 25 mM Tris

10x TBST:

24.23g Tris/HCl; 80.06 g NaCl; 10 ml Tween20; add 1 l ddH₂O

Fluorescence *in situ* hybridization:

0.9 M NaCl; 20 mM Tris/HCl, pH 7.3; 0.01% SDS

3.1.6 Oligonucleotides

3.1.6.1 Genotyping primers

Name	Sequence (5'-3')
<i>Csf1r</i> For	CATGGCTGTGGCCTAGAGA
<i>Csf1r</i> Rev	GGACTAGCCACCATGTCTCC
<i>miR-34a</i> For	ACCTTGCAGGTGCTCAGAAT
<i>miR-34a</i> Rev-a	TGGAGCTAACGGAGTGTGTG
<i>miR-34a</i> Rev-b	CTACCCAAGCTCGACGAAGT
<i>miR-34a</i> Rev-c	TGCAGCACTTCTAGGGCAGT
<i>Vil-Cre</i> For	CGCGAACATCTTCAGGTTCT
<i>Vil-Cre</i> Rev	CAAGCCTGGCTCGACGGCC
<i>Apc^{Min}</i> wt	GCCATCCCTTCACGTTAG
<i>Apc^{Min}</i> com	TTCCACTTTGGCATAAGGC
<i>Apc^{Min}</i> mut	TTCTGAGAAAGACAGAAGTTA

3.1.6.2 qPCR primers

Name	Sequence (5'-3')
Mouse- <i>Cyclophilin</i> -for	ATGGTCAACCCCACCGTGT
Mouse- <i>Cyclophilin</i> -rev	TTCTGCTGTCTTTGGAACCTTTGTC
Mouse- β - <i>actin</i> -for	CTAAGGCCAACCGTGAAAAG
Mouse- β - <i>actin</i> -rev	ACCAGAGGCATACAGGGACA
Mouse- <i>B2M</i> -for	CCGGCCTGTATGCTATCC
Mouse- <i>B2M</i> -rev	CTTGCTGAAGGACATATCTGACA
Mouse- <i>Csf1r</i> -for	CCCCACAGATAAAATTGGAGCC
Mouse- <i>Csf1r</i> -rev	TTGAATCCCCTTCGGCGTT
Mouse- <i>pri-mir-34a</i> -for	CTGTGCCCTCTTGCAAAA
Mouse- <i>pri-mir-34a</i> -rev	GGACATTCAGGTGAGGGT
Mouse- <i>Dkk2</i> -for	CGGCATAGAGATCGCAACCATG
Mouse- <i>Dkk2</i> -rev	GCAGTCTGATGACCGTAGGCAT
Mouse- <i>Fzd10</i> -for	CTGGCTTGCTACCTAGTCATCG
Mouse- <i>Fzd10</i> -rev	TGCGTACCATGAGCTTCTCCAG

Name	Sequence (5'-3')
Mouse- <i>Wnt10a</i> -for	GCTCCTGTTCTTCCTACTGCTG
Mouse- <i>Wnt10a</i> -rev	ATGTCAGGCACACTGTGTTGGC
Mouse- <i>Clec16a</i> -for	GAACACCACAGACGAGGAGAAG
Mouse- <i>Clec16a</i> -rev	CATACAGGAGGCAGAGCACGAA
Mouse- <i>Slc14a1</i> -for	TGGCTGTGTAGGAACTGTGGTC
Mouse- <i>Slc14a1</i> -rev	GGTGGCATTGTAACCTTGGAGC
Mouse- <i>Ptprm</i> -for	AGAGGAAGGAGACGATGAGCAG
Mouse- <i>Ptprm</i> -rev	AGAAGGCTTCGTCGCAGTTGGT
Mouse- <i>Ntn1</i> -for	GTCTGGTGTGTGACTGTAGGCA
Mouse- <i>Ntn1</i> -rev	CCGAGCATGGAGGTTGCAGTTG
Mouse- <i>Tagln</i> -for	ATATGGAGCCTGTGTGGAGTG
Mouse- <i>Tagln</i> -rev	CACTGGCTTCGATCCCTCAG
Mouse- <i>Dab2</i> -for	CTCTTCAAAGGCAATGCTCCTGC
Mouse- <i>Dab2</i> -rev	TATGGCTCCTGGGACCCACAGTT
Mouse- <i>Grem1</i> -for	AGGTGCTTGAGTCCAGCCAAGA
Mouse- <i>Grem1</i> -rev	TCCTCGTGGATGGTCTGCTTCA
Mouse- <i>Atp2b4</i> -for	CACCATCTCACTAGCCTACTCTG
Mouse- <i>Atp2b4</i> -rev	AGTGTGCCTGTCTTATCGGAGC
Mouse- <i>Ank2</i> -for	ATCGGAGTCAGATCAAGAGCCG
Mouse- <i>Ank2</i> -rev	AAGCCAGCCTTTCTTCCATCCG
Mouse- <i>Igf2</i> -for	CTTCAGTTTGTCTGTTCCGGACCG
Mouse- <i>Igf2</i> -rev	GTGGCACAGTATGTCTCCAGGA
Mouse- <i>Notch2</i> -for	CCACCTGCAATGACTTCATCGG
Mouse- <i>Notch2</i> -rev	TCGATGCAGGTGCCTCCATTCT
Mouse- <i>Epha4</i> -for	GGCTATACTGACAAGCAGAGGAG
Mouse- <i>Epha4</i> -rev	GGAAAGCATCCAAGGAGCCGTT
Mouse- <i>Sesn3</i> -for	GCGCATGTATGACAGCTACTGG
Mouse- <i>Sesn3</i> -rev	TCAGATGCCGAGTTATGGCTCG

Name	Sequence (5'-3')
Mouse- <i>Lef1</i> -for	ACTGTCAGGCGACACTTCCATG
Mouse- <i>Lef1</i> -rev	GTGCTCCTGTTTGACCTGAGGT
Mouse- <i>Jag1</i> -for	TGCGTGGTCAATGGAGACTCCT
Mouse- <i>Jag1</i> -rev	TCGCACCGATAACCAGTTGTCTC
Mouse- <i>Prickle1</i> -for	AACAGCTCCTGTACCAGTTGCC
Mouse- <i>Prickle1</i> -rev	CTTCCTCTGAGCACTGAACACC
Mouse- <i>Fgf9</i> -for	ACAGTGGACTCTACCTCGGCAT
Mouse- <i>Fgf9</i> -rev	GGTTGGAAGAGTAGGTGTTGTAC
Mouse- <i>Npnt</i> -for	GGAGCTACATCTGCAAGTGTCAC
Mouse- <i>Npnt</i> -rev	GCTACACTGGTGCTGTCCAAGA
Mouse- <i>Adam10</i> -for	TGCACCTGTGCCAGCTCTGATG
Mouse- <i>Adam10</i> -rev	GATAGTCCGACCACTGAACTGC
Mouse- <i>Notch1</i> -for	GCAGATGCTCAGGGTGTCTT
Mouse- <i>Notch1</i> -rev	GCCAGGATCAGTGGAGTTGT
Mouse- <i>Snai1</i> -for	CACACGCTGCCTTGTGTCT
Mouse- <i>Snai1</i> -rev	GGTCAGCAAAGCACGGTT
Human- <i>TAGLN</i> -for	CTTCCCTCTGACACATGCGG
Human- <i>TAGLN</i> -rev	GTCAGTGGGACACAGTGAGGC
Human- <i>NTN1</i> -for	CTGTCCCTCGGCAAGAAGTT
Human- <i>NTN1</i> -rev	GTAGATGGCCATGGACTCGG
Human- β - <i>actin</i> -for	TGACATTAAGGAGAAGCTGTGCTAC
Human- β - <i>actin</i> -rev	GAGTTGAAGGTAGTTTCGTGGATG

3.1.6.3 Oligonucleotides used for fluorescence *in situ* hybridization (FISH)

Name	Sequence (5'-3')	Company
EUB338	[FITC]-5'-GCTGCCTCCCGTAGGAGT-3'	Metabion
NON338	[Cy3]-5'-CGACGGAGGGCATCCTCA-3'	Metabion

3.1.6.4 Oligonucleotides used for cloning and mutagenesis

Name	Sequence (5'-3')	Company
Murine <i>Csf1r</i> 3'-UTR For	ATTACCGGTACATATGGACTTCGCCCTCA	Metabion
Murine <i>Csf1r</i> 3'-UTR Rev	ATTCTGCAGGGTGTTTGTGGTGTGGTCA	Metabion
Murine <i>Csf1r</i> 3'-UTR mutant For	CCCAGAGCCTGGGCCATCAGTCGGA GTGGGGTTCTCACAGT	Metabion
Murine <i>Csf1r</i> 3'-UTR mutant Rev	ACTGTGAGAACCCCACTCCGACTGATGGCCCAGGCTCTGGG	Metabion
Murine <i>Ntn1</i> 3'-UTR For	ATTACCGGTTCTCCATCACCCGCTGTCTAGG	Metabion
Murine <i>Ntn1</i> 3'-UTR Rev	ATTCTGCAGAGAGTGAATCCCTGCCTCGCAG	Metabion
Murine <i>Ntn1</i> 3'-UTR mutant For-1	GTTGTTGGTCTCTGTGTTTACCTGCTGGCTGGTCTCC	Metabion
Murine <i>Ntn1</i> 3'-UTR mutant Rev-1	ACACAGAGACCAACAACAAGTATCC CAGTGTCATCGGG	Metabion
Murine <i>Ntn1</i> 3'-UTR mutant For-2	GTGGTTGTGTTTTCTGCTGGAGCTGCCTGTG	Metabion
Murine <i>Ntn1</i> 3'-UTR mutant Rev-2	GCAGAAAACACAACCACCCGGCTTGA CTTCA	Metabion
Murine <i>Ntn1</i> 3'-UTR mutant For-3	CCCACATCACTGTGTTTACTTACTGAG CACCCTCTTGGTG	Metabion
Murine <i>Ntn1</i> 3'-UTR mutant Rev-3	AAACACAGTGATGTGGGCAGAAGTGGAG	Metabion
Murine <i>Tagln</i> 3'-UTR For	ATTGAATTCGCCTGCCTCACAAATGCC TATG	Metabion
Murine <i>Tagln</i> 3'-UTR Rev	ATTCTGCAGTGGGCTGGGTCTCCTTCAAAGG	Metabion
Murine <i>Tagln</i> 3'-UTR mutant For-1	AGCCACTGTGTTTCTGGCCCCTGTCCAGCT	Metabion
Murine <i>Tagln</i> 3'-UTR mutant Rev-1	CCAGAAACACAGTGGCTCTGGGGTAA GATGCT	Metabion
Murine <i>Tagln</i> 3'-UTR mutant For-2	AGCCTGGCTGTAGGCCAGCCCACTGTCCTT	Metabion

Name	Sequence (5'-3')	Company
Murine <i>Tagln</i> 3'-UTR mutant Rev-2	TGGCCTACAGCCAGGCTACCCCAGC	Metabion
Human <i>NTN1</i> 3'-UTR For	ATTGAATTCGTCTCCACTGCTACCTGCTG	Metabion
Human <i>NTN1</i> 3'-UTR Rev	ATTGATATCTCCCACAGGGTTGTCATGAG	Metabion
Human <i>NTN1</i> 3'-UTR mutant For-1	GTGGTCACCGCCTCATGCTGGAGCTGCC	Metabion
Human <i>NTN1</i> 3'-UTR mutant Rev-1	CATGAGGCGGTGACCACCCGGCTTGGG	Metabion
Human <i>NTN1</i> 3'-UTR mutant For-2	TCTCTGTGTGTTTCGGGCCTCTGGCCCACAT	Metabion
Human <i>NTN1</i> 3'-UTR mutant Rev-2	CCCGAAACACACAGAGAGCCCAGGAAAGCA	Metabion
Human <i>TAGLN</i> 3'-UTR For	ATTGAATTCCTTAGCCTGCCTCACCCACAC	Metabion
Human <i>TAGLN</i> 3'-UTR Rev	ATTGATATCACGGCAGCCAGGAACACATAC	Metabion
Human <i>TAGLN</i> 3'-UTR mutant For-1	GCATTGTGTTTTTGGCCCCTCCCTCCCGG	Metabion
Human <i>TAGLN</i> 3'-UTR mutant Rev-1	GGCCAAAAACACAATGCTTTCGGGTAAGAAGTTGG	Metabion
Human <i>TAGLN</i> 3'-UTR mutant For-2	TTTGCCCTGGTCACTTTTGTTATGGTTCAGATCTG	Metabion
Human <i>TAGLN</i> 3'-UTR mutant Rev-2	AAAGTGACCAGGGCAAATCAAACCTCTGCCA	Metabion

3.1.7 miRNA mimics

miRNA mimics	Sequence (5'-3')	Supplier
Pre-miR™ miRNA Precursor PM11030 (hsa-miR-34a-5p)	GGCCAGCUGUGAGUGUUUCUUUGG CAGUGUCUUAGCUGGUUGUUGUGA GCAAUAGUAAGGAAGCAAUCAGCAA GUAUACUGCCCUAGAAGUGCUGCA CGUUGUGGGGCC	Thermo Fisher Scientific

3.1.8 Vectors

Name	Insert	Source/Reference
pRTR	empty	(Jackstadt et al., 2013)
pRTR- <i>pri-miR-34a</i>	human <i>pri-miR-34a</i>	(Kaller et al., 2011)
pGL3-control-MCS	firefly luciferase	(Welch et al., 2007)
pGL3- <i>Csf1r</i> wt	mouse <i>Csf1r</i> 3'UTR	this work
pGL3- <i>Csf1r</i> mut	mouse <i>Csf1r</i> 3'UTR	this work
pGL3- <i>Tagln</i> wt	mouse <i>Tagln</i> 3'UTR	this work
pGL3- <i>Tagln</i> mut	mouse <i>Tagln</i> 3'UTR	this work
pGL3- <i>Ntn1</i> wt	mouse <i>Ntn1</i> 3'UTR	this work
pGL3- <i>Ntn1</i> mut	mouse <i>Ntn1</i> 3'UTR	this work
pGL3- <i>TAGLN</i> wt	human <i>TAGLN</i> 3'UTR	this work
pGL3- <i>TAGLN</i> mut	human <i>TAGLN</i> 3'UTR	this work
pGL3- <i>NTN1</i> wt	human <i>NTN1</i> 3'UTR	this work
pGL3- <i>NTN1</i> mut	human <i>NTN1</i> 3'UTR	this work
pRL	Renilla	(Pillai et al., 2005)
pGL3_as	complementary sequence of miR-34a	(Welch et al., 2007)
Bluescript II p695-pBS-mOlfm4	mouse <i>Olfm4</i> ORF	Prof. Dr. Hans Clevers
pBluescript II KS-mLgr5	mouse <i>Lgr5</i> ORF	(Jaeckel et al., 2018)
pBluescript II KS	empty	(Jaeckel et al., 2018)
pCMV6-Entry-Lgr5	mouse <i>Lgr5</i> ORF	Origene, cat.no. MR219702

3.1.9 Mice

Strain	Background	Source/Reference
<i>miR-34a</i> ^{fl/fl} mice	C57BL6/SV129	(Rokavec, Oner, et al., 2014)

Strain	Background	Source/Reference
<i>Csf1^{fl/fl}</i> mice	C57BL6/SV129	The Jackson Laboratory
<i>Villin-Cre</i> mice	C57BL6	The Jackson Laboratory
<i>Apc^{Min/+}</i> mice	C57BL6	Dr. Marlon Schneider (Ludwig- Maximilians- University of Munich)

3.1.10 Cell lines

Cell lines	Medium
CT26	RPMI 1640 Medium with L-glutamine, 10% FBS and 1% Pen/strep
H1299	DMEM with 10% FBS and 1% Pen/strep
SW480	
SW480/pRTR- <i>pri-miR-34a</i>	

3.1.11 Software

Application	Software	Supplier/Developer
IHC	Phenochart 1.0.12	PerkinElmer
	Axiovision	Zeiss
	ImageJ	Wayne Rasband (retired from NIH)
IF	ZEN 2009	Zeiss
PCR	AlphaEase ® Fc	Alpha Innotech
qPCR	LightCycler 480	Roche
WB	Skant Software 2.4.3	Thermo Fisher Scientific
	Image Studio Version 5.2	LI-COR Biosciences

Application	Software	Supplier/Developer
Sequencing analysis	Sequencing Analysis 5.2	Thermo Fisher Scientific
	Benchling	Benchling
Luciferase reporter assays	SIMPLICITY software	DLR
Tumoroids	NIS-Elements Analysis	Nikon
Ectopic expression	BD Accuri™ C6 Cytometer	BD Biosciences
Figure composition	PowerPoint 2016	Microsoft
	Affinity Designer	Serif
Data analysis and figure generation	Graphpad Prism 9.0	Graph Pad Software Inc.

3.1.12 Laboratory equipment

Device	Supplier
Alpha Innotech FluorChem FC2 Imaging System	ProteinSimple
Applied Biosystems® 3130 Genetic Analyzer	Thermo Fisher Scientific
Applied Biosystems® GeneAmp PCR System 9700	Thermo Fisher Scientific
AxioPlan 2 Microscope System	Zeiss
Axiovert 25 Microscope	Zeiss
AZ100 Multizoom Microscope	Nikon
B. Braun Biotech International Incubation Shake Cabinet CERTOMAT® IS	Bio-Rad
Cell culture flasks, Multiwall plates and Conical Tubes	Corning
CO2 incubators	BINDER
Eppendorf Centrifuge 5810R	Eppendorf
Eppendorf 5417C Centrifuge	Eppendorf
Eluator™ Vacuum Elution Device	Promega
Forma™ Water-Jacketed CO2 Incubator	Thermo Fisher Scientific
Heraeus Biofuge Primo Centrifuge	Thermo Fisher Scientific
Heraeus Fresco 17 Centrifuge	Thermo Fisher Scientific
Heraeus Megafuge 1.0R Centrifuge	Thermo Fisher Scientific
Heraeus Pico Microcentrifuge	Thermo Fisher Scientific

Device	Supplier
Herasafe™ KS, Class II Biological Safety Cabinet	Thermo Fisher Scientific
Hot Plate 062	Labotect
HTU SONI-130 MiniFIER	G. Heinemann Ultraschall- und Labortechnik
Julabo SW-20C Shake Water Bath	JULABO
LightCycler® 480 Instrument II	Roche
LSM700 Confocal Microscope	Zeiss
Mastercycler® Pro Thermal Cyclers	Eppendorf
Mini Trans-Blot Electrophoretic Transfer Cell	Bio-Rad
Mini-PROTEAN®-electrophoresis system	Bio-Rad
NanoDrop One	Thermo Fisher Scientific
NanoDrop® ND-1000	Thermo Fisher Scientific
Neubauer counting chamber	Carl Roth
Mr. Frosty™ Freezing Container	Thermo Fisher Scientific
Odyssey® Fc Imaging System	LI-COR Biosciences
Orion II luminometer	Berthold Technologies
peqPOWER 300 Volt Power Supply	BIOgenetiX
PowerPac 200 Power Supply	Bio-Rad
PowerPac 300 Power Supply	Bio-Rad
Thermomixer Comfort	Eppendorf
Varioskan Flash Spectral Scanning Multimode Reader	Thermo Fisher Scientific
Vectra® Polaris™ Automated Quantitative Pathology Imaging System	PerkinElmer
Waterbath WNB 45	Memmert

3.2 Methods

3.2.1 Generation and breeding of mice

Conditional *Csf1r* gene knockout mice (*Csf1r^{fl/fl}*), in which exon 5 of the *Csf1r* gene is flanked by *loxP* sites (J. Li, Chen, Zhu, & Pollard, 2006), were purchased from the Jackson Laboratory (*Csf1r^{lox}*, Stock No: 021212). The generation of *Mir34a^{fl/fl}* mice was described previously (Rokavec, Oner, et al., 2014). To generate the mice lacking *Csf1r* or *Mir34a* or both in intestinal epithelial cells (IECs), *Csf1r^{fl/fl}*, *Mir34a^{fl/fl}* and *Csf1r^{fl/fl};Mir34a^{fl/fl}* mice were crossed with *Villin-Cre* mice with a C57BL/6 background (el Marjou et al., 2004; Jaeckel et al., 2018; J. Li et al., 2006; Rokavec, Li, et al., 2014).

Csf1r^{ΔIEC}, *Mir34a^{ΔIEC}*, *Csf1r^{fl/fl};Mir34a^{fl/fl}* and *Csf1r^{ΔIEC};Mir34a^{ΔIEC}* mice were crossed with *Apc^{Min/+}* mice with a C57BL6 background, and the mice with the following genotypes were obtained: *Csf1r^{ΔIEC}; Apc^{Min/+}*, *Mir34a^{ΔIEC}; Apc^{Min/+}*, *Csf1r^{fl/fl};Mir34a^{fl/fl}; Apc^{Min/+}* and *Csf1r^{ΔIEC};Mir34a^{ΔIEC}; Apc^{Min/+}*.

Mice were housed in individually ventilated cages (IVC) with a 12:12 light–dark cycle and *ad libitum* access to water and standard rodent diet. And the offspring showed no overt phenotype, and the genotypes were obtained in normal Mendelian ratios. Animal experimentation was approved by the Government of Upper Bavaria, Germany (AZ55.2-1-54-2532-4-2014 and AZ55.2-2532.Vet_02-20-177).

3.2.2 Genotyping

2-3 mm tails of three-week-old mice were lysed overnight at 56°C in 95 μl Soriano Buffer supplemented with 5 μl Proteinase K. And then stop enzymatic digestion by heat inactivation at 95°C for 10 minutes. Supernatants containing

genomic DNA were collected for PCR genotyping after centrifugation of the sample at 13000 rpm for 5 minutes.

All genotyping primers are listed in Table 3.1.6.1.

The PCR conditions for each gene are listed below:

Apc^{Min/+} genotyping:

Master mix	
Component	Volume
10x Vogelstein buffer	2.5 ul
Tween20	0.5 ul
10 mM dNTPs	1 ul
Primer mixture	1 ul
Hot FIREPol® DNA Polymerase	0.5 ul
Nuclease-free Water	17.5 ul
Genomic DNA	2 ul
Total Volume	25 ul

Reaction parameters		
Step	Temperature	Time
Initial	95°C	15 minutes
37 cycles	95°C	30 seconds
	59°C	30 seconds
	72°C	40 seconds
Final	72°C	3 minutes
Hold	4°C	

Primer mixture: 10 ul mut Primer + 10 ul com Primer + 5 ul wt Primer + 75 ul
nuclease-free H₂O = 100 ul

miR-34a genotyping:

Master mix	
Component	Volume
10x Vogelstein buffer	2.5 ul
Tween20	0.5 ul
10 mM dNTPs	1 ul
Primer mixture	5 ul
Hot FIREPol® DNA Polymerase	0.5 ul
Nuclease-free Water	13.5 ul
Genomic DNA	2 ul
Total Volume	25 ul

Reaction parameters		
Step	Temperature	Time
Initial	95°C	15 minutes
37 cycles	95°C	30 seconds
	65°C	30 seconds
	72°C	30 seconds
Final	72°C	3 minutes
Hold	4°C	

Primer mixture: 20 ul For Primer + 10 ul Rev-a Primer + 15 ul Rev-b Primer + 5 ul Rev-c Primer + 50 ul nuclease-free H₂O = 100 ul

Csf1r genotyping:

Master mix	
Component	Volume
10x Vogelstein buffer	2.5 ul
Tween20	0.5 ul
10 mM dNTPs	1 ul
Primer mixture	1 ul
Hot FIREPol® DNA Polymerase	0.5 ul
Nuclease-free Water	17.5 ul
Genomic DNA	2 ul
Total Volume	25 ul

Reaction parameters		
Step	Temperature	Time
Initial	95°C	15 minutes
35 cycles	95°C	30 seconds
	63°C	30 seconds
	72°C	30 seconds
Final	72°C	3 minutes
Hold	4°C	

Primer mixture: 10 ul For Primer + 10 ul Rev Primer + 80 ul nuclease-free H₂O = 100 ul

Vil-Cre genotyping:

Master mix		Reaction parameters		
Component	Volume	Step	Temperature	Time
10x Vogelstein buffer	2 ul	Initial	95°C	5 minutes
10 mM dNTPs	2 ul	38 cycles	95°C	45 seconds
Primer mixture	4 ul		55°C	45 seconds
FIREPol® DNA Polymerase	0.5 ul		72°C	45 seconds
Nuclease-free Water	9.5 ul	Final	72°C	5 minutes
Genomic DNA	2 ul	Hold	4°C	
Total Volume	20 ul			

Primer mixture: 10 ul For Primer + 10 ul Rev Primer + 80 ul nuclease-free H₂O = 100 ul

3.2.3 Specimen preparation and adenoma counting

The mice were dissected after being euthanized by cervical dislocation. After careful removal of the mesentery and surrounding fat tissues, the entire mouse intestine was isolated. After gently flushing out the intestinal contents with cold PBS, the intestinal tract was cut longitudinally, and the small intestine (SI) was divided into three parts (duodenum, jejunum, and ileum). After the tissue was fixed in 4% neutral-buffered formalin at 4°C overnight, each part of the intestinal tract was photographed, and rolled up as a “swiss roll” and placed into a labeled tissue cassette. Dehydration, clearing, and wax infiltration were done by an automated tissue processing machine. Finally, the paraffin-embedded tissue blocks were made for later sectioning. The number and size of intestinal tumors were evaluated by using a ZEISS dissecting microscope.

3.2.4 Histology and immunohistochemistry

The 3-5 μm paraffin sections were cut on the microtome manually and mounted on glass slides. After adequate drying at room temperature, sectioned tissue slides were ready for staining applications.

For histologic analysis, hematoxylin and eosin (H&E) and periodic acid-Schiff (PAS) staining were conducted by the automated slide stainers according to the standard operating procedures. The intestinal adenomas were identified as low- or high-grade based on abnormal architectural features (Jiang & Hermeking, 2017). And PAS staining was used to detect the goblet cells on the villus and Paneth cells in the crypts.

Immunohistochemistry (IHC) was performed according to the standard protocol. Paraffin tissue was firstly deparaffinized after a series of immersions in xylene and graded alcohols, and rehydrated with ddH₂O. And then antigen unmasking was carried out by immersing slides into pH 6.0 Target Retrieval Solution (Dako) or pH 9.0 Tris-EDTA Buffer and heated in a scientific microwave (750 Watt) for 30 minutes. After the slides were naturally cooled down to room temperature and washed with PBS three times, the endogenous peroxidase activity was blocked by incubating the sections in 3% hydrogen peroxide for 10 minutes at room temperature. To reduce non-specific background staining, the 2.5% Normal Horse Serum (Dako) or 3% Bovine Serum Albumin solution was applied for incubation for 30 minutes at room temperature. The section slides were incubated with 70–100 μl primary antibody diluted in background-reducing antibody diluent (Dako) at 4 °C overnight. After being rinsed with PBS adequately, the sections were then incubated with the ready-to-use secondary antibody (ImmPRESS REAGENT Anti-Rabbit IgG or ImmPRESS REAGENT Anti-Rat IgG)

for 1 hour at room temperature. The detection of DAB (3,3'-Diaminobenzidine) for brown stainings and aminoethyl carbazole (AEC) for red stainings was using the DAB Peroxidase Substrate Kit (Vector) or AEC Substrate Kit (Abcam), respectively.

Antibodies and reagents are listed in Table 3.1.4.1 and Table 3.1.4.2. Staining slides were scanned with Vectra® Polaris™ Automated Quantitative Pathology Imaging System, and quantified by ImageJ software (Jiang & Hermeking, 2017).

3.2.5 *In situ* hybridization analysis

For the detection of intestinal stem cells (ISCs), the *Olfm4* and *Lgr5* RNA probes were generated using the Bluescript II SK plasmid p695-pBS-mOlfm4 (kindly provided by Prof. Hans Clevers), and the pBSII KS-mLgr5 plasmid. The *Lgr5* open reading frame (ORF) was obtained from the pCMV6 entry plasmid (bought from OriGene Technologies, Inc., catalog number MR219702), and cloned into the Bluescript II (pBSII) KS plasmid by using the restriction enzymes *NotI* and *KpnI*. For the generation of the probes the Bluescript II plasmid p695-pBS-mOlfm4 and the pBSII KS-mLgr5 were linearized with the *NotI* and the *EcoRI* restriction enzyme, respectively. The *Olfm4* and *Lgr5* RNA probes were *in vitro* transcribed with RNA-T7 Polymerase and labeled with digoxigenin (DIG) by using the DIG Northern Starter Kit (Roche Diagnostics).

In situ hybridization (ISH) was performed as described (Gregorieff & Clevers, 2010; Jaeckel et al., 2018). 5-µm fresh sections were deparaffinized and rehydrated through xylene (three times, 5 minutes each) and graded ethanol series (100%, 100%, 96%, 70%, 50%, and 25% ethanol, 5 minutes each), and then rinsed twice in DEPC-treated H₂O. After digestion of proteins, post-fixation,

and anhydryzation, each tissue section was covered with hybridization solution and incubated at 65°C for 2 hours. And after removing the excess hybridization solution, the sections were covered with new hybridization buffer containing 500 ng/ml of DIG-RNA-probe, and hybridized at 65°C for 48 hours. And after post-hybridization wash, the BCIP/NBT Substrate System (Sigma-Aldrich) was added to the sections, and the immunological reaction was performed for 24–36 hours at room temperature in the dark. Finally, the sections were mounted in Kaiser glycerine gelatin (Merck) and visualized under the microscope.

To assess bacterial infiltration in intestinal adenoma, fluorescence *in situ* hybridization (FISH) was applied (Öner et al., 2018). The fresh paraffin sections were deparaffinized and then rehydrated to DEPC-treated ddH₂O. And the slides with the probe-hybridization buffer mixture (probe in a final concentration of 1 µg/ml) on the tissue were incubated at 50°C overnight. The negative probe (NON338) and universal eubacteria probe (EUB338) were used here. After washing slides with prewarmed hybridization buffer, and rinsing in DEPC-treated ddH₂O, slides were mounted with ProLong Gold antifade reagent (Thermo Fisher Scientific), and later visualized with LSM700 Confocal Microscope. The oligonucleotides used for FISH are listed in Table 3.1.6.3.

3.2.6 Assessment of immunodetections

The assessment of immunodetections was performed with ImageJ software. For quantification of p-STAT3 expression the H-score was used (Goulding et al., 1995; Ishibashi et al., 2003; Jiang & Hermeking, 2017). The H-score is calculated by the formula: $H\text{-score} = \sum (I \times P_i)$, with a range of 0 to 300. “I” means the intensity of staining, and a score of 0, 1, 2, and 3 indicates no, moderate, and strong staining, respectively. And “P_i” is the percentage of positive

tumor cells (from 0 to 100%). For quantification of bacterial infiltration in intestinal adenomas, EUB338 scoring (Öner et al., 2018) was used according to the staining intensity (0, no staining; 1, weak; 2, moderate; 3, strong).

3.2.7 Cell lines and tumoroid culture

The lung cancer cell line H1299 and colorectal cancer cell line SW480 were kept in Dulbecco's modified Eagle's medium (DMEM). CT26, the murine colorectal carcinoma cell line, was cultured in RPMI 1640 Medium with L-glutamine (Thermo Fisher Scientific). All cell lines were grown in medium containing antibiotics (100 units/ml penicillin + 100 ug/ml streptomycin) and 10% Gibco™ Fetal Bovine Serum (FBS) (Thermo Fisher Scientific).

Intestinal adenoma cells from three tumors for each *Apc*^{Min/+} mouse were isolated by lysis in DMEM containing 4000 units Collagenase Type IV (Merck Millipore) and 125 µg/ml Dispase Type II (Sigma-Aldrich). 1.5×10^4 single cells were counted using a hemocytometer and then embedded in 50 µl Matrigel per well and seeded in 24-well plates.

The tumoroid culture medium was changed every 2 days, and tumoroids were passaged at a 1:4 – 1:6 ratio about every 6 days (Jaeckel et al., 2018; Sato et al., 2011). Tumoroids were documented with a Nikon AZ-100 microscope.

3.2.8 Immunofluorescence (IF) staining of tumoroids

Tumoroids were harvested for IF staining as previously described (Broutier et al., 2016; H. Li, Rokavec, Jiang, Horst, & Hermeking, 2017). After removing the medium and washing with the cold HBSS, the Matrigel drops were gently pipetted up and down using the 1 ml tips and then carefully transferred the tumoroid suspension to a 15 ml centrifuge tube. In order to wash the basement

matrix off, gently invert the tube five to ten times and then carefully remove the HBSS after the tumoroids settled down under gravity on ice for 10 minutes. Repeat the wash step above three times. Tumoroids were fixed with 4% PFA for 30 minutes on ice. After washing with HBSS three times, tumoroids were permeabilized with 0.1% Triton X-100 for 30 minutes. After removal of Triton X-100 solution, tumoroids were incubated with blocking solution (5% BSA in 1xHBSS) for 1 hour at room temperature. Tumoroids were incubated with diluted primary antibody at 4 °C for 24–48 hours and incubated with secondary antibody at room temperature for 2 hours. After each step, tumoroids were washed with cold HBSS for three times and settled under gravity during these processes. The antibodies used for IF staining are listed in Table 3.1.4.1 and Table 3.1.4.2. For EdU staining an EdU Click 555 Kit (baseclick GmbH) was used according to the manufacturer's protocol. The images of tumoroids were acquired with an LSM 700 confocal microscope (Zeiss).

3.2.9 Cryopreservation of mammalian cells and tumoroids

Cells in the exponential growth phase were used for cryopreservation. After trypsinization and determination of viability, centrifuge the desired amount of cells in a Falcon tube at 1200 rpm for 5 minutes. Remove the supernatant and then gently resuspend the cell pellet in freezing medium (90% FBS + 10% DMSO). Aliquot 1 ml of cell suspension per labeled cryovial and cap. And then immediately place the cryovials into a Mr. Frosty™ freezing container (kept at room temperature) and transfer to -80°C freezer overnight. After about 24 hours, put the cryovials in liquid nitrogen for long-term storage.

After removing the medium and gently washing with ice-cold HBSS, add 1ml of Cell Recovery Solution per well in a 24-well plate, detach the Matrigel

droplet with 1000 μ l tip and carefully transfer to a 15 ml tube and fill to 10ml with cold HBSS. Centrifuge at 400 rpm for 3 min at 16°C, remove the supernatant, and resuspend the cell pellets in 5 ml DMEM/F12 with 1:100 Glutamate and 1:100 HEPES gently, and then use an 18-gauge followed by a 22-gauge syringe to get single cells. After checking the number and viability under the microscope, centrifuge the desired amount of cells in a centrifuge tube at 1200 rpm for 5 min at 16°C. Remove the supernatant and then gently resuspend the cell pellet in cryopreserved solution (50% advanced DMEM/F12 + 40% FBS + 10% DMSO). Aliquot 1 ml of cell suspension per labeled cryovial. Place the cryovials in a Mr. Frosty™ freezing container, and store overnight in a -80°C freezer, then transfer to liquid nitrogen for long-term cryopreservation.

3.2.10 Generation of cell pools stably expressing conditional alleles

Stably transfected cells were generated as previously described (Jaeckel et al., 2018; H. Li et al., 2017). SW480 were transfected with pRTR-*pri-miR-34a* plasmids (Jackstadt et al., 2013) using Lipofectamin 2000 (Invitrogen) or FuGENE6 (Roche). After 24 hours, cells were transferred into media containing 4 μ g/ml puromycin for 7 days. Homogeneity of the derived cell pools was tested by addition of 100 ng/ml DOX for 2 days, and GFP expression was evaluated by fluorescence microscopy.

3.2.11 Dual 3'-UTR luciferase reporter assays

The 3'-UTR of the murine *Csf1r*, *Tagln* and *Ntn1* mRNA was PCR amplified from cDNA obtained from murine bone marrow-derived macrophages or murine genomic DNA. The 3'-UTR of the human *TAGLN* and *NTN1* mRNA were PCR amplified from cDNA obtained from SW480. Sequencing was applied to confirm the insertion of the target gene's 3'-UTR into the pGL3-control-MCS

vector. The QuikChange II XL Site-Directed Mutagenesis Kit (Stratagene) or the Mut Express II Fast Mutagenesis Kit V2 (Vazyme Biotech Co.,Ltd.) was used to carry out the mutagenesis of the miR-34a seed-matching sequences, and the results were confirmed by sequencing. H1299 or CT-26 cells were cultured in 12-well plates at a density of 30000 cells/well for 24 hours before being transfected with either a *pre-miR-34a* oligonucleotide (Ambion, PM11030) or a negative control oligonucleotide (Ambion, neg. control #1) at a concentration of 25 nM using the HiPerFect Transfection Reagent (Qiagen). Luciferase reporter assays were conducted at 48 hours post-transfection using the Luciferase Reporter Assay Kit (Promega), and then fluorescence intensity was measured using an Orion II luminometer (Berthold) and analyzed with the SIMPLICITY software package (DLR). The oligonucleotides and the primers used for cloning and mutagenesis are listed in Table 3.1.6.4.

3.2.12 Acquisition of plasmids

The competent cells E.coli XL1-blue strain was used for transformation, cloning, and production of plasmids here.

The 100 ul of XL1-blue cells stored at -80°C were thawed on ice. 100 ng of the plasmid DNA or 10µl of the recombinant product were added to competent cells, and then incubated in ice for 30 minutes. After heat shock at 42°C for 45 seconds, cells were incubated in ice for 2 minutes. And then 900 ul of LB liquid medium without antibiotics was added and incubated at 37°C for 1 hour (200 – 250 rpm). In order to increase colony number, centrifuge the tube at 5000 rpm for 5 min and discard the supernatant. Finally resuspend the bacteria with the remaining medium and spread gently with a sterile spreader on a pre-warmed (at

37°C) LB solid medium plate containing Ampicillin resistance, and incubate the plate overnight at 37°C.

After overnight culture, a number of single clones were picked and inoculated with 5 ml or 150 ml LB liquid medium containing Ampicillin (100 ug/ml) overnight at 37°C (shaking at 225 rpm).

For the small amount (5 ml) or large amount (150 ml) of plasmid DNA isolation, the QIAprep Spin Miniprep Kit (QIAGEN) or Pure Yield™ Plasmid Midiprep System (Promega) was used by following the instruction of the manufacturer, respectively.

3.2.13 DNA sequencing

For DNA sequence verification, Sanger sequencing was performed. The detailed components and cycling conditions are as followed:

Reaction mixtures		Thermocycling conditions		
Component	Volume	Step	Temperature	Time
Big Dye Terminator V1.1	1 ul	15 cycles	96°C	10 seconds
5 x Sequence Buffer	2 ul		60°C	90 seconds
Primer	0.5 ul	Hold	4°C	
Plasmid (1ug/ul)	1 ul			
ddH ₂ O	5.5 ul			
Total Volume	10 ul			

DyeEx 2.0 Spin Kit (QIAGEN) was used for purification of PCR-product according to the instruction of the manufacturer. And then purified DNA was mixed with Hi-Di Formamide (Applied Biosystems), and loaded into Applied Biosystems® 3130 Genetic Analyzer for sequencing. Data was collected with the

Sequencing Analysis 5.2 software and evaluated with Benchling cloud-based platform.

3.2.14 Quantitative real-time PCR (qPCR) analysis

Total RNA was isolated using the RNeasy Plus Mini Kit (Qiagen) or High Pure RNA Isolation Kit (Roche) according to the respective manufacturer's instruction manual. And complementary DNA (cDNA) was synthesized from an RNA template using the Verso cDNA Kit (Thermo Scientific), the reaction mixtures and procedures for reverse transcriptase PCR are listed as follows:

Reaction mixtures		PCR program		
Component	Volume	Step	Temperature	Time
5 x cDNA synthesis buffer	4 ul	1 cycle	42°C	60 minutes
dNTP Mix	2 ul	Final	95°C	2 minutes
RNA Primer (anchored oligo dT)	1 ul	Hold	4°C	
RT Enhancer	1 ul			
Verso Enzyme Mix	1 ul			
Template (RNA) (200 ng/ul)	3 ul			
Nuclease-free Water	8 ul			
Total Volume	20 ul			

qPCR was performed with Fast SYBR Green Master Mix (Applied Biosystems) on the LightCycler 480 II platform (Roche Diagnostics). Expression was normalized to *Cyclophilin*, *B2M* or β -*actin* expression and calculated using the $2^{-\Delta\Delta C_t}$ method (Livak & Schmittgen, 2001). Primers used for qPCR are listed in Table 3.1.6.2.

3.2.15 Western blot analysis

After harvesting cells in six-well plates, cell-lysates were collected in RIPA lysis buffer, then sonicated, followed by centrifugation at 12000 rpm for 20 min at 4°C, and the supernatant was saved for use. After determining the protein concentration using the Micro BCA™ Protein Assay Kit according to the manufacturer's instructions, the protein sample mixed with Laemmli sample buffer was denatured at 95°C for 8–10 min, then store at -80°C until use.

40-80 µg protein were separated on 12% sodium dodecyl sulfate-acrylamide gels, and gel electrophoresis was performed by using Mini-PROTEAN Tetra Cell (Bio-Rad) at a voltage of 60–120 with running buffer. And the transfer of proteins was performed using Mini Trans-Blot Electrophoretic Transfer Cell (Bio-Rad) at constant 380 mA with cold transfer buffer in a cold room (2-8°C), the proteins were transferred to Immobilon-P transfer membranes with 0.2 µm pore size (R1JB33689; Merck Millipore). To reduce signal background, the membranes were incubated with 5% skim milk in TBST at room temperature for 1 hour. And the membranes in the primary antibody solution were incubated overnight at 4°C with gentle rocking. Signals from horseradish-peroxidase-coupled secondary antibodies were generated by Immobilon® Western Chemiluminescent Horseradish Peroxidase (HRP) Substrate (WBKLS0100; Merck Millipore) and recorded with a CCD/Charged Coupled Device camera (Odyssey Fc; LI-COR, Lincoln, NE). Densitometric analysis of blots was conducted using Image Studio Version 5.2 software. Antibodies used here are listed in Table 3.1.4.1 and Table 3.1.4.2.

3.2.16 Transcriptomic analysis

The RNeasy Plus Mini Kit (Qiagen) was used to isolate total RNA from adenomas or tumoroids, followed by on-column DNase digestion (3 RNA samples per genotype; each tumor RNA sample represented a pool of 3 tumors isolated from the same mouse). We constructed and sequenced the random primed cDNA libraries using the HiSeq4000 (Illumina) platform by GATC (Konstanz, Germany). Each sample was covered by at least 30 million single reads of 50 bp length. We processed the NA-Seq FASTQ files using RNA-Seq module implemented in the CLC Genomics Workbench v20.0.2 software (Qiagen Bioinformatics) and mapped to the GRCm38/mm10 mouse reference genome and its associated gene and transcript annotation (ENSEMBL) with the settings mismatch cost = 2, insertion cost = 2, deletion cost = 3, length fraction = 0.8, similarity fraction = 0.8. RNA-Seq data were filtered to exclude weakly expressed transcripts with less than two mapped exon reads in all samples from the analysis and subjected to upper quartile normalization using the R/Bioconductor RUVSeq (remove unwanted variation from RNA-Seq data) package as described in Risso et al (Risso, Ngai, Speed, & Dudoit, 2014). After normalization with the RUVg method for removal of variation between RNA samples resulting from differences in library preparation, differential gene expression analysis was conducted with DESeq2 (Love, Huber, & Anders, 2014). We performed Principal Component Analysis (PCA) and Gene Set Enrichment Analysis (GSEA) using the PCA functionality of the EDASeq R package as implemented in RUVSeq, and the fgsea R package (Korotkevich, Sukhov, & Sergushichev, 2019), respectively. Prior to GSEA, the ash (adaptive shrinkage) estimator (Stephens, 2016) was used to adjust the expression changes from low count genes. We generated heatmaps with Morpheus (Broad Institute), and collected gene sets from the

Molecular Signatures database (MSigDB) (Liberzon et al., 2015) or as indicated (Merlos-Suarez et al., 2011; Munoz et al., 2012; Sveen et al., 2018; Tan et al., 2014; Taube et al., 2010). TargetScanMouse 7.1 (Agarwal, Bell, Nam, & Bartel, 2015) and 11 additional miRNA target prediction algorithms from the miRWalk2.0 (Dweep & Gretz, 2015) were used to predict miR-34a targets. Expression profiling data obtained in this study was deposited in the Gene Expression Omnibus website (accession no. GSE167449 and GSE167450).

3.2.17 Analysis of expression and clinical data from public databases

The STAT3 and c-JUN expression signatures were generated after RNA-Seq datasets from the NCBI Gene Expression Omnibus (GEO) were compiled, as described previously (Winter, Rokavec, & Hermeking, 2021). RNA-Seq data from cell lines and tissues with STAT3, c-JUN, or SRF ectopic expression or knockdown (KD)/knockout (KO) was analyzed for the identification of differentially regulated genes. In Supplemental Data 1–4, a list of RNA-Seq studies analyzed is shown along with the respective GEO accession numbers. By analyzing transcription factor ChIP-Seq data utilizing the Cistrome database (Zheng et al., 2019), direct regulation was evaluated. Only ChIP-Seq datasets that passed peak quality controls were included in the analysis. In Supplemental Data 1–4, ChIP-Seq studies analyzed are listed with the corresponding GEO accession numbers.

We obtained expression and clinical information for studying human colon cancer samples from TCGA-COAD and GSE39582 (Cancer Genome Atlas, 2012; Marisa et al., 2013), and retrieved associations between patient samples and CMS categories from the Colorectal Cancer Subtyping Consortium (CRCSC) at www.synapse.org. The classifications of tumor samples by CRC intrinsic subtypes (CRIS) were obtained from (Isella et al., 2017). We collected expression

data of human CRC cell lines from the Cancer Cell Line Encyclopedia (CCLE) (Barretina et al., 2012). By using the log-rank test, the statistics for Forest plots and survival curves were computed. The optimal cutoff values for binary classification (high/low expression) were determined with the Survminer R-package (<https://CRAN.R-project.org/package=survminer>). Using one-way ANOVA and a post-test for a linear trend from stage 1 to stage 4, the differential expression between tumors of different stages was assessed. As previously described (Shi et al., 2020), GSEA of curated gene sets acquired from the Molecular Signatures database (MSigDB) (Liberzon et al., 2015) or as indicated (Esnault et al., 2014; Winter et al., 2021), was carried out on pre-ranked gene lists organized by expression correlation coefficients (Pearson) with the $\Delta 34a$ expression signature, mature miR-34a, or *CSF1R* expression. The normalized enrichment scores (NES) and false discovery rate-adjusted q values were used to evaluate the significance of enrichments.

3.3 Statistical analyses

Statistical analyses were performed using GraphPad Prism 8.3.0 software. The one-way ANOVA and two-tailed unpaired Student's t-test were used to assess the statistical significance of differences in group mean values. In order to visualize the survival time, Kaplan-Meier curves were employed, and the outcomes were compared using a log-rank test. A *P*-value less than 0.05 was considered statistically significant and marked with the asterisk (**P* < 0.05, ***P* < 0.01, ****P* < 0.001, or *****P* < 0.0001).

The results that follow are in part derived from the manuscript: Liu et al., Csf1r mediates enhancement of intestinal tumorigenesis caused by inactivation of Mir34a. *Int J Biol Sci.* 2022;18(14):5415-5437. The publisher has stated that this material can be used in the author's doctoral thesis without obtaining permission from the publisher.

4. Results

4.1 Combined deletion of *Mir34a* and *Csf1r* in murine intestinal epithelium

Similar to the human *CSF1R* the 3'-UTR of the murine *Csf1r* contains a conserved *Mir34a* seed-matching sequence (SMS) (**Figure 9A**). In a reporter assay the murine *Csf1r* 3'-UTR was repressed by ectopic *Mir34a*, whereas a reporter with point mutations in the *Mir34a* SMS was refractory to repression by ectopic *Mir34a* in murine CT26 CRC cells (**Figure 9B**). In addition, expression of the endogenous *Csf1r* was repressed by ectopic *pre-miR-34a* in murine CT26 cells, similar to the known miR-34a targets *Snai1* and *Notch1*, whereas β -*actin* expression was not affected (**Figure 9C**). Therefore, *Csf1r* represents a direct, conserved target for repression by *Mir34a* in mice.

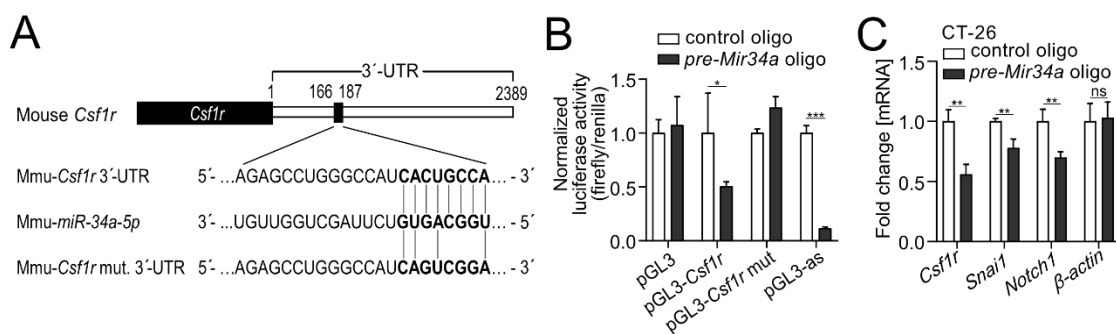


Figure 9. *Csf1r* represents a direct, conserved target for repression by *Mir34a* in mice.

A Scheme of the murine miR-34a seed, the seed-matching sequence and its targeted mutation in the 3'-UTR of the murine *Csf1r* mRNA.

B Dual-reporter assay after transfection of CT26 cells with *pre-Mir34a* oligonucleotides and the murine *Csf1r* 3'-UTR reporter constructs. Data represent mean \pm SD (n = 3).

C qPCR analysis of the indicated mRNAs in CT26 cells after transfection with control or *pre-Mir34a* oligonucleotides for 48 hours. Data represent mean \pm SD (n = 3).

Data information: In (**B,C**), results are presented as mean \pm SD using the two-tailed unpaired Student's t-test. * $P < 0.05$, ** $P < 0.01$, *** $P < 0.001$, or **** $P < 0.0001$.

B,C: Janine König performed the data analyses and generated the figures.

Next, we crossed mice harboring either *Mir34a* or *Csf1r* alleles flanked by two *loxP* sites with *Villin-Cre* mice (**Figure 10A**). As a result, the respective alleles

were inactivated in intestinal epithelial cells (IECs) from embryonic day 12.5 onwards. In IECs deficient for *Mir34a*, *Csf1r* expression, as well as expression of the known miR-34a targets *Snai1* and *Notch1*, was up-regulated, whereas β -actin expression was not affected (**Figure 10B**). In addition, *pri-Mir34a* expression was up-regulated in *Csf1r*-deficient IECs (**Figure 10B**). Therefore, the reciprocal repression between *miR-34a* and *CSF1R* previously detected in CRC cell lines was confirmed on the organismal level.

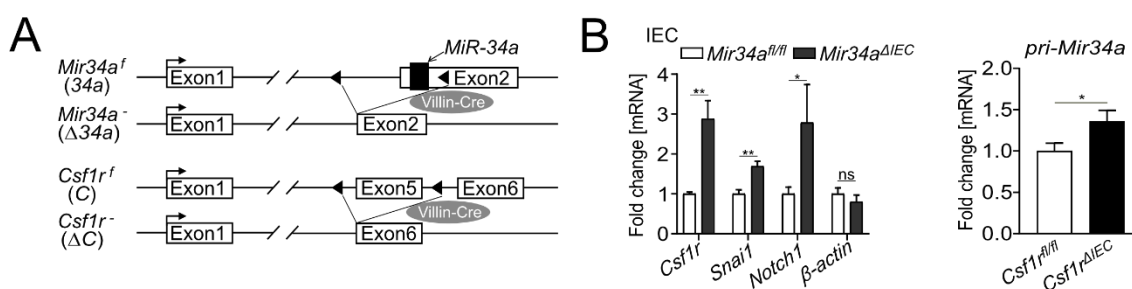


Figure 10. Analysis of the reciprocal repression between *miR-34a* and *CSF1R* on the organismal level.

A Scheme showing the generation of mice with intestinal epithelial cell-specific deletions.

B Analysis of the indicated mRNAs in intestinal epithelial cells (IECs) derived from the mice with the indicated genotypes. Data represent mean \pm SD (n \geq 3). Results are presented as mean \pm SD using the two-tailed unpaired Student's t-test. *P < 0.05, **P < 0.01, ***P < 0.001, or ****P < 0.0001. **B** (Right panel): Xiaolong Shi performed the data analysis of *pri-Mir34a* and generated the figure.

4.2 *Csf1r* mediates effects of *Mir34a* loss on intestinal architecture and secretory cell homeostasis

In order to determine, whether inactivation of *Mir34a* affects intestinal tumor formation in a *Csf1r*-dependent manner, we generated *Apc^{Min/+}* mice with inactivation of *Mir34a*, *Csf1r* or of both genes in IECs (F. Liu et al., 2022). In *Mir34a*-deficient *Apc^{Min/+}* mice, we observed a significant increase in total length of the small intestine, and in the width and depth of crypts, as well as in the villus height, but a decrease in villus width of the small intestine (**Figure 11**). Deletion of *Csf1r*, except for depth of crypts, had the opposite effect on these parameters in *Apc^{Min/+}* mice. However, combined deletion of *Mir34a* and *Csf1r* had no significant effect on intestinal architecture when compared with the control group

(**Figure 11**). The variations in the width of crypts presumably caused the differences in total length of the small intestine observed among the four genotypes. In addition, we evaluated goblet and Paneth cell numbers after immunohistochemical detection using specific markers (**Figure 12A and B**) as well as PAS staining (**Figure 13A and B**). A significant decrease in the number of goblet and an increase in Paneth cells was detected in *Mir34a*-deficient intestines. As reported previously (Huynh et al., 2009), inactivation of *Csf1r* resulted in a decreased number of Paneth cells, while the number and size of goblet cells increased. In addition, the number of entero-endocrine cells was increased in *Mir34a*-deficient *Apc*^{Min/+} mice, but decreased in *Csf1r*-deficient *Apc*^{Min/+} mice (**Figure 14**). When both genes were deleted the effects on goblet, Paneth and entero-endocrine cells were neutralized.

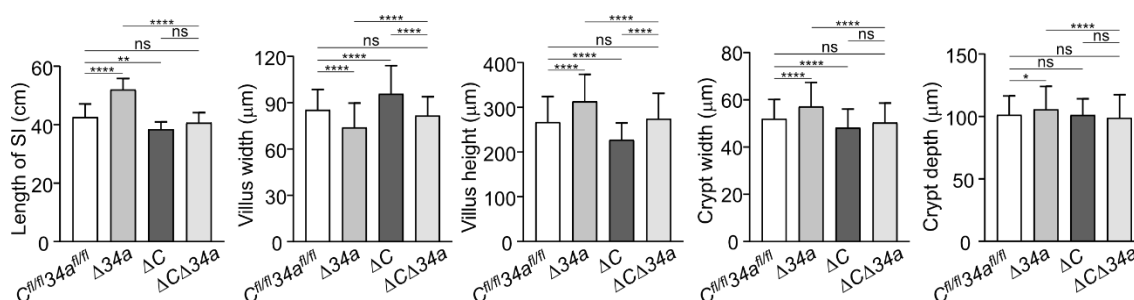
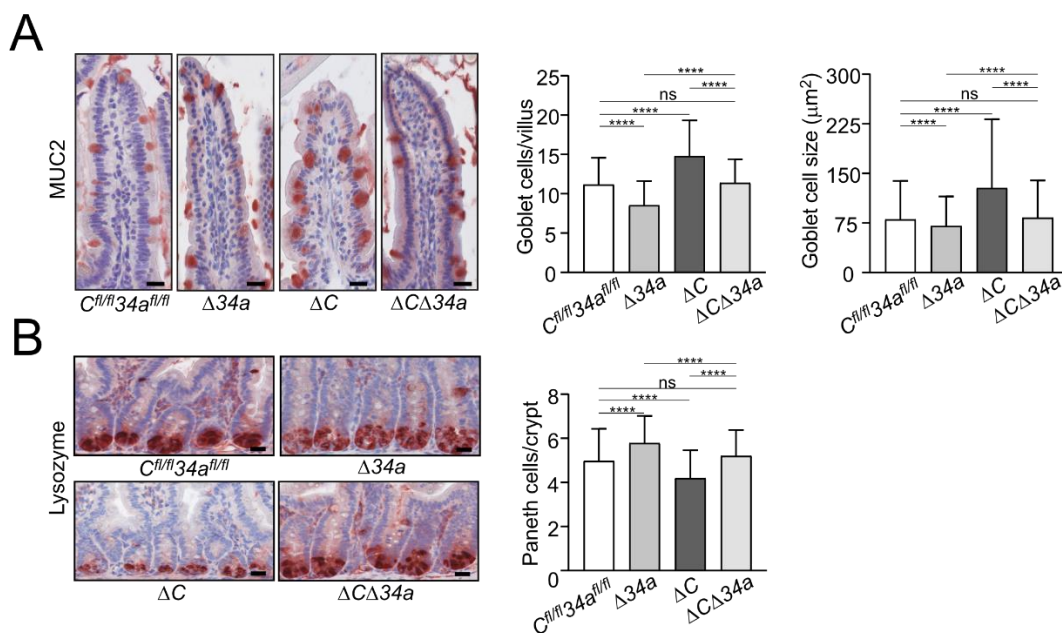


Figure 11. Determination of the length of the small intestine, and the width and height of villi and the width and depth of crypts in the small intestine from *Apc*^{Min/+} mice with the indicated genotypes (≥ 160 ileum villi or crypts per group and $n \geq 4$ mice per genotype). Results are presented as mean \pm SD using Tukey's multiple comparisons test. * $P < 0.05$, ** $P < 0.01$, *** $P < 0.001$, or **** $P < 0.0001$.



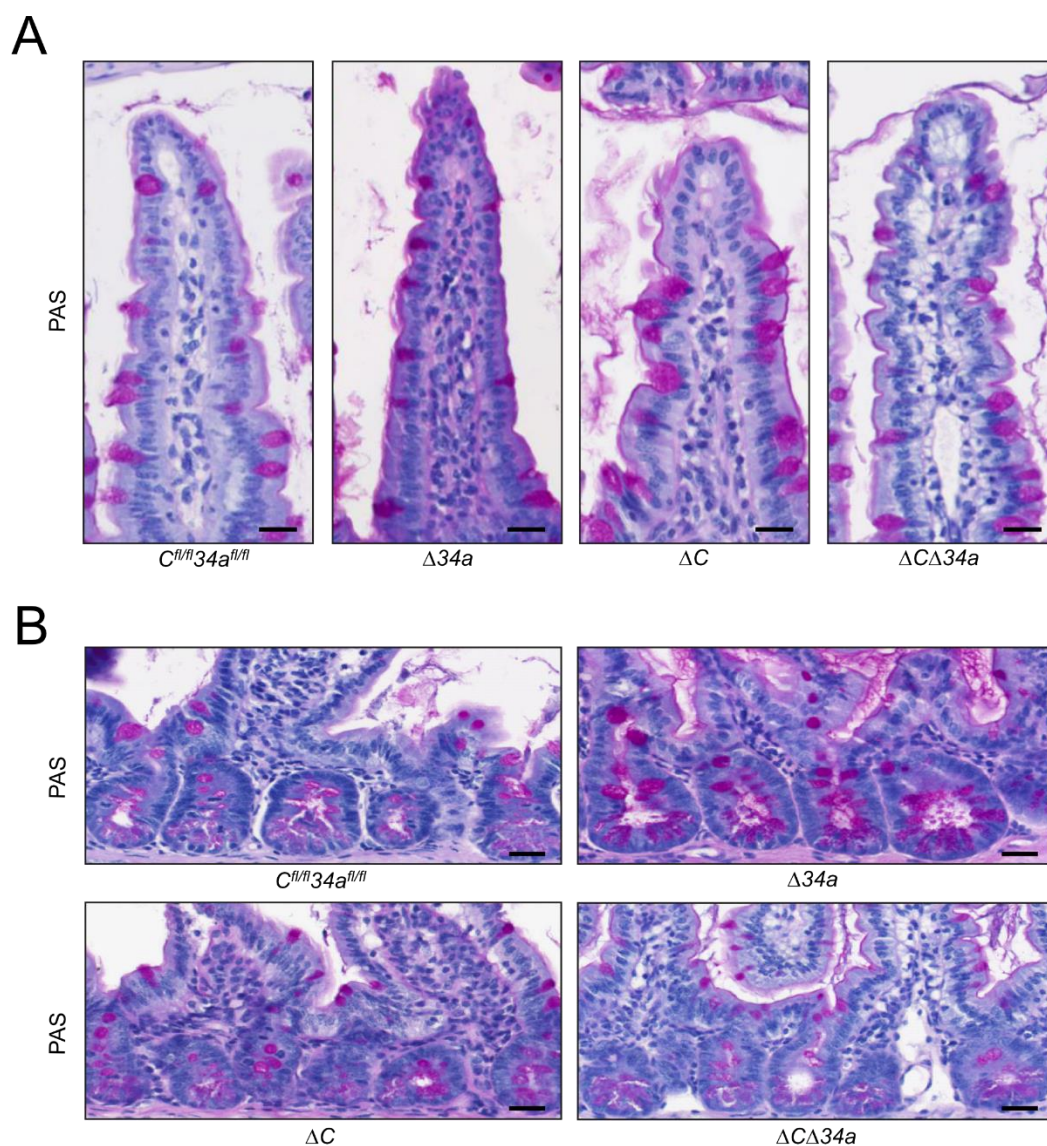


Figure 13. Detection of goblet cells on normal villus (**A**) and Paneth cells at normal crypt (**B**) from 18 weeks old $Apc^{Min/+}$ mice with the indicated genotype by Periodic acid-Schiff (PAS) staining. Scale bar: 20 μ m.

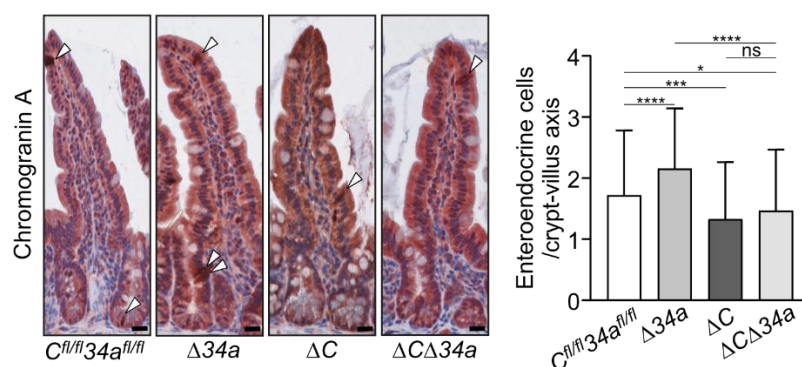


Figure 14. Quantification of entero-endocrine cells per crypt-villus axis from the $Apc^{Min/+}$ mice with the indicated genotypes after staining with Chromogranin A specific antibodies (≥ 150 crypt-villus axes per group and $n \geq 3$ mice per genotype). Scale bar: 20 μ m. Results are presented as mean \pm SD using Tukey's multiple comparisons test. * $P < 0.05$, ** $P < 0.01$, *** $P < 0.001$, or **** $P < 0.0001$.

4.3 *Mir34a* loss enhances intestinal tumorigenesis in a *Csf1r*-dependent manner

The expression of *Csf1r* was up-regulated in *Mir34a*-deficient adenomas and *pri-Mir34a* expression was increased in *Csf1r*-deficient adenomas on the mRNA and protein levels (**Figure 15A and B**). Notably, IEC-specific deletion of *Csf1r* in *Apc*^{Min/+} mice resulted in a significantly longer life-span, while loss of *Mir34a* resulted in a shorter overall survival (**Figure 15C**). In contrast, *Apc*^{Min/+} mice deficient for both *Csf1r* and *Mir34a* did not show a statistically significant change in survival when compared to *Csf1r*^{fl/fl};*Mir34a*^{fl/fl};*Apc*^{Min/+} mice (**Figure 15C**). When the entire small intestinal tract from 18 weeks old *Apc*^{Min/+} mice was examined, *Csf1r*-deficient *Apc*^{Min/+} mice showed a significantly reduced number of intestinal tumors, whereas *Mir34a*-deficient mice showed a dramatic increase in tumor numbers (**Figure 15D-F**). Notably, *Apc*^{Min/+} mice with deletion of both *Mir34a* and *Csf1r* displayed similar frequencies of intestinal tumors as *Csf1r*^{fl/fl};*Mir34a*^{fl/fl};*Apc*^{Min/+} mice. The size of adenomas was significantly larger in *Mir34a*-deficient and smaller in *Csf1r*-deficient *Apc*^{Min/+} mice when compared to *Csf1r*^{fl/fl};*Mir34a*^{fl/fl};*Apc*^{Min/+} mice (**Figure 15G**). Similarly, the frequency of large tumors (≥ 2 mm) was significantly higher in *Mir34a* ^{Δ IEC};*Apc*^{Min/+} mice, but lower in *Csf1r* ^{Δ IEC};*Apc*^{Min/+} mice. However, when *Mir34a* and *Csf1r* were inactivated concomitantly in IECs, the effects of the single inactivations on tumor size and its distribution were largely neutralized (**Figure 15G**). Furthermore, the deletion of *Mir34a* increased the number of tumors with high-grade dysplasia in *Apc*^{Min/+} mice, whereas deletion of *Csf1r* resulted in a lower percentage of tumors with high-grade dysplasia (**Figure 16A and B**). However, concomitant deletion of both genes resulted in the compensation of both effects. Taken together, the effects of the single deletions of *Mir34a* and *Csf1r* were neutralized by simultaneous

inactivation of both genes, implying that *Mir34a* and *Csf1r* functionally antagonize each other during intestinal tumor formation and progression. Therefore, *Csf1r* up-regulation caused by *Mir34a* deletion contributes to the increased number and size of intestinal adenomas observed in *miR-34a*-deficient mice, which ultimately determines the lifespan of these mice.

We hypothesized that the decreased tumor size observed after deletion of *Csf1r* in *Apc^{Min/+}* mice may be due to decreased tumor cell proliferation and increased apoptosis. Indeed, the proliferation-marker Ki67 was down-regulated and apoptosis was increased in adenomas of *Csf1r^{ΔIEC};Apc^{Min/+}* mice (**Figure 16C and D**). On the contrary, proliferation was increased and apoptosis was decreased in *Mir34a*-deficient adenomas (**Figure 16C and D**). When both deletions were combined, the rate of proliferation and apoptosis was similar as in adenomas of *Apc^{Min/+}* mice without deletion of these genes (**Figure 16C and D**). Consistent with the finding that activation of CSF1R induces STAT3 phosphorylation (p-STAT3) in CRC cell lines (Shi et al., 2020), the frequency of cells displaying STAT3 activation was decreased in adenomas of *Csf1r^{ΔIEC};Apc^{Min/+}* mice, whereas deletion of *Mir34a* increased the number of p-STAT3-positive tumor cells (**Figure 16E**). *Apc^{Min/+}* mice with combined deletion *Csf1r* and *Mir34a* did not show a significant change in the frequency of p-STAT3-positive cells when compared to control *Apc^{Min/+}* mice.

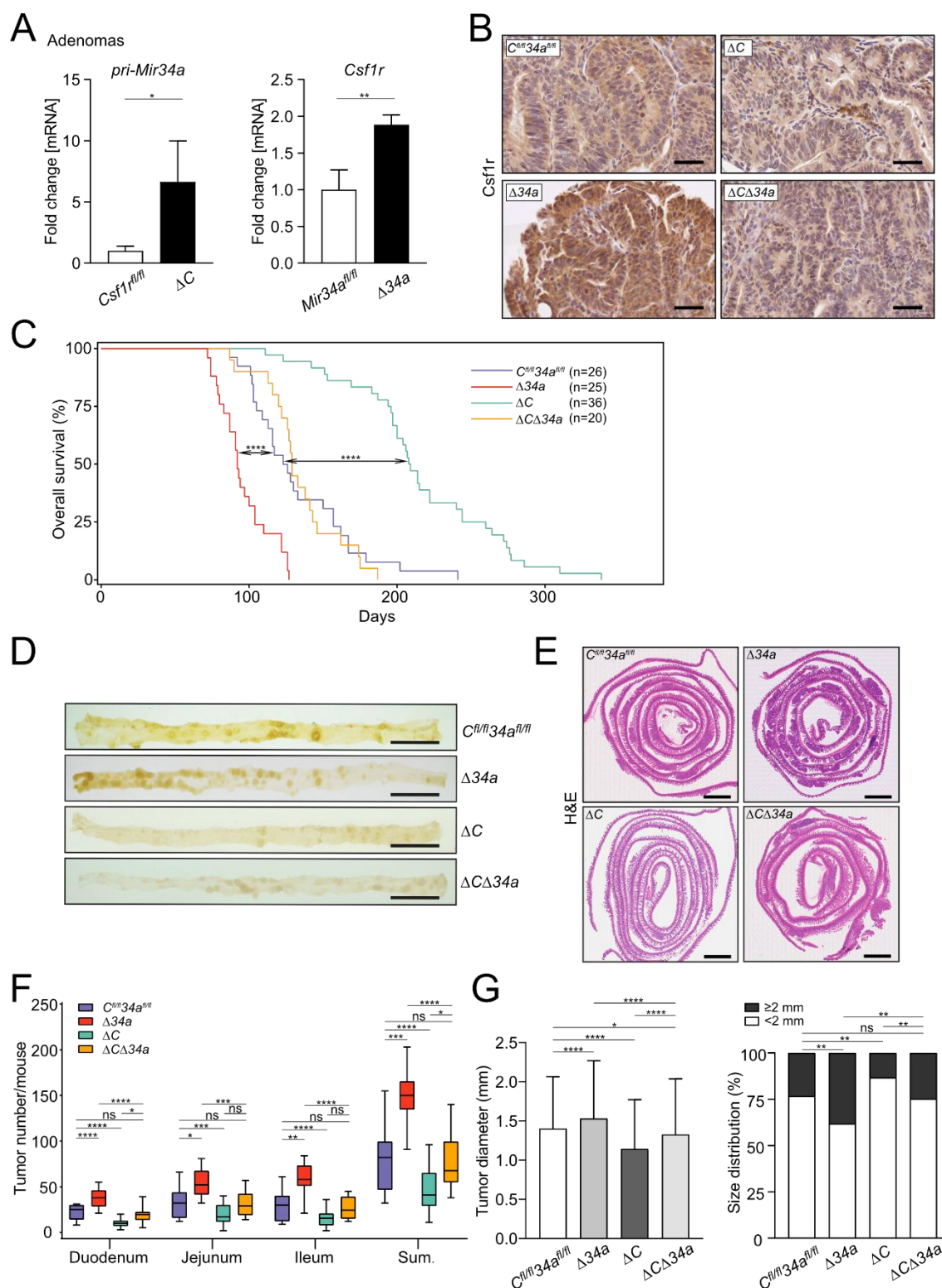


Figure 15. Effects of *Mir34a* and/or *Csf1r* deficiency on intestinal tumorigenesis in *Apc^{Min/+}* mice.

A qPCR analysis of *Csf1r* and *pri-miR-34a* in adenomas of *Apc^{Min/+}* mice with the indicated genotypes. Results are presented as mean values \pm SD (n \geq 3).

B IHC detection of *Csf1r* in intestinal adenomas in *Apc^{Min/+}* mice with the indicated genotypes. Scale bar: 50 μ m.

C Kaplan-Meier survival analysis of the *Apc^{Min/+}* mice with the indicated genotypes. Results were compared with a log-rank test.

D Representative macroscopic images of polyps in resected small intestines in 18 weeks old *Apc^{Min/+}* mice with the indicated genotypes. Scale bar: 2 cm.

E Representative “swiss-rolling” sections of the small intestine of 18 weeks old *Apc^{Min/+}* mice by hematoxylin and eosin (H&E) staining. Scale bar: 2 mm.

F Quantification of tumor number in small intestine of 18 weeks old *Apc^{Min/+}* mice with the indicated genotypes. The box plot extends from the 25th to 75th percentiles. The line in the middle of the box is plotted at the median. The whiskers underneath or above the boxes range from min. to max. value, respectively ($n \geq 7$ mice per genotype).

G Quantification of tumor size and distribution in small intestine of 18 weeks old *Apc^{Min/+}* mice with the indicated genotypes ($n \geq 7$ mice per genotype).

Data information: In (A), results are presented as mean \pm SD using the two-tailed unpaired Student's t-test. In (G), results are presented as mean \pm SD using Tukey's multiple comparisons test. * $P < 0.05$, ** $P < 0.01$, *** $P < 0.001$, or **** $P < 0.0001$.

A: Xiaolong Shi performed the data analyses and generated the figures.

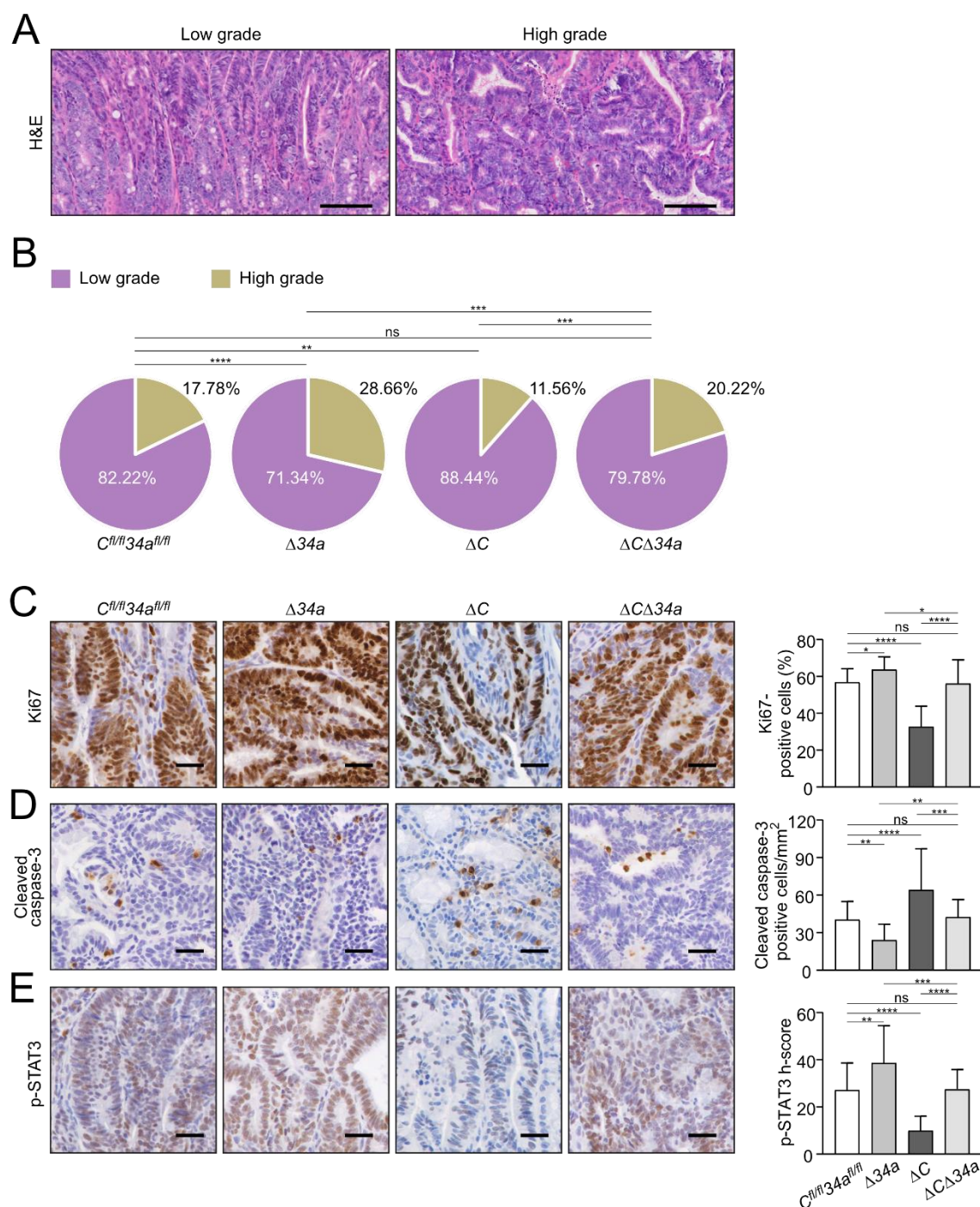


Figure 16. Cellular effects of *Mir34a* and/or *Csf1r* deficiency in intestinal adenomas.

A Representative images of low- and high-grade adenomas. Scale bar: 100 μ m.

B Quantification of tumor stage in adenomas from the small intestine in 18 weeks old *Apc*^{Min/+} mice with the indicated genotypes (n = 6 mice per genotype).

C, D, E, IHC detection of Ki67 (**C**), cleaved-caspase-3 (**D**) and phospho-STAT3 (**E**) in adenomas from the small intestine in 18 weeks old *Apc*^{Min/+} mice with the indicated genotypes. (n \geq 3 mice per genotype). Scale bar: 30 μ m.

Data information: In (**B-E**), results are presented as mean \pm SD using Tukey's multiple comparisons test. **P* < 0.05, ***P* < 0.01, ****P* < 0.001, or *****P* < 0.0001.

4.4 *Csf1r* loss largely reversed the effects of *Mir34a* deletion on tumor microenvironment

Tumor-associated fibroblasts were increased within adenomas in *Mir34a*-deficient adenomas, whereas deletion of *Csf1r* resulted in their decrease (**Figure 17A**). Notably, concomitant *Mir34a* and *Csf1r* deletion resulted in unchanged numbers of fibroblasts within adenomas. Therefore, *Csf1r* is required for the recruitment of fibroblasts in *Mir34a*-deficient adenomas. Similarly, *Mir34a* inactivation resulted in a *Csf1r*-dependent increase in CD3-positive T-cells (**Figure 17B**), CD45R-positive B-cells (**Figure 17C**) and CD68-positive macrophages (**Figure 17D**), as well as LY6G-positive neutrophils (**Figure 17E**). Furthermore, FISH with the universal eubacteria-specific probe (EUB338) revealed that *Mir34a*-deficient adenomas displayed more bacterial infiltration, whereas less bacterial infiltration was observed in *Csf1r*-deficient adenomas (**Figure 17F**). The degree of bacterial infiltration was similar in adenomas with deletion of both genes when compared to control mice (**Figure 17F**). Taken together, deletion of *Csf1r* largely reversed the effects of *Mir34a* loss on infiltration by fibroblasts, immune cells and bacteria in adenomas. Therefore, the up-regulation of *Csf1r* as a consequence of *Mir34a* inactivation in intestinal adenomas is an important mediator of tumor/stroma interactions, which may promote tumor initiation and progression.

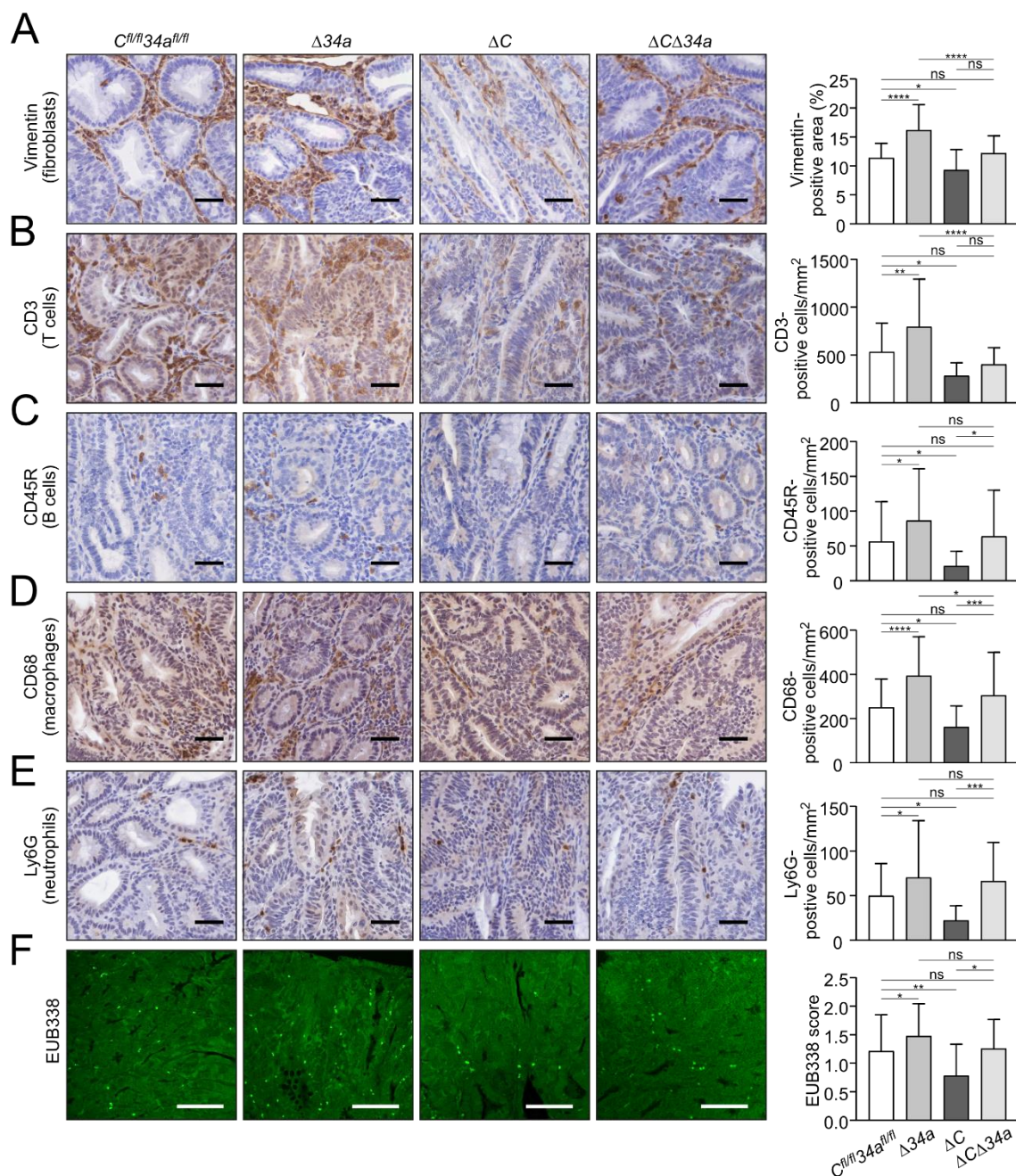


Figure 17. Effects of *Mir34a* and/or *Csf1R* deficiency on stromal cells and bacterial infiltration of *Apc*^{Min/+} adenomas.

A, B, C, D, E IHC detection of fibroblast cells (**A**) by Vimentin and infiltrated T cells (**B**), B cells (**C**), macrophages (**D**), neutrophils (**E**) by CD3, CD45R, CD68, Ly6G, respectively, in adenomas. ($n \geq 3$ mice per genotype). Scale bar: 40 μ m.

F Quantification of bacterial infiltration using FISH of universal eubacteria probe (EUB338) in adenomas. ($n \geq 3$ mice per genotype). Scale bar: 100 μ m.

Data information: In (**A-F**), results are presented as mean \pm SD using Tukey's multiple comparisons test. * $P < 0.05$, ** $P < 0.01$, *** $P < 0.001$, or **** $P < 0.0001$.

4.5 Role of *Csf1r* in *Mir34a*-loss induced stemness and Wnt signaling

In order to assess effects on tumor cell stemness, we determined the expression of the stem cell marker *Lgr5* in adenoma sections using *in situ* hybridization (ISH) (**Figure 18A**). *Lgr5*-positive areas were increased in intestinal adenomas of *Mir34a^{ΔIEC};Apc^{Min/+}* mice and decreased in adenomas of *Csf1r^{ΔIEC};Apc^{Min/+}* mice. However, the combined inactivation of *Mir34a* and *Csf1r* neutralized these effects (**Figure 18A**). In addition, a significant increase in the number of ISCs at the crypt base of *Mir34a^{ΔIEC};Apc^{Min/+}* mice was determined by detection of the stem cell markers *Olfm4* and *Lgr5* by ISH, while *Csf1r^{ΔIEC};Apc^{Min/+}* mice showed a decrease in ISCs (**Figure 18B and C**). Combined deletion of both genes resulted in an ISC frequency similar to that observed in wild-type *Apc^{Min/+}* mice. Therefore, the enhanced frequency of stem cells observed in *Mir34a*-deficient adenomas and normal intestinal crypts, was dependent on the increased expression of *Csf1r*.

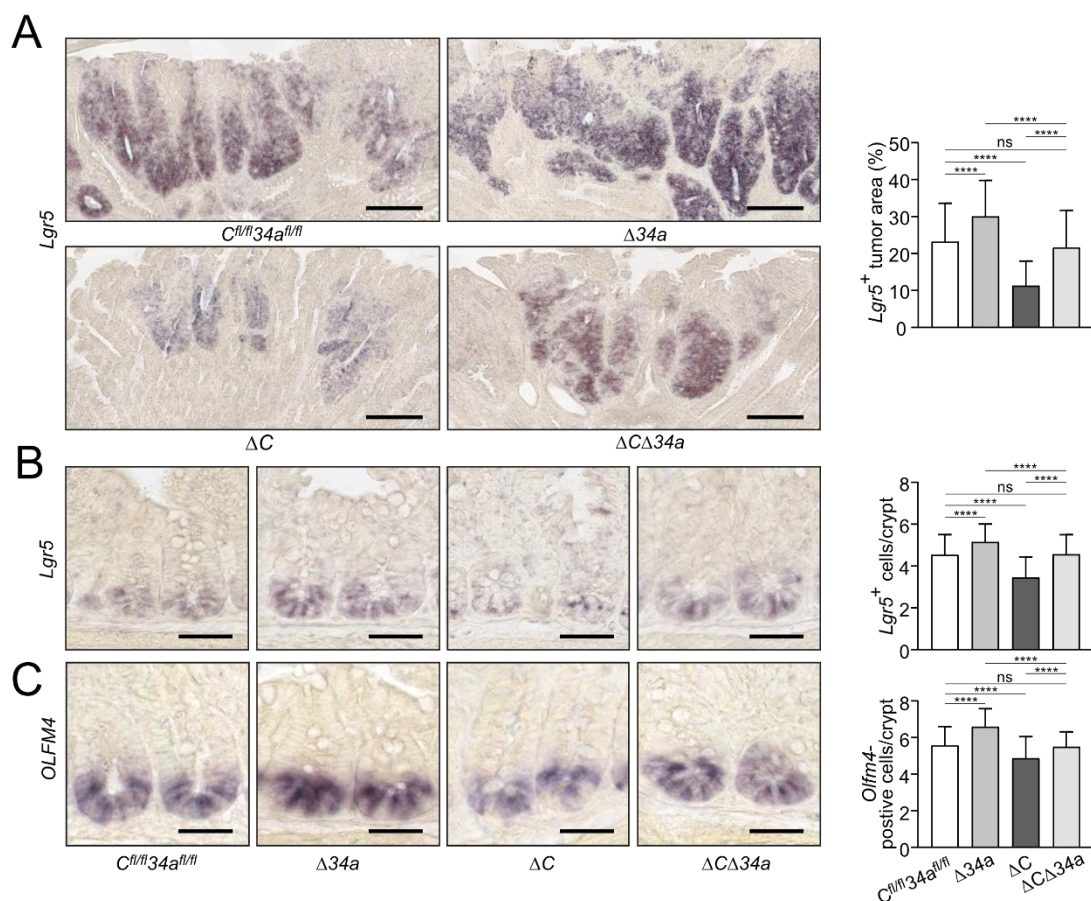


Figure 18. Effects of *Mir34a* and/or *Csf1r* deficiency on stemness.

A Quantification of *Lgr5*-positive area in ≥ 40 intestinal adenomas per group. ($n = 4$ mice per genotype). Scale bar: 140 μm .

B, C *in situ* hybridization detection of *Lgr5*-positive cells (**B**) and *Olfm4*-positive cells (**C**) at the crypt base of 18 weeks old *Apc^{Min/+}* mice with the indicated genotypes. At least 40 crypts per mouse ($n \geq 3$ mice per genotype) were counted. Scale bar: 40 μm .

Data information: In (**A-C**), results are presented as mean \pm SD using Tukey's multiple comparisons test. * $P < 0.05$, ** $P < 0.01$, *** $P < 0.001$, or **** $P < 0.0001$.

We had previously observed that *miR-34a/b/c*-deletion in combination of hemizygous *APC* inactivation promotes nuclear accumulation of β -catenin (Jiang & Hermeking, 2017). In order to assess the effect of the introduced deletions on Wnt signaling the β -catenin localization in the untransformed crypts of the *Apc^{Min/+}* mice with deletions of *Mir34a* or/and *Csf1r* was determined (**Figure 19**). As expected, an increased nuclear accumulation of β -catenin protein in cells at the crypt bases was observed after *Mir34a* deletion in *Apc^{Min/+}* mice. Interestingly, deletion of *Csf1r* decreased the number of cells with nuclear β -catenin at the crypt

base and concomitant deletion of *Mir34a* and *Csf1r* resulted in similar numbers of cells with nuclear β -catenin as observed in the controls. Therefore, loss of *Mir34a* contributes to β -catenin activation in a *Csf1r*-dependent manner.

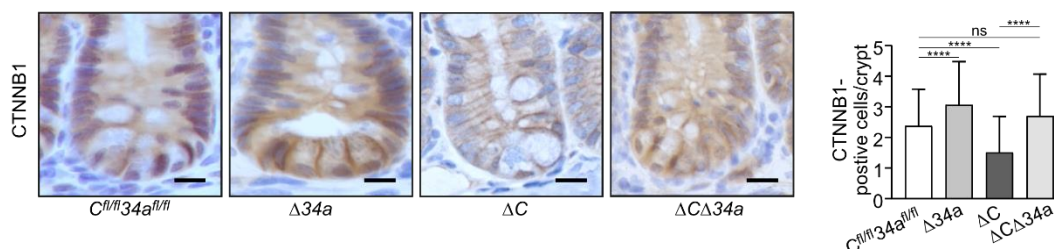


Figure 19. Effects of *Mir34a* and/or *Csf1r* deficiency on β -catenin localization.

Quantification of β -catenin nuclear positive cells in ≥ 180 normal crypts per group ($n = 3$ mice per genotype). Scale bar: 15 μ m. Results are presented as mean \pm SD using Tukey's multiple comparisons test. * $P < 0.05$, ** $P < 0.01$, *** $P < 0.001$, or **** $P < 0.0001$.

In order to obtain functional evidence for *Mir34a/Csf1r* mediated regulation of stemness in adenomas, we performed a tumoroid formation assay (**Figure 20**). Indeed, tumoroids derived from *Mir34a*-deficient adenomas displayed an increase in formation rate and mean size, whereas tumoroids derived from *Csf1r*-deficient adenomas formed at a decreased rate and were smaller. When both genes were deleted concomitantly, tumoroids were similar in number and size to *Mir34a/Csf1r*-proficient tumoroids. *Mir34a*-deficient tumoroids exhibited the highest frequency of actively proliferating cells as evidenced by EdU labeling (**Figure 21**), whereas *Csf1r*-deficient tumoroids showed the lowest rate of proliferation. The combined deletion of both genes nullified the single effects, implying that *Csf1r* is an important mediator of the increased proliferation resulting from *Mir-34a* inactivation. These effects on proliferation presumably explain the observed differences in tumoroid number and size among the genotypes.

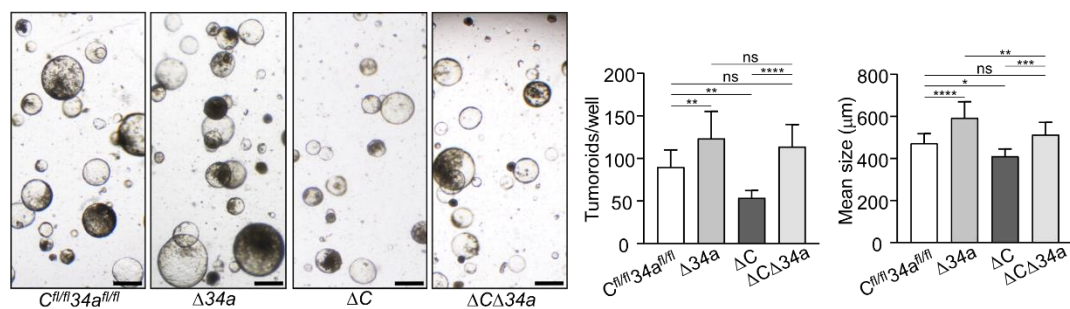


Figure 20. Effects of *Mir34a* and/or *Csf1r* deficiency on tumorigenesis.

Tumorigenesis assay of adenomas (three tumors per mouse) derived from *Ap^c^{Min/+}* mice with the indicated genotypes ($n = 3$ mice per genotype). Scale bar: 400 μm . Results are presented as mean \pm SD using Tukey's multiple comparisons test. * $P < 0.05$, ** $P < 0.01$, *** $P < 0.001$, or **** $P < 0.0001$.

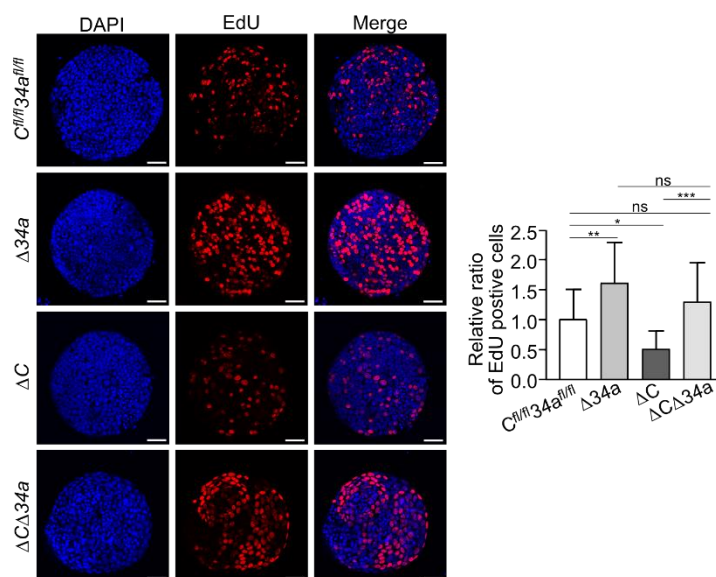


Figure 21. Effects of *Mir34a* and/or *Csf1r* deficiency on tumorigenesis proliferation.

Quantification of EdU labeling of proliferating cells in 20 tumoroids derived from adenomas per group ($n = 3$ mice per genotype), relative ratio was normalized to the corresponding control. Scale bar: 40 μm . Results are presented as mean \pm SD using Tukey's multiple comparisons test. * $P < 0.05$, ** $P < 0.01$, *** $P < 0.001$, or **** $P < 0.0001$.

4.6 Expression profiling of *Mir34a*- and/or *Csf1r*-deficient adenomas and tumoroids

Next, we determined the mRNA expression profiles of *Mir34a^{ΔIEC}*, *Csf1r^{ΔIEC}* and *Mir34a^{ΔIEC};Csf1r^{ΔIEC}* adenomas and compared them to *Mir34a^{fl/fl};Csf1r^{fl/fl}* adenomas from 18-weeks old in *Ap^c^{Min/+}* mice. For each genotype, 3 libraries were generated from RNA isolated from adenomas of 3 mice (3 adenomas from each mouse were pooled) and subjected to RNA-Seq analysis

with more than 30 million reads per library. Principal component analysis (PCA) showed that adenomas of *Mir34a*^{ΔIEC} and *Csf1r*^{ΔIEC} mice were indeed characterized by distinct transcriptomes, while the gene expression pattern in *Mir34a*^{ΔIEC};*Csf1r*^{ΔIEC} adenomas was more similar to *Mir34a*^{fl/fl};*Csf1r*^{fl/fl} adenomas (**Figure 22**). Differential gene expression analyses using DESeq2 showed that in adenomas from *Mir34a*-deficient mice, 301 genes were significantly up- and 127 genes were down-regulated when compared to adenomas from control mice (**Figure 23**, Supplemental Data 5). In *Csf1r*-deficient adenomas, rather moderate changes in gene expression with 28 significantly up- and 26 significantly down-regulated genes were observed when compared to adenomas from control mice (**Figure 23**, Supplemental Data 6). However, in adenomas from *Csf1r*/*Mir34a*-deficient mice *Apc*^{Min/+} mice only 15 genes were significantly up-, and 17 genes were down-regulated, indicating that the gene expression changes observed in *Mir34a*-deficient adenomas were largely abrogated by the concomitant deletion of *Csf1r* (**Figure 23**, Supplemental Data 7). In addition, we performed NGS analyses of tumoroids derived from tumor cells from *Mir34a* and/or *Csf1r*-deficient adenomas in order to identify cell autonomous changes in gene expression, which are not potentially confounded by interactions of tumor cells with the tumor-microenvironment, as in the adenomas. PCA showed that tumoroids of the respective genotypes were characterized by distinct transcriptomes (**Figure 24**). Differential gene expression analyses showed that in tumoroids from *Mir34a*-deficient mice, 232 genes were significantly up- and 202 genes were down-regulated (**Figure 25**, Supplemental Data 8). In tumoroids derived from *Csf1r*-deficient and *Csf1r*/*Mir34a*-deficient adenomas, moderate transcriptome changes with lower numbers of differentially regulated genes were observed (**Figure 25**, Supplemental Data 9 and Supplemental Data 10).

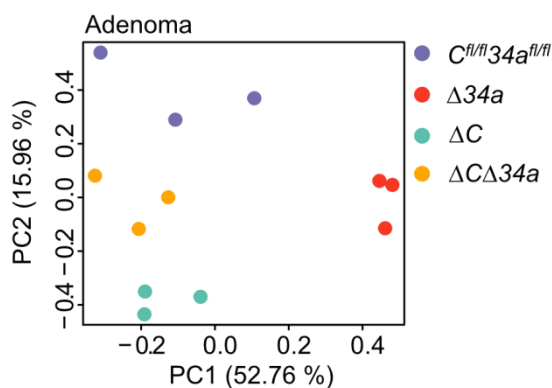


Figure 22. Principal component analysis (PCA) of RNA expression in adenomas from mice with the indicated genotypes. Dr. Markus Kaller performed the analysis and generated the figure.

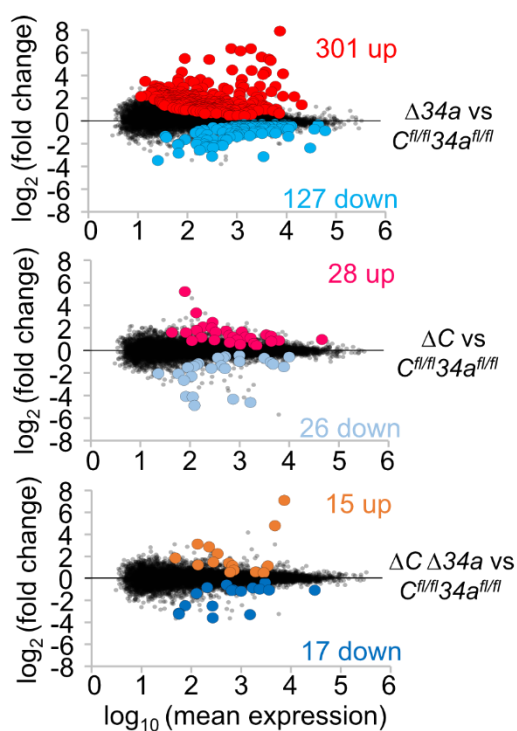


Figure 23. MA-plots showing differential RNA expression (FDR q-value < 0.05) between adenomas with the indicated genotypes from $Apc^{Min/+}$ mice. Significantly up- and down-regulated RNAs are highlighted as indicated. Non-significantly regulated genes are shown in gray. The numbers of differentially regulated RNAs are indicated. See also Supplemental Data 5–7. Dr. Markus Kaller performed the analysis and generated the figure.

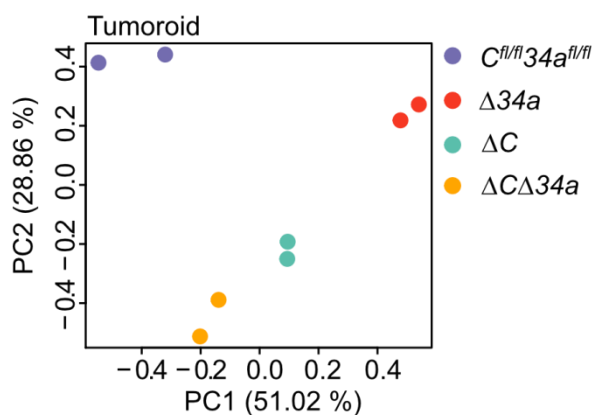


Figure 24. Principal component analysis (PCA) of RNA expression in tumoroids derived from adenomas from mice with the indicated genotypes. Dr. Markus Kaller performed the analysis and generated the figure.

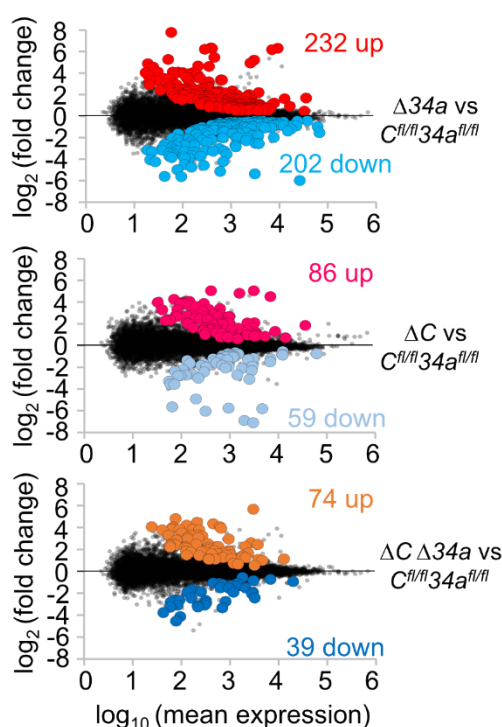


Figure 25. MA-plots showing differential RNA expression (FDR q-value <0.05) between tumoroids derived from adenomas of the respective loss-of-function mice and from $Apc^{Min/+}$ mice. Significantly up- and down-regulated RNAs are highlighted as indicated. Non-significantly regulated genes are shown in gray. The numbers of differentially regulated RNAs are indicated. See also Supplemental Data 8–10. Dr. Markus Kaller performed the analysis and generated the figure.

Interestingly, the overlap between mRNAs up-regulated in *Mir34a*-deficient adenomas and tumoroids, though limited, was statistically highly significant, and among the 23 mRNAs significantly up-regulated in both *Mir34a*-deficient adenomas and tumoroids were three factors involved in Wnt signaling

(*Dkk2*, *Fzd10* and *Wnt10a*) (**Figure 26**), suggesting that the tumor cell-autonomous repression of Wnt signaling by miR-34a may be a critical mechanism of miR-34a mediated tumor suppression, as reported previously (Kaller et al., 2011; N. H. Kim et al., 2011). However, the divergent effects of *Mir34a*-deficiency in adenomas and in tumoroids may in part be due to interactions between *Mir34a*-deficient tumor cells in the adenomas and cells within the tumor microenvironment, such as infiltrating macrophages, which do not occur in tumoroids. In addition, tumoroids are cultured in an artificial matrix, which may not fully represent the *in vivo* environment of tumor cells in adenomas (Guiu & Jensen, 2021), and therefore influence gene expression.

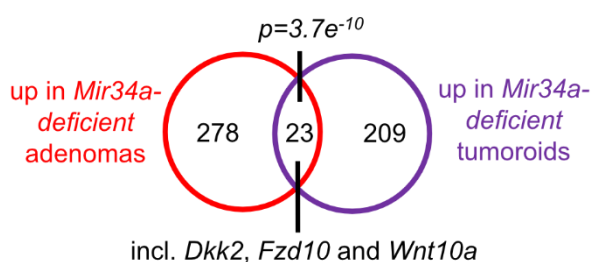


Figure 26. Venn diagram showing overlap between RNAs differentially up-regulated in *Mir34a*^{ΔIEC};*Apc*^{Min/+} adenomas or tumoroids. The numbers of differentially regulated RNAs are indicated. Statistical significance was determined by Fisher's Exact test. Dr. Markus Kaller performed the analysis and generated the figure.

Next we used Gene Set Enrichment Analyses (GSEA) to identify pathways that are differentially regulated in adenomas and tumoroids dependent on their *Mir34a* and *Csf1r* status (**Figure 27**). For this, we focused on processes relevant for tumor progression that are known to be suppressed by miR-34a, such as epithelial-mesenchymal transition (EMT), stemness, and Wnt signaling (**Figure 27**). In *Mir34a*-deficient adenomas, EMT-associated genes were strongly up-regulated. Moreover, extracellular matrix (ECM)-related factors, as well as Consensus Molecular Subtype (CMS)4-associated genes indicative of mesenchymal tumors (Guinney et al., 2015) were up-regulated (**Figure 27**). In

Mir34a-deficient tumoroids, gene signatures characteristic for ISCs, Wnt signaling, and, to a lesser extent, EMT and ECM-related gene signatures were up-regulated (**Figure 27**). Remarkably, the up-regulation of factors involved in EMT, stemness, Wnt signaling and extracellular matrix components in *Mir34a*-deficient adenomas and/or tumoroids was largely abrogated by co-deletion of *Csf1r* (**Figure 27**). Deletion of *Csf1r* alone had a very limited effect on the analyzed gene signatures. Taken together, these results imply that the up-regulation of *Csf1r* expression in *Mir34a*-deficient tumors represents a central mediator of the effects of *Mir34a* loss on gene expression in intestinal adenomas and/or tumoroids.

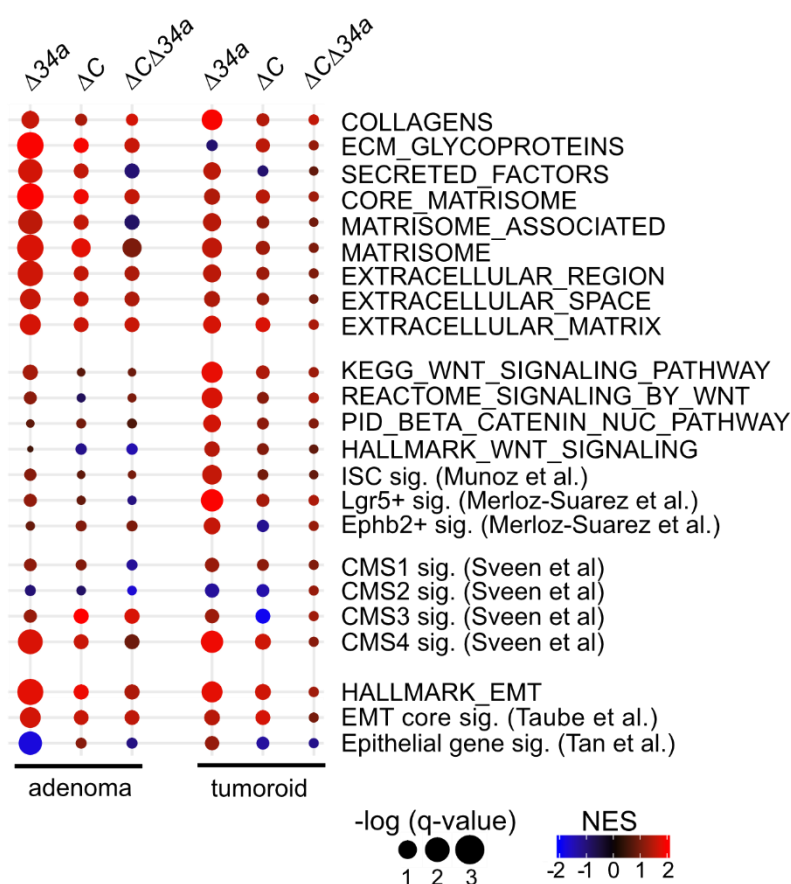


Figure 27. Dot plot representation of Gene Set Enrichment Analyses (GSEA) of the indicated functional categories obtained from pair-wise comparisons of *Mir34a* ^{Δ IEC};*Apc*^{Min/+}, *Csf1r* ^{Δ IEC};*Apc*^{Min/+}, or *Mir34a* ^{Δ IEC};*Csf1r* ^{Δ IEC};*Apc*^{Min/+} with *Mir34a*^{fl/fl};*Csf1r*^{fl/fl};*Apc*^{Min/+} adenomas and tumoroids. The significance of enrichments is presented by normalized enrichment scores (NES) and false discovery rate-adjusted q values. Dr. Markus Kaller performed the analysis and generated the figure.

4.7 Analysis of *Mir34a* target expression

Next, we analyzed which miR-34a targets were significantly up-regulated in either *Mir34a*-deficient adenomas and/or tumoroids. For the identification of up-regulated miR-34a targets, we employed the miRNA target prediction tools TargetScanMouse 7.1 and the mirWalk2.0 (mouse) archive.

In *Mir34a*-deficient adenomas, we identified a set of 62 significantly up-regulated mRNAs with *Mir34a* seed-matching sites in their 3'-UTR (**Figure 28A**). In addition, we identified a set of 58 mRNAs with *Mir34a* seed-matching sites that were up-regulated in tumoroids derived from *Mir34a*-deficient adenomas (**Figure 28B**). Among these were mRNAs, which encode factors relevant for the effects of *Mir34a* deletion described above, such as *Jag1*, *Kitl*, *Lef1*, *OLFM4*, *Met* and *Notch2*. Six predicted *Mir34a* targets (*Arhgap44*, *Ccnjl*, *Clec16a*, *Esy3*, *Golga7b*, *Grp*) were up-regulated in both *Mir34a*-deficient adenomas and tumoroids (**Figure 28A and B**). Remarkably, the up-regulation of predicted *Mir34a* targets in *Mir34a*-deficient adenomas was largely abrogated by co-deletion of *Csf1r* (**Figure 28A**). In *Csf1r/Mir34a*-deficient tumoroids, up-regulation of the majority of predicted *Mir34a* targets was strongly reduced, and only a subset of predicted *Mir34a* targets was also up-regulated when compared to *Csf1r^{fl/fl};Mir34a^{fl/fl}* tumoroids (**Figure 28B**). RNA-Seq results were confirmed by qPCR analysis of selected RNAs up-regulated in *Mir34a*-deficient adenomas and/or tumoroids (**Figure 29A and B**).

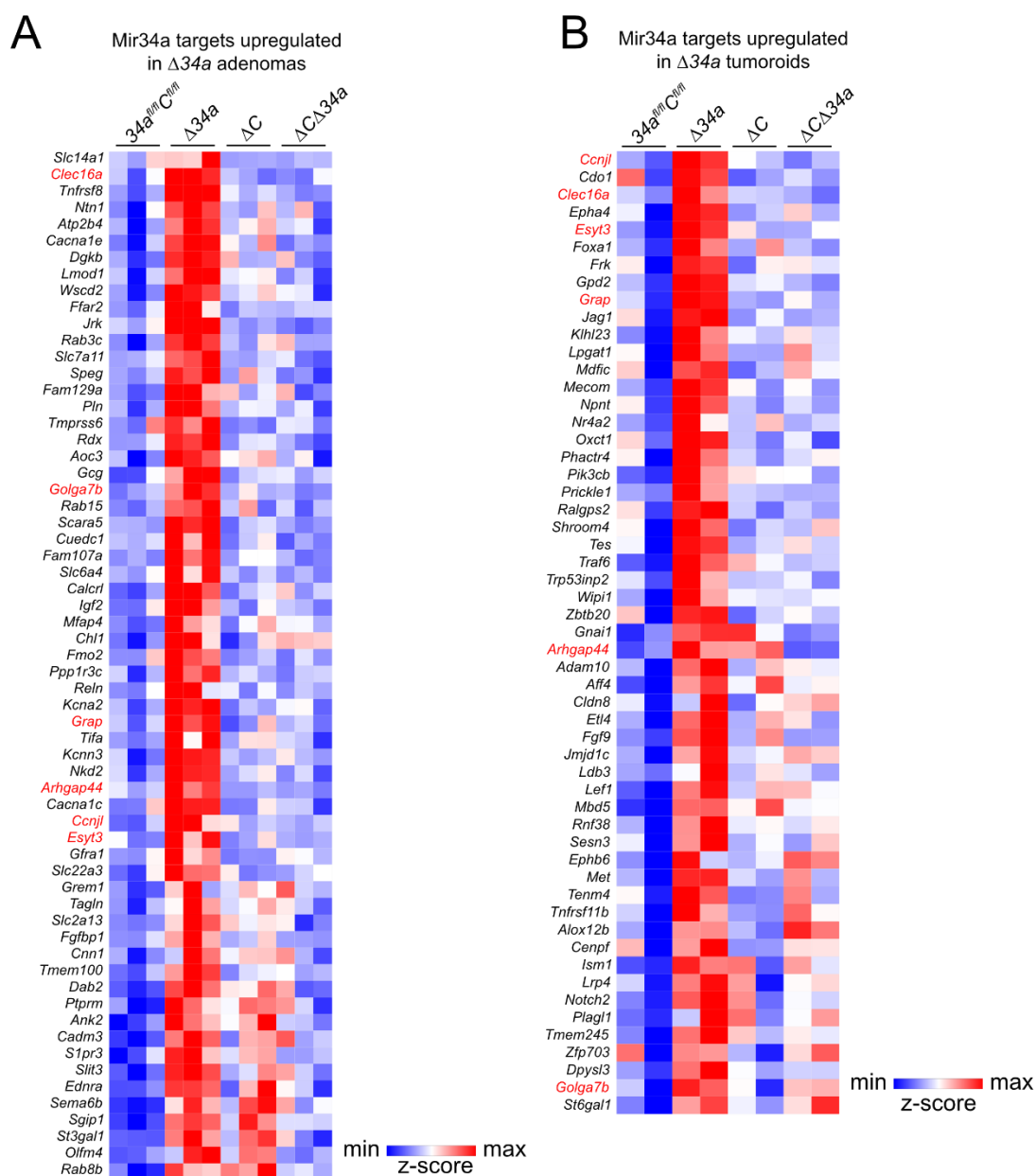


Figure 28. Heat-map of RNA expression of predicted Mir34a targets in **A**, adenomas or **B**, tumoroids with the indicated genotypes from $Apc^{Min/+}$ mice. RNAs with upregulation in $\Delta 34a$ vs $34a^{fl/fl}; C^{fl/fl}$ (FDR<0.05) are shown. RNAs up-regulated both in $\Delta 34a$ adenomas and tumoroids are indicated in red. Dr. Markus Kaller performed all data analyses and generated all figures.

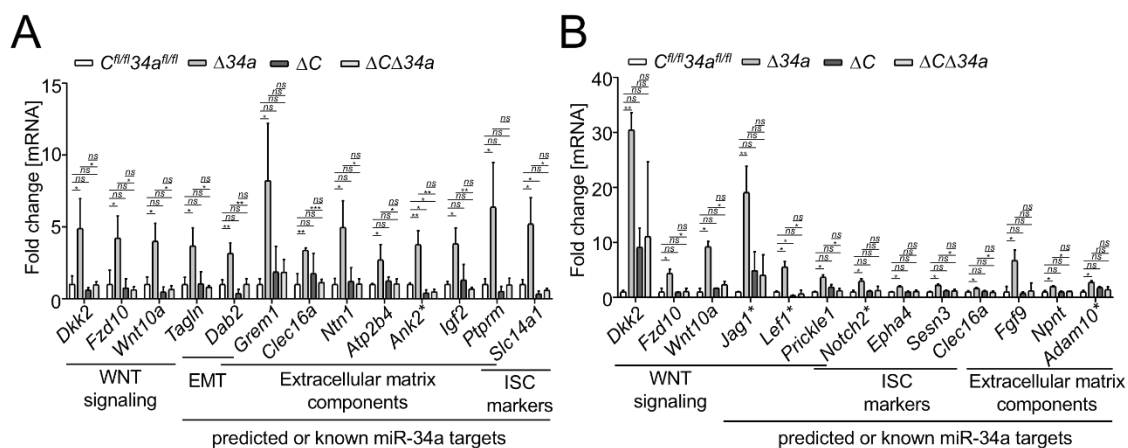


Figure 29. Validation of the exemplary *Mir34a* target genes differently regulated in adenomas (A) or tumoroids (B) with the indicated genotypes by qPCR. Published miR-34a target is labeled with an asterisk (*). Results were represented as mean \pm SD, and subjected to an unpaired, two-tailed Student's t-test with p -values * < 0.05, ** < 0.01, *** < 0.001, ns: not significant.

In order to understand the effect of co-deletion of *Csf1r* on *Mir34a* loss induced changes in gene expression, we analyzed if genes up-regulated after inactivation of *Mir34a* are potentially subject to opposing regulation by *Mir34a* and *Csf1r* signaling. Activation of *Csf1r* is known to induce several signaling pathways, such as the JAK-STAT, MAPK and Rho-actin cascades (Stanley & Chitu, 2014), which ultimately result in the activation of several downstream transcription factors (TFs) such as STAT3, AP1 (JUN:FOS) and SRF (Burrige & Wennerberg, 2004; Fang & Richardson, 2005; Finbloom & Larner, 1995; Gau & Roy, 2018). Therefore, we analyzed whether expression signatures comprising RNAs commonly up-regulated after induction of these TFs were associated with loss of *Mir34a* in adenomas and/or tumoroids. Indeed, GSEA showed that loss of *Mir34a* in adenomas, and to a lesser extent in tumoroids, was associated with the induction of STAT3, JUN and SRF expression signatures (Figure 30). Furthermore, loss of *Mir34a* in adenomas was associated with the induction of RNAs commonly up-regulated after IL6 treatment, which includes STAT3 activation (Figure 30). Remarkably, this effect was largely abrogated by co-deletion of *Csf1r* (Figure 30).

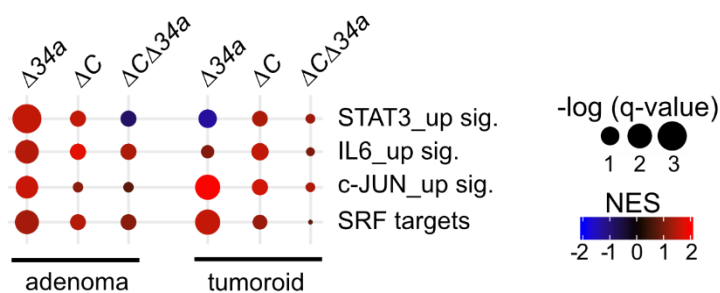


Figure 30. Gene Set Enrichment Analyses (GSEA) of the indicated gene signatures and SRF targets obtained from pair-wise comparisons of *Mir34a* ^{Δ IEC};*Apc*^{Min/+}, *Csf1r* ^{Δ IEC};*Apc*^{Min/+}, or *Mir34a* ^{Δ IEC};*Csf1r* ^{Δ IEC};*Apc*^{Min/+} with *Mir34a*^{fl/fl};*Csf1r*^{fl/fl};*Apc*^{Min/+} adenomas and tumoroids. The significance of enrichments is presented by normalized enrichment scores (NES) and false

discovery rate-adjusted q values. Dr. Markus Kaller performed the analysis and generated the figure.

In order to further characterize how concomitant deletion of *Csf1r* affects transcriptome changes induced by loss of *Mir34a* in adenomas, we determined which *Mir34a* targets may be coordinately regulated by both *Mir34a* and STAT3, AP1 (JUN:FOS) and SRF in a coherent feed-forward manner (hereinafter referred to as “*Mir34a*/TF targets”). Thereby, we identified 26 predicted *Mir34a* targets that are presumably directly regulated by either STAT3, JUN or SRF, as evidenced by analysis of previously published ChIP-Seq and RNA expression datasets (**Figure 31**). Of note, only two (*Ank2*, *Gfra1*) of the identified targets have been characterized as direct miR-34a targets previously (R. He et al., 2017; Zhu, Feng, Cheng, & Xiao, 2018). Next, two of these targets, *Ntn1/Netrin-1* and *Tagln/Transgelin* were selected for further analysis (**Figure 32** and **Figure 33**): *Ntn1* is known to mediate survival signals that contribute to tumorigenesis (Arakawa, 2004; Brisset, Grandin, Bernet, Mehlen, & Hollande, 2021; Mazelin et al., 2004). *Tagln* may exert oncogenic functions by regulation of multiple tumor-relevant processes, such as EMT, invasion and metastasis (Dvorakova, Nenutil, & Bouchal, 2014; Elsafadi et al., 2020). The 3'-UTR of murine *Ntn1* contains three *Mir34a* SMSs (**Figure 32A**). Ectopic *pre-Mir34a* significantly repressed a murine *Ntn1* 3'-UTR reporters and mutations of the three SMSs abrogated their repression by ectopic *Mir34a* (**Figure 32B**). In addition, *Ntn1* mRNA and protein expression was significantly repressed by ectopic *Mir34a* in the murine CRC cell line CT26 (**Figure 32C**). Similar results were obtained for *Tagln* (**Figure 32D-F**). Interestingly, the 3'-UTR of the human *NTN1* and *TAGLN* mRNA also harbors a miR-34a seed-matching site (**Figure 33A and D**). Human *NTN1* and *TAGLN* 3'-UTR-reporters were significantly repressed after co-transfection of *pre-miR-34a*

in an SMS-dependent manner (Figure 33B and E). Furthermore, ectopic expression of *pri-miR-34a* significantly decreased *NTN1* and *TAGLN* mRNA and protein expression levels in the human CRC cell line SW480 (Figure 33C and F). Taken together, these results show that *Ntn1* and *Tagln* are conserved and direct targets of miR-34a.

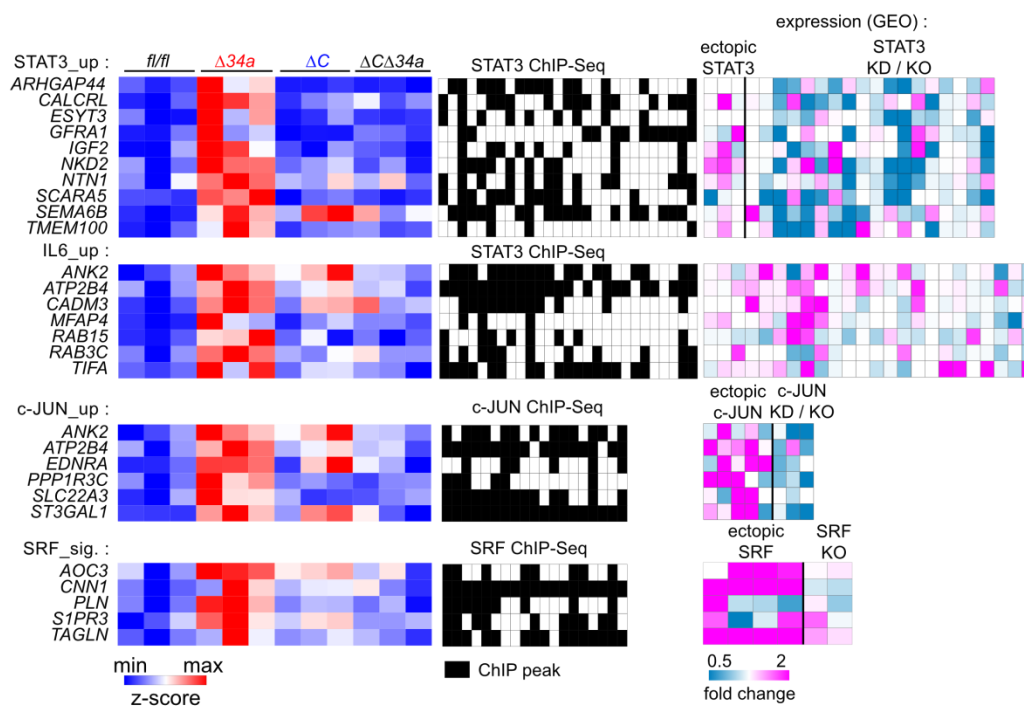


Figure 31. Characterization of coordinated regulation of Mir34a target mRNA expression by Mir34a and the transcription factors STAT3, AP1 (JUN:FOS) and SRF.

Left: Heat-maps showing the expression of indicated genes in adenomas from *Mir34a^{fl/fl};Csf1^{fl/fl};Apc^{Min/+}*, *Mir34a^{ΔIEC};Apc^{Min/+}*, *Csf1^{ΔIEC};Apc^{Min/+}*, or *Mir34a^{ΔIEC};Csf1^{ΔIEC};Apc^{Min/+}* mice. Middle: Heatmaps showing promoter occupancy by STAT3, c-JUN, or SRF according to GEO ChIP-seq datasets. Right: Heat-maps showing the fold change in expression of the indicated mRNAs in GEO datasets after STAT3 ectopic expression or knockdown (KD)/knockout (KO), IL6 treatment, and c-JUN or SRF ectopic expression or knockdown (KD)/knockout (KO). GEO data are shown from left to right in the order of the underlying datasets listed in Supplemental Data 1- 4. Dr. Markus Kaller performed the analysis and generated the figure.

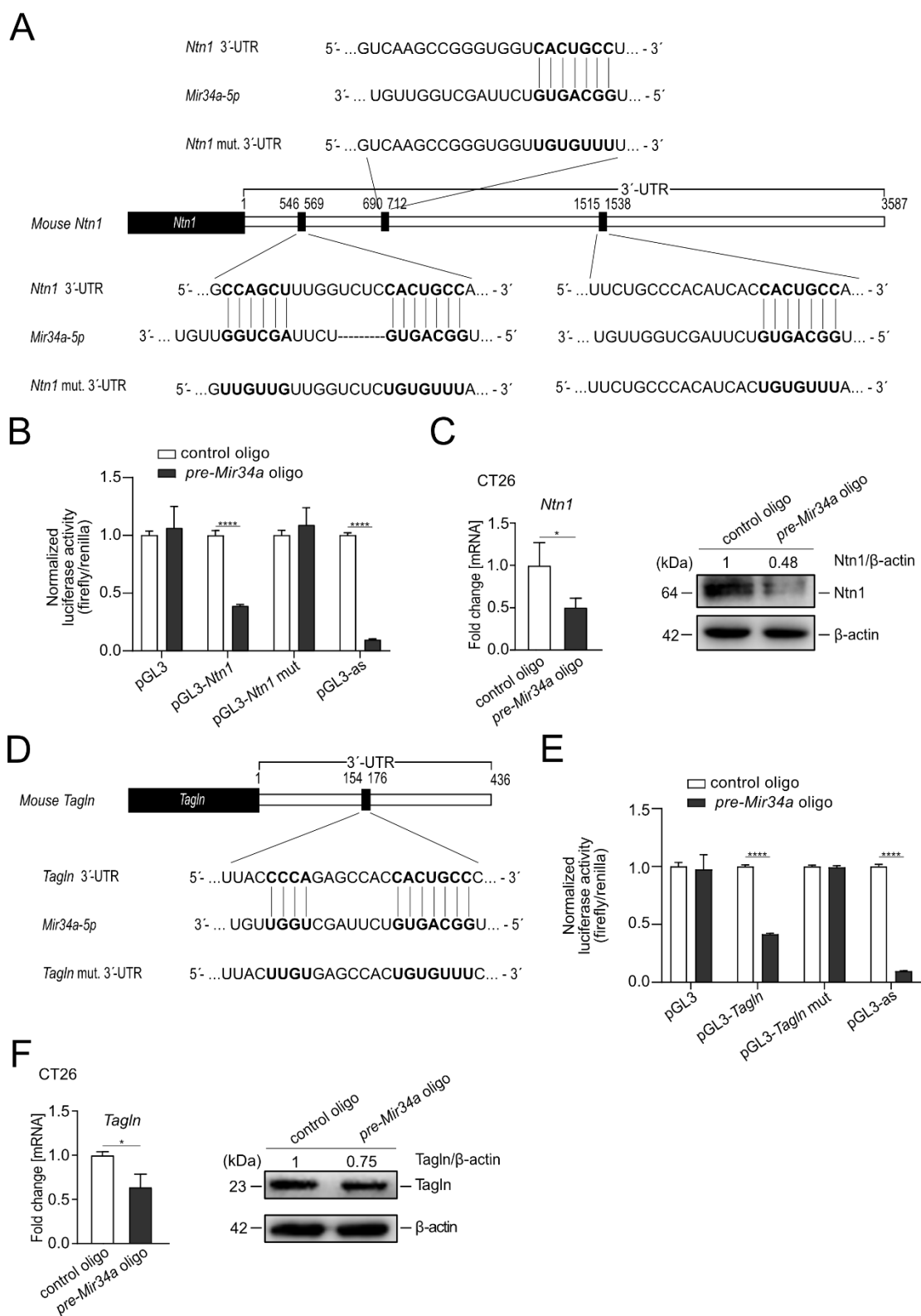


Figure 32. Characterization of *Ntn1* and *Tagln* as direct targets of *Mir34a*.

A Scheme of the *Mir34a* seed, the seed-matching sequences and its targeted mutation in the 3'-UTR of mouse *Ntn1* mRNA.

B Dual-reporter assay after transfection of H1299 cells with the indicated *pre-Mir34a* oligonucleotides using the murine *Ntn1* 3'-UTR reporter.

C qPCR (left panel) and Western blot analysis (right panel) of *Ntn1* in CT26 cells after addition of *pre-Mir34a* oligonucleotides.

D Scheme of the Mir34a seed, the seed-matching sequences and its targeted mutation in the 3'-UTR of mouse *Tagln* mRNA.

E Dual-reporter assay after transfection of H1299 cells with the indicated *pre-Mir34a* oligonucleotides using the murine *Tagln* 3'-UTR reporter.

F qPCR (left panel) and Western blot analysis (right panel) of *Tagln* in CT26 cells after addition of *pre-Mir34a* oligonucleotides.

Data information: In (**B, C, E, F**), results are presented as mean \pm SD (n=3) using the two-tailed unpaired Student's t-test. *P < 0.05, **P < 0.01, ***P < 0.001, or ****P < 0.0001.

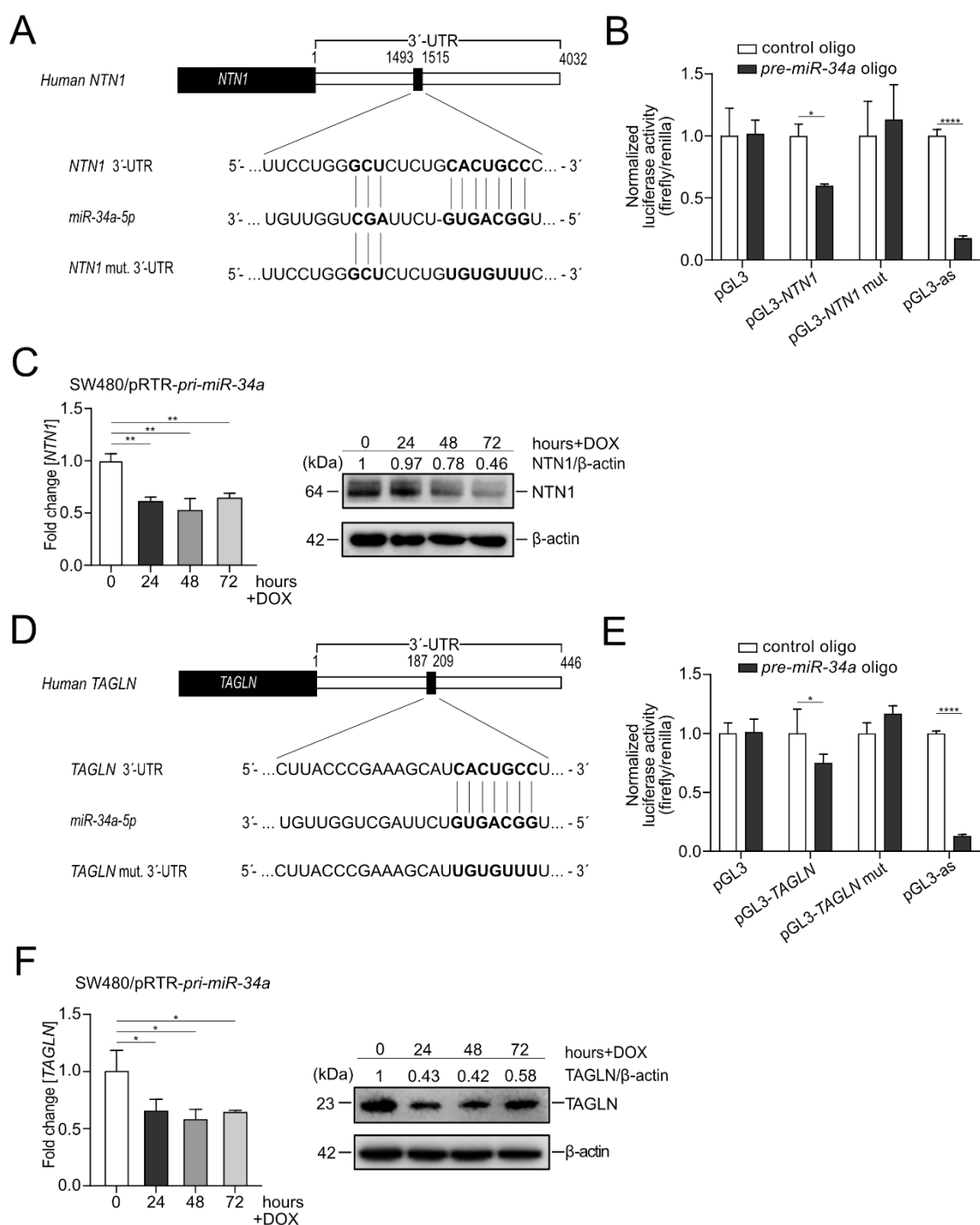


Figure 33. *NTN1* and *TAGLN* are the direct targets of miR-34a in human.

A Scheme of the miR-34a seed, the seed-matching sequences and its targeted mutation in the 3'-UTR of human *NTN1* mRNA.

B Dual-reporter assay after transfection of H1299 cells with the indicated *pre-miR-34a*

oligonucleotides using the human *NTN1* 3'-UTR reporter.

C qPCR (left panel) and Western blot analysis (right panel) of *NTN1* in SW480/pRTR-*pre-miR-34a* cells after addition of DOX.

D Scheme of the miR-34a seed, the seed-matching sequences and its targeted mutation in the 3'-UTR of human *TAGLN* mRNA.

E Dual-reporter assay after transfection of H1299 cells with the indicated *pre-miR-34a* oligonucleotides using the human *TAGLN* 3'-UTR reporter.

F qPCR (left panel) and Western blot analysis (right panel) of *TAGLN* in SW480/pRTR-*pre-miR-34a* cells after addition of DOX.

Data information: In (**B**, **C**, **E**, **F**), results are presented as mean \pm SD (n=3) using the two-tailed unpaired Student's t-test. *P < 0.05, **P < 0.01, ***P < 0.001, or ****P < 0.0001.

4.8 Clinical associations of *Mir34a*-related expression signatures

Next, we determined whether the expression signatures we identified in *Mir34a* ^{Δ IEC}, *Csf1r* ^{Δ IEC} and *Mir34a* ^{Δ IEC};*Csf1r* ^{Δ IEC} adenomas are associated with clinical parameters, such as patient survival and tumor stage, in two independent CRC patient cohorts (TCGA-COAD and GSE39582). Interestingly, in primary CRCs the *Mir34a* ^{Δ IEC} signature was associated with poor relapse free survival in both patient cohorts (**Figure 34A**). Moreover, a pooled patient cohort comprising 946 patients from both patient cohorts recapitulated these findings with increased statistical significance (**Figure 34B**). Conversely, the *Csf1r* ^{Δ IEC} signature was associated with improved relapse free survival (**Figure 34A**). The *Mir34a* ^{Δ IEC};*Csf1r* ^{Δ IEC} expression signature was not associated with a significant difference in relapse free survival (**Figure 34A**). Moreover, the *Mir34a* ^{Δ IEC} signature was elevated in advanced tumor stages, whereas the *Csf1r* ^{Δ IEC} and *Mir34a* ^{Δ IEC};*Csf1r* ^{Δ IEC} expression signatures were elevated in less advanced tumor stages (**Figure 34C**).

Next, we analyzed whether the *Mir34a* ^{Δ IEC} adenoma signature, mature miR-34a expression and *CSF1R* expression is associated with HALLMARK, KEGG, as well as TF expression and TF target signatures in human CR tumors or CRC cell lines (**Figure 34D**). In human CRCs, the *Mir34a* ^{Δ IEC} adenoma gene

signature was associated with EMT, inflammation and actin cytoskeleton signatures, as well as with the TNF- α /NF κ B, IL6/STAT3 and MAPK signaling pathways. Moreover, it was associated with STAT3 and JUN expression signatures. Remarkably, several SRF, AP1 and NF κ B target signatures were strongly associated with the *Mir34a* ^{Δ IEC} adenoma signature. Moreover, these associations could also be found in CRC cell lines, which strongly suggests tumor cell intrinsic regulations. Conversely, expression of mature miR-34a displayed a strong negative correlation with the large majority of the analyzed gene signatures. Furthermore, *CSF1R* expression positively correlated with the majority of the analyzed gene signatures, which largely reflected the associations found for the *Mir34a* ^{Δ IEC} adenoma signature. These findings indicate that loss of *miR-34a*, and the resulting elevated expression of CSF1R in human CRCs is also associated with the signaling pathways and TF expression signatures identified in *Mir34a*-deficient, murine adenomas in this study.

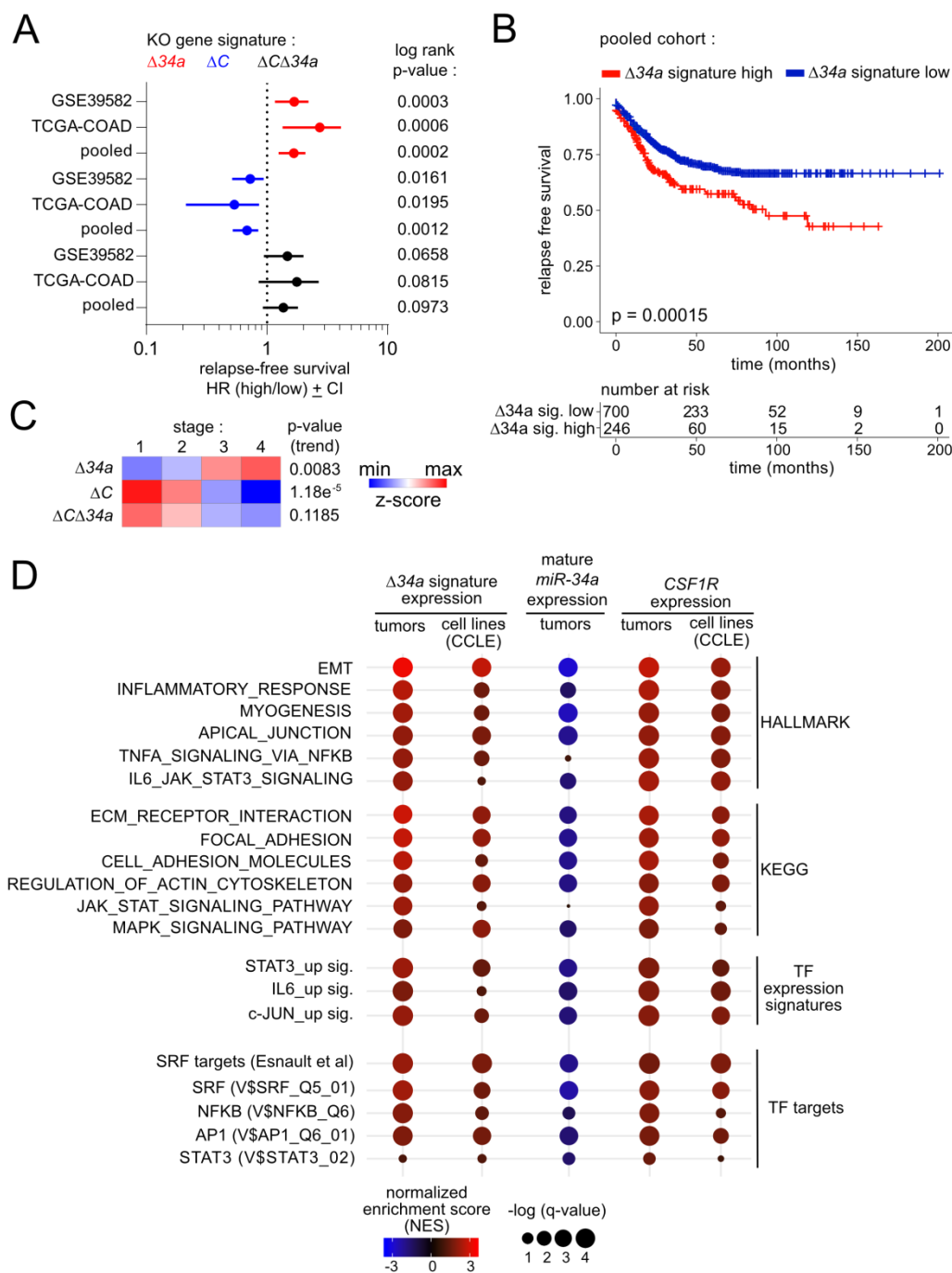


Figure 34. Clinical associations of *Mir34a*-related expression signatures.

A Forest plots showing hazard ratios for relapse free survival by comparing patients with high versus low expression of the $\Delta 34a$, ΔC and $\Delta 34a\Delta C$ expression signatures in the TCGA and GSE39582 patient cohorts, and the pooled cohort comprising both individual cohorts. Dots represent Hazard ratios and horizontal lines show 95% CI. P-values were calculated using the log-rank method.

B Kaplan-Meier analysis of relapse free survival for patients with high or low expression of the $\Delta 34a$ expression signature using the pooled dataset of the TCGA and GSE39582 patient cohorts (n = 946 patients). The significance was calculated with the log-rank test and the x-axis represents relapse free survival in months. Below the graph the numbers of patients at risk with high or low expression of the $\Delta 34a$ expression signature at the respective time point is provided.

C Heat-map showing the expression of the $\Delta 34a$, ΔC and $\Delta 34a\Delta C$ expression signatures in the indicated tumor stages using the pooled dataset of the TCGA and GSE39582 patient cohorts. The p-values for linear trend in expression from stage 1 to stage 4 are provided.

D Gene Set Enrichment Analysis (GSEA) of the indicated functional categories showing their association with the $\Delta 134a$ signature, mature *miR-34a* expression and *Csf1r* expression in tumors using the pooled dataset of the TCGA and GSE39582 patient cohorts (tumors) and cancer cell lines (CCLE). The significance of enrichments is presented by normalized enrichment scores (NES) and false discovery rate-adjusted q values.

Dr. Markus Kaller performed all data analyses and generated all figures.

Next we analyzed whether elevated expression of the “Mir34a/TF” targets (**Figure 31**) is associated with molecular subtypes and stages of CRC, or CRC patient survival (**Figure 35**). Remarkably, the majority of the Mir34a/TF targets showed elevated expression in CMS4 tumors. Moreover, numerous targets showed elevated expression in CRIS-B and -D subtypes. The CMS4 and CRISB and CRISD molecular subtypes display mesenchymal and WNT-associated expression signatures, respectively (Guinney et al., 2015; Isella et al., 2017). Furthermore, the majority of Mir34a targets displayed elevated expression in the advanced tumor stages 3 and 4. While this pattern was less evident for STAT3 target genes, it was found for the majority of direct JUN and SRF targets. Strikingly, the large majority of the Mir34a/TF targets displayed a negative correlation with mature miR-34a expression, as well as a positive correlation with *CSF1R* expression in human CRCs (**Figure 35**), suggesting that the proposed feed-forward regulation of these genes is conserved between murine and human cells. Moreover, elevated expression of the majority of “Mir34a/TF” target mRNAs was significantly associated with poor relapse free survival of CRC patients (**Figure 35**).

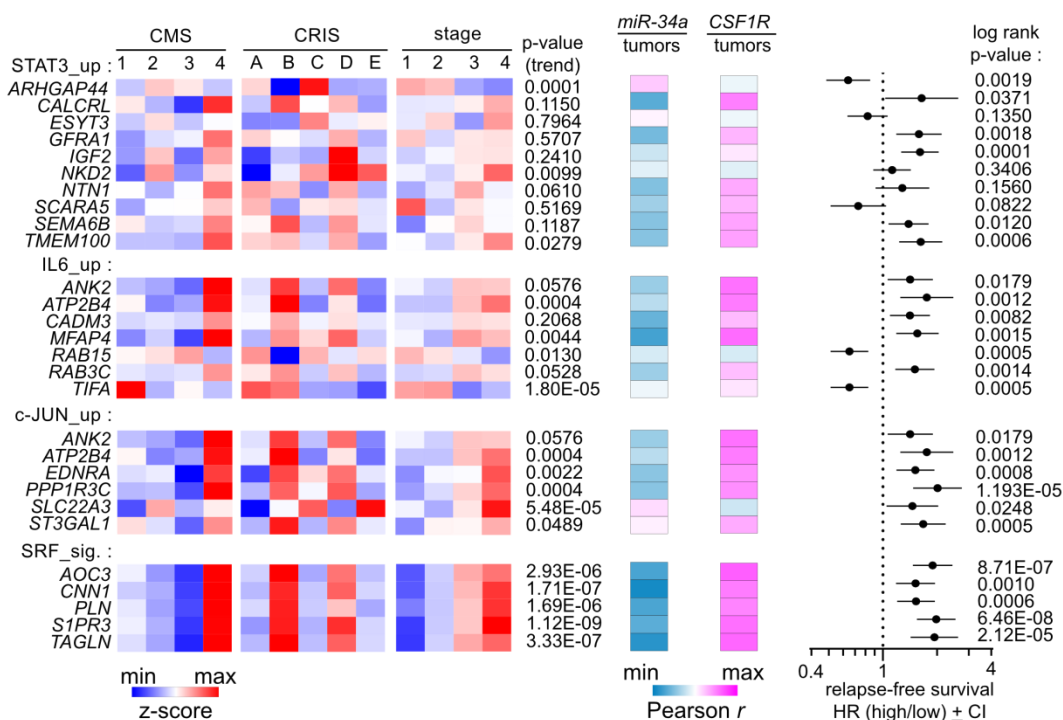


Figure 35. Associations of miR-34a target expression with clinico-pathological parameters. Left: Heat-maps showing the expression of indicated mRNAs in CMS and CRIS molecular subtypes and tumor stages. The p-values for linear trend in expression from stage 1 to stage 4 are indicated. Middle: Heat-maps showing the expression correlation between the indicated mRNAs and mature *miR-34a* and *CSF1R*. Right: Forest plot showing hazard ratios for relapse free survival by comparing patients with high versus low expression of the indicated mRNAs. Dots represent hazard ratios and horizontal lines show 95% CI. P-values were calculated using the log-rank method. Dr. Markus Kaller performed the analysis and generated the figure.

4.9 *Mir34a* and *Csf1r* influence therapeutic responses in tumoroids

We have previously reported a role of the miR-34/CSF1R/STAT3 axis in the response to 5-Fluorouracil (5-FU) in human CRC cell lines *ex vivo* (Shi et al., 2020). Therefore, we asked whether the genetic inactivation of *Mir34a* and/or *Csf1r* would modulate the response to 5-FU in tumoroids (**Figure 36**). Interestingly, we found that *Mir34a*-deficient tumoroids showed less apoptosis in response to 5-FU, while *Csf1r*-deficient tumoroids displayed more apoptosis in response to 5-FU. When both genes were deleted the response to 5-FU was not significantly different from tumoroids with intact *Mir34a* and *Csf1r* genes (**Figure 36**). Since the effects of deleting *Mir34a* and *Csf1r* abrogated the effect of single

deletions, these results showed that *Csf1r* is an important mediator of the 5-FU-resistance caused by *Mir34a* inactivation.

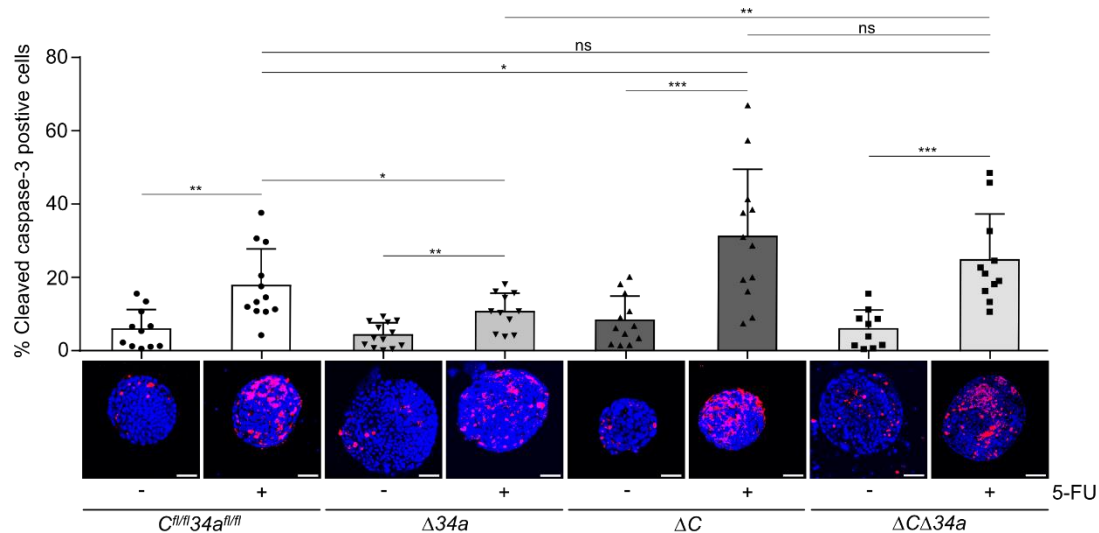


Figure 36. Effects of *Mir34a/Csf1r* loss on the response to 5-FU.

Tumoroids were cultured for 3 days and then treated with or without 5-FU (25 μ g/ml) for 48 hours. ≥ 10 tumoroids from 3 mice per group are analyzed. Scale bar: 50 μ m. Results are presented as mean \pm SD using a two-tailed unpaired Student's t-test. * $P < 0.05$, ** $P < 0.01$, *** $P < 0.001$, or **** $P < 0.0001$.

5. Discussion

In this thesis, the *in vivo* relevance of the suppression of *Csf1r* by miR-34a for intestinal tumorigenesis was studied using *Apc*^{Min/+} mice with IEC-specific deletions of the *miR-34a* and/or *Csf1r* genes. Our results showed tumor-suppressive effects of *Mir34a*, whereas a tumor-promoting role of *Csf1r* was determined in intestinal epithelial cells. The combined deletion of *Mir34a* and *Csf1r* demonstrated that activation of *Csf1r* is required for the effects of *Mir34a* loss during intestinal tumorigenesis. Therefore, the up-regulation of *Csf1r* expression that results from the inactivation of *Mir34a* is an important mediator of the pro-tumorigenic effects of *Mir34a* inactivation in mice and presumably also in human CRC. In our previous research, *CSF1R* was identified as a direct target of miR-34a in human CRC cells, and the CSF1R-STAT3-miR-34a feedback regulation was characterized (Shi et al., 2020). In the current study, we confirmed that *Csf1r* also represents a direct target of *Mir34a* in mice. Furthermore, we provide genetic evidence that this regulation occurs *in vivo*, since the reciprocal repression between *Mir34a* and *Csf1r* was also identified in murine intestinal epithelium and derived adenomas.

We have previously reported the combined deletion of *miR-34a* and *miR-34b/c* resulted in significant architectural changes, such as a longer SI, and increased crypt width and depth in *Apc*^{Min/+} mice (Jiang & Hermeking, 2017). And deletion of *miR-34a/b/c* also led to larger tumor size and shorter lifespan in *Apc*^{Min/+} mice (Jiang & Hermeking, 2017). Whereas deletion of miR-34a or miR-34b/c alone did not have these effects (Jiang & Hermeking, 2017). Here, we observed significant changes in intestinal architecture and cellular composition after *miR-34a* was deleted in *Apc*^{Min/+} mice, i.e. an increase of SI length, and an increase of the number of Paneth cells, and *miR-34a* loss results in a significant

increased tumor burden as well as decreased survival in *Apc*^{Min/+} mice. It is worth noting that in that in the previous study *miR-34* genes were deleted in all cells of the mice, whereas here we used a *Villin-Cre* allele for IEC-specific deletion of *Mir34a*. The diverging results between the two studies may be due to cell-type-specific effects of *miR-34* deletion, e.g. Mir34-deficient cells in the tumor micro-environment may influence tumor formation and progression. In addition, we detected an increase in entero-endocrine cells in *Mir34a*^{ΔIEC};*Apc*^{Min/+} mice. Interestingly, entero-endocrine cells control microbial and intestinal homeostasis via innate immune signaling (Watnick & Jugder, 2020).

Since the genetic deletion of *Mir34* did not promote the formation of B-cell lymphomas in *Eμ-Myc* mouse model (Concepcion et al., 2012), and the anti-proliferative effect of miR-34a was observed at high levels of expression but not upon endogenous expression levels, the role of *miR-34a* as a tumor suppressor gene has recently been questioned (Mockly, Houbron, & Seitz, 2022). However, miR-34a, in addition to its role in proliferation, has also been implicated in the regulation of many other tumor formation relevant processes, such as cell cycle arrest, apoptosis and chemo-sensitivity, by targeting master regulators of these processes (Bommer et al., 2007; Chang et al., 2007; L. He et al., 2007; Tarasov et al., 2007; W. Yin, Gao, & Zhang, 2020). The majority of these studies also employed miR-34a inactivating approaches to come to the conclusion that miR-34 has tumor suppressive properties. Therefore, miR-34a presumably harbors context-dependent tumor suppressive capacities. The results obtained in this thesis also support a tumor suppressive role of miR-34a and indicate that the repression of *Csf1r* by miR-34a is an important component of this tumor suppressive capacity.

CSF1R expression was found at an elevated level in various types of human cancer and correlated with poor prognosis of patients (Chambers, Kacinski, Ivins, & Carcangiu, 1997; Kluger et al., 2004; Okugawa et al., 2018; L. Yang et al., 2016), including CRC patients (Shi et al., 2020; X. Wang, Zhang, Hu, & Qian, 2022). Studies in mouse models showed that *Csf1r* plays a crucial role in the development of some human diseases including neoplasm (Arreola et al., 2021; Ide et al., 2002; Konno, Kasanuki, Ikeuchi, Dickson, & Wszolek, 2018). In *Csf1r*^{-/-} mice a reduced number of Paneth and enteroendocrine cells, and increased goblet cell numbers were previously detected in the SI, as well as a shortened length of the SI (Huynh et al., 2009). Furthermore, a decreased rate of SI-derived organoid formation combined with decreased expression of the stem cell markers were observed in *Csf1r*-deficient mice (Akcora et al., 2013; Huynh et al., 2009). These analyses were performed in mice with germ-line deletion of *Csf1r* (Huynh et al., 2009) or *Csf1r*^{fl/fl}; *Villin-Cre*^{ERT2} mice treated with tamoxifen (Akcora et al., 2013). However, so far the role of *Csf1r* in *Apc* loss-induced intestinal tumorigenesis has not been explored in mouse models. Here, we established *Apc*^{Min/+} mice with IEC-specific deletion of *Csf1r* via *Villin-Cre*, and found that *Csf1r* loss resulted in the modulation of SI architecture and a decrease of secretory and intestinal stem cells. The *Csf1r*^{ΔIEC}; *Apc*^{Min/+} mice had fewer and smaller adenomas and survived longer. Furthermore, the IECs-specific deletion of *Csf1r* in *Apc*^{Min/+} mice resulted in a decreased *Lgr5*-positive tumor area. Furthermore, a decreased in the number and mean size of tumoroids that could be obtained from *Csf1r*-deficient adenomas was observed. Our results suggest that *Csf1r* plays an important role in promoting tumor formation caused by loss of *Apc* in intestinal epithelial cells.

Here, we confirmed the critical role of *Csf1r* as a central component of the *Csf1r*-*STAT3*-*Mir34a* feed-back-regulation, which we had previously identified and characterized in human CRC cells (Shi et al., 2020). However, the relevance of the *Csf1r*/*Mir34a* feed-back loop in mice was so far unclarified. We observed that *Apc*^{Min/+} mice with deletions of *miR-34a* and *Csf1r* genes had a phenotype similar to that of *Apc*^{Min/+} mice, suggesting that the effects of *Mir34a* loss on intestinal tumorigenesis are at least partially mediated by up-regulation of *Csf1r* expression. It should however be mentioned that the *Csf1r* deletion studied here could have a dominant effect in the context of *Mir34a* inactivation which is not identical to reverting the elevation of *Csf1r* expression caused by *Mir34a* loss. To provide direct and formal evidence that *Mir34a* suppresses tumorigenesis through downregulation of *Csf1r*, the SMS for *Mir34a* should be deleted in the 3'-UTR of *Csf1r* of mice in the future and subjected to similar analyses as performed here.

Since *Csf1r* and *Mir34a* exhibited opposite effects on tumor proliferation, apoptosis, *STAT3* signaling, and intestinal cancer stem cells, their antagonistic effects might be responsible for the compensatory effect of deleting both genes. Here, *Mir34a* inactivation resulted in a *Csf1r*-dependent increase in tumor-associated fibroblasts, macrophages, neutrophils, T- and B-cells. Since cancer cells closely interact with surrounding microenvironment, the up-regulation of *Csf1r* presumably mediated the effects of *Mir34a* loss on these cells of within the microenvironment. Importantly, the tumor microenvironment modulates cancer onset and progression via establishing the vital and complex cell-cell interactive networks (Hinshaw & Shevde, 2019).

In this study, we showed that *Csf1r* is an important mediator of the effects of *Mir34a* loss on stemness and Wnt signaling. Intestinal stem cells are thought to represent the tumor initiating cells during intestinal tumorigenesis (Catalano et al., 2013; Ungefroren, Sebens, Seidl, Lehnert, & Hass, 2011), and multiple signaling pathways, including Wnt/ β -catenin pathways, regulate the cell-cell and cell-matrix interactions in the intestinal stem cell niche (Pastuła & Marcinkiewicz, 2019; Takahashi & Shiraishi, 2020). Interestingly, *Lgr5*, which was up-regulated in *Mir34a*-deficient adenomas and down-regulated in *Csf1r*-deficient adenomas, is not only a stem cell marker, but also potentiates Wnt/ β -catenin signaling. During intestinal tumorigenesis, intestinal stem cells are considered tumor-initiating cells (Barker et al., 2009), and the Wnt/ β -catenin pathway plays an important role in stem cell self-renewal (Mohammed et al., 2016). Here, we found that *Csf1r* up-regulation presumably mediated the effects of *Mir34a* loss on tumor stemness and Wnt signaling.

In this research, we also analyzed the expression profile of *Mir34a*- and/or *Csf1r*-deficient adenomas and tumoroids, and explored the expression of potential miR-34a targets in adenomas and tumoroids. In addition, pathways differentially regulated in adenomas and tumoroids dependent on the *Mir34a* and *Csf1r* status were identified. *Mir34a*-loss-associated expression signatures were found to be correlated with advanced clinical stage and poor survival in CRCs. In addition, the miR-34a/CSF1R axis was demonstrated to be involved in resistance to 5-FU in tumoroids. Among the identified, potential miR-34a targets, *Ntn1/Netrin-1* and *Transgelin/Tagln* were further validated and characterized as two novel miR-34a targets in human and murine cell lines. These two targets are coordinately regulated by both, miR-34a and the CSF1R-induced JAK-STAT,

MAPK and Rho-actin signaling pathways and represent attractive mediators of the effects of *Mir34a* inactivation in tumors.

Netrin-1 is a member of the netrin family that belongs to laminin-like proteins (Claro & Ferro, 2020; Rajasekharan & Kennedy, 2009). In addition to directing axon guidance (Kennedy, Serafini, de la Torre, & Tessier-Lavigne, 1994; Serafini et al., 1996), involvement of neuronal migration (Alcántara, Ruiz, De Castro, Soriano, & Sotelo, 2000; Kawasaki, Ito, & Hirata, 2006; S. Yamagishi, Bando, & Sato, 2020) and glial development (Jarjour et al., 2003; Rajasekharan et al., 2009; Tsai, Tessier-Lavigne, & Miller, 2003), Netrin-1 also plays an important part in regulating angiogenesis (Castets & Mehlen, 2010), inflammation (Rosenberger et al., 2009) and tumorigenesis (Arakawa, 2004; Mehlen & Furne, 2005; Paradisi & Mehlen, 2010). To exert its biological functions, Netrin-1 binds to several receptors, including deleted in colorectal cancer (DCC) (Keino-Masu et al., 1996), the DCC orthologue neogenin (NEO1) (Wilson & Key, 2007), the UNC5 orthologues, Down syndrome cell adhesion molecule (DSCAM) (G. Liu et al., 2009; Ly et al., 2008), and Cluster of differentiation 146 (CD146) (Tu et al., 2015). Notably, the tumor suppressor gene *DCC*, is localized on chromosome 18q, where frequent deletions are observed in CRC (Fearon et al., 1990), and is down-regulated in more than half of CRCs (Mehlen & Fearon, 2004). Contrary to the effect of Netrin-1, DCC acts as an effective inhibitor of cell invasion, tumor growth and metastasis (Rodrigues, De Wever, Bruyneel, Rooney, & Gespach, 2007), and limits the progression of intestinal tumors in mouse models (Castets et al., 2011). DCC regulates apoptosis as a dependency receptor (Mehlen et al., 1998): it suppresses cell apoptosis when engaged by Netrin-1, while it triggers apoptosis in the absence of Netrin-1. Therefore, *DCC* represents a conditional tumor suppressor. Abnormal expression of Netrin-1 was detected in multiple

cancers, including metastatic breast cancer (Fitamant et al., 2008), non-small cell lung cancer (X. Zhang et al., 2018), and pancreatic ductal adenocarcinoma (Dumartin et al., 2010) as well as CRC (Nakayama et al., 2022). Netrin-1 is involved in the maintenance and renewal of intestinal epithelium, and controls intestinal tumor formation and progression (Mazelin et al., 2004; Paradisi et al., 2009). The anti-apoptotic signal mediated by Netrin-1 may inhibit p53-induced apoptosis, and p53 is directly involved in the transcriptional regulation of Netrin-1 and its receptors (Arakawa, 2004, 2005; Tanikawa, Matsuda, Fukuda, Nakamura, & Arakawa, 2003). Furthermore, Netrin-1 regulates cancer cell motility and tumorigenesis via multiple pathways, including YAP signaling (Qi, Li, Luo, Guan, & Ye, 2015), ERK/MAPK signaling (Shimizu et al., 2013; K. Yin et al., 2018) and Notch signaling (Ylivinkka et al., 2013). Interestingly, protein kinase A (PKA), Rho/ROCK and PI3K-dependent pathways are intimately involved in pro-invasive activity induced by Netrin-1 in CRC (Rodrigues et al., 2007), and Netrin-1 up-regulation mediated by activation of the NF- κ B pathway inhibits the pro-apoptotic effect of the Netrin-1 receptors (Paradisi et al., 2008; Paradisi et al., 2009). Therefore, the down-regulation of Netrin-1 by miR-34a may inhibit multiple pro-tumorigenic pathways in CRC.

Transgelin, also named *WS3-10* and *SM22-Alpha*, is a gene encoding a cell shape-change and transformation-sensitive protein that belongs to the calponin family (Assinder, Stanton, & Prasad, 2009; Camoretti-Mercado et al., 1998; Shapland, Hsuan, Totty, & Lawson, 1993). It was first identified in smooth muscle cells (Lees-Miller, Heeley, Smillie, & Kay, 1987), and also found to be broadly expressed across other tissues, such as colon, endometrium, urinary bladder, prostate and stomach (Assinder et al., 2009; Dos Santos Hidalgo, Meola, Rosa, Paro de Paz, & Ferriani, 2011; Elsafadi et al., 2020). *Transgelin*, as a

member of actin-binding proteins (ABPs), is localized in the protoplasm. It is known as a typical marker of smooth muscle cells (Lees-Miller et al., 1987; L. Li, Miano, Cserjesi, & Olson, 1996), and also found to be expressed in other types of cells, including epithelial cells (Kunzmann, Ottensmeier, Speer, & Fehrholz, 2018; H. Yu et al., 2008), skeletal stem cells (Elsafadi et al., 2016), vascular endothelial cells (Cevallos et al., 2006; Tsuji-Tamura, Morino-Koga, Suzuki, & Ogawa, 2021), and fibroblasts (Lawson, Harrison, & Shapland, 1997; R. Liu, Hossain, Chen, & Jin, 2017). TAGLN is not only involved in vascular contraction (Je & Sohn, 2007; Xie et al., 2015; Zeidan et al., 2004), cell differentiation (Elsafadi et al., 2016; Pérot et al., 2014; Robin et al., 2013) and angiogenesis (Tsuji-Tamura et al., 2021), but has also been implicated in cellular transformation and tumor-related processes (Dvorakova et al., 2014), such as cell apoptosis (Mutalip et al., 2014), tumor growth (Fu, Wang, & Yue, 2020), proliferation and invasion (Tsui et al., 2019; Yang et al., 2021). TAGLN represents a promising diagnostic and prognostic biomarker and is a potential therapeutic target in multiple cancers, such as triple negative breast cancer (Rao et al., 2015), gastric adenocarcinoma (Huang et al., 2008), and ovarian cancer (Meagher et al., 2022; Wei et al., 2021) as well as colorectal cancer (Elsafadi et al., 2020; Y. Lin et al., 2009). In CRC, TAGLN might be involved in driving cancer progression as its expression increases with tumor stage, and high expression of TAGLN indicated a worse overall survival and decreased disease-free survival in CRC patients (Elsafadi et al., 2020). Furthermore, increased levels of TAGLN were found in node-positive CRCs and might therefore represent a candidate biomarker of node status in CRC (Y. Lin et al., 2009). In addition, enhanced expression of TAGLN correlates with aggressive tumor behaviors in CRC, it could promote cell proliferation, migration, growth and colony formation (Elsafadi et al., 2020). And

TAGLN, as one of cytoskeletal associated proteins, is also closely related to EMT and the metastasis of CRC (J. Liu, Zhang, Li, & Wang, 2020; Zhong et al., 2020; H. M. Zhou et al., 2016; Y. Zhou et al., 2020). Mechanistically, TAGLN has been reported to be a TGF β -inducible gene (S. Chen, Kulik, & Lechleider, 2003; Elsafadi et al., 2016; Qiu, Feng, & Li, 2003; H. Yu et al., 2008). And upregulation of TAGLN is mainly mediated by TGF β signaling, which is mediated through the Rho-MRTF-SRF signaling and Smad-dependent signaling pathways (Cevallos et al., 2006; S. Chen et al., 2003; Yokota et al., 2016). In CRC, altered expression of TAGLN could facilitate TGF β -induced tumor growth, migration and invasion (Elsafadi et al., 2020; Y. Zhou et al., 2020). In addition, transgelin could promote the progression and metastasis of CRC via the Rho signaling (Lew et al., 2020), as well as AKT and JNK signaling pathways (H. Zhou, Zhang, Chen, & Lin, 2016). Repression of transgelin may therefore mediate the tumor suppressive effects of miR-34a in CRC.

In summary, the present study shows that *Csf1r* is a central mediator of the effects of *Mir34a* loss on the intestinal tumor phenotypes. In addition, it provides genetic evidence for the functional relevance of the deregulation of the *Mir34a/Csf1r* double-negative feedback loop during intestinal tumorigenesis (**Figure 37**) (F. Liu et al., 2022). The findings suggest that *Csf1r* could serve as an effective and promising target in treating CRCs with defects in the p53/miR-34a pathway. Since epigenetic silencing of *miR-34a* was found in 75% of CRCs (Vogt et al., 2011), the combination of miR-34a restoration and CSF1R inhibition may be a viable therapeutic option for a significant number of CRC patients in the future.

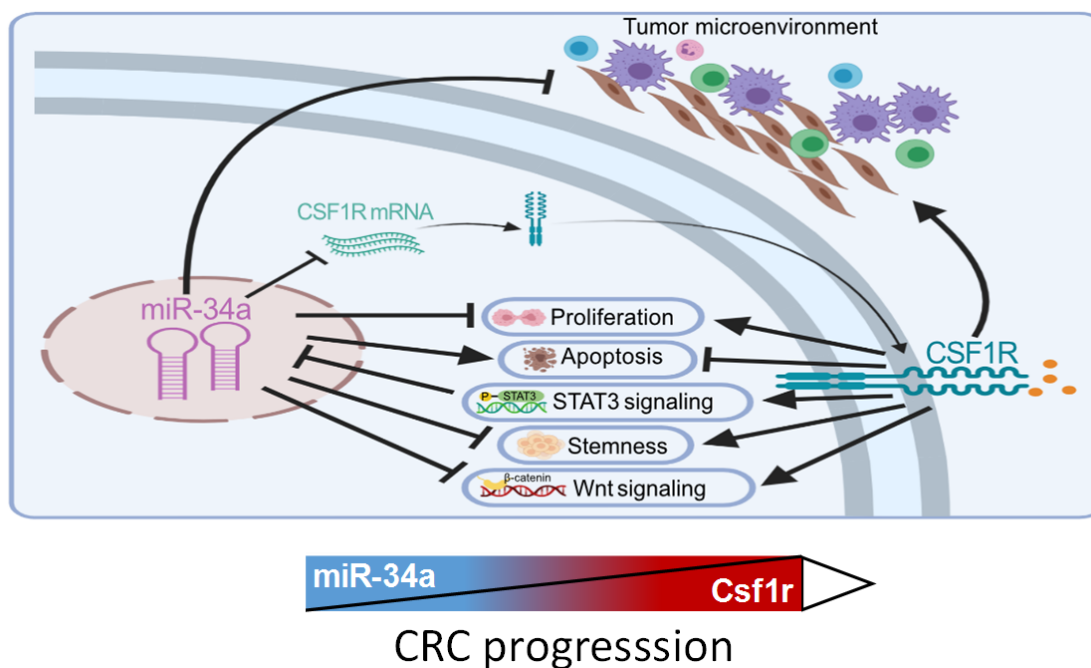


Figure 37. Summarizing model of the Mir34a/Csf1r double-negative feedback loop during intestinal tumorigenesis. During intestinal tumor formation, Csf1r up-regulation caused by *Mir34a* inactivation is a major mediator of the pro-tumorigenic effects of *Mir34a* loss. It mediates proliferation, stemness, Wnt signaling, and modulates the tumor microenvironment. Csf1r and Mir34a exert opposite effects on STAT3 signaling. Taken together, the results show that Csf1r is an important mediator of the effects of *Mir34a* inactivation on intestinal tumorigenesis. Activating or inhibiting effects of miR-34a and CSF1R are indicated by arrows and rectangles, respectively.

6. References

- Abancens, M., Bustos, V., Harvey, H., McBryan, J., & Harvey, B. J. (2020). Sexual Dimorphism in Colon Cancer. *Front Oncol*, *10*, 607909. doi:10.3389/fonc.2020.607909
- Abd-Aziz, N., Kamaruzman, N. I., & Poh, C. L. (2020). Development of MicroRNAs as Potential Therapeutics against Cancer. *J Oncol*, *2020*, 8029721. doi:10.1155/2020/8029721
- Abeykoon, J. P., Lasho, T. L., Dasari, S., Rech, K. L., Ranatunga, W. K., Manske, M. K., . . . Go, R. S. (2022). Sustained, complete response to pexidartinib in a patient with CSF1R-mutated Erdheim-Chester disease. *Am J Hematol*, *97*(3), 293-302. doi:10.1002/ajh.26441
- Abu-Duhier, F. M., Goodeve, A. C., Care, R. S., Gari, M., Wilson, G. A., Peake, I. R., & Reilly, J. T. (2003). Mutational analysis of class III receptor tyrosine kinases (C-KIT, C-FMS, FLT3) in idiopathic myelofibrosis. *Br J Haematol*, *120*(3), 464-470. doi:10.1046/j.1365-2141.2003.04108.x
- Agarwal, V., Bell, G. W., Nam, J. W., & Bartel, D. P. (2015). Predicting effective microRNA target sites in mammalian mRNAs. *Elife*, *4*. doi:10.7554/eLife.05005
- Ahmed, F. E. (2006). Gene-gene, gene-environment & multiple interactions in colorectal cancer. *J Environ Sci Health C Environ Carcinog Ecotoxicol Rev*, *24*(1), 1-101. doi:10.1080/10590500600614295
- Aihara, H., Kumar, N., & Thompson, C. C. (2014). Diagnosis, surveillance, and treatment strategies for familial adenomatous polyposis: rationale and update. *Eur J Gastroenterol Hepatol*, *26*(3), 255-262. doi:10.1097/meg.0000000000000010
- Akcora, D., Huynh, D., Lightowler, S., Germann, M., Robine, S., de May, J. R., . . . Ramsay, R. G. (2013). The CSF-1 receptor fashions the intestinal stem cell niche. *Stem Cell Res*, *10*(2), 203-212. doi:10.1016/j.scr.2012.12.001
- Al-Tassan, N., Chmiel, N. H., Maynard, J., Fleming, N., Livingston, A. L., Williams, G. T., . . . Cheadle, J. P. (2002). Inherited variants of MYH associated with somatic G:C-->T:A mutations in colorectal tumors. *Nat Genet*, *30*(2), 227-232. doi:10.1038/ng828
- Alcántara, S., Ruiz, M., De Castro, F., Soriano, E., & Sotelo, C. (2000). Netrin 1 acts as an attractive or as a repulsive cue for distinct migrating neurons during the development of the cerebellar system. *Development*, *127*(7), 1359-1372. doi:10.1242/dev.127.7.1359
- Amersi, F., Agustin, M., & Ko, C. Y. (2005). Colorectal cancer: epidemiology, risk factors, and health services. *Clin Colon Rectal Surg*, *18*(3), 133-140. doi:10.1055/s-2005-916274
- Arakawa, H. (2004). Netrin-1 and its receptors in tumorigenesis. *Nat Rev Cancer*, *4*(12), 978-987. doi:10.1038/nrc1504
- Arakawa, H. (2005). p53, apoptosis and axon-guidance molecules. *Cell Death Differ*, *12*(8), 1057-1065. doi:10.1038/sj.cdd.4401601

- Arnold, A., Tronser, M., Sers, C., Ahadova, A., Endris, V., Mamlouk, S., . . . Bläker, H. (2020). The majority of β -catenin mutations in colorectal cancer is homozygous. *BMC Cancer*, *20*(1), 1038. doi:10.1186/s12885-020-07537-2
- Arnold, M., Sierra, M. S., Laversanne, M., Soerjomataram, I., Jemal, A., & Bray, F. (2017). Global patterns and trends in colorectal cancer incidence and mortality. *Gut*, *66*(4), 683-691. doi:10.1136/gutjnl-2015-310912
- Arreola, M. A., Soni, N., Crapser, J. D., Hohsfield, L. A., Elmore, M. R. P., Matheos, D. P., . . . Green, K. N. (2021). Microglial dyshomeostasis drives perineuronal net and synaptic loss in a CSF1R(+/-) mouse model of ALSP, which can be rescued via CSF1R inhibitors. *Sci Adv*, *7*(35). doi:10.1126/sciadv.abg1601
- Assinder, S. J., Stanton, J. A., & Prasad, P. D. (2009). Transgelin: an actin-binding protein and tumour suppressor. *Int J Biochem Cell Biol*, *41*(3), 482-486. doi:10.1016/j.biocel.2008.02.011
- Azzani, M., Roslani, A. C., & Su, T. T. (2016). Financial burden of colorectal cancer treatment among patients and their families in a middle-income country. *Support Care Cancer*, *24*(10), 4423-4432. doi:10.1007/s00520-016-3283-2
- Bader, A. G., Brown, D., Stoudemire, J., & Lammers, P. (2011). Developing therapeutic microRNAs for cancer. *Gene Ther*, *18*(12), 1121-1126. doi:10.1038/gt.2011.79
- Baghdadi, M., Endo, H., Takano, A., Ishikawa, K., Kameda, Y., Wada, H., . . . Seino, K. I. (2018). High co-expression of IL-34 and M-CSF correlates with tumor progression and poor survival in lung cancers. *Sci Rep*, *8*(1), 418. doi:10.1038/s41598-017-18796-8
- Bailey, C. E., Hu, C. Y., You, Y. N., Bednarski, B. K., Rodriguez-Bigas, M. A., Skibber, J. M., . . . Chang, G. J. (2015). Increasing disparities in the age-related incidences of colon and rectal cancers in the United States, 1975-2010. *JAMA Surg*, *150*(1), 17-22. doi:10.1001/jamasurg.2014.1756
- Baker, S. J., Fearon, E. R., Nigro, J. M., Hamilton, S. R., Preisinger, A. C., Jessup, J. M., . . . Vogelstein, B. (1989). Chromosome 17 deletions and p53 gene mutations in colorectal carcinomas. *Science*, *244*(4901), 217-221. doi:10.1126/science.2649981
- Barker, N., Ridgway, R. A., van Es, J. H., van de Wetering, M., Begthel, H., van den Born, M., . . . Clevers, H. (2009). Crypt stem cells as the cells-of-origin of intestinal cancer. *Nature*, *457*(7229), 608-611. doi:10.1038/nature07602
- Barretina, J., Caponigro, G., Stransky, N., Venkatesan, K., Margolin, A. A., Kim, S., . . . Garraway, L. A. (2012). The Cancer Cell Line Encyclopedia enables predictive modelling of anticancer drug sensitivity. *Nature*, *483*(7391), 603-607. doi:10.1038/nature11003
- Beckman, R. A., & Loeb, L. A. (2005). Genetic instability in cancer: theory and experiment. *Semin Cancer Biol*, *15*(6), 423-435. doi:10.1016/j.semcan.2005.06.007

- Bibbins-Domingo, K., Grossman, D. C., Curry, S. J., Davidson, K. W., Epling, J. W., Jr., García, F. A. R., . . . Siu, A. L. (2016). Screening for Colorectal Cancer: US Preventive Services Task Force Recommendation Statement. *Jama*, *315*(23), 2564-2575. doi:10.1001/jama.2016.5989
- Bienz, M., & Clevers, H. (2000). Linking colorectal cancer to Wnt signaling. *Cell*, *103*(2), 311-320. doi:10.1016/S0092-8674(00)00122-7
- Bishehsari, F., Mahdavinia, M., Vacca, M., Malekzadeh, R., & Mariani-Costantini, R. (2014). Epidemiological transition of colorectal cancer in developing countries: environmental factors, molecular pathways, and opportunities for prevention. *World J Gastroenterol*, *20*(20), 6055-6072. doi:10.3748/wjg.v20.i20.6055
- Bommer, G. T., Gerin, I., Feng, Y., Kaczorowski, A. J., Kuick, R., Love, R. E., . . . Fearon, E. R. (2007). p53-mediated activation of miRNA34 candidate tumor-suppressor genes. *Curr Biol*, *17*(15), 1298-1307. doi:10.1016/j.cub.2007.06.068
- Bos, J. L., Fearon, E. R., Hamilton, S. R., Verlaan-de Vries, M., van Boom, J. H., van der Eb, A. J., & Vogelstein, B. (1987). Prevalence of ras gene mutations in human colorectal cancers. *Nature*, *327*(6120), 293-297. doi:10.1038/327293a0
- Brisset, M., Grandin, M., Bernet, A., Mehlen, P., & Hollande, F. (2021). Dependence receptors: new targets for cancer therapy. *EMBO Mol Med*, *13*(11), e14495. doi:10.15252/emmm.202114495
- Broutier, L., Andersson-Rolf, A., Hindley, C. J., Boj, S. F., Clevers, H., Koo, B. K., & Huch, M. (2016). Culture and establishment of self-renewing human and mouse adult liver and pancreas 3D organoids and their genetic manipulation. *Nat Protoc*, *11*(9), 1724-1743. doi:10.1038/nprot.2016.097
- Bu, P., Wang, L., Chen, K. Y., Srinivasan, T., Murthy, P. K., Tung, K. L., . . . Shen, X. (2016). A miR-34a-Numb Feedforward Loop Triggered by Inflammation Regulates Asymmetric Stem Cell Division in Intestine and Colon Cancer. *Cell Stem Cell*, *18*(2), 189-202. doi:10.1016/j.stem.2016.01.006
- Buc, E., Kwiatkowski, F., Alves, A., Panis, Y., Manton, G., & Slim, K. (2006). Tobacco smoking: a factor of early onset of colorectal cancer. *Dis Colon Rectum*, *49*(12), 1893-1896. doi:10.1007/s10350-006-0704-1
- Burridge, K., & Wennerberg, K. (2004). Rho and Rac take center stage. *Cell*, *116*(2), 167-179. doi:10.1016/s0092-8674(04)00003-0
- Bürtin, F., Mullins, C. S., & Linnebacher, M. (2020). Mouse models of colorectal cancer: Past, present and future perspectives. *World J Gastroenterol*, *26*(13), 1394-1426. doi:10.3748/wjg.v26.i13.1394
- Byrne, P. V., Guilbert, L. J., & Stanley, E. R. (1981). Distribution of cells bearing receptors for a colony-stimulating factor (CSF-1) in murine tissues. *J Cell Biol*, *91*(3 Pt 1), 848-853. doi:10.1083/jcb.91.3.848
- Byrne, R. M., & Tsikitis, V. L. (2018). Colorectal polyposis and inherited colorectal cancer syndromes. *Ann Gastroenterol*, *31*(1), 24-34. doi:10.20524/aog.2017.0218
- Camoretti-Mercado, B., Forsythe, S. M., LeBeau, M. M., Espinosa, R., 3rd, Vieira, J. E., Halayko, A. J., . . . Solway, J. (1998). Expression and cytogenetic

- localization of the human SM22 gene (TAGLN). *Genomics*, 49(3), 452-457. doi:10.1006/geno.1998.5267
- Campa, C. C., Ciraolo, E., Ghigo, A., Germena, G., & Hirsch, E. (2015). Crossroads of PI3K and Rac pathways. *Small GTPases*, 6(2), 71-80. doi:10.4161/21541248.2014.989789
- Cancer Genome Atlas, N. (2012). Comprehensive molecular characterization of human colon and rectal cancer. *Nature*, 487(7407), 330-337. doi:10.1038/nature11252
- Cannarile, M. A., Weisser, M., Jacob, W., Jegg, A. M., Ries, C. H., & Rüttinger, D. (2017). Colony-stimulating factor 1 receptor (CSF1R) inhibitors in cancer therapy. *J Immunother Cancer*, 5(1), 53. doi:10.1186/s40425-017-0257-y
- Caputo, F., Santini, C., Bardasi, C., Cerma, K., Casadei-Gardini, A., Spallanzani, A., . . . Gelsomino, F. (2019). BRAF-Mutated Colorectal Cancer: Clinical and Molecular Insights. *Int J Mol Sci*, 20(21). doi:10.3390/ijms20215369
- Carroll, K. L., Frugé, A. D., Heslin, M. J., Lipke, E. A., & Greene, M. W. (2022). Diet as a Risk Factor for Early-Onset Colorectal Adenoma and Carcinoma: A Systematic Review. *Front Nutr*, 9, 896330. doi:10.3389/fnut.2022.896330
- Cassetta, L., & Pollard, J. W. (2018). Targeting macrophages: therapeutic approaches in cancer. *Nat Rev Drug Discov*, 17(12), 887-904. doi:10.1038/nrd.2018.169
- Castets, M., Broutier, L., Molin, Y., Brevet, M., Chazot, G., Gadot, N., . . . Mehlen, P. (2011). DCC constrains tumour progression via its dependence receptor activity. *Nature*, 482(7386), 534-537. doi:10.1038/nature10708
- Castets, M., & Mehlen, P. (2010). Netrin-1 role in angiogenesis: to be or not to be a pro-angiogenic factor? *Cell Cycle*, 9(8), 1466-1471. doi:10.4161/cc.9.8.11197
- Catalano, V., Turdo, A., Di Franco, S., Dieli, F., Todaro, M., & Stassi, G. (2013). Tumor and its microenvironment: a synergistic interplay. *Semin Cancer Biol*, 23(6 Pt B), 522-532. doi:10.1016/j.semcancer.2013.08.007
- Cathomas, G. (2014). PIK3CA in Colorectal Cancer. *Front Oncol*, 4, 35. doi:10.3389/fonc.2014.00035
- Cevallos, M., Riha, G. M., Wang, X., Yang, H., Yan, S., Li, M., . . . Chen, C. (2006). Cyclic strain induces expression of specific smooth muscle cell markers in human endothelial cells. *Differentiation*, 74(9-10), 552-561. doi:10.1111/j.1432-0436.2006.00089.x
- Chambers, S. K., Kacinski, B. M., Ivins, C. M., & Carcangiu, M. L. (1997). Overexpression of epithelial macrophage colony-stimulating factor (CSF-1) and CSF-1 receptor: a poor prognostic factor in epithelial ovarian cancer, contrasted with a protective effect of stromal CSF-1. *Clin Cancer Res*, 3(6), 999-1007.
- Chang, T. C., Wentzel, E. A., Kent, O. A., Ramachandran, K., Mullendore, M., Lee, K. H., . . . Mendell, J. T. (2007). Transactivation of miR-34a by p53 broadly influences gene expression and promotes apoptosis. *Mol Cell*, 26(5), 745-752. doi:10.1016/j.molcel.2007.05.010

- Chen, S., Kulik, M., & Lechleider, R. J. (2003). Smad proteins regulate transcriptional induction of the SM22alpha gene by TGF-beta. *Nucleic Acids Res*, 31(4), 1302-1310. doi:10.1093/nar/gkg224
- Chen, W. S., Chen, J. Y., Liu, J. M., Lin, W. C., King, K. L., Whang-Peng, J., & Yang, W. K. (1997). Microsatellite instability in sporadic-colon-cancer patients with and without liver metastases. *Int J Cancer*, 74(4), 470-474. doi:10.1002/(sici)1097-0215(19970822)74:4<470::aid-ijc20>3.0.co;2-c
- Cheng, C. Y., Hwang, C. I., Corney, D. C., Flesken-Nikitin, A., Jiang, L., Öner, G. M., . . . Nikitin, A. Y. (2014). miR-34 cooperates with p53 in suppression of prostate cancer by joint regulation of stem cell compartment. *Cell Rep*, 6(6), 1000-1007. doi:10.1016/j.celrep.2014.02.023
- Cheng, M., Bhujwala, Z. M., & Glunde, K. (2016). Targeting Phospholipid Metabolism in Cancer. *Front Oncol*, 6, 266. doi:10.3389/fonc.2016.00266
- Chim, C. S., Wong, K. Y., Qi, Y., Loong, F., Lam, W. L., Wong, L. G., . . . Liang, R. (2010). Epigenetic inactivation of the miR-34a in hematological malignancies. *Carcinogenesis*, 31(4), 745-750. doi:10.1093/carcin/bgq033
- Claro, V., & Ferro, A. (2020). Netrin-1: Focus on its role in cardiovascular physiology and atherosclerosis. *JRSM Cardiovasc Dis*, 9, 2048004020959574. doi:10.1177/2048004020959574
- Concepcion, C. P., Han, Y. C., Mu, P., Bonetti, C., Yao, E., D'Andrea, A., . . . Ventura, A. (2012). Intact p53-dependent responses in miR-34-deficient mice. *PLoS Genet*, 8(7), e1002797. doi:10.1371/journal.pgen.1002797
- De Robertis, M., Massi, E., Poeta, M. L., Carotti, S., Morini, S., Cecchetelli, L., . . . Fazio, V. M. (2011). The AOM/DSS murine model for the study of colon carcinogenesis: From pathways to diagnosis and therapy studies. *J Carcinog*, 10, 9. doi:10.4103/1477-3163.78279
- Dos Santos Hidalgo, G., Meola, J., Rosa, E. S. J. C., Paro de Paz, C. C., & Ferriani, R. A. (2011). TAGLN expression is deregulated in endometriosis and may be involved in cell invasion, migration, and differentiation. *Fertil Steril*, 96(3), 700-703. doi:10.1016/j.fertnstert.2011.06.052
- Dumartin, L., Quemener, C., Laklai, H., Herbert, J., Bicknell, R., Bousquet, C., . . . Hagedorn, M. (2010). Netrin-1 mediates early events in pancreatic adenocarcinoma progression, acting on tumor and endothelial cells. *Gastroenterology*, 138(4), 1595-1606, 1606.e1591-1598. doi:10.1053/j.gastro.2009.12.061
- Dvorakova, M., Nenutil, R., & Bouchal, P. (2014). Transgelins, cytoskeletal proteins implicated in different aspects of cancer development. *Expert Rev Proteomics*, 11(2), 149-165. doi:10.1586/14789450.2014.860358
- Dweep, H., & Gretz, N. (2015). miRWalk2.0: a comprehensive atlas of microRNA-target interactions. *Nat Methods*, 12(8), 697. doi:10.1038/nmeth.3485
- Dwyer, A. R., Greenland, E. L., & Pixley, F. J. (2017). Promotion of Tumor Invasion by Tumor-Associated Macrophages: The Role of CSF-1-Activated Phosphatidylinositol 3 Kinase and Src Family Kinase Motility Signaling. *Cancers (Basel)*, 9(6). doi:10.3390/cancers9060068

- Ebi, H., Costa, C., Faber, A. C., Nishtala, M., Kotani, H., Juric, D., . . . Engelman, J. A. (2013). PI3K regulates MEK/ERK signaling in breast cancer via the Rac-GEF, P-Rex1. *Proc Natl Acad Sci U S A*, *110*(52), 21124-21129. doi:10.1073/pnas.1314124110
- el Marjou, F., Janssen, K. P., Chang, B. H., Li, M., Hindie, V., Chan, L., . . . Robine, S. (2004). Tissue-specific and inducible Cre-mediated recombination in the gut epithelium. *Genesis*, *39*(3), 186-193. doi:10.1002/gene.20042
- Elsafadi, M., Manikandan, M., Almalki, S., Mahmood, A., Shinwari, T., Vishnubalaji, R., . . . Alajez, N. M. (2020). Transgelin is a poor prognostic factor associated with advanced colorectal cancer (CRC) stage promoting tumor growth and migration in a TGF β -dependent manner. *Cell Death Dis*, *11*(5), 341. doi:10.1038/s41419-020-2529-6
- Elsafadi, M., Manikandan, M., Dawud, R. A., Alajez, N. M., Hamam, R., Alfayez, M., . . . Mahmood, A. (2016). Transgelin is a TGF β -inducible gene that regulates osteoblastic and adipogenic differentiation of human skeletal stem cells through actin cytoskeleton organization. *Cell Death Dis*, *7*(8), e2321. doi:10.1038/cddis.2016.196
- Esnault, C., Stewart, A., Gualdrini, F., East, P., Horswell, S., Matthews, N., & Treisman, R. (2014). Rho-actin signaling to the MRTF coactivators dominates the immediate transcriptional response to serum in fibroblasts. *Genes Dev*, *28*(9), 943-958. doi:10.1101/gad.239327.114
- Fang, J. Y., & Richardson, B. C. (2005). The MAPK signalling pathways and colorectal cancer. *Lancet Oncol*, *6*(5), 322-327. doi:10.1016/s1470-2045(05)70168-6
- Fearon, E. R., Cho, K. R., Nigro, J. M., Kern, S. E., Simons, J. W., Ruppert, J. M., . . . et al. (1990). Identification of a chromosome 18q gene that is altered in colorectal cancers. *Science*, *247*(4938), 49-56. doi:10.1126/science.2294591
- Fearon, E. R., & Vogelstein, B. (1990). A genetic model for colorectal tumorigenesis. *Cell*, *61*(5), 759-767. doi:10.1016/0092-8674(90)90186-i
- Finbloom, D. S., & Larner, A. C. (1995). Regulation of the Jak/STAT signalling pathway. *Cell Signal*, *7*(8), 739-745. doi:10.1016/0898-6568(95)02004-7
- Fitamant, J., Guenebeaud, C., Coissieux, M. M., Guix, C., Treilleux, I., Scoazec, J. Y., . . . Mehlen, P. (2008). Netrin-1 expression confers a selective advantage for tumor cell survival in metastatic breast cancer. *Proc Natl Acad Sci U S A*, *105*(12), 4850-4855. doi:10.1073/pnas.0709810105
- Fu, J., Wang, X., & Yue, Q. (2020). Functional loss of TAGLN inhibits tumor growth and increases chemosensitivity of non-small cell lung cancer. *Biochem Biophys Res Commun*, *529*(4), 1086-1093. doi:10.1016/j.bbrc.2020.06.066
- Galiatsatos, P., & Foulkes, W. D. (2006). Familial adenomatous polyposis. *Am J Gastroenterol*, *101*(2), 385-398. doi:10.1111/j.1572-0241.2006.00375.x
- Gao, J., Li, N., Dong, Y., Li, S., Xu, L., Li, X., . . . Yu, J. (2015). miR-34a-5p suppresses colorectal cancer metastasis and predicts recurrence in patients with stage II/III colorectal cancer. *Oncogene*, *34*(31), 4142-4152. doi:10.1038/onc.2014.348

- Gau, D., & Roy, P. (2018). SRF'ing and SAP'ing - the role of MRTF proteins in cell migration. *J Cell Sci*, 131(19). doi:10.1242/jcs.218222
- Gérard, C., De Mot, L., Cordi, S., van Eyll, J., & Lemaigre, F. P. (2021). Temporal dynamics of a CSF1R signaling gene regulatory network involved in epilepsy. *PLoS Comput Biol*, 17(4), e1008854. doi:10.1371/journal.pcbi.1008854
- Goulding, H., Pinder, S., Cannon, P., Pearson, D., Nicholson, R., Snead, D., . . . et al. (1995). A new immunohistochemical antibody for the assessment of estrogen receptor status on routine formalin-fixed tissue samples. *Hum Pathol*, 26(3), 291-294. doi:10.1016/0046-8177(95)90060-8
- Gregorieff, A., & Clevers, H. (2010). In situ hybridization to identify gut stem cells. *Curr Protoc Stem Cell Biol*, Chapter 2, Unit 2F.1. doi:10.1002/9780470151808.sc02f01s12
- Gu, W. J., Pei, J. P., Lyu, J., Akimoto, N., Haruki, K., Ogino, S., & Zhang, C. D. (2022). The Burden of Early-Onset Colorectal Cancer and Its Risk Factors from 1990 to 2019: A Systematic Analysis for the Global Burden of Disease Study 2019. *Cancers (Basel)*, 14(14). doi:10.3390/cancers14143502
- Guan, H., Wang, X., Song, Y., Gao, P., Li, Y., Wu, Z., . . . Wang, Z. (2021). Is CSF1R Expression Localization Crucial for its Prognostic Value in Colorectal Cancer? *Appl Immunohistochem Mol Morphol*, 29(1), 68-75. doi:10.1097/pai.0000000000000844
- Guilbert, L. J., & Stanley, E. R. (1980). Specific interaction of murine colony-stimulating factor with mononuclear phagocytic cells. *J Cell Biol*, 85(1), 153-159. doi:10.1083/jcb.85.1.153
- Guinney, J., Dienstmann, R., Wang, X., de Reyniès, A., Schlicker, A., Soneson, C., . . . Tejpar, S. (2015). The consensus molecular subtypes of colorectal cancer. *Nat Med*, 21(11), 1350-1356. doi:10.1038/nm.3967
- Guiu, J., & Jensen, K. B. (2021). Counter Piece to Organoid vs Mouse Models: Which is a Better Research Tool.... *Cell Mol Gastroenterol Hepatol*. doi:10.1016/j.jcmgh.2021.09.011
- Guo, Y. J., Pan, W. W., Liu, S. B., Shen, Z. F., Xu, Y., & Hu, L. L. (2020). ERK/MAPK signalling pathway and tumorigenesis. *Exp Ther Med*, 19(3), 1997-2007. doi:10.3892/etm.2020.8454
- Halberg, R. B., Waggoner, J., Rasmussen, K., White, A., Clipson, L., Prunuske, A. J., . . . Dove, W. F. (2009). Long-lived Min mice develop advanced intestinal cancers through a genetically conservative pathway. *Cancer Res*, 69(14), 5768-5775. doi:10.1158/0008-5472.can-09-0446
- Half, E., Bercovich, D., & Rozen, P. (2009). Familial adenomatous polyposis. *Orphanet J Rare Dis*, 4, 22. doi:10.1186/1750-1172-4-22
- Halling, K. C., Harper, J., Moskaluk, C. A., Thibodeau, S. N., Petroni, G. R., Yustein, A. S., . . . Powell, S. M. (1999). Origin of microsatellite instability in gastric cancer. *Am J Pathol*, 155(1), 205-211. doi:10.1016/s0002-9440(10)65114-0

- He, L., He, X., Lim, L. P., de Stanchina, E., Xuan, Z., Liang, Y., . . . Hannon, G. J. (2007). A microRNA component of the p53 tumour suppressor network. *Nature*, *447*(7148), 1130-1134. doi:10.1038/nature05939
- He, R., Liu, P., Xie, X., Zhou, Y., Liao, Q., Xiong, W., . . . Tang, H. (2017). circGFRA1 and GFRA1 act as ceRNAs in triple negative breast cancer by regulating miR-34a. *J Exp Clin Cancer Res*, *36*(1), 145. doi:10.1186/s13046-017-0614-1
- Henderson, R. H., French, D., Maughan, T., Adams, R., Allemani, C., Minicozzi, P., . . . Lawler, M. (2021). The economic burden of colorectal cancer across Europe: a population-based cost-of-illness study. *Lancet Gastroenterol Hepatol*, *6*(9), 709-722. doi:10.1016/s2468-1253(21)00147-3
- Hermeking, H. (2007). p53 enters the microRNA world. *Cancer Cell*, *12*(5), 414-418. doi:10.1016/j.ccr.2007.10.028
- Hermeking, H. (2010). The miR-34 family in cancer and apoptosis. *Cell Death Differ*, *17*(2), 193-199. doi:10.1038/cdd.2009.56
- Hermeking, H. (2012). MicroRNAs in the p53 network: micromanagement of tumour suppression. *Nat Rev Cancer*, *12*(9), 613-626. doi:10.1038/nrc3318
- Hidalgo-Sastre, A., Lubeseder-Martellato, C., Engleitner, T., Steiger, K., Zhong, S., Deszitics, J., . . . von Figura, G. (2020). Mir34a constrains pancreatic carcinogenesis. *Sci Rep*, *10*(1), 9654. doi:10.1038/s41598-020-66561-1
- Hinshaw, D. C., & Shevde, L. A. (2019). The Tumor Microenvironment Innately Modulates Cancer Progression. *Cancer Res*, *79*(18), 4557-4566. doi:10.1158/0008-5472.can-18-3962
- Hollstein, M., Sidransky, D., Vogelstein, B., & Harris, C. C. (1991). p53 mutations in human cancers. *Science*, *253*(5015), 49-53. doi:10.1126/science.1905840
- Huang, Q., Huang, Q., Chen, W., Wang, L., Lin, W., Lin, J., & Lin, X. (2008). Identification of transgelin as a potential novel biomarker for gastric adenocarcinoma based on proteomics technology. *J Cancer Res Clin Oncol*, *134*(11), 1219-1227. doi:10.1007/s00432-008-0398-y
- Huynh, D., Akçora, D., Malaterre, J., Chan, C. K., Dai, X. M., Bertoncillo, I., . . . Ramsay, R. G. (2013). CSF-1 receptor-dependent colon development, homeostasis and inflammatory stress response. *PLoS One*, *8*(2), e56951. doi:10.1371/journal.pone.0056951
- Huynh, D., Dai, X. M., Nandi, S., Lightowler, S., Trivett, M., Chan, C. K., . . . Stanley, E. R. (2009). Colony stimulating factor-1 dependence of paneth cell development in the mouse small intestine. *Gastroenterology*, *137*(1), 136-144, 144.e131-133. doi:10.1053/j.gastro.2009.03.004
- Ide, H., Seligson, D. B., Memarzadeh, S., Xin, L., Horvath, S., Dubey, P., . . . Witte, O. N. (2002). Expression of colony-stimulating factor 1 receptor during prostate development and prostate cancer progression. *Proc Natl Acad Sci U S A*, *99*(22), 14404-14409. doi:10.1073/pnas.222537099
- Isella, C., Brundu, F., Bellomo, S. E., Galimi, F., Zanella, E., Porporato, R., . . . Bertotti, A. (2017). Selective analysis of cancer-cell intrinsic transcriptional

- traits defines novel clinically relevant subtypes of colorectal cancer. *Nat Commun*, 8, 15107. doi:10.1038/ncomms15107
- Ishibashi, H., Suzuki, T., Suzuki, S., Moriya, T., Kaneko, C., Takizawa, T., . . . Sasano, H. (2003). Sex steroid hormone receptors in human thymoma. *J Clin Endocrinol Metab*, 88(5), 2309-2317. doi:10.1210/jc.2002-021353
- Jackstadt, R., Roh, S., Neumann, J., Jung, P., Hoffmann, R., Horst, D., . . . Hermeking, H. (2013). AP4 is a mediator of epithelial-mesenchymal transition and metastasis in colorectal cancer. *J Exp Med*, 210(7), 1331-1350. doi:10.1084/jem.20120812
- Jackstadt, R., & Sansom, O. J. (2016). Mouse models of intestinal cancer. *J Pathol*, 238(2), 141-151. doi:10.1002/path.4645
- Jaeckel, S., Kaller, M., Jackstadt, R., Götz, U., Müller, S., Boos, S., . . . Hermeking, H. (2018). Ap4 is rate limiting for intestinal tumor formation by controlling the homeostasis of intestinal stem cells. *Nat Commun*, 9(1), 3573. doi:10.1038/s41467-018-06001-x
- Jarjour, A. A., Manitt, C., Moore, S. W., Thompson, K. M., Yuh, S. J., & Kennedy, T. E. (2003). Netrin-1 is a chemorepellent for oligodendrocyte precursor cells in the embryonic spinal cord. *J Neurosci*, 23(9), 3735-3744. doi:10.1523/jneurosci.23-09-03735.2003
- Je, H. D., & Sohn, U. D. (2007). SM22alpha is required for agonist-induced regulation of contractility: evidence from SM22alpha knockout mice. *Mol Cells*, 23(2), 175-181.
- Jenkins, M. A., Croitoru, M. E., Monga, N., Cleary, S. P., Cotterchio, M., Hopper, J. L., & Gallinger, S. (2006). Risk of colorectal cancer in monoallelic and biallelic carriers of MYH mutations: a population-based case-family study. *Cancer Epidemiol Biomarkers Prev*, 15(2), 312-314. doi:10.1158/1055-9965.Epi-05-0793
- Jiang, L., & Hermeking, H. (2017). miR-34a and miR-34b/c Suppress Intestinal Tumorigenesis. *Cancer Res*, 77(10), 2746-2758. doi:10.1158/0008-5472.Can-16-2183
- Kaller, M., & Hermeking, H. (2016). Interplay Between Transcription Factors and MicroRNAs Regulating Epithelial-Mesenchymal Transitions in Colorectal Cancer. *Adv Exp Med Biol*, 937, 71-92. doi:10.1007/978-3-319-42059-2_4
- Kaller, M., Liffers, S. T., Oeljeklaus, S., Kuhlmann, K., Röh, S., Hoffmann, R., . . . Hermeking, H. (2011). Genome-wide characterization of miR-34a induced changes in protein and mRNA expression by a combined pulsed SILAC and microarray analysis. *Mol Cell Proteomics*, 10(8), M111.010462. doi:10.1074/mcp.M111.010462
- Kambara, T., Whitehall, V. L., Spring, K. J., Barker, M. A., Arnold, S., Wynter, C. V., . . . Jass, J. R. (2004). Role of inherited defects of MYH in the development of sporadic colorectal cancer. *Genes Chromosomes Cancer*, 40(1), 1-9. doi:10.1002/gcc.20011
- Kawasaki, T., Ito, K., & Hirata, T. (2006). Netrin 1 regulates ventral tangential migration of guidepost neurons in the lateral olfactory tract. *Development*, 133(5), 845-853. doi:10.1242/dev.02257

- Keino-Masu, K., Masu, M., Hinck, L., Leonardo, E. D., Chan, S. S., Culotti, J. G., & Tessier-Lavigne, M. (1996). Deleted in Colorectal Cancer (DCC) encodes a netrin receptor. *Cell*, *87*(2), 175-185. doi:10.1016/s0092-8674(00)81336-7
- Kennedy, T. E., Serafini, T., de la Torre, J. R., & Tessier-Lavigne, M. (1994). Netrins are diffusible chemotropic factors for commissural axons in the embryonic spinal cord. *Cell*, *78*(3), 425-435. doi:10.1016/0092-8674(94)90421-9
- Kim, B. H., Yi, E. H., & Ye, S. K. (2016). Signal transducer and activator of transcription 3 as a therapeutic target for cancer and the tumor microenvironment. *Arch Pharm Res*, *39*(8), 1085-1099. doi:10.1007/s12272-016-0795-8
- Kim, N. H., Kim, H. S., Kim, N. G., Lee, I., Choi, H. S., Li, X. Y., . . . Weiss, S. J. (2011). p53 and microRNA-34 are suppressors of canonical Wnt signaling. *Sci Signal*, *4*(197), ra71. doi:10.1126/scisignal.2001744
- Kim, W. S., Park, C., Hong, S. K., Park, B. K., Kim, H. S., & Park, K. (2000). Microsatellite instability(MSI) in non-small cell lung cancer(NSCLC) is highly associated with transforming growth factor-beta type II receptor(TGF-beta RII) frameshift mutation. *Anticancer Res*, *20*(3a), 1499-1502.
- Kinzler, K. W., Nilbert, M. C., Su, L. K., Vogelstein, B., Bryan, T. M., Levy, D. B., . . . et al. (1991). Identification of FAP locus genes from chromosome 5q21. *Science*, *253*(5020), 661-665. doi:10.1126/science.1651562
- Kluger, H. M., Dolled-Filhart, M., Rodov, S., Kacinski, B. M., Camp, R. L., & Rimm, D. L. (2004). Macrophage colony-stimulating factor-1 receptor expression is associated with poor outcome in breast cancer by large cohort tissue microarray analysis. *Clin Cancer Res*, *10*(1 Pt 1), 173-177. doi:10.1158/1078-0432.ccr-0699-3
- Kolch, W. (2005). Coordinating ERK/MAPK signalling through scaffolds and inhibitors. *Nat Rev Mol Cell Biol*, *6*(11), 827-837. doi:10.1038/nrm1743
- Kong, F., Zhou, K., Zhu, T., Lian, Q., Tao, Y., Li, N., . . . Tang, R. (2019). Interleukin-34 mediated by hepatitis B virus X protein via CCAAT/enhancer-binding protein α contributes to the proliferation and migration of hepatoma cells. *Cell Prolif*, *52*(6), e12703. doi:10.1111/cpr.12703
- Konno, T., Kasanuki, K., Ikeuchi, T., Dickson, D. W., & Wszolek, Z. K. (2018). CSF1R-related leukoencephalopathy: A major player in primary microgliopathies. *Neurology*, *91*(24), 1092-1104. doi:10.1212/wnl.0000000000006642
- Koopman, M., Kortman, G. A., Mekenkamp, L., Ligtenberg, M. J., Hoogerbrugge, N., Antonini, N. F., . . . van Krieken, J. H. (2009). Deficient mismatch repair system in patients with sporadic advanced colorectal cancer. *Br J Cancer*, *100*(2), 266-273. doi:10.1038/sj.bjc.6604867
- Kordowski, F., Kolarova, J., Schafmayer, C., Buch, S., Goldmann, T., Marwitz, S., . . . Reiss, K. (2018). Aberrant DNA methylation of ADAMTS16 in

- colorectal and other epithelial cancers. *BMC Cancer*, 18(1), 796. doi:10.1186/s12885-018-4701-2
- Korotkevich, G., Sukhov, V., & Sergushichev, A. (2019). Fast gene set enrichment analysis. *bioRxiv*, 060012. doi:10.1101/060012
- Kovalchuk, I. (2016). Chapter 1 - Genome Stability: An Evolutionary Perspective. In I. Kovalchuk & O. Kovalchuk (Eds.), *Genome Stability* (pp. 1-18). Boston: Academic Press.
- Kunzmann, S., Ottensmeier, B., Speer, C. P., & Fehrholz, M. (2018). Effect of progesterone on Smad signaling and TGF- β /Smad-regulated genes in lung epithelial cells. *PLoS One*, 13(7), e0200661. doi:10.1371/journal.pone.0200661
- Lawson, D., Harrison, M., & Shapland, C. (1997). Fibroblast transgelin and smooth muscle SM22alpha are the same protein, the expression of which is down-regulated in many cell lines. *Cell Motil Cytoskeleton*, 38(3), 250-257. doi:10.1002/(sici)1097-0169(1997)38:3<250::aid-cm3>3.0.co;2-9
- Lee, A. W. (1999). Synergistic activation of mitogen-activated protein kinase by cyclic AMP and myeloid growth factors opposes cyclic AMP's growth-inhibitory effects. *Blood*, 93(2), 537-553.
- Lee, A. W., & States, D. J. (2000). Both src-dependent and -independent mechanisms mediate phosphatidylinositol 3-kinase regulation of colony-stimulating factor 1-activated mitogen-activated protein kinases in myeloid progenitors. *Mol Cell Biol*, 20(18), 6779-6798. doi:10.1128/mcb.20.18.6779-6798.2000
- Lees-Miller, J. P., Heeley, D. H., Smillie, L. B., & Kay, C. M. (1987). Isolation and characterization of an abundant and novel 22-kDa protein (SM22) from chicken gizzard smooth muscle. *J Biol Chem*, 262(7), 2988-2993.
- Lengauer, C., Kinzler, K. W., & Vogelstein, B. (1998). Genetic instabilities in human cancers. *Nature*, 396(6712), 643-649. doi:10.1038/25292
- Lew, Z. X., Zhou, H. M., Fang, Y. Y., Ye, Z., Zhong, W., Yang, X. Y., . . . Lin, Y. (2020). Transgelin interacts with PARP1 in human colon cancer cells. *Cancer Cell Int*, 20, 366. doi:10.1186/s12935-020-01461-y
- Li, H., Rokavec, M., Jiang, L., Horst, D., & Hermeking, H. (2017). Antagonistic Effects of p53 and HIF1A on microRNA-34a Regulation of PPP1R11 and STAT3 and Hypoxia-induced Epithelial to Mesenchymal Transition in Colorectal Cancer Cells. *Gastroenterology*, 153(2), 505-520. doi:10.1053/j.gastro.2017.04.017
- Li, J., Chen, K., Zhu, L., & Pollard, J. W. (2006). Conditional deletion of the colony stimulating factor-1 receptor (c-fms proto-oncogene) in mice. *Genesis*, 44(7), 328-335. doi:10.1002/dvg.20219
- Li, L., Miano, J. M., Cserjesi, P., & Olson, E. N. (1996). SM22 alpha, a marker of adult smooth muscle, is expressed in multiple myogenic lineages during embryogenesis. *Circ Res*, 78(2), 188-195. doi:10.1161/01.res.78.2.188
- Li, L., Zhao, G. D., Shi, Z., Qi, L. L., Zhou, L. Y., & Fu, Z. X. (2016). The Ras/Raf/MEK/ERK signaling pathway and its role in the occurrence and development of HCC. *Oncol Lett*, 12(5), 3045-3050. doi:10.3892/ol.2016.5110

- Li, M., Li, M., Yang, Y., Liu, Y., Xie, H., Yu, Q., . . . He, Q. (2020). Remodeling tumor immune microenvironment via targeted blockade of PI3K- γ and CSF-1/CSF-1R pathways in tumor associated macrophages for pancreatic cancer therapy. *J Control Release*, 321, 23-35. doi:10.1016/j.jconrel.2020.02.011
- Li, S., Wei, X., He, J., Cao, Q., Du, D., Zhan, X., . . . Sun, L. (2021). The comprehensive landscape of miR-34a in cancer research. *Cancer Metastasis Rev*, 40(3), 925-948. doi:10.1007/s10555-021-09973-3
- Li, W. J., Wang, Y., Liu, R., Kasinski, A. L., Shen, H., Slack, F. J., & Tang, D. G. (2021). MicroRNA-34a: Potent Tumor Suppressor, Cancer Stem Cell Inhibitor, and Potential Anticancer Therapeutic. *Front Cell Dev Biol*, 9, 640587. doi:10.3389/fcell.2021.640587
- Liberzon, A., Birger, C., Thorvaldsdottir, H., Ghandi, M., Mesirov, J. P., & Tamayo, P. (2015). The Molecular Signatures Database (MSigDB) hallmark gene set collection. *Cell Syst*, 1(6), 417-425. doi:10.1016/j.cels.2015.12.004
- Lin, H., Lee, E., Hestir, K., Leo, C., Huang, M., Bosch, E., . . . Williams, L. T. (2008). Discovery of a cytokine and its receptor by functional screening of the extracellular proteome. *Science*, 320(5877), 807-811. doi:10.1126/science.1154370
- Lin, X., Lin, B.-w., Chen, X.-l., Zhang, B.-l., Xiao, X.-j., Shi, J.-s., . . . Chen, X. (2017). PAI-1/PIAS3/Stat3/miR-34a forms a positive feedback loop to promote EMT-mediated metastasis through Stat3 signaling in Non-small cell lung cancer. *Biochem Biophys Res Commun*, 493(4), 1464-1470.
- Lin, Y., Buckhaults, P. J., Lee, J. R., Xiong, H., Farrell, C., Podolsky, R. H., . . . Dynan, W. S. (2009). Association of the actin-binding protein transgelin with lymph node metastasis in human colorectal cancer. *Neoplasia*, 11(9), 864-873. doi:10.1593/neo.09542
- Liu, C., Kelnar, K., Liu, B., Chen, X., Calhoun-Davis, T., Li, H., . . . Tang, D. G. (2011). The microRNA miR-34a inhibits prostate cancer stem cells and metastasis by directly repressing CD44. *Nat Med*, 17(2), 211-215. doi:10.1038/nm.2284
- Liu, F., Bouznad, N., Kaller, M., Shi, X., König, J., Jaeckel, S., & Hermeking, H. (2022). Csf1r mediates enhancement of intestinal tumorigenesis caused by inactivation of Mir34a. *Int J Biol Sci*, 18(14), 5415-5437. doi:10.7150/ijbs.75503
- Liu, G., Li, W., Wang, L., Kar, A., Guan, K. L., Rao, Y., & Wu, J. Y. (2009). DSCAM functions as a netrin receptor in commissural axon pathfinding. *Proc Natl Acad Sci U S A*, 106(8), 2951-2956. doi:10.1073/pnas.0811083106
- Liu, J., Zhang, Y., Li, Q., & Wang, Y. (2020). Transgelins: Cytoskeletal Associated Proteins Implicated in the Metastasis of Colorectal Cancer. *Front Cell Dev Biol*, 8, 573859. doi:10.3389/fcell.2020.573859
- Liu, R., Hossain, M. M., Chen, X., & Jin, J. P. (2017). Mechanoregulation of SM22 α /Transgelin. *Biochemistry*, 56(41), 5526-5538. doi:10.1021/acs.biochem.7b00794

- Livak, K. J., & Schmittgen, T. D. (2001). Analysis of relative gene expression data using real-time quantitative PCR and the 2(-Delta Delta C(T)) Method. *Methods*, 25(4), 402-408. doi:10.1006/meth.2001.1262
- Lodygin, D., Tarasov, V., Epanchintsev, A., Berking, C., Knyazeva, T., Korner, H., . . . Hermeking, H. (2008). Inactivation of miR-34a by aberrant CpG methylation in multiple types of cancer. *Cell Cycle*, 7(16), 2591-2600. doi:10.4161/cc.7.16.6533
- Loh, C. Y., Arya, A., Naema, A. F., Wong, W. F., Sethi, G., & Looi, C. Y. (2019). Signal Transducer and Activator of Transcription (STATs) Proteins in Cancer and Inflammation: Functions and Therapeutic Implication. *Front Oncol*, 9, 48. doi:10.3389/fonc.2019.00048
- Lothe, R. A., Peltomäki, P., Meling, G. I., Aaltonen, L. A., Nyström-Lahti, M., Pylkkänen, L., . . . et al. (1993). Genomic instability in colorectal cancer: relationship to clinicopathological variables and family history. *Cancer Res*, 53(24), 5849-5852.
- Love, M. I., Huber, W., & Anders, S. (2014). Moderated estimation of fold change and dispersion for RNA-seq data with DESeq2. *Genome Biol*, 15(12), 550. doi:10.1186/s13059-014-0550-8
- Ly, A., Nikolaev, A., Suresh, G., Zheng, Y., Tessier-Lavigne, M., & Stein, E. (2008). DSCAM is a netrin receptor that collaborates with DCC in mediating turning responses to netrin-1. *Cell*, 133(7), 1241-1254. doi:10.1016/j.cell.2008.05.030
- Ma, Y., Qin, H., & Cui, Y. (2013). MiR-34a targets GAS1 to promote cell proliferation and inhibit apoptosis in papillary thyroid carcinoma via PI3K/Akt/Bad pathway. *Biochem Biophys Res Commun*, 441(4), 958-963. doi:10.1016/j.bbrc.2013.11.010
- MacDonald, K. P., Rowe, V., Bofinger, H. M., Thomas, R., Sasmono, T., Hume, D. A., & Hill, G. R. (2005). The colony-stimulating factor 1 receptor is expressed on dendritic cells during differentiation and regulates their expansion. *J Immunol*, 175(3), 1399-1405. doi:10.4049/jimmunol.175.3.1399
- Maher, M. G., Sapi, E., Turner, B., Gumbs, A., Perrotta, P. L., Carter, D., . . . Haffty, B. G. (1998). Prognostic significance of colony-stimulating factor receptor expression in ipsilateral breast cancer recurrence. *Clin Cancer Res*, 4(8), 1851-1856.
- Marisa, L., de Reyniès, A., Duval, A., Selves, J., Gaub, M. P., Vescovo, L., . . . Boige, V. (2013). Gene expression classification of colon cancer into molecular subtypes: characterization, validation, and prognostic value. *PLoS Med*, 10(5), e1001453. doi:10.1371/journal.pmed.1001453
- Mazelin, L., Bernet, A., Bonod-Bidaud, C., Pays, L., Arnaud, S., Gespach, C., . . . Mehlen, P. (2004). Netrin-1 controls colorectal tumorigenesis by regulating apoptosis. *Nature*, 431(7004), 80-84. doi:10.1038/nature02788
- McCubrey, J. A., Steelman, L. S., Chappell, W. H., Abrams, S. L., Wong, E. W., Chang, F., . . . Franklin, R. A. (2007). Roles of the Raf/MEK/ERK pathway in cell growth, malignant transformation and drug resistance. *Biochim Biophys Acta*, 1773(8), 1263-1284. doi:10.1016/j.bbamcr.2006.10.001

- Meagher, N. S., Gorringer, K. L., Wakefield, M. J., Bolithon, A., Pang, C. N. I., Chiu, D. S., . . . Ramus, S. J. (2022). Gene expression profiling of mucinous ovarian tumors and comparison with upper and lower gastrointestinal tumors identifies markers associated with adverse outcomes. *Clin Cancer Res*. doi:10.1158/1078-0432.Ccr-22-1206
- Mehlen, P., & Fearon, E. R. (2004). Role of the dependence receptor DCC in colorectal cancer pathogenesis. *J Clin Oncol*, 22(16), 3420-3428. doi:10.1200/jco.2004.02.019
- Mehlen, P., & Furne, C. (2005). Netrin-1: when a neuronal guidance cue turns out to be a regulator of tumorigenesis. *Cell Mol Life Sci*, 62(22), 2599-2616. doi:10.1007/s00018-005-5191-3
- Mehlen, P., Rabizadeh, S., Snipas, S. J., Assa-Munt, N., Salvesen, G. S., & Bredesen, D. E. (1998). The DCC gene product induces apoptosis by a mechanism requiring receptor proteolysis. *Nature*, 395(6704), 801-804. doi:10.1038/27441
- Menter, D. G., Davis, J. S., Broom, B. M., Overman, M. J., Morris, J., & Kopetz, S. (2019). Back to the Colorectal Cancer Consensus Molecular Subtype Future. *Curr Gastroenterol Rep*, 21(2), 5. doi:10.1007/s11894-019-0674-9
- Mercurio, L., Cecchetti, S., Ricci, A., Pacella, A., Cigliana, G., Bozzuto, G., . . . Carpinelli, G. (2017). Phosphatidylcholine-specific phospholipase C inhibition down-regulates CXCR4 expression and interferes with proliferation, invasion and glycolysis in glioma cells. *PLoS One*, 12(4), e0176108. doi:10.1371/journal.pone.0176108
- Merlos-Suarez, A., Barriga, F. M., Jung, P., Iglesias, M., Cespedes, M. V., Rossell, D., . . . Batlle, E. (2011). The intestinal stem cell signature identifies colorectal cancer stem cells and predicts disease relapse. *Cell Stem Cell*, 8(5), 511-524. doi:10.1016/j.stem.2011.02.020
- Misso, G., Di Martino, M. T., De Rosa, G., Farooqi, A. A., Lombardi, A., Campani, V., . . . Caraglia, M. (2014). Mir-34: a new weapon against cancer? *Mol Ther Nucleic Acids*, 3(9), e194. doi:10.1038/mtna.2014.47
- Mockly, S., Houbron, É., & Seitz, H. (2022). A rationalized definition of general tumor suppressor microRNAs excludes miR-34a. *Nucleic Acids Res*, 50(8), 4703-4712. doi:10.1093/nar/gkac277
- Mohammed, M. K., Shao, C., Wang, J., Wei, Q., Wang, X., Collier, Z., . . . Lee, M. J. (2016). Wnt/ β -catenin signaling plays an ever-expanding role in stem cell self-renewal, tumorigenesis and cancer chemoresistance. *Genes Dis*, 3(1), 11-40. doi:10.1016/j.gendis.2015.12.004
- Morandi, A., Barbetti, V., Rivero, M., Dello Sbarba, P., & Rovida, E. (2011). The colony-stimulating factor-1 (CSF-1) receptor sustains ERK1/2 activation and proliferation in breast cancer cell lines. *PLoS One*, 6(11), e27450. doi:10.1371/journal.pone.0027450
- Moser, A. R., Luongo, C., Gould, K. A., McNeley, M. K., Shoemaker, A. R., & Dove, W. F. (1995). ApcMin: a mouse model for intestinal and mammary tumorigenesis. *Eur J Cancer*, 31a(7-8), 1061-1064. doi:10.1016/0959-8049(95)00181-h

- Moser, A. R., Pitot, H. C., & Dove, W. F. (1990). A dominant mutation that predisposes to multiple intestinal neoplasia in the mouse. *Science*, 247(4940), 322-324. doi:10.1126/science.2296722
- Mouchemore, K. A., Sampaio, N. G., Murrey, M. W., Stanley, E. R., Lannutti, B. J., & Pixley, F. J. (2013). Specific inhibition of PI3K p110 δ inhibits CSF-1-induced macrophage spreading and invasive capacity. *Febs j*, 280(21), 5228-5236. doi:10.1111/febs.12316
- Mun, S. H., Park, P. S. U., & Park-Min, K. H. (2020). The M-CSF receptor in osteoclasts and beyond. *Exp Mol Med*, 52(8), 1239-1254. doi:10.1038/s12276-020-0484-z
- Munoz, J., Stange, D. E., Schepers, A. G., van de Wetering, M., Koo, B. K., Itzkovitz, S., . . . Clevers, H. (2012). The Lgr5 intestinal stem cell signature: robust expression of proposed quiescent '+4' cell markers. *Embo j*, 31(14), 3079-3091. doi:10.1038/emboj.2012.166
- Munteanu, I., & Mastalier, B. (2014). Genetics of colorectal cancer. *J Med Life*, 7(4), 507-511.
- Murga-Zamalloa, C., Rolland, D. C. M., Polk, A., Wolfe, A., Dewar, H., Chowdhury, P., . . . Wilcox, R. A. (2020). Colony-Stimulating Factor 1 Receptor (CSF1R) Activates AKT/mTOR Signaling and Promotes T-Cell Lymphoma Viability. *Clin Cancer Res*, 26(3), 690-703. doi:10.1158/1078-0432.Ccr-19-1486
- Murphy, N., Ward, H. A., Jenab, M., Rothwell, J. A., Boutron-Ruault, M. C., Carbonnel, F., . . . Gunter, M. J. (2019). Heterogeneity of Colorectal Cancer Risk Factors by Anatomical Subsite in 10 European Countries: A Multinational Cohort Study. *Clin Gastroenterol Hepatol*, 17(7), 1323-1331.e1326. doi:10.1016/j.cgh.2018.07.030
- Mutalip, S. S., Yunos, N. M., Abdul-Rahman, P. S., Jauri, M. H., Osman, A., & Adenan, M. I. (2014). Mechanisms of action of 17 β H-neriifolin on its anticancer effect in SKOV-3 ovarian cancer cell line. *Anticancer Res*, 34(8), 4141-4151.
- Nakayama, H., Ohnuki, H., Nakahara, M., Nishida-Fukuda, H., Sakaue, T., Fukuda, S., . . . Kusumoto, C. (2022). Inactivation of axon guidance molecule netrin-1 in human colorectal cancer by an epigenetic mechanism. *Biochem Biophys Res Commun*, 611, 146-150. doi:10.1016/j.bbrc.2022.04.069
- Nandi, S., Gokhan, S., Dai, X. M., Wei, S., Enikolopov, G., Lin, H., . . . Stanley, E. R. (2012). The CSF-1 receptor ligands IL-34 and CSF-1 exhibit distinct developmental brain expression patterns and regulate neural progenitor cell maintenance and maturation. *Dev Biol*, 367(2), 100-113. doi:10.1016/j.ydbio.2012.03.026
- Nguyen, L. H., Liu, P. H., Zheng, X., Keum, N., Zong, X., Li, X., . . . Cao, Y. (2018). Sedentary Behaviors, TV Viewing Time, and Risk of Young-Onset Colorectal Cancer. *JNCI Cancer Spectr*, 2(4), pky073. doi:10.1093/jncics/pky073
- Novak, U., Harpur, A. G., Paradiso, L., Kanagasundaram, V., Jaworowski, A., Wilks, A. F., & Hamilton, J. A. (1995). Colony-stimulating factor 1-induced STAT1 and STAT3 activation is accompanied by phosphorylation of Tyk2

- in macrophages and Tyk2 and JAK1 in fibroblasts. *Blood*, 86(8), 2948-2956.
- Noy, R., & Pollard, J. W. (2014). Tumor-associated macrophages: from mechanisms to therapy. *Immunity*, 41(1), 49-61. doi:10.1016/j.immuni.2014.06.010
- O'Sullivan, D. E., Sutherland, R. L., Town, S., Chow, K., Fan, J., Forbes, N., . . . Brenner, D. R. (2022). Risk Factors for Early-Onset Colorectal Cancer: A Systematic Review and Meta-analysis. *Clin Gastroenterol Hepatol*, 20(6), 1229-1240.e1225. doi:10.1016/j.cgh.2021.01.037
- Okada, N., Lin, C. P., Ribeiro, M. C., Biton, A., Lai, G., He, X., . . . He, L. (2014). A positive feedback between p53 and miR-34 miRNAs mediates tumor suppression. *Genes Dev*, 28(5), 438-450. doi:10.1101/gad.233585.113
- Okugawa, Y., Toiyama, Y., Ichikawa, T., Kawamura, M., Yasuda, H., Fujikawa, H., . . . Kusunoki, M. (2018). Colony-stimulating factor-1 and colony-stimulating factor-1 receptor co-expression is associated with disease progression in gastric cancer. *Int J Oncol*, 53(2), 737-749. doi:10.3892/ijo.2018.4406
- Öner, M. G., Rokavec, M., Kaller, M., Bouznad, N., Horst, D., Kirchner, T., & Hermeking, H. (2018). Combined Inactivation of TP53 and MIR34A Promotes Colorectal Cancer Development and Progression in Mice Via Increasing Levels of IL6R and PAI1. *Gastroenterology*, 155(6), 1868-1882. doi:10.1053/j.gastro.2018.08.011
- Paradisi, A., Maise, C., Bernet, A., Coissieux, M. M., Maccarrone, M., Scoazec, J. Y., & Mehlen, P. (2008). NF-kappaB regulates netrin-1 expression and affects the conditional tumor suppressive activity of the netrin-1 receptors. *Gastroenterology*, 135(4), 1248-1257. doi:10.1053/j.gastro.2008.06.080
- Paradisi, A., Maise, C., Coissieux, M. M., Gadot, N., Lépinasse, F., Delloye-Bourgeois, C., . . . Mehlen, P. (2009). Netrin-1 up-regulation in inflammatory bowel diseases is required for colorectal cancer progression. *Proc Natl Acad Sci U S A*, 106(40), 17146-17151. doi:10.1073/pnas.0901767106
- Paradisi, A., & Mehlen, P. (2010). Netrin-1, a missing link between chronic inflammation and tumor progression. *Cell Cycle*, 9(7), 1253-1262. doi:10.4161/cc.9.7.11072
- Parker, T. W., Rudeen, A. J., & Neufeld, K. L. (2020). Oncogenic Serine 45-Deleted β -Catenin Remains Susceptible to Wnt Stimulation and APC Regulation in Human Colonocytes. *Cancers (Basel)*, 12(8). doi:10.3390/cancers12082114
- Parri, M., & Chiarugi, P. (2010). Rac and Rho GTPases in cancer cell motility control. *Cell Commun Signal*, 8, 23. doi:10.1186/1478-811x-8-23
- Pastuła, A., & Marcinkiewicz, J. (2019). Cellular Interactions in the Intestinal Stem Cell Niche. *Archivum Immunologiae et Therapiae Experimentalis*, 67(1), 19-26. doi:10.1007/s00005-018-0524-8
- Patel, P., & De, P. (2016). Trends in colorectal cancer incidence and related lifestyle risk factors in 15-49-year-olds in Canada, 1969-2010. *Cancer Epidemiol*, 42, 90-100. doi:10.1016/j.canep.2016.03.009

- Peltomäki, P., Sistonen, P., Mecklin, J. P., Pylkkänen, L., Järvinen, H., Simons, J. W., . . . de la Chapelle, A. (1991). Evidence supporting exclusion of the DCC gene and a portion of chromosome 18q as the locus for susceptibility to hereditary nonpolyposis colorectal carcinoma in five kindreds. *Cancer Res*, *51*(16), 4135-4140.
- Pérot, G., Mendiboure, J., Brouste, V., Velasco, V., Terrier, P., Bonvalot, S., . . . Chibon, F. (2014). Smooth muscle differentiation identifies two classes of poorly differentiated pleomorphic sarcomas with distinct outcome. *Mod Pathol*, *27*(6), 840-850. doi:10.1038/modpathol.2013.205
- Peyraud, F., Cousin, S., & Italiano, A. (2017). CSF-1R Inhibitor Development: Current Clinical Status. *Curr Oncol Rep*, *19*(11), 70. doi:10.1007/s11912-017-0634-1
- Pikor, L., Thu, K., Vucic, E., & Lam, W. (2013). The detection and implication of genome instability in cancer. *Cancer Metastasis Rev*, *32*(3-4), 341-352. doi:10.1007/s10555-013-9429-5
- Pillai, R. S., Bhattacharyya, S. N., Artus, C. G., Zoller, T., Cougot, N., Basyuk, E., . . . Filipowicz, W. (2005). Inhibition of translational initiation by Let-7 MicroRNA in human cells. *Science*, *309*(5740), 1573-1576. doi:10.1126/science.1115079
- Pino, M. S., & Chung, D. C. (2010). The chromosomal instability pathway in colon cancer. *Gastroenterology*, *138*(6), 2059-2072. doi:10.1053/j.gastro.2009.12.065
- Pixley, F. J., & Stanley, E. R. (2004). CSF-1 regulation of the wandering macrophage: complexity in action. *Trends Cell Biol*, *14*(11), 628-638. doi:10.1016/j.tcb.2004.09.016
- Podo, F., Paris, L., Cecchetti, S., Spadaro, F., Abalsamo, L., Ramoni, C., . . . Iorio, E. (2016). Activation of Phosphatidylcholine-Specific Phospholipase C in Breast and Ovarian Cancer: Impact on MRS-Detected Choline Metabolic Profile and Perspectives for Targeted Therapy. *Front Oncol*, *6*, 171. doi:10.3389/fonc.2016.00171
- Powell, S. M., Zilz, N., Beazer-Barclay, Y., Bryan, T. M., Hamilton, S. R., Thibodeau, S. N., . . . Kinzler, K. W. (1992). APC mutations occur early during colorectal tumorigenesis. *Nature*, *359*(6392), 235-237. doi:10.1038/359235a0
- Qi, Q., Li, D. Y., Luo, H. R., Guan, K. L., & Ye, K. (2015). Netrin-1 exerts oncogenic activities through enhancing Yes-associated protein stability. *Proc Natl Acad Sci U S A*, *112*(23), 7255-7260. doi:10.1073/pnas.1505917112
- Qiu, P., Feng, X. H., & Li, L. (2003). Interaction of Smad3 and SRF-associated complex mediates TGF-beta1 signals to regulate SM22 transcription during myofibroblast differentiation. *J Mol Cell Cardiol*, *35*(12), 1407-1420. doi:10.1016/j.yjmcc.2003.09.002
- Quail, D. F., Bowman, R. L., Akkari, L., Quick, M. L., Schuhmacher, A. J., Huse, J. T., . . . Joyce, J. A. (2016). The tumor microenvironment underlies acquired resistance to CSF-1R inhibition in gliomas. *Science*, *352*(6288), aad3018. doi:10.1126/science.aad3018

- Rabeneck, L., Chiu, H. M., & Senore, C. (2020). International Perspective on the Burden of Colorectal Cancer and Public Health Effects. *Gastroenterology*, *158*(2), 447-452. doi:10.1053/j.gastro.2019.10.007
- Rajasekharan, S., Baker, K. A., Horn, K. E., Jarjour, A. A., Antel, J. P., & Kennedy, T. E. (2009). Netrin 1 and Dcc regulate oligodendrocyte process branching and membrane extension via Fyn and RhoA. *Development*, *136*(3), 415-426. doi:10.1242/dev.018234
- Rajasekharan, S., & Kennedy, T. E. (2009). The netrin protein family. *Genome Biol*, *10*(9), 239. doi:10.1186/gb-2009-10-9-239
- Ramesh, A., Brouillard, A., Kumar, S., Nandi, D., & Kulkarni, A. (2020). Dual inhibition of CSF1R and MAPK pathways using supramolecular nanoparticles enhances macrophage immunotherapy. *Biomaterials*, *227*, 119559. doi:10.1016/j.biomaterials.2019.119559
- Rao, D., Kimler, B. F., Nothnick, W. B., Davis, M. K., Fan, F., & Tawfik, O. (2015). Transgelin: a potentially useful diagnostic marker differentially expressed in triple-negative and non-triple-negative breast cancers. *Hum Pathol*, *46*(6), 876-883. doi:10.1016/j.humpath.2015.02.015
- Reedijk, M., Liu, X., van der Geer, P., Letwin, K., Waterfield, M. D., Hunter, T., & Pawson, T. (1992). Tyr721 regulates specific binding of the CSF-1 receptor kinase insert to PI 3'-kinase SH2 domains: a model for SH2-mediated receptor-target interactions. *Embo j*, *11*(4), 1365-1372. doi:10.1002/j.1460-2075.1992.tb05181.x
- Ren, J., Sui, H., Fang, F., Li, Q., & Li, B. (2019). The application of Apc(Min/+) mouse model in colorectal tumor researches. *J Cancer Res Clin Oncol*, *145*(5), 1111-1122. doi:10.1007/s00432-019-02883-6
- Risinger, J. I., Berchuck, A., Kohler, M. F., Watson, P., Lynch, H. T., & Boyd, J. (1993). Genetic instability of microsatellites in endometrial carcinoma. *Cancer Res*, *53*(21), 5100-5103.
- Risso, D., Ngai, J., Speed, T. P., & Dudoit, S. (2014). Normalization of RNA-seq data using factor analysis of control genes or samples. *Nat Biotechnol*, *32*(9), 896-902. doi:10.1038/nbt.2931
- Robin, Y. M., Penel, N., Pérot, G., Neuville, A., Vélasco, V., Ranchère-Vince, D., . . . Coindre, J. M. (2013). Transgelin is a novel marker of smooth muscle differentiation that improves diagnostic accuracy of leiomyosarcomas: a comparative immunohistochemical reappraisal of myogenic markers in 900 soft tissue tumors. *Mod Pathol*, *26*(4), 502-510. doi:10.1038/modpathol.2012.192
- Rodrigues, S., De Wever, O., Bruyneel, E., Rooney, R. J., & Gespach, C. (2007). Opposing roles of netrin-1 and the dependence receptor DCC in cancer cell invasion, tumor growth and metastasis. *Oncogene*, *26*(38), 5615-5625. doi:10.1038/sj.onc.1210347
- Rokavec, M., Li, H., Jiang, L., & Hermeking, H. (2014). The p53/miR-34 axis in development and disease. *J Mol Cell Biol*, *6*(3), 214-230. doi:10.1093/jmcb/mju003
- Rokavec, M., Oner, M. G., Li, H., Jackstadt, R., Jiang, L., Lodygin, D., . . . Hermeking, H. (2014). IL-6R/STAT3/miR-34a feedback loop promotes

- EMT-mediated colorectal cancer invasion and metastasis. *J Clin Invest*, 124(4), 1853-1867. doi:10.1172/JCI73531
- Rosenberger, P., Schwab, J. M., Mirakaj, V., Masekowsky, E., Mager, A., Morote-Garcia, J. C., . . . Eltzschig, H. K. (2009). Hypoxia-inducible factor-dependent induction of netrin-1 dampens inflammation caused by hypoxia. *Nat Immunol*, 10(2), 195-202. doi:10.1038/ni.1683
- Roussel, M. F., Cleveland, J. L., Shurtleff, S. A., & Sherr, C. J. (1991). Myc rescue of a mutant CSF-1 receptor impaired in mitogenic signalling. *Nature*, 353(6342), 361-363. doi:10.1038/353361a0
- Roussel, M. F., Davis, J. N., Cleveland, J. L., Ghysdael, J., & Hiebert, S. W. (1994). Dual control of myc expression through a single DNA binding site targeted by ets family proteins and E2F-1. *Oncogene*, 9(2), 405-415.
- Royal, I., Lamarche-Vane, N., Lamorte, L., Kaibuchi, K., & Park, M. (2000). Activation of cdc42, rac, PAK, and rho-kinase in response to hepatocyte growth factor differentially regulates epithelial cell colony spreading and dissociation. *Mol Biol Cell*, 11(5), 1709-1725. doi:10.1091/mbc.11.5.1709
- Rui, X., Zhao, H., Xiao, X., Wang, L., Mo, L., & Yao, Y. (2018). MicroRNA-34a suppresses breast cancer cell proliferation and invasion by targeting Notch1. *Exp Ther Med*, 16(6), 4387-4392. doi:10.3892/etm.2018.6744
- Saad El Din, K., Loree, J. M., Sayre, E. C., Gill, S., Brown, C. J., Dau, H., & De Vera, M. A. (2020). Trends in the epidemiology of young-onset colorectal cancer: a worldwide systematic review. *BMC Cancer*, 20(1), 288. doi:10.1186/s12885-020-06766-9
- Salmaninejad, A., Valilou, S. F., Soltani, A., Ahmadi, S., Abarghan, Y. J., Rosengren, R. J., & Sahebkar, A. (2019). Tumor-associated macrophages: role in cancer development and therapeutic implications. *Cell Oncol (Dordr)*, 42(5), 591-608. doi:10.1007/s13402-019-00453-z
- Salvatore, L., Calegari, M. A., Loupakis, F., Fassan, M., Di Stefano, B., Bensi, M., . . . Tortora, G. (2019). PTEN in Colorectal Cancer: Shedding Light on Its Role as Predictor and Target. *Cancers (Basel)*, 11(11). doi:10.3390/cancers11111765
- Sampaio, N. G., Yu, W., Cox, D., Wyckoff, J., Condeelis, J., Stanley, E. R., & Pixley, F. J. (2011). Phosphorylation of CSF-1R Y721 mediates its association with PI3K to regulate macrophage motility and enhancement of tumor cell invasion. *J Cell Sci*, 124(Pt 12), 2021-2031. doi:10.1242/jcs.075309
- Sato, T., Stange, D. E., Ferrante, M., Vries, R. G., Van Es, J. H., Van den Brink, S., . . . Clevers, H. (2011). Long-term expansion of epithelial organoids from human colon, adenoma, adenocarcinoma, and Barrett's epithelium. *Gastroenterology*, 141(5), 1762-1772. doi:10.1053/j.gastro.2011.07.050
- Serafini, T., Colamarino, S. A., Leonardo, E. D., Wang, H., Beddington, R., Skarnes, W. C., & Tessier-Lavigne, M. (1996). Netrin-1 is required for commissural axon guidance in the developing vertebrate nervous system. *Cell*, 87(6), 1001-1014. doi:10.1016/s0092-8674(00)81795-x
- Shapland, C., Hsuan, J. J., Totty, N. F., & Lawson, D. (1993). Purification and properties of transgelin: a transformation and shape change sensitive

- actin-gelling protein. *J Cell Biol*, 121(5), 1065-1073. doi:10.1083/jcb.121.5.1065
- Shen, Z. (2011). Genomic instability and cancer: an introduction. *J Mol Cell Biol*, 3(1), 1-3. doi:10.1093/jmcb/mjq057
- Shi, X., Kaller, M., Rokavec, M., Kirchner, T., Horst, D., & Hermeking, H. (2020). Characterization of a p53/miR-34a/CSF1R/STAT3 Feedback Loop in Colorectal Cancer. *Cell Mol Gastroenterol Hepatol*, 10(2), 391-418. doi:10.1016/j.jcmgh.2020.04.002
- Shimizu, A., Nakayama, H., Wang, P., König, C., Akino, T., Sandlund, J., . . . Klagsbrun, M. (2013). Netrin-1 promotes glioblastoma cell invasiveness and angiogenesis by multiple pathways including activation of RhoA, cathepsin B, and cAMP-response element-binding protein. *J Biol Chem*, 288(4), 2210-2222. doi:10.1074/jbc.M112.397398
- Shouqing, L., & Dexian, Z. (1998). Signal transduction pathways mediated by colony stimulating factor-1 receptor. *Chinese Science Bulletin*, 43(12), 969-974. doi:10.1007/BF02884628
- Siegel, R. L., Miller, K. D., Goding Sauer, A., Fedewa, S. A., Butterly, L. F., Anderson, J. C., . . . Jemal, A. (2020). Colorectal cancer statistics, 2020. *CA Cancer J Clin*, 70(3), 145-164. doi:10.3322/caac.21601
- Siemens, H., Neumann, J., Jackstadt, R., Mansmann, U., Horst, D., Kirchner, T., & Hermeking, H. (2013). Detection of miR-34a promoter methylation in combination with elevated expression of c-Met and β -catenin predicts distant metastasis of colon cancer. *Clin Cancer Res*, 19(3), 710-720. doi:10.1158/1078-0432.ccr-12-1703
- Singh, G., Sharma, S. K., & Singh, S. K. (2022). miR-34a negatively regulates cell cycle factor Cdt2/DTL in HPV infected cervical cancer cells. *BMC Cancer*, 22(1), 777. doi:10.1186/s12885-022-09879-5
- Smeester, B. A., Slipek, N. J., Pomeroy, E. J., Laoharawee, K., Osum, S. H., Larsson, A. T., . . . Largaespada, D. A. (2020). PLX3397 treatment inhibits constitutive CSF1R-induced oncogenic ERK signaling, reduces tumor growth, and metastatic burden in osteosarcoma. *Bone*, 136, 115353. doi:10.1016/j.bone.2020.115353
- Smith-Ravin, J., Pack, K., Hodgson, S., Tay, S. K., Phillips, R., & Bodmer, W. (1994). APC mutation associated with late onset of familial adenomatous polyposis. *J Med Genet*, 31(11), 888-890. doi:10.1136/jmg.31.11.888
- Stanley, E. R., & Chitu, V. (2014). CSF-1 receptor signaling in myeloid cells. *Cold Spring Harb Perspect Biol*, 6(6). doi:10.1101/cshperspect.a021857
- Stephens, M. (2016). False discovery rates: a new deal. *Biostatistics*, 18(2), 275-294. doi:10.1093/biostatistics/kxw041
- Stoffel, E. M., & Kastrinos, F. (2014). Familial colorectal cancer, beyond Lynch syndrome. *Clin Gastroenterol Hepatol*, 12(7), 1059-1068. doi:10.1016/j.cgh.2013.08.015
- Su, L. K., Kinzler, K. W., Vogelstein, B., Preisinger, A. C., Moser, A. R., Luongo, C., . . . Dove, W. F. (1992). Multiple intestinal neoplasia caused by a mutation in the murine homolog of the APC gene. *Science*, 256(5057), 668-670. doi:10.1126/science.1350108

- Sung, H., Ferlay, J., Siegel, R. L., Laversanne, M., Soerjomataram, I., Jemal, A., & Bray, F. (2021). Global Cancer Statistics 2020: GLOBOCAN Estimates of Incidence and Mortality Worldwide for 36 Cancers in 185 Countries. *CA Cancer J Clin*, *71*(3), 209-249. doi:10.3322/caac.21660
- Sung, J. J. Y., Chiu, H. M., Jung, K. W., Jun, J. K., Sekiguchi, M., Matsuda, T., & Kyaw, M. H. (2019). Increasing Trend in Young-Onset Colorectal Cancer in Asia: More Cancers in Men and More Rectal Cancers. *Am J Gastroenterol*, *114*(2), 322-329. doi:10.14309/ajg.000000000000133
- Sveen, A., Bruun, J., Eide, P. W., Eilertsen, I. A., Ramirez, L., Murumägi, A., . . . Lothe, R. A. (2018). Colorectal Cancer Consensus Molecular Subtypes Translated to Preclinical Models Uncover Potentially Targetable Cancer Cell Dependencies. *Clin Cancer Res*, *24*(4), 794-806. doi:10.1158/1078-0432.ccr-17-1234
- Takahashi, T., & Shiraishi, A. (2020). Stem Cell Signaling Pathways in the Small Intestine. *Int J Mol Sci*, *21*(6), 2032. doi:10.3390/ijms21062032
- Tan, T. Z., Miow, Q. H., Miki, Y., Noda, T., Mori, S., Huang, R. Y., & Thiery, J. P. (2014). Epithelial-mesenchymal transition spectrum quantification and its efficacy in deciphering survival and drug responses of cancer patients. *EMBO Mol Med*, *6*(10), 1279-1293. doi:10.15252/emmm.201404208
- Tanikawa, C., Matsuda, K., Fukuda, S., Nakamura, Y., & Arakawa, H. (2003). p53RDL1 regulates p53-dependent apoptosis. *Nat Cell Biol*, *5*(3), 216-223. doi:10.1038/ncb943
- Tarasov, V., Jung, P., Verdoodt, B., Lodygin, D., Epanchintsev, A., Menssen, A., . . . Hermeking, H. (2007). Differential regulation of microRNAs by p53 revealed by massively parallel sequencing: miR-34a is a p53 target that induces apoptosis and G1-arrest. *Cell Cycle*, *6*(13), 1586-1593. doi:10.4161/cc.6.13.4436
- Taube, J. H., Herschkowitz, J. I., Komurov, K., Zhou, A. Y., Gupta, S., Yang, J., . . . Mani, S. A. (2010). Core epithelial-to-mesenchymal transition interactome gene-expression signature is associated with claudin-low and metaplastic breast cancer subtypes. *Proc Natl Acad Sci U S A*, *107*(35), 15449-15454. doi:10.1073/pnas.1004900107
- Tong, Y., Yang, W., & Koeffler, H. P. (2011). Mouse models of colorectal cancer. *Chin J Cancer*, *30*(7), 450-462. doi:10.5732/cjc.011.10041
- Truong, A. D., Hong, Y., Lee, J., Lee, K., Kil, D. Y., Lillehoj, H. S., & Hong, Y. H. (2018). Interleukin-34 Regulates Th1 and Th17 Cytokine Production by Activating Multiple Signaling Pathways through CSF-1R in Chicken Cell Lines. *Int J Mol Sci*, *19*(6). doi:10.3390/ijms19061665
- Tsai, H. H., Tessier-Lavigne, M., & Miller, R. H. (2003). Netrin 1 mediates spinal cord oligodendrocyte precursor dispersal. *Development*, *130*(10), 2095-2105. doi:10.1242/dev.00424
- Tse, J. W. T., Jenkins, L. J., Chionh, F., & Mariadason, J. M. (2017). Aberrant DNA Methylation in Colorectal Cancer: What Should We Target? *Trends Cancer*, *3*(10), 698-712. doi:10.1016/j.trecan.2017.08.003
- Tsui, K. H., Lin, Y. H., Chang, K. S., Hou, C. P., Chen, P. J., Feng, T. H., & Juang, H. H. (2019). Transgelin, a p53 and PTEN-Upregulated Gene, Inhibits the

- Cell Proliferation and Invasion of Human Bladder Carcinoma Cells in Vitro and in Vivo. *Int J Mol Sci*, 20(19). doi:10.3390/ijms20194946
- Tsuji-Tamura, K., Morino-Koga, S., Suzuki, S., & Ogawa, M. (2021). The canonical smooth muscle cell marker TAGLN is present in endothelial cells and is involved in angiogenesis. *J Cell Sci*, 134(15). doi:10.1242/jcs.254920
- Tu, T., Zhang, C., Yan, H., Luo, Y., Kong, R., Wen, P., . . . Yan, X. (2015). CD146 acts as a novel receptor for netrin-1 in promoting angiogenesis and vascular development. *Cell Res*, 25(3), 275-287. doi:10.1038/cr.2015.15
- Ungefroren, H., Sebens, S., Seidl, D., Lehnert, H., & Hass, R. (2011). Interaction of tumor cells with the microenvironment. *Cell Commun Signal*, 9, 18-18. doi:10.1186/1478-811X-9-18
- Vogelstein, B., & Kinzler, K. W. (2002). *The genetic basis of human cancer*. McGraw-Hill Professional.
- Vogt, M., Munding, J., Gruner, M., Liffers, S. T., Verdoodt, B., Hauk, J., . . . Hermeking, H. (2011). Frequent concomitant inactivation of miR-34a and miR-34b/c by CpG methylation in colorectal, pancreatic, mammary, ovarian, urothelial, and renal cell carcinomas and soft tissue sarcomas. *Virchows Arch*, 458(3), 313-322. doi:10.1007/s00428-010-1030-5
- Vuik, F. E., Nieuwenburg, S. A., Bardou, M., Lansdorp-Vogelaar, I., Dinis-Ribeiro, M., Bento, M. J., . . . Spaander, M. C. (2019). Increasing incidence of colorectal cancer in young adults in Europe over the last 25 years. *Gut*, 68(10), 1820-1826. doi:10.1136/gutjnl-2018-317592
- Wang, B., Li, D., Kovalchuk, I., Apel, I. J., Chinnaiyan, A. M., Wóycicki, R. K., . . . Kovalchuk, O. (2018). miR-34a directly targets tRNA(i)(Met) precursors and affects cellular proliferation, cell cycle, and apoptosis. *Proc Natl Acad Sci U S A*, 115(28), 7392-7397. doi:10.1073/pnas.1703029115
- Wang, X., Zhang, J., Hu, B., & Qian, F. (2022). High Expression of CSF-1R Predicts Poor Prognosis and CSF-1R(high) Tumor-Associated Macrophages Inhibit Anti-Tumor Immunity in Colon Adenocarcinoma. *Front Oncol*, 12, 850767. doi:10.3389/fonc.2022.850767
- Watnick, P. I., & Jugder, B. E. (2020). Microbial Control of Intestinal Homeostasis via Enteroendocrine Cell Innate Immune Signaling. *Trends Microbiol*, 28(2), 141-149. doi:10.1016/j.tim.2019.09.005
- Wei, X., Lou, H., Zhou, D., Jia, Y., Li, H., Huang, Q., . . . Gao, Q. (2021). TAGLN mediated stiffness-regulated ovarian cancer progression via RhoA/ROCK pathway. *J Exp Clin Cancer Res*, 40(1), 292. doi:10.1186/s13046-021-02091-6
- Welch, C., Chen, Y., & Stallings, R. L. (2007). MicroRNA-34a functions as a potential tumor suppressor by inducing apoptosis in neuroblastoma cells. *Oncogene*, 26(34), 5017-5022. doi:10.1038/sj.onc.1210293
- Wheeler, J. M., Bodmer, W. F., & Mortensen, N. J. (2000). DNA mismatch repair genes and colorectal cancer. *Gut*, 47(1), 148-153. doi:10.1136/gut.47.1.148
- Wilson, N. H., & Key, B. (2007). Neogenin: one receptor, many functions. *Int J Biochem Cell Biol*, 39(5), 874-878. doi:10.1016/j.biocel.2006.10.023

- Winter, M., Rokavec, M., & Hermeking, H. (2021). 14-3-3 σ Functions as an Intestinal Tumor Suppressor. *Cancer Res*, 81(13), 3621-3634. doi:10.1158/0008-5472.can-20-4192
- Wong, J. J., Hawkins, N. J., Ward, R. L., & Hitchins, M. P. (2011). Methylation of the 3p22 region encompassing MLH1 is representative of the CpG island methylator phenotype in colorectal cancer. *Mod Pathol*, 24(3), 396-411. doi:10.1038/modpathol.2010.212
- Xi, Y., & Xu, P. (2021). Global colorectal cancer burden in 2020 and projections to 2040. *Transl Oncol*, 14(10), 101174. doi:10.1016/j.tranon.2021.101174
- Xiang, C., Li, H., & Tang, W. (2022). Targeting CSF-1R represents an effective strategy in modulating inflammatory diseases. *Pharmacol Res*, 187, 106566. doi:10.1016/j.phrs.2022.106566
- Xie, X. L., Nie, X., Wu, J., Zhang, F., Zhao, L. L., Lin, Y. L., . . . Han, M. (2015). Smooth muscle 22 α facilitates angiotensin II-induced signaling and vascular contraction. *J Mol Med (Berl)*, 93(5), 547-558. doi:10.1007/s00109-014-1240-4
- Yamagishi, H., Kuroda, H., Imai, Y., & Hiraishi, H. (2016). Molecular pathogenesis of sporadic colorectal cancers. *Chin J Cancer*, 35, 4. doi:10.1186/s40880-015-0066-y
- Yamagishi, S., Bando, Y., & Sato, K. (2020). Involvement of Netrins and Their Receptors in Neuronal Migration in the Cerebral Cortex. *Front Cell Dev Biol*, 8, 590009. doi:10.3389/fcell.2020.590009
- Yang, B., Chen, Q., Wan, C., Sun, S., Zhu, L., Zhao, Z., . . . Wang, B. (2021). Transgelin Inhibits the Malignant Progression of Esophageal Squamous Cell Carcinomas by Regulating Epithelial-Mesenchymal Transition. *Front Oncol*, 11, 709486. doi:10.3389/fonc.2021.709486
- Yang, L., Liu, Y., An, H., Chang, Y., Zhang, W., Zhu, Y., . . . Xu, J. (2016). High Expression of Colony-Stimulating Factor 1 Receptor Associates with Unfavorable Cancer-Specific Survival of Patients with Clear Cell Renal Cell Carcinoma. *Ann Surg Oncol*, 23(3), 1044-1052. doi:10.1245/s10434-015-4911-7
- Yang, S., Jiang, S., Wang, Y., Tu, S., Wang, Z., & Chen, Z. (2016). Interleukin 34 Upregulation Contributes to the Increment of MicroRNA 21 Expression through STAT3 Activation Associated with Disease Activity in Rheumatoid Arthritis. *J Rheumatol*, 43(7), 1312-1319. doi:10.3899/jrheum.151253
- Yin, K., Shang, M., Dang, S., Wang, L., Xia, Y., Cui, L., . . . Xu, Z. (2018). Netrin -1 induces the proliferation of gastric cancer cells via the ERK/MAPK signaling pathway and FAK activation. *Oncol Rep*, 40(4), 2325-2333. doi:10.3892/or.2018.6614
- Yin, W., Gao, F., & Zhang, S. (2020). MicroRNA-34a inhibits the proliferation and promotes the chemosensitivity of retinoblastoma cells by downregulating Notch1 expression. *Mol Med Rep*, 22(2), 1613-1620. doi:10.3892/mmr.2020.11238
- Ylivinkka, I., Hu, Y., Chen, P., Rantanen, V., Hautaniemi, S., Nyman, T. A., . . . Hyytiäinen, M. (2013). Netrin-1-induced activation of Notch signaling

- mediates glioblastoma cell invasion. *J Cell Sci*, 126(Pt 11), 2459-2469. doi:10.1242/jcs.120022
- Yokota, M., Kojima, M., Higuchi, Y., Nishizawa, Y., Kobayashi, A., Ito, M., . . . Ochiai, A. (2016). Gene expression profile in the activation of subperitoneal fibroblasts reflects prognosis of patients with colon cancer. *Int J Cancer*, 138(6), 1422-1431. doi:10.1002/ijc.29851
- Young, J. P., Win, A. K., Rosty, C., Flight, I., Roder, D., Young, G. P., . . . Price, T. J. (2015). Rising incidence of early-onset colorectal cancer in Australia over two decades: report and review. *J Gastroenterol Hepatol*, 30(1), 6-13. doi:10.1111/jgh.12792
- Yu, H., Königshoff, M., Jayachandran, A., Handley, D., Seeger, W., Kaminski, N., & Eickelberg, O. (2008). Transgelin is a direct target of TGF-beta/Smad3-dependent epithelial cell migration in lung fibrosis. *Faseb j*, 22(6), 1778-1789. doi:10.1096/fj.07-083857
- Yu, W., Chen, J., Xiong, Y., Pixley, F. J., Yeung, Y. G., & Stanley, E. R. (2012). Macrophage proliferation is regulated through CSF-1 receptor tyrosines 544, 559, and 807. *J Biol Chem*, 287(17), 13694-13704. doi:10.1074/jbc.M112.355610
- Zeidan, A., Swärd, K., Nordström, I., Ekblad, E., Zhang, J. C., Parmacek, M. S., & Hellstrand, P. (2004). Ablation of SM22alpha decreases contractility and actin contents of mouse vascular smooth muscle. *FEBS Lett*, 562(1-3), 141-146. doi:10.1016/s0014-5793(04)00220-0
- Zhang, X., Cui, P., Ding, B., Guo, Y., Han, K., Li, J., . . . Zhang, W. (2018). Netrin-1 elicits metastatic potential of non-small cell lung carcinoma cell by enhancing cell invasion, migration and vasculogenic mimicry via EMT induction. *Cancer Gene Ther*, 25(1-2), 18-26. doi:10.1038/s41417-017-0008-8
- Zhang, Y., & Liu, Z. (2017). STAT1 in cancer: friend or foe? *Discov Med*, 24(130), 19-29.
- Zheng, R., Wan, C., Mei, S., Qin, Q., Wu, Q., Sun, H., . . . Liu, X. S. (2019). Cistrome Data Browser: expanded datasets and new tools for gene regulatory analysis. *Nucleic Acids Res*, 47(D1), D729-d735. doi:10.1093/nar/gky1094
- Zhong, W., Hou, H., Liu, T., Su, S., Xi, X., Liao, Y., . . . Wang, B. (2020). Cartilage Oligomeric Matrix Protein promotes epithelial-mesenchymal transition by interacting with Transgelin in Colorectal Cancer. *Theranostics*, 10(19), 8790-8806. doi:10.7150/thno.44456
- Zhou, H., Zhang, Y., Chen, Q., & Lin, Y. (2016). AKT and JNK Signaling Pathways Increase the Metastatic Potential of Colorectal Cancer Cells by Altering Transgelin Expression. *Dig Dis Sci*, 61(4), 1091-1097. doi:10.1007/s10620-015-3985-1
- Zhou, H. M., Fang, Y. Y., Weinberger, P. M., Ding, L. L., Cowell, J. K., Hudson, F. Z., . . . Lin, Y. (2016). Transgelin increases metastatic potential of colorectal cancer cells in vivo and alters expression of genes involved in cell motility. *BMC Cancer*, 16, 55. doi:10.1186/s12885-016-2105-8

-
- Zhou, Y., Bian, S., Zhou, X., Cui, Y., Wang, W., Wen, L., . . . Tang, F. (2020). Single-Cell Multiomics Sequencing Reveals Prevalent Genomic Alterations in Tumor Stromal Cells of Human Colorectal Cancer. *Cancer Cell*, 38(6), 818-828.e815. doi:10.1016/j.ccell.2020.09.015
- Zhou, Y., Ding, B. Z., Lin, Y. P., & Wang, H. B. (2018). MiR-34a, as a suppressor, enhance the susceptibility of gastric cancer cell to luteolin by directly targeting HK1. *Gene*, 644, 56-65. doi:10.1016/j.gene.2017.10.046
- Zhou, Y., Zeng, J., Tu, Y., Li, L., Du, S., Zhu, L., . . . Liu, X. (2021). CSF1/CSF1R-mediated Crosstalk Between Choroidal Vascular Endothelial Cells and Macrophages Promotes Choroidal Neovascularization. *Invest Ophthalmol Vis Sci*, 62(3), 37. doi:10.1167/iovs.62.3.37
- Zhu, Y., Feng, Z., Cheng, W., & Xiao, Y. (2018). MicroRNA-34a mediates atrial fibrillation through regulation of Ankyrin-B expression. *Mol Med Rep*, 17(6), 8457-8465. doi:10.3892/mmr.2018.8873
- Zwaenepoel, O., Tzenaki, N., Vergetaki, A., Makrigiannakis, A., Vanhaesebroeck, B., & Papakonstanti, E. A. (2012). Functional CSF-1 receptors are located at the nuclear envelope and activated via the p110 δ isoform of PI 3-kinase. *Faseb j*, 26(2), 691-706. doi:10.1096/fj.11-189753

7. Supplements

7.1 Supplemental Data 1

Related to materials and methods.

STAT3-related public datasets used to identify potential STAT3 target genes

Microarray/RNA-seq		
datasets :	ectopic STAT3 expression	
Homo sapiens	MKN28, const. active STAT3	GSE78714
Mus musculus	mammary tumor, const. active STAT3	GSE17182
Mus musculus	MEFs, const. active STAT3	GSE21507
Microarray/RNA-seq		
datasets :	STAT3 knockout/knockdown	
Homo sapiens	DU145 STAT3 siRNA	GSE25944
Homo sapiens	A375 STAT3 siRNA	GSE31534
Homo sapiens	HCC1143 STAT3 siRNA	GSE85579
Homo sapiens	HCC70 STAT3 siRNA	GSE85579
Homo sapiens	MDA231 STAT3 siRNA	GSE85579
Homo sapiens	MDA157 STAT3 siRNA	GSE85579
Homo sapiens	MDA468 STAT3 siRNA	GSE85579
Homo sapiens	LY10 STAT3 siRNA	GSE106844
Homo sapiens	TMD8 STAT3 siRNA	GSE106844
Homo sapiens	Du145 STAT3 siRNA	GSE17482
Homo sapiens	Hela - STAT3 KO	GSE108495
Homo sapiens	SKOV STAT3 KO	GSE134375
Homo sapiens	OV3 STAT3 KO	GSE134375
Homo sapiens	OV8 STAT3 KO	GSE134375
Homo sapiens	CWR STAT3 siRNA	GSE17482
Homo sapiens	SKOV STAT3 siRNA	GSE20597
Mus musculus	STAT3 KO	GSE6846
Mus musculus	STAT3 KO	GSE151447
STAT3 ChIP-Seq		
datasets		
Homo sapiens	Tumor cells	GSM2278006
Homo sapiens	OCI-Ly7; B cell lymphoma; Blood	GSM1227207
Homo sapiens	MCF-10A; Epithelium; Breast	GSM935457
Homo sapiens	MDA-MB-231; mDA	GSM2278002
Homo sapiens	HCC1143	GSM2278010
Homo sapiens	U-2932; B Lymphocyte	GSM1227212

Homo sapiens	OCI-Ly3; B Lymphocyte; Bone Marrow	GSM1227206
Homo sapiens	H358; Lung	GSM2752894
Homo sapiens	SU-DHL4; B Lymphocyte; Peritoneal Effusion	GSM1227210
Homo sapiens	HCC70; Epithelium; Breast	GSM2278004
Homo sapiens	OCI-Ly10; B Lymphocyte; Bone Marrow	GSM1227204
Homo sapiens	MDA-MB-157; mDA	GSM2278001
Homo sapiens	MDA-MB-468; mDA	GSM2278009
Homo sapiens	SU-DHL2; B Lymphocyte	GSM1227209
Mus musculus	Mammary Gland	GSM2300477
Mus musculus	Th17	GSM1004860
Mus musculus	AtT-20; Corticotroph; Pituitary	GSM926625
Mus musculus	Embryonic Stem Cell	GSM2561450
Mus musculus	T Lymphocyte	GSM1601733
Mus musculus	T Lymphocyte; Blood	GSM494691
Mus musculus	Dendritic Cell; Spleen	GSM671415
Mus musculus	AtT-20; Corticotroph; Pituitary	GSM2445278
Mus musculus	T Lymphocyte; Spleen	GSM1543812
Mus musculus	T Lymphocyte; Blood	GSM580756
Mus musculus	in vitro polarized Th17 T cells	GSM540722
Mus musculus	primary CD4+ T cells	GSM652877
Mus musculus	Primary Cortical Oligodendrocyte Progenitor (OLP) cells	GSM2650745

7.2 Supplemental Data 2

Related to materials and methods.

IL6/STAT3-related public datasets used to identify potential STAT3 target genes

Microarray/RNA-seq datasets :	IL6-treatment	
Homo sapiens	MCF7 + IL6 1h	GSE126003
Homo sapiens	T47D + IL6 1h	GSE126003
Homo sapiens	DLD1 +IL6 24h	GSE149262
Homo sapiens	CMEC/D3 +IL6 72h	GSE138309
Homo sapiens	airways epithelial cells +IL6	GSE113185
Homo sapiens	macrophages +IL6	GSE123603
Homo sapiens	ANBL6 MM +IL6 24h	GSE115558
Homo sapiens	FLAM76 MM +IL6 24h	GSE115558
Homo sapiens	HUVEC +IL6	GSE163649

Homo sapiens	endothelial cells +IL6 1h	GSE19082
Homo sapiens	macrophages +IL6 4h	GSE8515
Homo sapiens	HepG2 +IL6 4h	GSE411
Homo sapiens	HK2 +IL6 1.5h	GSE68826
Homo sapiens	HK2 +IL6 1.5h	GSE68940
Homo sapiens	keratinocytes +IL6 24h	GSE53751
Homo sapiens	trachea cells +IL6 24h	GSE67361
Mus musculus	macrophages +IL6 6h	GSE411
Mus musculus	hepatocytes +IL6 4h	GSE21031
Mus musculus	liver +IL6 1h	GSE21060
Mus musculus	gastric tumors +IL6 1h	GSE43800
Mus musculus	hepatocytes +IL6 24h	GSE69928
STAT3 ChIP-Seq		
datasets		
Homo sapiens	Tumor cells	GSM2278006
Homo sapiens	OCI-Ly7; B cell lymphoma; Blood	GSM1227207
Homo sapiens	MCF-10A; Epithelium; Breast	GSM935457
Homo sapiens	MDA-MB-231; mDA	GSM2278002
Homo sapiens	HCC1143	GSM2278010
Homo sapiens	U-2932; B Lymphocyte	GSM1227212
Homo sapiens	OCI-Ly3; B Lymphocyte; Bone Marrow	GSM1227206
Homo sapiens	H358; Lung	GSM2752894
Homo sapiens	SU-DHL4; B Lymphocyte; Peritoneal Effusion	GSM1227210
Homo sapiens	HCC70; Epithelium; Breast	GSM2278004
Homo sapiens	OCI-Ly10; B Lymphocyte; Bone Marrow	GSM1227204
Homo sapiens	MDA-MB-157; mDA	GSM2278001
Homo sapiens	MDA-MB-468; mDA	GSM2278009
Homo sapiens	SU-DHL2; B Lymphocyte	GSM1227209
Mus musculus	Mammary Gland	GSM2300477
Mus musculus	Th17	GSM1004860
Mus musculus	AtT-20; Corticotroph; Pituitary	GSM926625
Mus musculus	Embryonic Stem Cell	GSM2561450
Mus musculus	T Lymphocyte	GSM1601733
Mus musculus	T Lymphocyte; Blood	GSM494691
Mus musculus	Dendritic Cell; Spleen	GSM671415
Mus musculus	AtT-20; Corticotroph; Pituitary	GSM2445278
Mus musculus	T Lymphocyte; Spleen	GSM1543812
Mus musculus	T Lymphocyte; Blood	GSM580756
Mus musculus	in vitro polarized Th17 T cells	GSM540722
Mus musculus	primary CD4+ T cells	GSM652877

Mus musculus	Primary Cortical Oligodendrocyte Progenitor (OLP) cells	GSM2650745
--------------	---	------------

7.3 Supplemental Data 3

Related to materials and methods.

c-JUN-related public datasets used to identify potential c-JUN target genes

Microarray/RNA-seq datasets :	ectopic c-JUN expression	
Homo sapiens	141 cells cJUN OE	GSE57520
Homo sapiens	510 cells cJUN OE	GSE57520
Homo sapiens	LPS12 cells cJUN OE	GSE57520
Mus musculus	mouse ESC cJUN OE	GSE50776
Mus musculus	mouse MEF cJUN OE	GSE50776
Microarray/RNA-seq datasets :	c-JUN knockout/knockdown	
Homo sapiens	BT549 cJUN siRNA	GSE71915
Mus musculus	mouse MEF cJUN KO	GSE26205
Mus musculus	mouse ESC cJUN KO	GSE127925
c-JUN CHIP-Seq datasets		
Homo sapiens	A549; Epithelium; Lung	GSM2437886
Homo sapiens	K562; Erythroblast; Bone Marrow	GSM935467
Homo sapiens	MDA-MB-231; Epithelium; Breast	GSM3070218
Homo sapiens	MDA-MB-231; Epithelium; Breast	GSM1700785
Homo sapiens	JHU-06; Endothelial Cell	GSM2576177
Homo sapiens	K562; Erythroblast; Bone Marrow	GSM935569
Homo sapiens	hESC; Embryonic Stem Cell	GSM2945834
Homo sapiens	Coronary artery smooth muscle	GSM1503219
Homo sapiens	LoVo; Colon	GSM1239467
Homo sapiens	Calu-3; Lung	GSM2266291
Homo sapiens	MCF-7; Epithelium; Breast	GSM2736190
Mus musculus	BMDM; Bone Marrow	GSM2974800
Mus musculus	Bone Marrow	GSM2974851
Mus musculus	CH12; Lymphoblastoid; Blood	GSM912901
Mus musculus	T Lymphocyte; Blood	GSM978770
Mus musculus	Chondrocyte; Rib	GSM1891979
Mus musculus	3T3-L1; Preadipocyte; Adipose	GSM1370451
Mus musculus	Th17; Spleen	GSM978770
Mus musculus	Myoblast; Muscle	GSM1354747

7.4 Supplemental Data 4

Related to materials and methods.

SRF-related public datasets used to identify potential SRF target genes

Microarray/RNA-seq datasets :	ectopic SRF expression / SRF induction	
Mus musculus	MEFs, serum-induction	GSE45888
Mus musculus	MEFs, TPA-treatment	GSE75667
Mus musculus	cardiomyocytes, Srf OE	GSE116030
Mus musculus	Neural progenitor cells, Srf OE	GSE90034
Microarray/RNA-seq datasets :	SRF knockout/knockdown	
Mus musculus	Srf KO cardiomyocyte, postnatal day 14	GSE109425
Mus musculus	Srf KO cardiomyocyte, postnatal day 90	GSE109425
SRF ChIP-Seq datasets		
Homo sapiens	HCT-116; Colon	GSM1010851
Homo sapiens	HUES64; Embryonic Stem Cell; Embryo	GSM1505777
Homo sapiens	ECC-1; Epithelium; Endometrium	GSM1010762
Homo sapiens	MCF-7; Epithelium; Breast	GSM1010839
Homo sapiens	A673; Polygonal; Muscle	GSM2436678
Homo sapiens	H1; Embryonic Stem Cell; Embryo	GSM803425
Homo sapiens	K562; Erythroblast; Bone Marrow	GSM803520
Homo sapiens	GM12878; B Lymphocyte; Blood	GSM803477
Homo sapiens	HepG2; Epithelium; Liver	GSM803502
Mus musculus	Neural Progenitor Cell	GSM2835909
Mus musculus	HL-1; Cardiomyocyte; Muscle	GSM471926
Mus musculus	Macrophage; Bone Marrow	GSM1645124
Mus musculus	MEFs; Embryonic Fibroblast	GSM1963110
Mus musculus	10T1/2; Fibroblast; Embryo	GSM992343
Mus musculus	Smooth Muscle Cell; Muscle	GSM3069844
Mus musculus	HL-1; Cardiomyocyte; Muscle	GSM558907
Mus musculus	NIH-3T3; Fibroblast; Embryo	GSM1118304
Mus musculus	Cornea	GSM1310233
Mus musculus	C2C12; Myoblast; Muscle	GSM915168
Mus musculus	Cornea	GSM1310232

7.5 Supplemental Data 5

Related to Figure 23 (upper panel).

List of the significantly up-regulated and down-regulated mRNAs in *Mir34a*-deficient adenomas compared to APCmin adenomas.

Significantly up-regulated mRNAs				Significantly down-regulated mRNAs			
Gene symbol	Base mean	Log ₂ fold change	padj	Gene symbol	Base mean	Log ₂ fold change	padj
<i>Rps3a3</i>	7365.848	7.900	5.03E-192	<i>Gabarapl2</i>	3202.215	-0.303	0.029481797
<i>Fabp6</i>	767.475	6.368	0.01538984	<i>Ergic3</i>	5896.202	-0.307	0.004985113
<i>Plb1</i>	1915.384	6.354	0.022477423	<i>Spns1</i>	1388.700	-0.316	0.027956778
<i>Defa2</i>	1181.559	6.155	0.000655073	<i>Irf2</i>	2226.794	-0.321	0.039577983
<i>Rpl3-ps1</i>	3154.752	5.619	7.35E-29	<i>Prdx1</i>	43626.677	-0.328	0.013437061
<i>Ighv1-14</i>	88.538	5.483	0.004199661	<i>Gstp1</i>	9014.622	-0.333	0.013909296
<i>Gm15308</i>	4457.504	5.439	0.003596828	<i>Ndufs2</i>	11298.639	-0.370	0.045873581
<i>Rps15a-ps8</i>	276.792	5.394	0.002694744	<i>Ifngr2</i>	8121.770	-0.371	0.046564398
<i>Rps3a2</i>	4774.443	5.315	8.82E-134	<i>Pias4</i>	1121.766	-0.373	0.047914688
<i>Gm3608</i>	805.717	4.473	3.25E-17	<i>Cldn3</i>	8208.716	-0.376	0.036137412
<i>Rps13-ps1</i>	1983.568	4.431	0.007955448	<i>Tarbp2</i>	1136.451	-0.378	0.031695187
<i>Defa21</i>	3706.476	4.322	0.006304795	<i>Yeats4</i>	1733.899	-0.383	0.012563872
<i>AA465934</i>	77.127	4.297	2.13E-20	<i>Ctla</i>	7721.149	-0.397	0.009153475
<i>Defa22</i>	3855.396	4.265	0.002466613	<i>Reps1</i>	1045.399	-0.428	0.030962392
<i>Defa20</i>	8548.141	4.142	0.004196561	<i>Atox1</i>	1836.608	-0.429	0.028218178
<i>Gm7861</i>	3360.437	4.073	0.000323885	<i>Cers2</i>	5373.356	-0.441	0.01538984
<i>Art2a-ps</i>	183.008	3.650	8.50E-13	<i>Pgap2</i>	1416.924	-0.442	0.006777366
<i>Gm45187</i>	65.610	3.650	0.001411018	<i>Gadd45a</i>	1024.789	-0.448	0.009020599
<i>Gm14851</i>	1259.746	3.649	0.000145422	<i>Rpl23a-ps3</i>	10540.275	-0.453	0.029481797
<i>Defa26</i>	114.578	3.503	0.000417858	<i>Ptms</i>	8250.755	-0.454	0.043934443
<i>Ighv1-79</i>	14.107	3.476	0.01538984	<i>Mknk2</i>	5343.088	-0.463	0.014760848
<i>Myo18b</i>	134.365	3.398	6.65E-25	<i>Chp1</i>	12646.494	-0.464	0.007879368
<i>BC021767</i>	64.456	3.391	0.001147298	<i>ErbB2</i>	3870.487	-0.479	0.033014213
<i>Aqp4</i>	261.910	3.359	1.54E-07	<i>Slc22a18</i>	2124.810	-0.485	0.048792327
<i>Defa-rs1</i>	1201.228	3.163	2.14E-11	<i>Atg2a</i>	1473.816	-0.488	0.008790228
<i>Miat</i>	22.298	3.108	0.002253683	<i>Mrpl48</i>	1607.691	-0.489	0.013402095
<i>Defa5</i>	2904.156	3.066	0.01475314	<i>Gins4</i>	846.685	-0.490	0.011241874
<i>Gm14850</i>	6012.373	3.039	0.035921244	<i>Hmgb1</i>	4378.909	-0.490	0.000655073
<i>Hand1</i>	27.773	3.007	0.01278381	<i>Prr15l</i>	4483.967	-0.498	0.009259377
<i>Nrcam</i>	42.075	2.995	0.00586178	<i>Sdf2</i>	2426.141	-0.518	0.012190125
<i>Thbs4</i>	83.274	2.955	0.020008038	<i>Gsto1</i>	11944.443	-0.523	0.021332972
<i>AY761184</i>	1350.587	2.947	0.027503502	<i>Tpra1</i>	959.220	-0.524	0.014760848
<i>Defa3</i>	550.794	2.911	0.02480173	<i>Ccdc34</i>	4462.785	-0.525	0.000782987
<i>Kcne4</i>	199.865	2.890	0.007303028	<i>Irf6</i>	7954.086	-0.535	0.011338462
<i>Duox1</i>	26.797	2.844	0.002836718	<i>Prune</i>	1687.158	-0.542	2.91E-05
<i>Golga7b</i>	25.428	2.817	0.004387201	<i>1700037H04Rik</i>	874.154	-0.546	0.045873581
<i>Lipf</i>	657.991	2.750	0.036908696	<i>Mrpl9</i>	2542.514	-0.559	0.000380263

<i>Mamdc2</i>	20.509	2.746	0.011941856	<i>Lfng</i>	859.884	-0.559	0.02934946
<i>Gpr182</i>	156.057	2.742	7.82E-10	<i>Rnf41</i>	972.869	-0.564	0.027503502
<i>Dgkb</i>	29.136	2.692	0.01250952	<i>Phldb3</i>	328.312	-0.571	0.037543532
<i>Calb2</i>	19.154	2.634	0.006097704	<i>Cdc42ep5</i>	2133.673	-0.578	0.025068965
<i>Rfx6</i>	37.882	2.583	0.030360614	<i>Plin2</i>	3099.749	-0.588	0.002088621
<i>Pcdhgb7</i>	62.021	2.582	0.023879709	<i>Tcat2</i>	1069.726	-0.589	0.00238409
<i>Scn7a</i>	72.802	2.579	0.003431915	<i>Grb7</i>	3886.749	-0.605	0.009630487
<i>Grem1</i>	2077.216	2.567	0.018053765	<i>Fbln1</i>	3926.405	-0.611	0.008493992
<i>Gm20633</i>	26.420	2.558	0.025806832	<i>Gm19680</i>	629.006	-0.618	0.041547738
<i>Gm15284</i>	4958.415	2.554	0.01250952	<i>Atg101</i>	1338.362	-0.621	0.007961059
<i>Kcna2</i>	34.843	2.538	0.009144102	<i>Krt23</i>	8932.446	-0.622	0.034723281
<i>Angptl1</i>	20.343	2.514	0.008806327	<i>Mettl23</i>	485.021	-0.644	0.037857791
<i>Scgb3a1</i>	19.532	2.486	0.00689615	<i>Aamdc</i>	916.824	-0.648	0.004578594
<i>Susd2</i>	1132.678	2.446	0.02934946	<i>Ing4</i>	1571.023	-0.658	0.00173874
<i>Retnlb</i>	332.232	2.417	2.35E-05	<i>St3gal6</i>	1880.357	-0.659	0.032240436
<i>Tmem116</i>	34.355	2.416	0.000245695	<i>Apobec3</i>	3317.659	-0.667	0.019296155
<i>Scara5</i>	53.498	2.414	0.001512289	<i>Shisa2</i>	1372.872	-0.688	0.001646867
<i>Tmem100</i>	33.667	2.409	0.000481879	<i>Rarg</i>	694.579	-0.710	0.009020599
<i>Chrm2</i>	171.085	2.345	0.004196561	<i>Capza1</i>	7491.254	-0.714	0.018573937
<i>Scn3b</i>	93.753	2.345	0.006795926	<i>Slc26a6</i>	4021.419	-0.714	0.013402095
<i>Mfap4</i>	133.454	2.313	8.80E-05	<i>Eif3j1</i>	1293.122	-0.716	0.013192269
<i>Kcnn3</i>	38.473	2.286	0.002203296	<i>Rpl28</i>	10034.868	-0.719	0.001462614
<i>Slit3</i>	99.178	2.284	5.76E-06	<i>Nectin4</i>	653.866	-0.721	0.024939507
<i>Lgr6</i>	39.258	2.284	0.009153475	<i>Ptgr1</i>	11085.631	-0.724	0.007876924
<i>Slc22a3</i>	38.608	2.277	0.014064026	<i>Zfpm1</i>	3487.555	-0.728	0.000199802
<i>Kcnp2</i>	27.307	2.270	0.040486325	<i>Cdc25b</i>	1056.552	-0.730	0.012586633
6330403A02Rik	65.759	2.268	0.000265291	<i>Rpl3</i>	36457.453	-0.735	0.000664812
<i>Ackr1</i>	38.321	2.264	0.008687209	<i>Ppfbp2</i>	1386.982	-0.749	0.009020599
<i>Gcg</i>	89.144	2.260	9.86E-05	<i>Ovol2</i>	398.038	-0.763	0.035524674
<i>Fbln2</i>	128.008	2.256	1.25E-05	AA467197	5407.425	-0.775	0.01191737
<i>Pgm5</i>	344.438	2.237	6.07E-06	<i>Klhl42</i>	882.789	-0.788	0.030360614
<i>Diras2</i>	29.314	2.220	0.008493992	<i>Sytl4</i>	215.104	-0.791	0.012035597
<i>Tnfrsf8</i>	14.841	2.219	0.009020599	<i>Scnm1</i>	685.689	-0.807	0.000499371
<i>Vstm2b</i>	53.779	2.219	0.045873581	<i>Gm42528</i>	215.563	-0.876	0.034723281
<i>Adamts13</i>	50.448	2.211	0.010044251	<i>Rplp0</i>	60447.318	-0.879	0.033505958
<i>Sdk1</i>	32.962	2.210	0.027503502	<i>Rhebl1</i>	169.444	-0.893	0.039189471
<i>Chrdl1</i>	107.589	2.198	0.023700698	<i>Ltbp4-1</i>	2946.853	-0.909	0.034223382
<i>Olfm4</i>	1117.010	2.197	0.000180627	<i>Epn3</i>	992.638	-0.914	0.004728021
<i>Hsd11b1</i>	145.683	2.191	2.25E-06	<i>Pop4</i>	934.059	-0.925	2.09E-08
<i>Kcna1</i>	39.678	2.189	0.006171304	<i>Gsta4</i>	2253.318	-0.933	0.017731618
<i>Ildr2</i>	215.074	2.181	0.002088621	<i>Gnal</i>	1382.861	-0.940	0.001540291
<i>Popdc2</i>	47.047	2.174	0.034723281	<i>Ckb</i>	6138.712	-0.957	0.017165872
<i>Defa17</i>	8516.947	2.172	1.61E-06	<i>Pccb</i>	4874.959	-0.960	8.08E-05
<i>Slc14a1</i>	456.593	2.170	0.027503502	<i>Foxq1</i>	2665.362	-1.002	0.034223382
<i>Chrdl2</i>	79.967	2.168	0.02682833	<i>Plcd3</i>	525.744	-1.025	0.002775875
<i>Mgp</i>	177.467	2.166	0.000792201	<i>Rbbp8nl</i>	144.988	-1.050	0.041007313
<i>Hcar1</i>	27.790	2.164	0.017165872	<i>Prss12</i>	1416.146	-1.084	0.000631404

<i>Myh11</i>	3067.121	2.153	0.000414054	<i>4930523C07Rik</i>	763.511	-1.086	0.001240333
<i>Serpina3f</i>	119.859	2.150	0.040486325	<i>Sord</i>	6041.751	-1.090	0.014345091
<i>Wscd2</i>	23.518	2.148	0.030689281	<i>Jmjd7</i>	190.205	-1.093	0.014064026
<i>Bmpr1b</i>	11.583	2.142	0.040486325	<i>Slc46a1</i>	2152.544	-1.101	0.008724678
<i>Fgfbp1</i>	190.898	2.141	0.000732548	<i>Fer1f4</i>	931.099	-1.102	0.029481797
<i>Fmo2</i>	207.033	2.136	0.035524674	<i>T</i>	1084.098	-1.117	0.014064026
<i>Defa24</i>	14430.425	2.133	1.74E-05	<i>Hist1h2bc</i>	3224.411	-1.118	0.012331324
<i>Fgl1</i>	47.000	2.116	0.043273222	<i>Hist2h2be</i>	252.395	-1.208	0.023134605
<i>Pyroxd2</i>	139.202	2.108	5.62E-05	<i>Aadac</i>	1301.692	-1.230	0.030962392
<i>Cd177</i>	2520.281	2.094	5.94E-06	<i>Prr18</i>	1073.154	-1.232	8.34E-05
<i>Chl1</i>	58.221	2.093	0.0010807	<i>Cyp2c68</i>	991.413	-1.315	0.019743052
<i>Cadm3</i>	45.212	2.064	0.000198378	<i>Hr</i>	1810.114	-1.320	0.044858355
<i>Ifi205</i>	88.261	2.058	1.71E-08	<i>2310058D17Rik</i>	36.065	-1.332	0.035243839
<i>Pln</i>	42.448	2.057	0.025068965	<i>2210407C18Rik</i>	11009.390	-1.376	0.020749515
<i>Egfl6</i>	68.381	2.035	0.037466502	<i>Car2</i>	1009.671	-1.403	0.046094557
<i>Exd1</i>	39.342	2.033	0.000128272	<i>Grhl3</i>	703.120	-1.430	4.69E-05
<i>Adamts8</i>	36.693	2.019	0.007876924	<i>Spag4</i>	37.618	-1.471	0.027503502
<i>Arhgap44</i>	77.808	1.992	0.000481879	<i>1700020L24Rik</i>	208.739	-1.608	0.027581575
<i>Rspo3</i>	79.339	1.966	0.00230325	<i>Gm13408</i>	91.275	-1.610	0.007879368
<i>Adcy5</i>	124.989	1.963	0.002029719	<i>Mmp28</i>	600.427	-1.641	0.002754647
<i>Hmcr2</i>	129.101	1.933	0.009630487	<i>Nlrp10</i>	339.620	-1.650	0.001512289
<i>Cxcl12</i>	571.126	1.917	0.001150611	<i>5830444B04Rik</i>	90.065	-1.652	0.005218856
<i>St6galnac3</i>	39.810	1.911	0.009306822	<i>RP23-359B23.11</i>	535.444	-1.669	0.025418747
<i>Fam107a</i>	21.798	1.876	0.012331324	<i>Ighv1-26</i>	618.296	-1.673	0.041664063
<i>Clip4</i>	59.985	1.869	0.001641294	<i>Rn18s-rs5</i>	248.780	-1.706	0.009203985
<i>Plscr2</i>	71.482	1.869	0.002612845	<i>Tmprss11e</i>	160.150	-1.886	0.001937704
<i>Gm14434</i>	128.696	1.868	0.009115883	<i>Ighv1-85</i>	220.677	-2.036	0.013402095
<i>Vip</i>	278.915	1.861	0.000193318	<i>Acat3</i>	66.353	-2.041	0.01002361
<i>Gfra1</i>	126.998	1.849	0.000582725	<i>Slc9a4</i>	154.024	-2.057	0.030251791
<i>Sgip1</i>	28.069	1.839	0.005147696	<i>Gm5586</i>	64.144	-2.120	0.0010807
<i>Mptx2</i>	2685.756	1.834	0.005050337	<i>Ighv1-72</i>	346.927	-2.156	0.006304795
<i>Lrrn1</i>	51.574	1.833	0.014213123	<i>1500015A07Rik</i>	486.008	-2.158	7.35E-29
<i>Slc24a3</i>	163.056	1.825	0.009354026	<i>Cldn18</i>	516.076	-2.171	0.008724678
<i>Dpt</i>	184.713	1.797	0.023879709	<i>Ighv5-4</i>	238.273	-2.224	0.005218856
<i>Sspn</i>	92.837	1.793	9.85E-07	<i>Pgc</i>	278.417	-2.311	0.006328943
<i>4930481B07Rik</i>	39.901	1.793	0.046988981	<i>Ivl</i>	244.012	-2.333	0.009306822
<i>Lama2</i>	49.077	1.787	0.036740585	<i>Igkv17-121</i>	331.207	-2.368	0.017165872
<i>P3h2</i>	67.029	1.780	0.031695187	<i>Rps3a1</i>	30160.999	-2.394	2.90E-45
<i>Synm</i>	619.552	1.773	0.002232397	<i>Ighm</i>	177.569	-2.597	0.017552181
<i>Clca3a1</i>	230.328	1.765	0.035436368	<i>Anxa9</i>	66.465	-2.848	1.10E-05
<i>Slc5a12</i>	1187.123	1.753	0.027581575	<i>Tff1</i>	315.259	-3.129	0.032889928
<i>Ogn</i>	111.501	1.733	0.046312028	<i>Reg1</i>	3434.803	-3.154	0.025068965
<i>Gm16685</i>	29.011	1.722	0.022957788	<i>Marcks1-ps4</i>	25.306	-3.486	0.02934946
<i>Ceacam10</i>	616.562	1.710	0.000792201				
<i>Scg3</i>	27.950	1.708	0.030360614				
<i>Ldhb</i>	293.015	1.702	6.05E-06				
<i>Crispld2</i>	439.633	1.701	0.005944366				

<i>Ror1</i>	49.156	1.692	0.040486325
<i>Rims1</i>	164.029	1.688	0.025068965
<i>Sfrp1</i>	365.529	1.688	0.000433835
<i>Rdh16</i>	399.418	1.687	0.026866872
<i>Actg2</i>	2107.656	1.682	0.027503502
<i>Lgi2</i>	135.524	1.663	0.025806832
<i>Tbx1</i>	349.553	1.659	3.67E-06
<i>Lipg</i>	161.669	1.654	0.041007313
<i>Cnn1</i>	906.427	1.652	0.026062685
<i>Nkd2</i>	79.037	1.652	0.009354026
<i>Tchh</i>	113.748	1.650	2.41E-05
<i>Galnt15</i>	59.749	1.631	0.030962392
<i>Tnxb</i>	119.838	1.631	0.005682432
<i>Hoxb8</i>	28.826	1.630	0.027503502
<i>Gpm6a</i>	31.285	1.601	0.025621987
<i>Fibin</i>	48.407	1.601	0.049876245
<i>Col8a1</i>	81.304	1.589	0.010542741
<i>Cygb</i>	256.459	1.580	0.007694842
<i>Mrgprf</i>	38.265	1.571	0.006304795
<i>Mmn1</i>	269.169	1.566	0.011338462
<i>Wnt2b</i>	51.620	1.561	0.006467812
<i>Slc7a11</i>	468.273	1.546	0.007879368
<i>Pcdh20</i>	71.666	1.541	0.017165872
<i>Phactr1</i>	42.458	1.537	0.03856856
<i>Tmem252</i>	437.823	1.535	0.025590556
<i>Slc1a1</i>	401.313	1.527	0.000713188
<i>Cap2</i>	149.616	1.526	0.014975205
<i>Tgfb3</i>	208.448	1.519	0.020749332
<i>Tgm4</i>	139.989	1.518	0.041336149
<i>Tpm2</i>	2129.924	1.514	0.027754834
<i>Ak1</i>	125.795	1.505	0.001512289
<i>Jph2</i>	199.656	1.499	0.00989613
<i>Rgs7bp</i>	81.145	1.489	0.000200618
<i>Kcnmb1</i>	96.798	1.476	0.020749515
<i>C4b</i>	1110.783	1.468	0.002760684
<i>9130208D14Rik</i>	664.824	1.465	0.046922751
<i>Adgrd1</i>	428.596	1.464	0.01250952
<i>Svep1</i>	63.346	1.461	0.005050337
<i>Col23a1</i>	135.872	1.461	0.005653967
<i>Atp1a2</i>	272.819	1.459	0.014345091
<i>Wnt10a</i>	52.028	1.457	0.031681957
<i>Ntn1</i>	180.815	1.454	0.041329523
<i>Frzb</i>	67.584	1.452	0.017165872
<i>Il18r1</i>	32.299	1.448	0.027087442
<i>Slc6a4</i>	664.185	1.443	0.005815348
<i>Rab3c</i>	58.671	1.418	0.003431915
<i>Reg4</i>	20307.094	1.411	0.035436368

<i>Serpina3g</i>	324.859	1.405	0.046090485
<i>Tagln</i>	3364.471	1.403	0.01288103
<i>Colec12</i>	194.425	1.402	6.01E-05
<i>Scpep1</i>	1808.205	1.391	3.56E-08
<i>Atp2b4</i>	442.674	1.387	0.008790228
<i>Nsg2</i>	47.760	1.383	0.034223382
<i>Afap111</i>	419.403	1.373	4.85E-08
<i>Madcaml</i>	75.981	1.361	0.024205518
<i>Slc13a2os</i>	42.923	1.357	0.036661955
<i>Ctsk</i>	160.736	1.355	0.042074167
<i>Cacna1e</i>	34.799	1.350	0.034723281
<i>Map3k8</i>	58.561	1.344	0.015838215
<i>Aoc3</i>	174.877	1.342	0.029481797
<i>Slc16a7</i>	66.883	1.338	0.018875724
<i>Ccnjl</i>	244.400	1.320	0.00024649
<i>Bhlha15</i>	144.712	1.314	1.03E-05
<i>Robo2</i>	113.323	1.307	0.034223382
<i>Lcn2</i>	3451.916	1.297	2.86E-10
<i>Gatm</i>	207.704	1.284	0.005850832
<i>Fzd10</i>	473.166	1.281	0.002754647
<i>Spon1</i>	679.469	1.279	0.01538984
<i>Gm8995</i>	148.133	1.270	0.018622276
<i>Islr</i>	125.884	1.263	0.027956778
<i>Scube1</i>	516.106	1.254	0.025068965
<i>Acta2</i>	3799.431	1.251	0.035436368
<i>Gem</i>	398.075	1.248	0.024541839
<i>Lmod1</i>	246.029	1.239	0.015245364
<i>Tmprss6</i>	131.498	1.233	0.044018441
<i>Reln</i>	175.611	1.233	0.036740585
<i>Gm10221</i>	1353.661	1.229	0.049493666
<i>Slc2a13</i>	114.435	1.213	0.035524674
<i>Ppp1r3c</i>	59.817	1.203	0.011161326
<i>Cacna1c</i>	180.309	1.196	0.034723281
<i>Ffar2</i>	247.244	1.189	0.001932919
<i>Abcc9</i>	627.487	1.186	0.038751848
<i>Bpifb5</i>	4212.674	1.180	0.030708576
<i>Cdh11</i>	281.891	1.167	0.009144102
<i>Clmp</i>	550.804	1.161	0.00989613
<i>Alpl</i>	118.604	1.159	0.022581697
<i>Ank2</i>	52.010	1.145	0.037319884
<i>Igf2</i>	233.996	1.137	0.00388279
<i>Aebp1</i>	199.246	1.136	0.039577983
<i>Dab2</i>	348.936	1.134	0.000199329
<i>S1pr3</i>	110.543	1.130	0.012190125
<i>Ly6c1</i>	360.606	1.123	0.01538984
<i>Esyt3</i>	446.819	1.121	0.005302339
<i>Grb10</i>	352.096	1.119	0.045824379

<i>Fxyd6</i>	365.293	1.103	0.038520262
<i>Enpp2</i>	269.676	1.088	0.034723281
<i>Naip6</i>	1361.947	1.078	0.000664812
<i>Map9</i>	183.603	1.077	0.019837731
<i>1810041L15Rik</i>	61.867	1.070	0.038751848
<i>Dennd2a</i>	174.331	1.067	0.035524674
<i>Myom1</i>	97.922	1.064	0.010297742
<i>Ednra</i>	248.043	1.063	0.036661955
<i>Speg</i>	71.379	1.050	0.030345512
<i>Rab15</i>	571.196	1.038	0.004988689
<i>Cps1</i>	6236.874	1.037	0.000169271
<i>Lbp</i>	350.987	1.036	0.000364096
<i>Abhd3</i>	1886.627	1.029	0.021616191
<i>Rasgrp3</i>	271.629	1.028	0.009825326
<i>Dram1</i>	143.411	1.028	0.046090485
<i>Timp3</i>	2118.665	1.026	0.012586633
<i>2610528A11Rik</i>	999.919	1.026	0.03856856
<i>Dlc1</i>	367.866	1.021	0.017165872
<i>Zcchc24</i>	455.524	1.016	0.014064026
<i>Gm8797</i>	4024.288	1.013	0.000180627
<i>Dkk2</i>	749.595	1.012	0.036137412
<i>C3</i>	1230.079	1.005	0.029481797
<i>Ramp2</i>	148.665	0.999	0.009144102
<i>Tmem154</i>	136.608	0.998	0.028315757
<i>Ddr2</i>	416.252	0.996	0.003596828
<i>Rgs5</i>	3589.823	0.995	0.008335317
<i>Tifa</i>	2135.205	0.994	0.014760848
<i>Calcr1</i>	300.951	0.988	7.13E-08
<i>Adgra2</i>	205.363	0.984	0.027246381
<i>Fam129a</i>	744.024	0.977	0.006586479
<i>Ptpm</i>	189.448	0.970	0.030813463
<i>Prickle2</i>	130.732	0.969	0.001932919
<i>Naip3</i>	158.740	0.968	0.046528149
<i>Rab3il1</i>	85.077	0.958	0.036661955
<i>Rdx</i>	912.403	0.952	0.000256631
<i>Bbs12</i>	92.916	0.950	0.026408953
<i>Nr1h4</i>	897.947	0.939	0.002709267
<i>Socs1</i>	131.853	0.926	0.034223382
<i>Scnn1a</i>	296.339	0.904	0.031055812
<i>Trps1</i>	134.942	0.904	0.04636375
<i>Sparcl1</i>	2663.433	0.901	0.037543532
<i>Sorbs1</i>	332.042	0.895	0.00589292
<i>Msr1</i>	312.164	0.891	0.015757774
<i>Aldh1b1</i>	5403.622	0.876	0.004988689
<i>Itih5</i>	419.200	0.838	0.037056702
<i>Xrcc3</i>	154.468	0.835	0.006343772
<i>Lss</i>	1720.971	0.831	0.024205518

<i>Zeb2</i>	283.027	0.825	0.034723281
<i>Apod</i>	185.497	0.824	0.016268569
<i>9130409J20Rik</i>	1488.501	0.791	0.00213228
<i>Nrbp2</i>	466.891	0.787	6.07E-06
<i>Itga9</i>	772.020	0.769	0.037319884
<i>Cuedc1</i>	784.792	0.767	0.019743052
<i>Grap</i>	211.826	0.759	0.023455023
<i>Hsd17b7</i>	1653.746	0.750	0.003431915
<i>Man2a2</i>	647.197	0.735	0.002775875
<i>Acad10</i>	345.546	0.731	0.00571129
<i>St3gal1</i>	703.224	0.720	0.043418421
<i>Frdm6</i>	553.840	0.719	0.003689416
<i>Sema6b</i>	300.766	0.692	0.027503502
<i>Heg1</i>	1533.529	0.662	0.019743052
<i>Mylk</i>	7195.280	0.650	0.034723281
<i>Fgf1</i>	386.073	0.646	0.030962392
<i>Kdm2b</i>	915.433	0.639	0.006304795
<i>Pwwp2a</i>	677.469	0.633	0.000323885
<i>Jrk</i>	225.394	0.630	0.003689416
<i>Pq/c3</i>	633.138	0.629	0.000200618
<i>Ttip11</i>	1944.493	0.536	0.000582725
<i>Pmp</i>	694.032	0.527	0.032795982
<i>Ikbip</i>	789.909	0.517	0.045693103
<i>Fam46c</i>	1216.773	0.495	0.031695187
<i>Guf1</i>	829.006	0.463	0.027956778
<i>Clec16a</i>	716.946	0.459	0.013402095
<i>Thg1l</i>	705.235	0.458	0.036740585
<i>Rab8b</i>	1037.103	0.445	0.023879709
<i>Txndc11</i>	1424.988	0.435	0.015757774

7.6 Supplemental Data 6

Related to Figure 23 (middle panel).

List of the significantly up-regulated and down-regulated mRNAs in *Csf1r*-deficient adenomas compared to APCmin adenomas.

Significantly up-regulated mRNAs				Significantly down-regulated mRNAs			
Gene symbol	Base mean	Log ₂ fold change	padj	Gene symbol	Base mean	Log ₂ fold change	padj
<i>Gm5855</i>	79.263	5.220	3.23E-06	<i>Fam195b</i>	991.830	-0.451	0.04707577
<i>Myo18b</i>	134.365	3.328	1.93E-27	<i>Snx33</i>	514.073	-0.539	0.04912398
<i>Gm10073</i>	284.797	2.487	0.03412056	<i>Rpl28</i>	10034.868	-0.581	0.04152231
<i>Art2a-ps</i>	183.008	2.095	0.00086333	<i>Gm12396</i>	471.435	-0.652	0.04083381
<i>Igkv4-57</i>	276.786	1.980	2.83E-09	<i>Sytl1</i>	365.210	-0.652	0.03078012

<i>Lgi2</i>	135.524	1.784	0.02721687	<i>Plip</i>	3145.911	-0.675	0.00297421
<i>RP23-359B23.11</i>	535.444	1.731	0.03412056	<i>Tacstd2</i>	998.534	-0.983	0.03643623
<i>Olfm4</i>	1117.010	1.645	0.02751039	<i>Dynlt1b</i>	4265.072	-1.050	0.0122282
<i>Cxcl5</i>	327.741	1.624	0.01837011	<i>Gm10116</i>	149.433	-1.159	0.00707855
<i>Ccr10</i>	43.466	1.595	0.04519266	<i>Rps3a2</i>	4774.443	-1.208	1.63E-05
<i>Ccdc109b</i>	83.369	1.586	0.04912398	<i>A930005H10Rik</i>	136.660	-1.270	0.00689268
<i>Lcn2</i>	3451.916	1.392	3.96E-13	<i>Gm44364</i>	427.610	-1.362	0.02262992
<i>Ceacam10</i>	616.562	1.323	0.04707577	<i>4930452B06Rik</i>	120.028	-1.410	0.0224567
<i>Pgk1-rs7</i>	4328.375	1.276	0.00299794	<i>Slc30a2</i>	7831.799	-1.448	0.01527869
<i>Igkv10-96</i>	1302.762	1.173	0.02944119	<i>5830444B04Rik</i>	90.065	-1.508	0.02948249
<i>Zc3h12a</i>	744.107	1.169	0.00305893	<i>Otof</i>	270.110	-1.590	0.01123515
<i>Emp3</i>	171.801	1.148	0.01428724	<i>Prom2</i>	510.368	-1.613	0.00462801
<i>Igkv1-110</i>	1678.083	1.095	0.02632293	<i>Gm44639</i>	23.103	-2.046	0.02191538
<i>Pigr</i>	45894.595	0.963	0.01123515	<i>Upk3a</i>	58.324	-2.069	0.04733272
<i>Ccdc88b</i>	894.810	0.939	0.0122282	<i>4930480K23Rik</i>	106.807	-2.299	5.85E-05
<i>Msr1</i>	312.164	0.911	0.02721687	<i>Psca</i>	75.779	-2.658	0.00037792
<i>Cps1</i>	6236.874	0.876	0.00508292	<i>Gm3716</i>	82.965	-4.069	0.00028973
<i>Parp8</i>	110.106	0.857	0.03822121	<i>Gm5292</i>	114.493	-4.124	0.00023307
<i>Elov6</i>	4376.025	0.796	0.006574	<i>Gdpd3</i>	744.287	-4.319	4.60E-05
<i>Pqlc3</i>	633.138	0.694	1.52E-05	<i>Gm10020</i>	1658.950	-4.611	0.00707855
<i>Tfip11</i>	1944.493	0.614	2.07E-05	<i>Gm14094</i>	123.550	-4.882	2.07E-05
<i>Rab8b</i>	1037.103	0.525	0.00689268				
<i>Tbc1d1</i>	2199.426	0.424	0.04774773				

7.7 Supplemental Data 7

Related to Figure 23 (lower panel).

List of the significantly up-regulated and down-regulated mRNAs in *Csf1r/Mir34a*-deficient adenomas compared to APCmin adenomas.

Significantly up-regulated mRNAs				Significantly down-regulated mRNAs			
Gene symbol	Base mean	Log ₂ fold change	padj	Gene symbol	Base mean	Log ₂ fold change	padj
<i>Rps3a3</i>	7365.848	7.080	1.94E-148	<i>Tet3</i>	3028.933	-0.398	0.04349876
<i>Rps3a2</i>	4774.443	4.781	1.31E-104	<i>Snx33</i>	514.073	-0.599	0.04718123
<i>Myo18b</i>	134.365	3.104	1.60E-19	<i>2310007B03Rik</i>	208.929	-0.837	0.00630993
<i>Igkv4-74</i>	228.277	2.848	3.45E-13	<i>Tst</i>	1714.678	-0.880	0.00069462
<i>Igkv8-21</i>	338.034	2.234	0.03279428	<i>lhh</i>	2353.000	-1.001	0.02624866

<i>Zik1</i>	47.770	1.831	0.03447439	<i>Grhl3</i>	703.120	-1.065	0.04349876
<i>Igkv4-57</i>	276.786	1.468	0.00093579	<i>Pitx1</i>	3637.836	-1.084	0.0285036
<i>Dclk1</i>	574.268	1.376	0.03469885	<i>Rps3a1</i>	30160.999	-1.088	1.03E-07
<i>Tmem154</i>	136.608	1.204	0.02596738	<i>Nectin4</i>	653.866	-1.120	0.00013334
<i>Ighv3-6</i>	676.428	1.128	0.04349876	<i>Tacstd2</i>	998.534	-1.185	0.0117698
<i>Lcn2</i>	3451.916	1.120	7.04E-07	<i>Smtnl2</i>	126.920	-1.389	0.0174334
<i>Ythdc2</i>	714.383	0.721	0.04065494	<i>Psca</i>	75.779	-2.489	0.00713858
<i>Ttip11</i>	1944.493	0.575	0.00080029	<i>Amd2</i>	266.155	-2.525	0.01024457
<i>Cacna2d1</i>	598.594	0.540	0.00796881	<i>Prss56</i>	56.568	-3.182	0.02468076
<i>Yipf5</i>	2860.125	0.491	0.03164122	<i>Mrpl23</i>	56.739	-3.261	0.0174334
				<i>Gpx5</i>	1509.304	-3.309	7.04E-07
				<i>Otof</i>	270.110	-3.610	1.86E-14

7.8 Supplemental Data 8

Related to Figure 25 (upper panel).

List of the significantly up-regulated and down-regulated mRNAs in *Mir34a*-deficient tumoroids compared to APCmin tumoroids.

Significantly up-regulated mRNAs				Significantly down-regulated mRNAs			
Gene symbol	Base mean	Log ₂ fold change	padj	Gene symbol	Base mean	Log ₂ fold change	padj
<i>Gm26983</i>	58.479	7.7867	2.13E-06	<i>Rplp1</i>	38053.806	-0.4389	0.02686749
<i>Rps15a-ps8</i>	388.681	6.3442	6.85E-26	<i>Ptdn2</i>	3141.819	-0.4619	0.039301847
<i>Rps3a3</i>	9251.682	6.3149	0.033622703	<i>Gm10288</i>	23568.680	-0.4624	0.01254258
<i>Eif5a13-ps</i>	407.649	6.2895	3.27E-23	<i>Txn2</i>	4596.942	-0.4629	0.03226749
<i>Pcna-ps2</i>	288.898	6.2178	0.035074212	<i>Atp5g1</i>	3889.207	-0.4699	0.025179762
<i>Rpl3-ps1</i>	7061.173	6.1786	3.47E-73	<i>Pdlim1</i>	3650.079	-0.5009	0.043745185
<i>Dkk2</i>	453.441	5.4580	6.61E-11	<i>Polr2f</i>	2310.410	-0.5103	0.031096841
<i>Map2</i>	50.565	5.2654	0.00029331	<i>Yars</i>	3734.939	-0.5143	0.044491147
<i>Gm10182</i>	3021.766	5.2066	5.50E-05	<i>Farsb</i>	3720.800	-0.5321	0.031486728
<i>Rps13-ps1</i>	2526.239	4.9347	1.24E-35	<i>Exosc5</i>	1997.158	-0.5329	0.040526834
<i>Gna14</i>	19.121	4.8714	0.017247803	<i>Mrps35</i>	2076.005	-0.5401	0.011986291
<i>Zfp462</i>	209.491	4.6563	0.000535601	<i>Avpi1</i>	2223.613	-0.5433	0.044447523
<i>Osr2</i>	353.031	4.6128	4.01E-07	<i>Uqcr11</i>	2683.728	-0.5457	0.03593397
<i>Gm13067</i>	24.628	4.5651	0.003838555	<i>Ak2</i>	6996.502	-0.5471	0.041861089
<i>Gm29865</i>	63.006	4.1001	1.56E-06	<i>Nars</i>	12209.446	-0.5560	0.018804648
<i>Lce6a</i>	31.040	4.1000	0.001224934	<i>Gm12191</i>	5621.323	-0.5564	0.044447523

<i>Lrrn3</i>	81.537	4.0977	9.01E-07	<i>Josd2</i>	965.835	-0.5688	0.047747905
<i>Ncf2</i>	100.728	4.0479	7.67E-05	<i>Phf10</i>	2539.081	-0.5741	0.032323626
<i>Sh3tc2</i>	164.916	4.0409	0.000377131	<i>Cd3eap</i>	1211.518	-0.5833	0.030189793
<i>Gm4742</i>	17.256	4.0299	0.021414412	<i>Sepw1</i>	3144.474	-0.5844	0.009181118
<i>Prickle1</i>	102.734	3.9337	3.87E-08	<i>Bpnt1</i>	3236.641	-0.5868	0.007005518
<i>Pcdh7</i>	133.184	3.9325	2.76E-05	<i>lfrd2</i>	3023.251	-0.5956	0.017055556
<i>Col14a1</i>	201.523	3.8356	0.00040056	<i>Tspan13</i>	1561.084	-0.6035	0.017247803
<i>Adams16</i>	65.187	3.8186	0.008705004	<i>Htra2</i>	1798.309	-0.6037	0.006506994
<i>Cd1d2</i>	19.639	3.7583	0.021414412	<i>Rdm1</i>	864.919	-0.6062	0.033216916
<i>Clstn2</i>	124.617	3.6177	0.012789462	<i>Ndufc2</i>	3251.713	-0.6075	0.016166281
<i>Gm10167</i>	119.470	3.5994	5.36E-09	<i>Sars</i>	9547.795	-0.6082	0.008705004
<i>Gm20765</i>	30.015	3.5701	0.038940547	<i>Cisd3</i>	3970.507	-0.6089	0.020028688
<i>Gm12669</i>	217.052	3.5623	0.006482775	<i>Pla2g16</i>	1816.482	-0.6106	0.005569682
<i>Tmprss13</i>	233.005	3.5214	6.94E-08	<i>Mrpl48</i>	1501.526	-0.6201	0.044491147
<i>Syt14</i>	41.957	3.4989	0.002399799	<i>Lgals9</i>	3997.136	-0.6225	0.025439644
<i>C2cd4b</i>	53.132	3.4960	0.003073485	<i>Ablim1</i>	8085.867	-0.6251	0.028181189
<i>Krt6a</i>	622.517	3.3619	1.95E-07	<i>Adi1</i>	2129.068	-0.6357	0.032846535
<i>Irx5</i>	654.455	3.3569	8.77E-07	<i>Fau</i>	5507.797	-0.6359	0.004346964
<i>5830418P13Rik</i>	29.126	3.3070	0.010918488	<i>Hspe1</i>	6125.856	-0.6373	0.00029331
<i>Wnt10a</i>	134.731	3.2749	7.23E-06	<i>Seps2</i>	6156.994	-0.6399	0.007281661
<i>A730046J19Rik</i>	20.756	3.2640	0.031145921	<i>Slc25a33</i>	587.962	-0.6475	0.046495889
<i>RP23-145I16.5</i>	350.152	3.1835	0.000857117	<i>Etfb</i>	3480.838	-0.6508	0.00608095
<i>Ism1</i>	66.649	3.0383	0.001851081	<i>Stc2</i>	3233.118	-0.6572	0.044447523
<i>Sema3e</i>	46.535	2.9431	0.017645334	<i>Ccdc115</i>	959.053	-0.6577	0.023385194
<i>Gpr157</i>	136.064	2.9149	2.01E-06	<i>Srm</i>	2837.704	-0.6725	0.02074829
<i>Sema3a</i>	20.760	2.9028	0.044491147	<i>Slc1a5</i>	8623.988	-0.6786	0.010463607
<i>H2-Q1</i>	76.012	2.9001	0.000442197	<i>Pgm1</i>	2955.085	-0.6830	0.00437696
<i>Ldb3</i>	148.811	2.7480	0.008773847	<i>Comtd1</i>	941.625	-0.6882	0.008705004
<i>AA465934</i>	54.151	2.7433	0.000199587	<i>Psat1</i>	10218.800	-0.7085	0.022622615
<i>Rassf4</i>	342.221	2.7352	0.00017682	<i>Elf4ebp1</i>	2434.218	-0.7108	0.017375236
<i>Col16a1</i>	348.416	2.6824	5.65E-06	<i>Aldh18a1</i>	4267.609	-0.7233	0.022622615
<i>Hydin</i>	54.207	2.6007	0.022622615	<i>Mrps14</i>	1319.839	-0.7265	0.001851081
<i>Znf41-ps</i>	118.132	2.5969	0.000226429	<i>Stra13</i>	1024.293	-0.7281	0.024255873
<i>Tpbp</i>	262.197	2.5805	7.57E-07	<i>Ankrd54</i>	1071.513	-0.7291	0.002533876
<i>Gm12603</i>	116.628	2.5030	0.011619079	<i>Rangrf</i>	932.487	-0.7395	0.008320802
<i>Crnpe</i>	233.410	2.5025	0.019067493	<i>Uqcrq</i>	4420.500	-0.7404	0.001084068
<i>Gm20463</i>	77.245	2.4822	0.00044797	<i>Gsdmd</i>	5121.295	-0.7415	0.017247803
<i>Foxc1</i>	135.177	2.4768	0.014067655	<i>Abhd14b</i>	804.064	-0.7447	0.044447523
<i>Cald1</i>	235.175	2.4538	7.10E-05	<i>Hacd1</i>	580.779	-0.7524	0.008705004
<i>Htra1</i>	58.451	2.4441	0.005027141	<i>1700021F05Rik</i>	743.671	-0.7640	0.00438845
<i>Pla2g4c</i>	131.244	2.4269	0.00634789	<i>Paax</i>	1104.511	-0.7659	0.02857225
<i>Alox12b</i>	34.856	2.4038	0.038461557	<i>Bcat2</i>	3863.999	-0.7695	0.005720174
<i>Dpysl3</i>	1071.417	2.3457	1.99E-12	<i>Mib2</i>	1440.506	-0.7833	0.039139573
<i>Cubn</i>	189.357	2.3409	0.024723452	<i>Ldhd</i>	709.184	-0.7901	0.023877748
<i>Bmp3</i>	143.041	2.3184	0.006394847	<i>Creg1</i>	1175.404	-0.7967	0.021093708
<i>St6gal1</i>	576.819	2.3022	1.31E-06	<i>Vkorc1</i>	499.561	-0.7980	0.009621267
<i>Map9</i>	73.987	2.2764	0.003995557	<i>Shmt2</i>	8341.442	-0.8005	0.001851081

<i>Tenn4</i>	1017.163	2.2691	1.25E-07	<i>Fam195a</i>	559.201	-0.8018	0.038582858
<i>Golga7b</i>	475.245	2.2624	1.55E-07	<i>Aldh2</i>	10127.622	-0.8041	0.030315134
<i>Cldn8</i>	448.057	2.2237	0.047326482	<i>Alg8</i>	1148.273	-0.8088	0.026951216
<i>Grap</i>	127.581	2.2232	5.67E-06	<i>Palld</i>	1415.799	-0.8168	0.045827358
<i>Arhgap44</i>	637.247	2.2028	4.23E-08	<i>Ifi2712b</i>	898.811	-0.8213	0.002872761
<i>Vim</i>	3736.819	2.1884	9.87E-05	<i>Cd63</i>	7825.030	-0.8334	0.017645334
<i>Neur11a</i>	408.601	2.1805	0.000951084	<i>Slc18a1</i>	546.427	-0.8381	0.042408344
<i>Dst</i>	784.736	2.1662	7.22E-05	<i>Slc12a8</i>	1296.432	-0.8390	0.000517548
<i>Scube1</i>	254.954	2.1612	0.002540607	<i>Rpp25</i>	401.410	-0.8401	0.045979893
<i>Irx3</i>	66.315	2.1591	0.02314818	<i>Gm15459</i>	8150.535	-0.8479	0.025941192
<i>Gm28036</i>	366.737	2.1545	0.007841188	<i>Aamdc</i>	394.177	-0.8761	0.007005518
<i>Ccdc80</i>	533.932	2.1180	0.000277774	<i>lah1</i>	931.838	-0.8809	0.01144003
<i>Mreg</i>	60.312	2.1104	0.046880565	<i>Rps15a</i>	18242.775	-0.8809	0.0001203
<i>Zc3h12c</i>	495.719	2.1073	2.21E-09	<i>Gas5</i>	12386.082	-0.8864	5.25E-05
<i>RP23-45713.2</i>	223.702	2.1043	0.00628501	<i>Ifitm3</i>	22541.062	-0.9191	0.004900801
<i>Fgf9</i>	101.482	2.0671	0.013851881	<i>Gstm1</i>	6780.965	-0.9263	1.82E-05
<i>Atp7a</i>	148.126	2.0521	0.044491147	<i>Mocs1</i>	1177.157	-0.9298	0.027529268
<i>Sytl2</i>	173.480	2.0187	0.006394847	<i>Cbr1</i>	2799.021	-0.9358	0.016536621
<i>Tnfrsf11b</i>	2360.995	2.0046	1.87E-10	<i>Pck2</i>	4748.555	-0.9458	8.09E-05
<i>Ccnjl</i>	98.451	2.0013	0.002360541	<i>Tada2a</i>	1147.561	-0.9552	0.000339326
<i>Wnt6</i>	1342.586	1.9839	0.003112336	<i>Mtfp1</i>	505.204	-0.9609	0.025941192
<i>Gm38394</i>	961.573	1.9562	0.009621267	<i>Car12</i>	979.140	-0.9641	0.003540452
<i>Shroom4</i>	178.786	1.9402	0.026951216	<i>Gm26825</i>	61907.963	-0.9710	1.49E-07
<i>4933404012Rik</i>	106.656	1.9371	0.00608095	<i>Gpt2</i>	530.673	-0.9735	0.022633197
<i>Fzd10</i>	328.381	1.9228	0.007069839	<i>Mthfd2</i>	2306.739	-0.9916	1.31E-05
<i>Lifr</i>	290.619	1.9062	0.032767491	<i>Slc6a9</i>	1851.847	-0.9916	0.041861089
<i>Arhgap6</i>	259.923	1.9023	0.009710561	<i>Retsat</i>	1850.948	-0.9997	0.000845633
<i>Myh10</i>	302.782	1.8871	0.030258457	<i>Homer2</i>	2889.558	-1.0006	0.013223948
<i>Rdh9</i>	777.053	1.8738	1.69E-10	<i>Myo1a</i>	4369.252	-1.0129	0.016228803
<i>Gm10676</i>	66.753	1.8565	0.045811139	<i>Atp2a3</i>	788.180	-1.0291	0.043027834
<i>R3hdml</i>	326.455	1.8513	0.011986291	<i>Fuom</i>	253.021	-1.0540	0.015409889
<i>Gcnt1</i>	348.333	1.8203	0.002586935	<i>Camkk2</i>	451.907	-1.0580	0.021074871
<i>Apcdd1</i>	2075.022	1.8154	0.008705004	<i>Prr18</i>	478.717	-1.0713	0.037051369
<i>Lef1</i>	234.227	1.8088	0.000315284	<i>Ggh</i>	685.781	-1.0778	0.003798507
<i>Enpp2</i>	201.155	1.7969	0.009212052	<i>Galnt6</i>	637.388	-1.0882	0.026951216
<i>Ptprd</i>	2082.306	1.7372	9.57E-09	<i>Gm8355</i>	6799.964	-1.0959	0.042305672
<i>Entpd3</i>	1195.274	1.6964	0.001323435	<i>Fabp2</i>	693.495	-1.1017	0.020560865
<i>Slc16a10</i>	682.693	1.6864	4.46E-05	<i>Asns</i>	5033.910	-1.1032	0.000946951
<i>Fam89a</i>	321.894	1.6851	0.000517548	<i>Cbx7</i>	2098.511	-1.1244	9.40E-07
<i>Hspa8</i>	35831.502	1.6831	1.45E-10	<i>Gsto1</i>	17551.616	-1.1913	0.041770402
<i>Gchfr</i>	76.956	1.6731	0.047442082	<i>Reep6</i>	2576.645	-1.2026	0.000377131
<i>Cd244</i>	155.590	1.6603	0.009784393	<i>Pfkfb4</i>	280.570	-1.2163	0.004467261
<i>Klhl23</i>	77.846	1.6510	0.021506823	<i>Ppm1h</i>	268.301	-1.2230	0.000407839
<i>Sema5a</i>	933.533	1.6253	8.36E-07	<i>Abcg2</i>	197.057	-1.2414	0.04771045
<i>Hspb1</i>	415.251	1.6239	0.002677615	<i>Gpd1</i>	1454.474	-1.2708	0.000179201
<i>Nuak1</i>	145.986	1.6185	0.007005518	<i>Hpdl</i>	276.112	-1.2941	0.04771045
<i>Mmp7</i>	12865.237	1.6130	1.87E-10	<i>Foxa2</i>	480.382	-1.2960	0.014962492

<i>Mecom</i>	1168.648	1.5897	1.07E-10	<i>Trib3</i>	452.548	-1.2983	0.000105424
<i>Nr4a2</i>	365.375	1.5884	0.028630607	<i>Tmem158</i>	693.071	-1.3071	0.00011563
<i>Wdfy1</i>	1219.487	1.5460	4.83E-06	<i>Sfn9</i>	242.798	-1.3140	0.0351581
<i>Cd1d1</i>	227.936	1.5404	0.013629106	<i>Dync2li1</i>	172.505	-1.3270	0.033345276
<i>Irs1</i>	210.175	1.5232	0.011986291	<i>Psph</i>	1242.742	-1.3478	3.14E-06
<i>Map6</i>	790.800	1.5231	0.001226583	<i>Apob</i>	1304.153	-1.3750	0.002465045
<i>Plagl1</i>	476.784	1.5219	0.04771045	<i>Ptgr1</i>	14991.733	-1.3912	0.002424496
<i>Esyt3</i>	97.694	1.5182	0.021968632	<i>Grb14</i>	174.911	-1.4271	0.03141421
<i>Mm2610528A11Rik</i>	283.786	1.5101	0.009420265	<i>Itpril2</i>	689.463	-1.4348	0.026819819
<i>Ephb6</i>	566.105	1.5079	0.004711752	<i>Gstm2</i>	730.663	-1.4493	0.00702117
<i>Gdgd3</i>	1422.754	1.4990	0.009673225	<i>Tm6sf2</i>	150.051	-1.4720	0.015236993
<i>Tbx1</i>	2699.388	1.4848	0.031486728	<i>Tmie</i>	147.575	-1.4915	0.038582858
<i>Cep112</i>	256.866	1.4838	0.00376951	<i>St3gal6</i>	1449.498	-1.4952	0.001851081
<i>Ccser1</i>	340.704	1.4759	0.007131688	<i>Epdr1</i>	334.421	-1.5181	0.021494353
<i>Mttr11</i>	740.967	1.4281	1.59E-06	<i>Agr2</i>	2132.400	-1.5266	0.000123572
<i>RP24-390A22.1</i>	939.211	1.4092	0.028630607	<i>Atf5</i>	2080.136	-1.5354	1.92E-08
<i>Slc17a4</i>	594.914	1.3995	0.000187708	<i>Rpl3</i>	67237.730	-1.5519	2.80E-26
<i>Mttr7</i>	299.410	1.3851	0.010034771	<i>Aspa</i>	1155.638	-1.5672	0.002829565
<i>Cdo1</i>	2147.931	1.3732	0.007841188	<i>Cth</i>	1414.812	-1.6361	4.64E-07
<i>Slc22a1</i>	309.731	1.3672	0.005559578	<i>Slc7a3</i>	80.778	-1.6496	0.024412673
<i>Kcnu1</i>	298.891	1.3517	0.001740226	<i>Anxa13</i>	1085.666	-1.6500	0.031793623
<i>Fgfr3</i>	289.820	1.3397	0.026951216	<i>Cbx6</i>	3439.443	-1.6879	1.58E-07
<i>Tcf4</i>	1757.854	1.3391	0.002335503	<i>Pard3b</i>	294.829	-1.7039	0.023997461
<i>Frdm6</i>	809.722	1.3317	2.81E-06	<i>Lgals1</i>	189.230	-1.7053	0.031793623
<i>Gpcpd1</i>	788.994	1.3171	7.11E-06	<i>Gltd1</i>	193.059	-1.7113	0.008705004
<i>Gpc1</i>	1164.617	1.3135	0.001593348	<i>Rpl11</i>	2971.549	-1.7943	0.000385464
<i>Casp12</i>	234.405	1.2904	0.031486728	<i>Gsta1</i>	2811.844	-1.8094	2.99E-06
<i>Clec16a</i>	532.059	1.2598	0.003557959	<i>Apobec3</i>	3684.982	-1.8317	8.87E-16
<i>Zbtb20</i>	2818.947	1.2440	0.003253948	<i>Muc6</i>	318.750	-1.8736	4.92E-06
<i>Mdfic</i>	336.098	1.2433	0.02141478	<i>Sox17</i>	7712.417	-1.9922	1.49E-05
<i>Pkhd1</i>	261.251	1.2274	0.026836288	<i>Vwf</i>	1279.576	-1.9982	0.007516341
<i>Ceacam1</i>	7830.912	1.2195	0.024255873	<i>Etv5</i>	1381.747	-2.0014	7.14E-11
<i>Slc5a9</i>	868.032	1.2151	0.010376921	<i>Gstm3</i>	679.570	-2.0361	1.74E-09
<i>Epha4</i>	1218.758	1.2108	0.000139306	<i>Arhgap10</i>	215.362	-2.0389	0.00724401
<i>Gata6</i>	1582.668	1.2014	0.020028688	<i>3110045C21Rik</i>	61.440	-2.0467	0.020789776
<i>Ly6g</i>	574.137	1.1990	0.002012077	<i>Ugt1a7c</i>	2168.057	-2.0718	1.92E-05
<i>Tle4</i>	830.484	1.1987	0.000199721	<i>Sytl4</i>	126.776	-2.1443	0.002677615
<i>Wls</i>	2773.564	1.1872	0.024412673	<i>Dnah2os</i>	82.659	-2.1699	0.002162978
<i>Evl</i>	417.657	1.1841	0.005632033	<i>Ripply3</i>	79.970	-2.1949	0.041861089
<i>Met</i>	1175.914	1.1778	5.76E-07	<i>Cdh5</i>	401.295	-2.1979	1.82E-10
<i>Ralgs2</i>	3013.544	1.1476	8.15E-11	<i>Ces2c</i>	254.584	-2.2508	2.31E-05
<i>Nbea</i>	1074.953	1.1284	0.006333272	<i>Gata4</i>	2081.080	-2.2968	5.36E-09
<i>Serpib11</i>	1597.953	1.1226	0.020948649	<i>Khdrbs3</i>	150.130	-2.3533	0.041877058
<i>Sesn3</i>	1609.353	1.1221	0.026168086	<i>Cyp2c55</i>	317.265	-2.4327	0.027809854
<i>Gm8797</i>	2848.687	1.1031	0.004043122	<i>Epha3</i>	149.757	-2.5006	0.010750799
<i>Pdlim2</i>	796.960	1.0960	0.004755074	<i>Ifitm6</i>	84.501	-2.5174	0.037116376
<i>Pbx1</i>	3957.006	1.0858	7.33E-05	<i>Cep85</i>	3224.738	-2.5444	4.51E-17

<i>Mex3b</i>	236.609	1.0814	0.022299697	<i>lhh</i>	3761.400	-2.5703	1.56E-17
<i>Npnt</i>	2706.981	1.0667	2.17E-07	<i>Adgrg2</i>	170.771	-2.6128	0.008609952
<i>Lmo7</i>	6853.652	1.0329	8.40E-05	<i>Glb1l2</i>	42.797	-2.6280	0.041861089
<i>Zfp618</i>	734.995	1.0262	0.015051676	<i>Ugt1a6a</i>	1246.516	-2.7007	6.02E-05
<i>Mfap3l</i>	351.835	1.0158	0.01478608	<i>Trim47</i>	110.299	-2.7381	0.031486728
<i>Arl5b</i>	575.591	0.9980	0.029535976	<i>Gm7357</i>	64.423	-2.7593	0.004872248
<i>Trio</i>	1492.193	0.9917	0.000198067	<i>Gabre</i>	176.990	-2.7720	0.004446303
<i>Gnai1</i>	775.339	0.9905	0.02697543	<i>Oprd1</i>	73.005	-2.7929	0.01104423
<i>Fam168a</i>	1115.710	0.9826	0.000253632	<i>Tmem266</i>	1261.409	-2.8620	6.80E-09
<i>Sema3c</i>	4214.939	0.9820	0.000510395	<i>Arg1</i>	39.507	-2.9121	0.014368032
<i>Itpkb</i>	367.206	0.9769	0.03593397	<i>Apoc2</i>	59.957	-2.9698	0.008609952
<i>Frk</i>	1101.942	0.9758	0.028606055	<i>Adh1</i>	565.692	-3.0239	0.00017682
<i>Ptk7</i>	2294.898	0.9755	0.038582858	<i>Fam183b</i>	18.756	-3.1630	0.042716155
<i>Serinc5</i>	2956.797	0.9633	0.000989153	<i>Akr1c14</i>	66.426	-3.1630	0.004517555
<i>Mcam</i>	4053.665	0.9583	0.007841188	<i>Gldc</i>	38.050	-3.1831	0.036816825
<i>Tgfb1</i>	1150.426	0.9428	0.010918488	<i>Cyp2c65</i>	286.693	-3.2278	7.22E-05
<i>Mgat4c</i>	1198.926	0.9413	9.01E-06	<i>Gm14851</i>	75.935	-3.2336	0.04771045
<i>Dsp</i>	16442.643	0.9273	3.43E-05	<i>Cyp4b1</i>	726.770	-3.2546	1.96E-06
<i>Rgs12</i>	1601.375	0.9150	0.024709039	<i>Slc28a2</i>	430.714	-3.2624	1.06E-17
<i>Zfp26</i>	471.377	0.9044	0.035705253	<i>Ugt8a</i>	111.884	-3.2883	0.003995557
<i>Peli1</i>	863.636	0.9025	0.02141478	<i>Gm37788</i>	23.518	-3.2988	0.041861089
<i>Pik3cb</i>	939.780	0.8940	0.007127572	<i>Sult1c2</i>	166.486	-3.3588	0.005632033
<i>Zcchc11</i>	983.508	0.8834	0.007438679	<i>T</i>	62.162	-3.4451	0.000111932
<i>Cblb</i>	428.432	0.8826	0.013754336	<i>St3gal5</i>	52.834	-3.4674	0.02314818
<i>Fam83d</i>	462.082	0.8799	0.025555099	<i>Prap1</i>	811.752	-3.5589	2.38E-09
<i>Gp1bb</i>	1250.692	0.8687	0.02857225	<i>Aqp5</i>	58.878	-3.6262	0.042414975
<i>Atp11a</i>	2297.482	0.8678	0.001309896	<i>Tcf23</i>	160.267	-3.6895	9.00E-05
<i>Ptprj</i>	3344.064	0.8642	0.002424496	<i>Dmtn</i>	53.711	-3.7410	0.041861089
<i>Lrp4</i>	3121.582	0.8556	0.026951216	<i>Akp3</i>	236.491	-3.7470	0.000115093
<i>Btbd7</i>	530.295	0.8427	0.045348902	<i>Clec2f</i>	103.898	-3.7685	0.010219868
<i>Mbd5</i>	355.041	0.8382	0.045155934	<i>Anxa10</i>	59.517	-3.8672	0.000664969
<i>Nhsl1</i>	2443.992	0.8274	0.003138478	<i>Pr2c3</i>	137.452	-3.9051	0.008445669
<i>Apaf1</i>	1833.873	0.8269	0.000229283	<i>Smoc1</i>	109.444	-3.9095	0.02697543
<i>Ptpre</i>	1241.255	0.8163	0.00017682	<i>Pcdhgb7</i>	21.423	-4.0649	0.017290909
<i>Arid5b</i>	1035.497	0.8140	0.013203002	<i>RP23-359B23.11</i>	692.619	-4.2458	5.00E-60
<i>Gpd2</i>	4167.941	0.8070	2.84E-05	<i>Cd59a</i>	27.208	-4.2570	0.0295267
<i>Pam</i>	3607.388	0.7900	0.00702117	<i>Adh7</i>	109.722	-4.5185	0.031808902
<i>Cenpf</i>	1858.433	0.7896	0.02408616	<i>Olfml2b</i>	274.122	-4.5860	9.80E-12
<i>Ghl3</i>	1997.402	0.7876	0.046874231	<i>Myo7a</i>	152.766	-4.7548	6.61E-11
<i>Wsb1</i>	2356.787	0.7865	0.008320802	<i>Vsig2</i>	77.927	-4.9937	1.82E-12
<i>Foxa1</i>	2979.478	0.7829	0.04771045	<i>Tff2</i>	602.197	-5.1415	0.009420265
<i>Notch2</i>	1487.157	0.7827	0.010090541	<i>Lipf</i>	3117.599	-5.3635	0.005027141
<i>Wipi1</i>	1142.096	0.7775	0.017247803	<i>Cfh</i>	42.786	-5.6052	0.000194505
<i>Cdk17</i>	656.058	0.7688	0.012053334	<i>Rps4l</i>	93.687	-5.6304	5.15E-06
<i>Tfip11</i>	2752.693	0.7642	0.048431765	<i>Gm43305</i>	26435.609	-5.9909	3.86E-05
<i>Farp1</i>	1989.846	0.7497	0.005302767				
<i>Ptbp2</i>	831.446	0.7494	0.024255873				

<i>Cobl</i>	2719.000	0.7472	0.022622615
<i>Trp53inp2</i>	1819.459	0.7456	0.04771045
<i>Jag1</i>	1452.110	0.7341	0.032767491
<i>Bcl9</i>	1586.685	0.7316	0.002533876
<i>Kitl</i>	4642.004	0.7041	0.038002848
<i>Afap111</i>	5835.163	0.6953	0.049142352
<i>Scpep1</i>	2850.151	0.6916	0.001657384
<i>Epc2</i>	894.154	0.6909	0.040526834
<i>Zfp703</i>	6066.750	0.6892	0.047975601
<i>Etl4</i>	2288.212	0.6878	0.04148622
<i>Jmjd1c</i>	1522.959	0.6875	0.017395901
<i>Adam10</i>	4150.597	0.6834	0.020912016
<i>Itga6</i>	6482.326	0.6694	0.00029331
<i>Nudt4</i>	5160.221	0.6608	0.0295267
<i>Fryl</i>	2750.545	0.6502	0.006904233
<i>Rnf38</i>	2177.811	0.6082	0.036627682
<i>Aff4</i>	2951.017	0.6057	0.039242954
<i>Lpgat1</i>	2062.510	0.6047	0.020926743
<i>Phactr4</i>	1961.552	0.5829	0.032767491
<i>Zdhhc21</i>	1329.859	0.5713	0.045439476
<i>Tmem245</i>	1702.351	0.5654	0.022622615
<i>Lrrc16a</i>	2282.516	0.5601	0.047178664
<i>Oxct1</i>	5867.987	0.5593	0.017127546
<i>Exoc6b</i>	1550.392	0.5561	0.036816825
<i>Traf6</i>	1239.292	0.5518	0.044447523
<i>Tes</i>	4735.285	0.5420	0.022622615
<i>Macf1</i>	3543.230	0.5079	0.024255873
<i>Anxa4</i>	32898.066	0.4631	0.042305672

7.9 Supplemental Data 9

Related to Figure 25 (middle panel).

List of the significantly up-regulated and down-regulated mRNAs in *Csf1r*-deficient tumoroids compared to APC^{min} tumoroids.

Significantly up-regulated mRNAs				Significantly down-regulated mRNAs			
Gene symbol	Base mean	Log ₂ fold change	padj	Gene symbol	Base mean	Log ₂ fold change	padj
<i>Eno1b</i>	2115.547	8.545	0.005264977	<i>Taldo1</i>	12320.003	-0.552	0.006527818
<i>Lipf</i>	3117.599	5.033	0.032217819	<i>Slc12a8</i>	1296.432	-0.660	0.049604636
<i>Eif5a13-ps</i>	407.649	5.032	1.19E-11	<i>Cda</i>	919.923	-0.739	0.012908849
<i>Reg3b</i>	1578.899	4.797	0.010926405	<i>Gm26825</i>	61907.963	-0.768	0.000605867
<i>Chd9</i>	6859.116	4.488	0.00024203	<i>2810428115Rik</i>	1027.442	-0.773	0.029781772
<i>Nid2</i>	70.791	4.246	0.008182885	<i>Septin5</i>	11872.794	-0.783	0.004852742

<i>Ildr2</i>	148.520	4.046	2.85E-05	<i>Bmp8b</i>	1501.902	-0.786	0.001513872
<i>Nyap1</i>	122.601	4.019	0.01115132	<i>Tmem180</i>	948.149	-0.813	0.037485635
<i>Gm11942</i>	32.764	3.965	0.005278321	<i>Phlda1</i>	12248.270	-0.890	0.000988203
<i>Slco5a1</i>	105.067	3.951	5.87E-10	<i>Rccd1</i>	1050.616	-0.892	0.001657048
<i>Tmod2</i>	291.368	3.857	0.000331018	<i>Mgst2</i>	1191.236	-0.912	0.017159244
<i>Klhl13</i>	105.530	3.856	7.07E-09	<i>Ldhd</i>	709.184	-0.919	0.013846932
<i>Dio1</i>	115.796	3.846	0.000782316	<i>Fhdc1</i>	744.435	-1.028	0.005452637
<i>Trpm6</i>	93.381	3.828	0.027130829	<i>Aim1l</i>	926.467	-1.042	0.005425664
<i>Ackr3</i>	147.564	3.643	0.022826051	<i>Eefsec</i>	834.524	-1.044	0.004060918
<i>Enpp2</i>	201.155	3.575	1.54E-09	<i>Gp1bb</i>	1250.692	-1.047	0.011612686
<i>Gm10052</i>	628.537	3.389	0.000307527	<i>Acs1l</i>	1160.101	-1.083	0.001623629
<i>Gm28036</i>	366.737	3.315	1.02E-05	<i>Cdhr2</i>	3046.022	-1.192	8.90E-05
<i>1700003F12Rik</i>	82.768	3.311	0.001158154	<i>Lrrc66</i>	631.904	-1.210	0.000971269
<i>Gm5148</i>	40.408	3.283	0.017159244	<i>Gm12744</i>	453.349	-1.218	0.003689542
<i>Olfm2b</i>	274.122	3.168	9.71E-06	<i>Al506816</i>	6888.954	-1.235	8.16E-11
<i>Arhgap44</i>	637.247	2.901	2.39E-12	<i>Galnt6</i>	637.388	-1.257	0.018379296
<i>Dkk2</i>	453.441	2.822	0.013846932	<i>Itln1</i>	2362.524	-1.293	5.43E-05
<i>Ifit1</i>	77.962	2.802	0.0079409	<i>Tm4sf5</i>	885.553	-1.336	0.005393062
<i>Ccdc33</i>	170.411	2.785	0.005262043	<i>3930402G23Rik</i>	132.081	-1.371	0.034288645
<i>Cyp2f2</i>	128.239	2.700	0.039165153	<i>Il3ra</i>	451.682	-1.477	0.000440972
<i>Reg3g</i>	983.822	2.668	4.13E-06	<i>Gm8355</i>	6799.964	-1.511	0.003618566
<i>Plac9b</i>	304.759	2.646	0.000156357	<i>Cwh43</i>	526.966	-1.613	0.014464497
<i>Cd200</i>	80.474	2.643	0.007590836	<i>Tm6sf2</i>	150.051	-1.642	0.013846932
<i>Hip1</i>	583.885	2.633	0.001285767	<i>2610528A11Rik</i>	283.786	-1.657	0.009428004
<i>RP24-390A22.1</i>	939.211	2.600	1.15E-06	<i>Fabp2</i>	693.495	-1.837	9.14E-06
<i>2210418O10Rik</i>	195.445	2.482	1.08E-05	<i>Ces2c</i>	254.584	-1.845	0.005262043
<i>Rhbdl2</i>	240.854	2.443	0.001158154	<i>2210407C18Rik</i>	2916.869	-1.920	0.021286363
<i>Rarb</i>	360.379	2.437	5.87E-10	<i>Oit1</i>	951.318	-1.954	0.001623629
<i>Gm10073</i>	349.913	2.394	9.49E-13	<i>Bcas1</i>	324.096	-2.000	2.87E-05
<i>Htra1</i>	58.451	2.382	0.019673334	<i>Prap1</i>	811.752	-2.067	0.013846932
<i>Serpinb7</i>	58.653	2.309	0.036645791	<i>Gm10036</i>	1791.573	-2.118	6.41E-06
<i>Trib2</i>	47.392	2.289	0.042319558	<i>Bnpl</i>	107.914	-2.215	0.041163186
<i>RP23-359B23.11</i>	692.619	2.217	3.03E-15	<i>Gsta1</i>	2811.844	-2.329	1.71E-09
<i>Irx5</i>	654.455	2.163	0.022448647	<i>Gm20699</i>	73.768	-2.389	0.001742256
<i>Tbx3os1</i>	128.414	2.091	0.000397301	<i>Trim29</i>	293.204	-2.443	0.019660527
<i>Cep85</i>	3224.738	2.087	4.88E-10	<i>Ereg</i>	168.653	-2.645	3.03E-05
<i>Tmem254c</i>	2306.541	2.075	0.019673334	<i>Gdpd3</i>	1422.754	-2.729	3.21E-08
<i>Socs3</i>	975.398	2.064	0.008239514	<i>4930452B06Rik</i>	125.072	-2.735	0.001158154
<i>Tmem254b</i>	675.334	1.988	0.009428004	<i>Gm37335</i>	96.624	-2.784	0.001847746
<i>Slc4a3</i>	136.680	1.985	0.000228556	<i>Rpgrip1</i>	85.153	-2.794	0.005262043
<i>Tmem254a</i>	700.793	1.951	0.005264977	<i>RP23-45713.2</i>	223.702	-3.019	2.15E-05
<i>Lrch4</i>	467.626	1.858	0.001272615	<i>Gm26377</i>	2536.232	-3.124	0.045318862
<i>Hspa8</i>	35831.502	1.842	1.66E-11	<i>Gm8885</i>	55.853	-3.292	0.000152853
<i>Jdp2</i>	355.774	1.686	0.021552668	<i>Anxa10</i>	59.517	-3.568	0.008747472
<i>Mtmr7</i>	299.410	1.636	0.004774663	<i>Fut10</i>	72.175	-3.582	0.000458363
<i>Rilpl1</i>	176.654	1.612	0.006527818	<i>Gm5292</i>	199.915	-4.934	4.20E-30
<i>Rpl11</i>	2971.549	1.596	0.010208959	<i>Cyp2c29</i>	64.591	-5.655	0.000379312

<i>Gm37376</i>	1504.388	1.585	0.032217819	<i>Gm10704</i>	940.745	-5.777	1.18E-48
<i>Rnf24</i>	314.334	1.564	0.013846932	<i>Gm10020</i>	4645.692	-5.822	1.07E-06
<i>Gm14226</i>	548.793	1.556	0.015813486	<i>Gm14094</i>	315.824	-6.057	8.90E-39
<i>Chac1</i>	391.144	1.493	0.010749668	<i>Gm10093</i>	1986.903	-6.911	6.46E-120
<i>Atp2b4</i>	284.465	1.411	0.000417447	<i>Gm10182</i>	3021.766	-7.110	2.24E-08
<i>Eno3</i>	790.059	1.402	0.043479661	<i>Gm8420</i>	2800.915	-8.425	1.47E-132
<i>Cdh5</i>	401.295	1.402	0.001158154				
<i>Ifi27</i>	555.921	1.388	0.042022706				
<i>Zfp532</i>	391.439	1.387	0.039165153				
<i>Smarca2</i>	1084.414	1.379	0.009636562				
<i>Plat</i>	2312.407	1.343	0.005262043				
<i>Gm4294</i>	547.551	1.337	0.000704746				
<i>Cmtrn3</i>	284.671	1.322	0.000873517				
<i>Rpl15-ps3</i>	8562.884	1.287	0.005262043				
<i>Gm6206</i>	321.412	1.193	0.019673334				
<i>Asah1</i>	3488.842	1.145	0.002067016				
<i>Gpt2</i>	530.673	1.140	0.012014694				
<i>Sema6a</i>	676.229	1.123	0.045072294				
<i>Pisd-ps1</i>	3559.954	1.001	0.011010573				
<i>Tmem150a</i>	308.229	0.983	0.026953258				
<i>Bahcc1</i>	2313.376	0.948	0.008239514				
<i>Atp11a</i>	2297.482	0.947	0.001207801				
<i>Slc17a5</i>	1027.990	0.944	0.013846932				
<i>Vegfa</i>	3634.098	0.873	0.005264977				
<i>Cdh13</i>	3191.281	0.847	1.05E-05				
<i>Tbx3</i>	5316.960	0.838	0.047066946				
<i>Arid5b</i>	1035.497	0.818	0.039845208				
<i>Large</i>	840.153	0.808	0.012908849				
<i>Galnt11</i>	639.879	0.766	0.01561526				
<i>Hsd12</i>	923.246	0.728	0.044984804				
<i>Cd24a</i>	14100.979	0.700	0.001513872				
<i>Sap30</i>	1461.658	0.611	0.039165153				
<i>Runx1</i>	1436.232	0.600	0.046228427				

7.10 Supplemental Data 10

Related to Figure 25 (lower panel).

List of the significantly up-regulated and down-regulated mRNAs in *Csf1r/Mir34a*-deficient tumoroids compared to APCmin tumoroids.

Significantly up-regulated mRNAs				Significantly down-regulated mRNAs			
Gene symbol	Base mean	Log ₂ fold change	padj	Gene symbol	Base mean	Log ₂ fold change	padj
<i>Gm10182</i>	3021.766	5.666	1.59E-05	<i>Htra2</i>	1798.309	-0.555	0.041544
<i>Gpc3</i>	75.939	4.812	0.000112	<i>Gstm1</i>	6780.965	-0.737	0.005879
<i>Zfp462</i>	209.491	4.460	0.003653	<i>Cdhr2</i>	3046.022	-0.853	0.019161
<i>Dkk2</i>	453.441	4.338	2.64E-06	<i>Ccnd2</i>	19892.557	-0.945	0.034215
<i>Cyp2f2</i>	128.239	4.204	5.21E-06	<i>Camkk2</i>	451.907	-1.068	0.046562
<i>Gm13067</i>	24.628	4.064	0.038304	<i>1110028F11Rik</i>	595.344	-1.104	0.022368
<i>Krt6a</i>	622.517	4.048	1.96E-10	<i>Cth</i>	1414.812	-1.116	0.009021
<i>Spink1</i>	68.628	4.042	0.022515	<i>Gstm3</i>	679.570	-1.165	0.01257
<i>Rtn1</i>	64.786	3.964	0.010003	<i>Anpep</i>	720.996	-1.246	0.046199
<i>Irx5</i>	654.455	3.921	6.40E-09	<i>Slc40a1</i>	1100.126	-1.297	0.000394
<i>Slc15a2</i>	172.769	3.845	0.017163	<i>St3gal6</i>	1449.498	-1.331	0.022368
<i>Gm29865</i>	63.006	3.836	3.06E-05	<i>Apob</i>	1304.153	-1.396	0.005601
<i>Fam43b</i>	92.413	3.824	0.004269	<i>Galnt6</i>	637.388	-1.509	0.000836
<i>Crnde</i>	233.410	3.784	3.85E-05	<i>Gata4</i>	2081.080	-1.518	0.00226
<i>Gm5148</i>	40.408	3.779	0.000636	<i>Oit1</i>	951.318	-1.554	0.030775
<i>Ncf2</i>	100.728	3.490	0.004269	<i>Ereg</i>	168.653	-1.660	0.048455
<i>Gm12669</i>	217.052	3.296	0.038703	<i>Tm6sf2</i>	150.051	-1.763	0.004396
<i>Cxcl14</i>	54.669	3.273	0.011498	<i>Ces2c</i>	254.584	-1.865	0.003241
<i>Gm45062</i>	160.126	3.254	0.040073	<i>Acta1</i>	134.371	-1.908	0.000705
<i>Car1</i>	269.064	3.215	0.010679	<i>Ccdc141</i>	1178.872	-1.917	0.021743
<i>Gpr157</i>	136.064	3.093	9.85E-07	<i>Rpl11</i>	2971.549	-1.920	0.000275
<i>RP23-45713.2</i>	223.702	3.069	6.07E-06	<i>Gsta1</i>	2811.844	-2.053	1.35E-07
<i>Pcdh7</i>	133.184	2.950	0.016184	<i>Cep85</i>	3224.738	-2.431	8.47E-15
<i>RP24-390A22.1</i>	939.211	2.943	2.34E-09	<i>Pla2g4a</i>	159.974	-2.454	0.014701
<i>Lrrn3</i>	81.537	2.893	0.008453	<i>Trf</i>	72.579	-2.613	0.016652
<i>Dynap</i>	78.475	2.826	0.009571	<i>Tgfb3</i>	91.135	-2.646	0.00226
<i>Tbx1</i>	2699.388	2.605	3.22E-06	<i>Muc6</i>	318.750	-2.668	2.33E-11
<i>Irx3</i>	66.315	2.550	0.009064	<i>Prap1</i>	811.752	-2.753	4.32E-05
<i>RP23-145116.5</i>	350.152	2.527	0.047585	<i>Apoc2</i>	59.957	-2.838	0.0346
<i>Enpp2</i>	201.155	2.472	8.00E-05	<i>Tek</i>	324.310	-2.893	0.043686
<i>Vim</i>	3736.819	2.455	1.47E-05	<i>Plac9b</i>	304.759	-3.078	1.57E-06
<i>Mreg</i>	60.312	2.415	0.034215	<i>Dzip1l</i>	83.364	-3.099	0.032962
<i>Gm20463</i>	77.245	2.412	0.00226	<i>Tmem45a</i>	216.013	-3.181	0.014701
<i>Serpib7</i>	58.653	2.350	0.019161	<i>Cybrd1</i>	219.553	-3.263	0.000187
<i>Gm14226</i>	548.793	2.265	4.27E-06	<i>Anxa10</i>	59.517	-3.278	0.016913
<i>Gm25287</i>	123.035	2.252	0.006312	<i>RP23-359B23.11</i>	692.619	-3.337	1.08E-39
<i>Apccdd1</i>	2075.022	2.251	0.000836	<i>Cfh</i>	42.786	-3.773	0.023116

<i>St6gal1</i>	576.819	2.239	8.45E-06	<i>Gkn3</i>	94.745	-4.141	0.016184
<i>Htra1</i>	58.451	2.203	0.04251	<i>Vsig2</i>	77.927	-4.546	1.25E-10
<i>Znf41-ps</i>	118.132	2.178	0.013182				
<i>Col16a1</i>	348.416	2.172	0.00226				
<i>Rerg</i>	130.070	2.087	0.030775				
<i>Rassf4</i>	342.221	2.008	0.046562				
<i>Gm38394</i>	961.573	1.891	0.035358				
<i>Golga7b</i>	475.245	1.871	0.000123				
<i>Tgfb1</i>	300.710	1.843	0.028586				
<i>Gm22918</i>	125.585	1.828	0.033746				
<i>Rdh9</i>	777.053	1.792	4.85E-09				
<i>Tpbp</i>	262.197	1.778	0.010003				
<i>Gm13139</i>	155.515	1.751	0.010003				
<i>Reg3g</i>	983.822	1.751	0.01436				
<i>Tnfrsf11b</i>	2360.995	1.656	1.76E-06				
<i>Mtmr11</i>	740.967	1.599	9.70E-08				
<i>Ephb6</i>	566.105	1.589	0.006291				
<i>Hspb1</i>	415.251	1.581	0.010679				
<i>Tenn4</i>	1017.163	1.485	0.009746				
<i>Tbx3os1</i>	128.414	1.481	0.035104				
<i>Fbxo32</i>	816.623	1.461	0.018058				
<i>Casp12</i>	234.405	1.424	0.030819				
<i>Gm10036</i>	1791.573	1.392	0.016913				
<i>Slc16a10</i>	682.693	1.267	0.018529				
<i>Robo1</i>	731.218	1.245	0.02306				
<i>Tcf4</i>	1757.854	1.241	0.016913				
<i>Ptprd</i>	2082.306	1.230	0.000836				
<i>Dpysl3</i>	1071.417	1.165	0.016184				
<i>Mmp7</i>	12865.237	1.131	0.000155				
<i>Rarb</i>	360.379	1.122	0.048455				
<i>Zc3h12c</i>	495.719	1.097	0.04301				
<i>Itpkb</i>	367.206	1.084	0.034215				
<i>Bnip3</i>	3814.478	1.077	0.017631				
<i>Kitl</i>	4642.004	0.985	0.001501				
<i>Met</i>	1175.914	0.720	0.0346				
<i>Sap30</i>	1461.658	0.639	0.018258				
<i>Cdh13</i>	3191.281	0.528	0.036342				

Acknowledgements

First of all, my deepest gratitude goes first and foremost to my supervisor, doctoral father- Prof. Dr. rer. nat. Heiko Hermeking, for offering me the valuable opportunity to conduct cancer research in the well-designed and fully-equipped laboratories, and also for his great patience, scientific guidance, and continuous support during my doctoral study. I am really grateful to him for providing me with a precious opportunity to learn basic experimental techniques, cultivate scientific thinking, and understand life attitudes. And without his consistent helpful advice and careful instruction, this project could not be completed.

Moreover, I would like to thank all the members of AG Hermeking and AG Peter Jung for their kind help and support throughout the past years. Working with all of you is lucky and unforgettable for me. In particular, I would like to thank Dr. Nassim Bouznad for designing the mouse crossings and initial performance of genotyping, Dr. Markus Kaller for performing bioinformatics analysis and interpretation professionally, Janine König for dual-reporter assays of murine *Csf1r* 3'-UTR, and qPCR analysis of *Csf1r* in CT26 cells, Dr. Stephanie Jaeckel for her great support for *in situ* hybridization and analysis of tumoroids, Dr. Markus Winter for technical advice, and Dr. Peter Jung for interesting discussions in the lab meetings. I also would like to thank Ursula Götz for her great technical support and assistance in the lab. In addition, I would like to thank Xiaolong Shi, Jinjiang Chou, Chunfeng Liu, Wenjing Shi, Zekai Huang, Yuyun Dun, Xiaoyan Chen for their help and support during these times.

Last but not least, I'm very grateful to my parents, who have been supporting me without a word of complaint. Words cannot express my love for my family. All that I am, or hope to be, I owe to my dear parents. I love them.

Affidavit



LUDWIG-
MAXIMILIANS-
UNIVERSITÄT
MÜNCHEN

Promotionsbüro
Medizinische Fakultät



Affidavit

Liu, Fangteng

Surname, first name

Street

Zip code, town, country

I hereby declare, that the submitted thesis entitled:

Csf1r mediates enhancement of intestinal tumorigenesis caused by inactivation of *Mir34a*

is my own work. I have only used the sources indicated and have not made unauthorized use of services of a third party. Where the work of others has been quoted or reproduced, the source is always given.

I further declare that the dissertation presented here has not been submitted in the same or similar form to any other institution for the purpose of obtaining an academic degree.

Munich, 28.07.2023

place, date

Fangteng Liu

Signature doctoral candidate

List of publications

- Liu, F., Bouznad, N., Kaller, M., Shi, X., König, J., Jaeckel, S., & Hermeking, H. (2022). Csf1r mediates enhancement of intestinal tumorigenesis caused by inactivation of Mir34a. *Int J Biol Sci*, 18(14), 5415-5437. doi:10.7150/ijbs.75503
- Liu, F., Dong, Q., & Huang, J. (2017). Overexpression of LncRNA PVT1 Predicts Advanced Clinicopathological Features and Serves as an Unfavorable Risk Factor for Survival of Patients with Gastrointestinal Cancers. *Cell Physiol Biochem*, 43(3), 1077-1089. doi:10.1159/000481719
- Liu, F., Gao, H., Li, S., Ni, X., & Zhu, Z. (2017). Long non-coding RNA ZFAS1 correlates with clinical progression and prognosis in cancer patients. *Oncotarget*, 8(37), 61561-61569. doi:10.18632/oncotarget.18633
- Liu, F., Gao, H., Zhao, Y., & Zhu, Z. (2017). Transducin (β)-like 1 X-linked receptor 1 correlates with clinical prognosis and clinicopathological characteristics in human solid carcinomas. *Oncotarget*, 8(37), 61626-61636. doi:10.18632/oncotarget.18650
- Liu, F., Ou, Y., Lin, Q. S., Qiu, C., Luo, H. L., & Zhu, P. Q. (2016). Low expression of long non-coding RNA-LET can indicate metastasis and a poor prognosis: a meta-analysis. *Minerva Med*.
- Liu, F. T., Dong, Q., Gao, H., & Zhu, Z. M. (2017). The prognostic significance of UCA1 for predicting clinical outcome in patients with digestive system malignancies. *Oncotarget*, 8(25), 40620-40632. doi:10.18632/oncotarget.16534
- Liu, F. T., Gao, H., Wu, C. W., & Zhu, Z. M. (2017). The association of plasma fibrinogen with clinicopathological features and prognosis in esophageal cancer patients. *Oncotarget*, 8(54), 93029-93038. doi:10.18632/oncotarget.21746
- Liu, F. T., Ou, Y. X., Zhang, G. P., Qiu, C., Luo, H. L., & Zhu, P. Q. (2016). HOXB7 as a promising molecular marker for metastasis in cancers: a meta-analysis. *Onco Targets Ther*, 9, 2693-2699. doi:10.2147/ott.S104000
- Liu, F. T., Pan, H., Xia, G. F., Qiu, C., & Zhu, Z. M. (2016). Prognostic and clinicopathological significance of long noncoding RNA H19 overexpression in human solid tumors: evidence from a meta-analysis. *Oncotarget*, 7(50), 83177-83186. doi:10.18632/oncotarget.13076
- Liu, F. T., Xue, Q. Z., Zhang, Y., Hao, T. F., Luo, H. L., & Zhu, P. Q. (2016). Long Non-Coding RNA HOXA Transcript at the Distal Tip as a Putative Biomarker of Metastasis and Prognosis: a Meta-Analysis. *Clin Lab*, 62(11), 2091-2098. doi:10.7754/Clin.Lab.2016.160224
- Liu, F. T., Xue, Q. Z., Zhu, P. Q., Luo, H. L., Zhang, Y., & Hao, T. (2016). Long noncoding RNA AFAP1-AS1, a potential novel biomarker to predict the clinical outcome of cancer patients: a meta-analysis. *Onco Targets Ther*, 9, 4247-4254. doi:10.2147/ott.S107188
- Liu, F. T., Zhou, L., Qiu, C., Xia, G., Zhu, P. Q., & Luo, H. L. (2016). Association of the HOTAIR rs4759314 polymorphism with cancer risk: a meta-analysis. *J buon*, 21(4), 1016-1023.
- Liu, F. T., Zhu, P. Q., Luo, H. L., Zhang, Y., Hao, T. F., Xia, G. F., . . . Qiu, C. (2016). Long noncoding RNA ANRIL: a potential novel prognostic marker in cancer: a meta-analysis. *Minerva Med*, 107(2), 77-83.
- Liu, F. T., Zhu, P. Q., Luo, H. L., Zhang, Y., & Qiu, C. (2016). Prognostic value of long non-coding RNA UCA1 in human solid tumors. *Oncotarget*, 7(36), 57991-58000. doi:10.18632/oncotarget.11155
- Liu, F. T., Zhu, P. Q., Ou, Y. X., Lin, Q. S., Qiu, C., & Luo, H. L. (2016). Long non-coding RNA-LET can indicate metastasis and a poor prognosis: a meta-analysis. *Minerva Med*, 107(2), 101-107.
- Liu, F. T., Zhu, P. Q., Ou, Y. X., Liu, W. W., Xia, G. F., & Luo, H. L. (2016). Positive association between IL-16 rs1131445 polymorphism and cancer risk: a meta-analysis. *Minerva Med*, 107(2), 84-91.